Evaluation of RADARSAT-1 for Monitoring and Mapping Land Use / Land Cover in Thailand.

by

Rébecca Filion
Bachelor in Geography, Université Laval, Québec, 2000

A Thesis Submitted in Partial Fulfillment of the Requirements for the Degree of

MASTER IN SCIENCE

in the Department of Geography

We accept this thesis as conforming to the required standard

[redacted]

Dr. K.Olaf Niemann, Supervisor (Department of Geography)

[redacted]

Dr. Mark S. Flaherty, Departmental Member (Department of Geography)

[redacted]

Dr. David G. Goodenough, Outside Member (Pacific Forestry Centre / Computer Science Department)

[redacted]

Dr. Monique Bernier, External Member (Institut National de la Recherche Scientifique, Centre Eau, Terre et Environnement, Université du Québec)

Supervisor: Dr. K.Olaf Niemann

ABSTRACT

Shrimp farming is an important part of the world aquaculture market. Thailand has, for the last 10 years, been the world's leader in the intensive shrimp culture industry. However, intensive shrimp farming has major social, economic and environmental impacts. It is therefore paramount to manage this activity in order to make it sustainable.

In response to the Thai government's search for a cost effective approach to the regular monitoring of large areas, a project was started in 1998 using optical LANDSAT data to identify shrimp farms, as well as other land cover and land use. The high frequency of cloud cover, however, made regular data collection impossible. RADARSAT-1 imagery, on the other hand, has great potential for this type of application as the images are firstly highly influenced by the presence of water and, secondly, not influenced by clouds and other typical effects of tropical weather such as dust and haze.

In this thesis, RADARSAT-1 imagery was evaluated as a tool to monitor and map shrimp farms as well as different land use and land cover in the area of Changwat Chachoengsao, southeastern Thailand. Multi-temporal and multi-angle image combinations were used in order to augment the quantity of information usually available when only one image channel is used. Five fine beam modes (F1, F4 and F5) RADARSAT-1 scenes were taken between May and September 2001.

Image pre-processing techniques such as radiometric correction, geometric correction, principal components analysis, speckle filtering and texture analysis were performed on all the images. Subsequent pixel-based classifications, unsupervised and supervised, as well as segmentation-based classifications, were performed on the pre-

processed images. A comparison was carried out between possible combinations of multi-temporal and multi-angle classified images.

The best results were obtained using a supervised maximum likelihood classification of four (rice paddies, human settlements, orchard plantations, and all water bodies) and five (rice paddies, human settlements, orchard plantations water bodies, and shrimp farms) land use / land cover classes using multi-temporal mean texture components produced from the two images having steeper incidence angles: May 24 2001 (F1) and July 11 2001 (F1).

Examiners:

[redacted]

Dr. K.Olaf Niemann, Supervisor (Department of Geography)

[redacted]

Dr. Mark S. Flaherty, Departmental Member (Department of Geography)

[redacted]

Dr. David G. Goodenough, Outside Member (Pacific Forestry Center / Computer Science Department)

[redacted]

Dr. Monique Bernier, External Member (Institut National de la Recherche Scientifique, Centre Eau, Terre et Environnement, Université du Québec)

TABLE OF CONTENTS

LIST OF TABLES

LIST OF FIGURES

ACKNOWLEDGEMENTS

I would like particularly to thank my supervisor Dr. Olaf Niemann for his support, encouragement, and trust, without which this project would never have been completed. I would also like to thank my committee members, Dr. Mark Flaherty and Dr. Goodenough, for their time and help. Thanks to my excellent English tutor, Peter Fothergill-Payne, who encouraged me so much in spending his precious time reviewing each single word of this document. Thanks to Dr. Monique Bernier for supporting me, personally, financially and academically, as well as allowing me to do all my analyses at the INRS (*Institut National de la Recherche Scientifique*). Thanks also to Yves Gauthier (INRS) for his incredible technical help and support.

Particular acknowledgements to the *Fonds pour la formation des chercheurs et l'aide à la recherche (FCAR), Gouvernement du Québec*, for the scholarship they have given me (Bourse de maîtrise en recherche, B1). Thanks to the financial support from the Rockefeller Brothers Fund for the purchase of the RADARSAT-1 satellite images. Thanks also to the Canadian Space Agency (CSA) for facilitating the acquisition of the RADARSAT-1 satellite images used in this project.

Thanks to my friend and geographer colleague, Carrie Steckler, for assisting me in Thailand during this amazing field campaign, as well as helping and encouraging me during the final miles of this project. Special thanks to Jenn Yakimishyn, for sitting in front of that computer that day..., and becoming my excellent friend, and source of motivation! Thanks to Caroline Poulin for spending so much time reading and editing my work. I will bring you back some good cider my friend! Thanks to Elizabeth Malta, my geographer colleague and very good friend, who constantly helps and encourages me truly without respite, and for being a model of success. Thanks to Missey for wearing that fuzzy hat on the Rugby field, thanks for being my mate and friend! Thanks to my fantastic friend Grant Sullivan, who helped me so much to go on during my first year, and who always listened to my great stories, like the one about the "big apple"! Thanks to Geneviève-Isabelle Picard for being my best friend and my soul mate. "*Tu es mon idole, mon idole, Geneviève...*". Thanks to Julie Bergeron for being there, even from far away, during the whole progression of the thesis, supporting me in an incredible way, and promising me a "*Félicitations*" banner!

Thanks to all my supportive friends who cheer me all along the way, and with whom I had a wonderful time traveling, chatting, celebrating, playing rugby, going at the beach, snowboarding and skateboarding, in other words, my precious friends with whom I enjoy life and I have great fun outside my graduate studies.

Thanks to my parents Serge Filion and Mariette Simard, my sister Catherine Filion and brother Frédéric Filion, for their wise advice and moral support through that whole process. Thank you for encouraging me from beginning to end, and believing in me. "*Nos difficultés sont nos maitres...*".

Finally, exceptional thanks to Frédéric Poulin for his love and ultimate support, but also for being the most patient person in the world... *je t'aime.*

DEDICATION

Pour toi ma belle grand-mère,

Juliana Simard,

qui a toujours été si fière de moi et de mon travail.

CHAPTER ONE

INTRODUCTION

1.1 Nature of the Problem

Among all aquaculture sectors in the global economy, shrimp farming is one of the fastest growing. In 1998, 737,000 tonnes of shrimp were produced by the world's shrimp farmers, yielding an estimated value of 6 billions US dollars (Flaherty et al., 2000). The production of cultured shrimp started increasing drastically in the 1980's. Since the 1990's, this type of aquaculture has exceeded captured shrimp production (Patmasiriwat *et al.*, 1998). Thailand, since 1991, has been the world largest producer and exporter of cultured shrimp, exporting up to 90% of its own production and supplying 20% of the world trade of shrimp and prawn (Huitric *et al.*, 2002; Flaherty *et al.*, 2000; 1999; Patmasiriwat *et al*, 1998). During the past few years, Thai farmers have developed new aquaculture techniques using low salinity water, which allows cultivation of black tiger shrimp (*Penaeus monodon*) a marine species further inland, so that direct access to the ocean is no longer necessary (Flaherty and Vandergeest, 1998). Farmers transport salt water inland so that they can establish their farms in freshwater areas, primarily rice paddies (Flaherty *et al.*, 2000). For rice farmers, the conversion of their field into shrimp ponds is tempting because the profits are higher, and easy because they already have extensive irrigation infrastructure (Flaherty *et al.*, 2000). The rapid establishment of low salinity shrimp farming, into rich farmland of Thailand's rice growing Central Plain, has lead to important social, economic and environmental concerns (Flaherty *et al.*, 2000; 1999; Flaherty and Vandergeest, 1998). It is an important land and water management

challenge due to its potential negative impacts, resulting in an unsustainable aquaculture industry (Flaherty *et al.*, 2000; Dierberg and Kiattisimkul, 1996). In turning part of their fields into shrimp ponds, some rice farmers make more profits. For example, based on the price for small shrimp in 1998, in converting only 1 ha of their rice field into shrimp ponds (yielding 2 crops during the year), rice farmers annual income can be 16 times more than is usual with rice alone (Flaherty et al., 2000). In 1995, there were about 26,145 inland shrimp farms in Thailand, 80% of them being small (less then 1.6 ha, with an average of 3 ponds of around 0.5 ha each) and occupying a total area of approximately 74,942 ha (Patmasiriwat *et al.*, 1998). This explains why "*inventory and monitoring of shrimp farms are essential tools for decision-making on aquaculture development, including regulatory laws, environmental protection and revenue collection*" (Travaglia *et al.*, 1999, p.1). Because of this rapid and continuous development, on July 22, 1998, Prime Minister Chuan Leekpai of the Thai government banned low salinity inland shrimp farming in some areas in order to control and minimise the negative impacts of this growing commercial activity (Flaherty *et al.*, 1999; 2000). It was decided to ban shrimp farming in freshwater areas, while allowing it to continue in areas with brackish water. There is a need to collect regular information for the coastline, and beyond, in order to locate the farms and evaluate their expansion. However, the task of collecting information by ground inventory for the purposes of monitoring this resource and environmental planning is very difficult, time consuming, and therefore expensive. The availability of an accurate and fast methodology for observing remote areas is of significant importance. Satellite remote sensing is potentially an economical solution to this methodological problem.

Between the two types of existing satellite sensors, the passive and the active, the second has many advantages in mapping and monitoring tropical areas such as Thailand. In these zones, it is hard to acquire data regularly with near infrared and visible sensors because of the effects of heavy clouds and haze (Forster, 1996). Synthetic Aperture Radar (SAR) using an active sensor, such as the Canadian satellite RADARSAT-1, has the advantage of being able to penetrate clouds, haze, dust, and darkness. Moreover, radar can also be used in multiple modes (multiple wavelengths, multiple incidence angles, multiple polarizations and multiple antennas), or synergistically with visible and near-infrared data, to furnish additional information (Forster, 1996). The presence of water is readily detected by radar imagery and is usually represented by dark grey or black areas on the images, which can be very useful for distinguishing shrimp ponds from other types of land cover. This explains the advantage of RADARSAT-1 compared to aircraft or optical satellites in viewing the earth under almost any conditions at any time (CSA, 2000). Furthermore, compared with the other satellites, RADARSAT-1 offers a superior frequency of image capture compared with other satellites and allows for a more precise temporal study of the shrimp farms.

The identification of shrimp farms with RADARSAT-1 imagery is an interesting goal. To identify the farms, as water bodies is one thing, but to differentiate the farms from the other water bodies is another. Shrimp farms are of a different shape and size from reservoirs or fish farms, and they are also the only ones to use aerators. In this project, multi-angle and multi-temporal images were used in order to see how RADARSAT-1 had the potential to identify and monitor shrimp farms. A combination of images, with various dates of acquisition, can help in the identification of seasonally variable land cover, and with various incidence angles, can help in the identification of

water bodies as well as the differentiation of vegetation cover. Pre-processing and processing analysis were applied on different image combinations.

1.2 Goal and Objectives of the Study

The goal of this study was to evaluate the potential of multi-temporal, and/or multi-angle, RADARSAT-1 imagery as a tool in monitoring and mapping shrimp farms, as well as other land cover and land use types, present in the Bang Pakong River basin situated in the Central Plain of southeastern Thailand.

The objectives of this project were to:

1. find the best RADARSAT-1 image classification procedure to identify shrimp farms, and other land uses / land covers present on the study area,
    a) selecting from the following image pre-processing techniques:
        - principal component analysis (PCA)
        - speckle filtering
        - texture analysis
    b) selecting from the following image processing techniques:
        - pixel-based classifications:
            -unsupervised classification
            - supervised classification
        - segmentation-based classification
    c) selecting from the following image combinations:
        - multi-temporal images
        - multi-angle images

2. verify if the shrimp farms could be differentiated from other water bodies in a supervised classification,
    a) assessing if polygons grouping pixels representing shrimp ponds only (water and possibly aerators, if detectable by the RADARSAT-1 satellite), could be differentiated from the water class in a resulting classification.
    b) assessing if polygons grouping pixels representing shrimp farm areas (water and dykes surrounding the ponds, if detectable by the RADARSAT-1 satellite), could be differentiated from the water class in a resulting classification.

1.3 Structure of the Thesis

This thesis contains seven chapters. Chapter 2 presents the history, status and trends of shrimp farming in Thailand, also defining the difference between coastal and inland farming. This chapter furthermore, explains the structure and geographic distribution of inland shrimp farms, as well as their major economic, environmental and socio-economic impacts. Chapter 3 concerns remote sensing, SAR data, and the potential of RADARSAT-1 as a tool to monitor shrimp farming in Thailand. Descriptions of the study area, the data source, as well as the field methodology, are presented in Chapter 4. The methodology of the image pre-processing and processing analysis is described in Chapter 5. In this chapter, every image analysis procedure, used in Chapter 6 to obtain a classification with great accuracy in results, is defined based on a literature review. Chapter 6 evaluates RADARSAT-1 as a tool for monitoring and mapping shrimp farms and other land cover / land use present in the study area. Chapter 7 presents the final

conclusions of the analysis in relation to this thesis goal and the objectives outlined in Chapter 1.

CHAPTER TWO

SHRIMP FARMING IN THAILAND

2.1 History, Status and Trends

The culture of fish and other aquatic species in Asia has a long history. The first descriptions of pond culture were recorded in China during the 12th century B.C.. However, marine shrimp culture started later. By the 15th century A.D., marine shrimp culture often occurred on a large scale in Indonesia in brackish water (mix of fresh and seawater) ponds (Menasveta and Fast, 1998). In Thailand, extensive shrimp farming started in Rayong and Chanthaburi, two coastal provinces situated east of Bangkok, around 1935 (Huitric *et al*, 2002; Patmasiriwat, 1998; Flaherty and Karnjanakesorn, 1995). Shrimp farming in brackish water evolved from extensive, to semi intensive, and finally to intensive systems in order to increase profit. However, intensive coastal systems have contributed to the loss of mangrove forest leading to habitat loss for aquatic species, as well as contamination of coastal water with nutrients from the shrimp ponds and intrusion of salt water into rice paddies (Flaherty and Vandergeest, 1999). Approximately 10 years ago in Thailand, inland shrimp farmers began to grow black tiger shrimp using a low-salinity system. According to a convention established in the literature, the term "prawn" is used for freshwater species and "shrimp" for others, particularly marine ones (Flaherty and Vandergeest, 1998; Pillay, 1990). This section will review the rapid evolution of shrimp farming in Thailand, from extensive coastal aquaculture to intensive inland low-salinity farming, that has brought with it many concerns about its economical,

environmental and social impacts. These concerns will be discussed in sections 2.3, 2.4 and 2.5.

2.1.1 Coastal aquaculture

Originally, Thai shrimp culture was practiced in coastal areas, using seawater flooding to trap shrimp larvae and adults (Dierberg and Kiattisimkul, 1996). This method did not need any water exchange, food was only natural, the stocking density was low (natural), as well as the yield (Dierberg and Kiattisimkul, 1996). Open extensive shrimp farming first occurred in the 1935, in the provinces south of Bangkok, in the upper Gulf of Thailand (Dierberg and Kiattisimkul, 1996). This traditional technique used tidal flats (low elevation areas) and mangrove forest, converted into trapping ponds (8 to 16 ha each), to capture wild shrimp and then raise them in these brackish water areas (FAO/SEAFDEC, 1997). The shrimp were principally grown for domestic consumption but also to sell at the local market (Huitric *et al.*, 2002). This traditional approach to farming used basic technologies, with construction and operating costs being low, and not requiring any special technical or management skills. Tides naturally exchanged the water in the pond (5 to 10% of daily water exchange), keeping it clean and decreasing the chance of disease, only natural food was used and the stocking density, as well as the yield, were low (Lebel *et al.,* 2002; Dierberg and Kiattisimkul, 1996; Flaherty and Karnjanakesorn, 1995). In 1947, the price of salt fell considerably, leading to a major expansion in extensive shrimp farming in the coastal provinces (Samut Songkhram, Samut Sakhon and Samut Prakarn) situated south of Bangkok (Flaherty and Karnjanakesorn, 1995). Many small-scale salt producers converted their salt fields to shrimp ponds so as to increase profits (Flaherty and Karnjanakesorn, 1995). Because of

the high soil salinity, rice farmers situated in mangrove areas with low yields were harvesting shrimp during low tide periods, for domestic consumption and to augment their incomes (Flaherty and Karnjanakesorn, 1995). Gradually, more farmers permanently changed their rice fields into extensive shrimp farms. With its tropical climate allowing year round cultivation and 2,600km of largely undeveloped coastline, Thailand was a favourable environment for promoting extensive coastal shrimp farming, but also later semi-intensive and intensive coastal farming (Flaherty et al., 1999).

In 1973, semi-intensive shrimp farming, requiring less area (3 to 5 ha for each pond) but more daily water exchange (5 to 40%), started to be promoted by the Thai Department of Fisheries (DFO) (Dierberg and Kiattisimkul, 1996; Flaherty and Karnjanakesorn, 1995). Because of high consumer demand and consequently high prices for shrimp, farmers increased their productivity (Menasveta and Fast, 1998). Semi-intensive farming required more work and additional technology. As mentioned by Flaherty and Karnjanakesorn (1995, p. 29), "*semi-intensive marine shrimp culture requires supplementary feeding in addition to the natural food in the ponds because of higher stocking densities*", resulting in yields two to three times higher than with extensive systems (Dierberg and Kiattisimkul, 1996). Also, the young shrimp were no longer wild, but provided by hatcheries belonging to the Department of Fisheries (Flaherty and Karnjanakesorn, 1995). Black tiger shrimp (*Penaeus monodon*) was preferred as it matures quickly and grows large in size when raised in ponds (Figure 2.1).

Figure 2.1 Black tiger shrimp (Penaeus monodon)

Until 1984, 90% of the shrimp production was harvested in coastal natural environments for the most part in the Gulf of Thailand (Lavallee, 1996). Extensive and semi-intensive shrimp farming needed to be on the coast, in tidal areas, leading to the destruction of mangrove forest. The result being that 55% of the mangrove forests have been cut down between 1961 and 1993 because of these farming techniques (Menasveta, 1996).

Between 1981 and 1993, cultured shrimp production increased from 10,729 tonnes to 225,514 tonnes with the intensification of the farms around 1986, and the captured shrimp production decrease from 122,706 tonnes to 100,000 tonnes (Table 2.1 and Figure 2.2).

Table 2.1. Captured and cultured shrimp production and areas involved in Thailand, 1981 to 1997 (Royal Thai Department of Fisheries (1997), Customs Department and Department of Business Economics).

Year	Production By capture (Tonnes)	Production By culture (Tonnes)	Total Production (Tonnes)	Shrimp Culture area (ha)	Number of Farms
1981	122 706	10 729	133 435	27 459	3 657
1982	156 523	10 091	166 614	30 792	3 943
1983	127 584	11 550	139 134	35 537	4 327
1984	104 394	13 007	117 401	36 792	4 519
1985	91 632	15 840	107 472	40 769	4 939
1986	102 227	17 886	120 113	45 368	5 534
1987	128 100	23 566	151 666	44 770	5 899
1988	110 200	55 633	165 833	54 778	10 246
1989	110 800	93 495	204 295	71 166	12 545
1990	107 400	118 227	225 627	64 606	15 072
1991	129 10	162 070	291 170	75 332	18 998
1992	116 800	184 884	301 684	72 796	19 403
1993	100 000	225 514	325 514	71 887	20 027
1994	N/A	263 446	N/A	73 247	22 198
1995	N/A	259 541	N/A	74 942	26 145
1996	N/A	259 541	N/A	N/A	N/A
1997	N/A	258 000	N/A	N/A	N/A

Intensive shrimp farming in Thailand was first established in the early 1980's in the provinces of Samut Sakhon, Samut Prakan, Samut Songkhram, Chachoengsao, Phetchaburi and Bangkok located in the upper Gulf of Thailand (Huitric *et al.*, 2002; Flaherty and Karnjanakesorn, 1995). Intensive shrimp farms were open ponds (less than 1 ha each) requiring more capital as well as greater technical skills. These systems necessitated daily water exchange of 30 to 40% and water quality control using pumps, aerators and filters due to high stoking densities and high diet feeding resulting in yields that were three to four times greater than semi-intensive systems (Flaherty et al., 1999; Dierberg and Kiattisimkul, 1996; Flaherty and Karnjanakesorn, 1995).

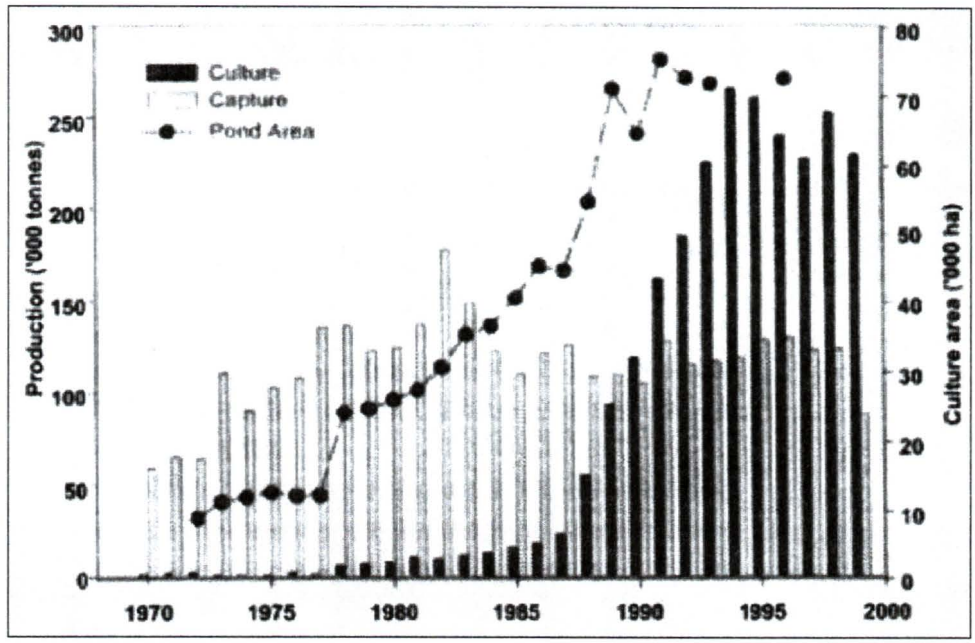

Figure 2.2 Growth of the shrimp aquaculture industry in Thailand from 1970 to 2000. Production of shrimp in tones from aquaculture is shown as black solid bars, and from capture is shown as white solid bars. Pond areas are shown as dashed line (Lebel et al., 2002, p312; Thai Department of Fisheries, FAO, 2000)

With this technique, ponds needed to be situated along the coast because of the large amounts of salt water needed for water exchange during the grow-out period (Flaherty et al., 2000; Flaherty and Vandergeest, 1995). In the late 80s, as mentioned by Flaherty *et al.*, (2000, p.174), "*... the lack of suitable sites remaining along the coast, increased monitoring of mangroves forests by Thai government agencies and NGOs, and sharp increases in land values due to competition with other coastal land uses*", limited the operations of coastal farmers. Because of this situation, and also concerned about the risk of pollutant and disease intrusion into their farms, farmers developed more "closed" ponds, surrounded by mud dykes, in order not to operate directly on the coast (Flaherty et al., 2000). These first "closed" intensive systems needed less daily water exchange and the farmers used mechanical water pumps to fill the ponds with salt water, as well as to exchange the water (Flaherty et al., 2000). In order to operate, farmers needed to have

access to an adequate water supply and drainage, as well as special facilities such as storage sheds and refrigeration units. Closed systems lead to the development of a new low-salinity shrimp culture technique, where direct access to the ocean was no longer necessary (Flaherty et al., 2000).

2.1.2 Inland Shrimp Farming

Thai shrimp farmers recently adopted a low-salinity system, using trucks to transport the saltwater or saltpan water further inland, as an alternative method of intense cultivation (Flaherty *et al*, 1999; Flaherty and Vandergeest, 1995). Initially, low salinity farms were situated next to the main river estuaries in the upper part of the Gulf of Thailand. (Bang Pakong, Chao Praya, Tha Chin and Mae Khlong). Intrusion of salt water into these rivers promoted the development of shrimp farming (Flaherty *et al.,* 1999; 2000). However, the subsequent removal of salt water by the heavy rains of the wet season also limited farming to a seasonal activity. Experimentation demonstrated that black tiger shrimp (*Penaeus monodon*) could be effectively grown in very low salinity conditions, if the newly hatched larvae were properly acclimated to a low salinity environment (Lebel *et al.,* 2002; Flaherty *et al.*, 2000). The acclimation of the shrimp starts in early post larval stages, for a period of three to five days, the salinity level of the tanks are slowly reduced by adding fresh water (Flaherty *et al.*, 2000). *Penaeus monodon* is the most successful species to grow in a low salinity system because it tolerates large variations of temperature and salinity (Flaherty et al., 2000; Laubier, 1990). The development of this system in the hatcheries allowed the farmers to successfully grow farm-raised shrimp further and further from the coast, in any place where there was a source of fresh water (Flaherty et al., 2000).

Rice farmers found that it was possible and profitable to grow shrimp in their rice fields, and this conversion promoted the establishment of shrimp farms much further from the coast than previously encountered (Flaherty and Karnjanakesorn, 1995). Most of the shrimp farmers have very little aquaculture knowledge or experience and they generally copy the infrastructure and techniques of their neighbours, resulting in a potential misuse of materials and products (Flaherty *et al.*, 2000).

According to Flaherty et al. (2000), it is difficult to evaluate the impact of low salinity inland shrimp farms because data from Thailand's Department of Fisheries do not identify if the shrimp are the result of coastal or an inland production. However, they suggested that probably 30-40% of the total output of the country was the result of black tiger shrimp grown in low salinity conditions in intensive inland farms (Flaherty *et al.*, 2000).

2.2 Geographic Distribution and Structure of Inland Shrimp Farms

The first provinces where the intensive shrimp farming industry took hold were situated around the upper Gulf of Thailand: Samut Sakhon, Samut Prakan, Samut Songkhram, Chachoengsao, Phetchaburi and Bangkok (Figure 2.3).

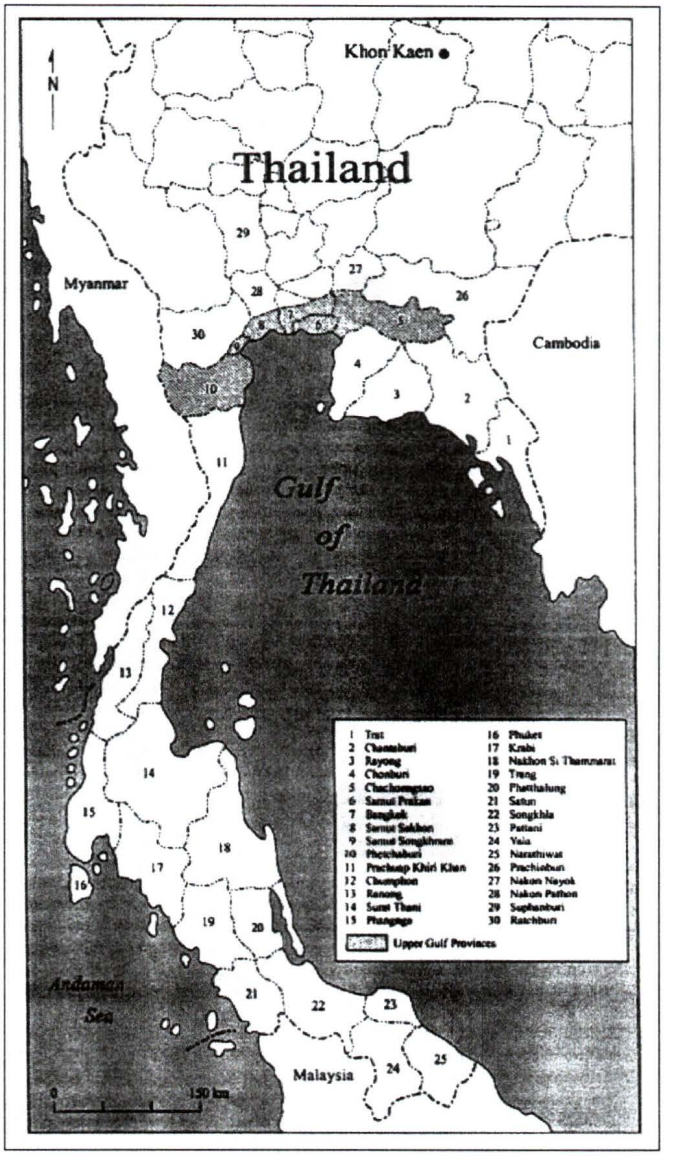

Figure 2.3 Thailand's first provinces using intensive shrimp farming techniques. (Flaherty and Vandergeest, 1998, p.819)

Currently, a large number of rice farmers have adopted low-salinity culture systems in order to generate higher incomes. This explains why a greater number of shrimp farms are being established further from the coast, into the rich farmland of Thailand's rice growing Central Plain (Flaherty and Karnjanakesorn, 1995). According to Miller *et al.* (1999) and Arbhabhirama *et al.* (1988), inland shrimp farmers of the Central and Eastern Thailand can harvest between one and three crops per year, depending on

crop prices and diseases. Except for the wet season, approximately from June until October, crops can be grown at any time of the year. During the wet season, it becomes very difficult to control the salinity of the ponds, and therefore, most farmers avoid this period. The growth cycle is approximately 100-120 days. Although, before putting a new crop in, the farmers need to clean the pond and this can take from a week to a month. Usually, the first crop is put into the pond in December, during the cool and dry season, and harvested in the hot season, March/April approximately. The second crop can be raised from April/May to August. In limiting the time of the cleaning period of both ponds, farmers can try to grow a third pond during the wet season, from around August to November. (Miller *et al.*, 1999; Arbhabhirama *et al.*, 1988).

The size of the inland shrimp farms is usually very small, typically a couple of ponds, each having a typical size of 0.64ha (6,400m², so around 80mX80m) (Flaherty et al., 2000). The ponds are separated from each other by a thick wall of soil called a dyke. The dyke's thickness can vary from 0.5 meter to several meters, and its elevation above the water is at most 1 meter (Travaglia et al., 1999). What differentiates shrimp farms from other water bodies is their size, shape and organisation. Firstly, they are smaller than water reservoirs and fishponds; secondly, each pond has the same rectangular form; finally, there are always many ponds situated right beside each other, separated by dykes. A water reservoir, or a canal, is also located next to the ponds. Another difference with other water bodies is that intensive shrimp farmers have to equip each pond with an aerator system to oxygenate the water (Figure 2.4.).

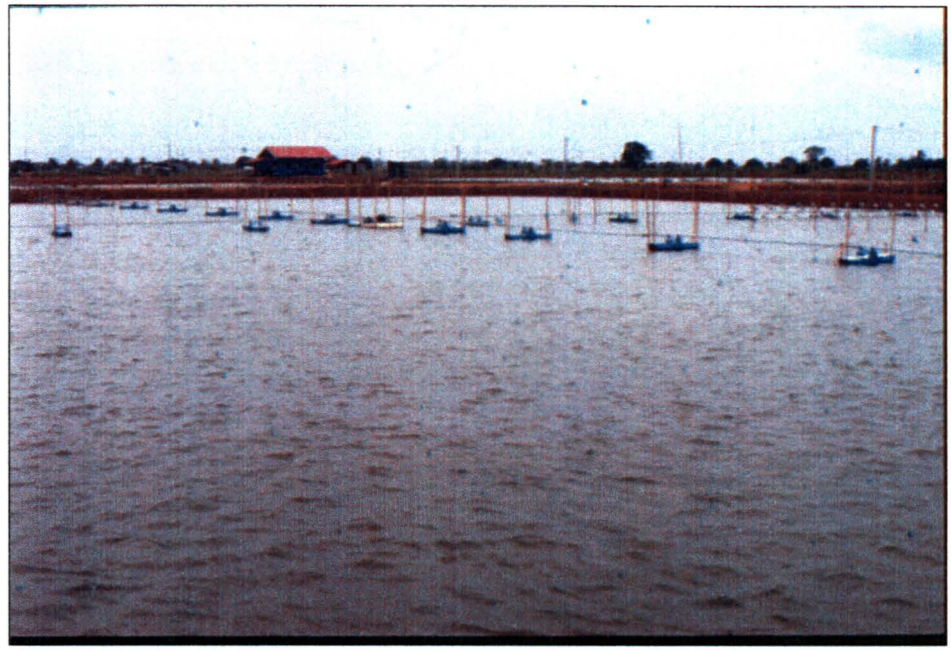

Figure 2.4 Inland shrimp farm in the province of Chachoengsao, Thailand

2.3 Economic Impacts

Among all the seafood available on the market, shrimp is the one that has the highest economic value, and the species with the greatest global production is the black tiger shrimp (Flaherty and Vandergeest, 1998; Flaherty and Karnjanakesorn, 1995). In 1998, total world production of farm-raised shrimp was 737,000 tonnes estimated to be worth US$ 6 billion (Flaherty et al, 2000), an increase of over 400% compared with 1983 total world production of approximately 147,000 tonnes (Anderson and Fong, 1997). The world largest producing and exporting countries are situated in South Asia, growing black tiger shrimp (*Penaeus monodon*), and in South America, growing western white shrimp (*Penaeus vannemei*) (Flaherty *et al.*, 2000; Flaherty and Karnjanakesorn, 1995). Most of the farmed shrimp are raised in tropical regions because of the climatic advantages and lowest operating costs (Flaherty and Karnjanakesorn, 1995). For more than a decade,

Ecuador has been the most important producer and exporter of farm-raised shrimp in the Western Hemisphere, but significant industries also exist in Mexico, Honduras, and Colombia (Anderson and Fong, 1997). In the Eastern Hemisphere, , since 1991, Thailand has become the leader among the other large South Asian producing countries, including Indonesia and India (Flaherty *et al.*, 2000; Anderson and Fong, 1997). China, Vietnam, Bangladesh, Taiwan and the Philippines have also contributed significantly to the world production of farm-raised shrimp (Anderson and Fong, 1997).

According to Flaherty *et al.* (2000), a successful yield for an inland shrimp farm is between 4 and 5 tonnes per ha per crop. Thai farmers usually growth 2 crops per year. The price of the shrimp is size dependent; the larger they are, the better the price. Average income, per ha per crop, for an inland shrimp farm is approximately US$ 32,000 (Flaherty *et al.*, 2000; Patmasiriwat *et al.*, 1998). After deducting all the variable and fixed costs the farmers have to cover, they clear a profit of from 17% to 26%. An income that varies between US$ 5,440 and US$ 8,320 is considerably greater than anything they could earn from rice. (Patmasiriwat *et al.*, 1998). In 1997, Thailand produced 258,000 tonnes of *Penaeus monodon* and exported 212,868 tonnes. The value of the merchandise was 75,959 baht, equivalent of US$ 1,899 million (Patmasiriwat *et al.*, 1998).

Developed countries, such as the United States, Japan and some countries in Western Europe, constitute the principal world markets (Aquasol, 2002b; Patmasiriwat *et al.*, 1998; Khor, 1995; FAO, 1990). However, some of them also raise a small number of shrimp, using high technology techniques but their small yields are not comparable to those of most tropical countries.

Because of its prominent place in the aquaculture economy, inland shrimp farming in Thailand needs to be managed in a sustainable way. Non-existent or incorrect

management of land use can lead to environmental damage. Most of the farms are run by small-scale producers who are interested in maximum profits, but usually have very little knowledge of sustainable management (Flaherty *et al,* 2000; Patmasiriwat *et al.*, 1998). In order to achieve their goals, farmers use many chemicals and fertilisers to make the shrimp grow bigger faster and reduce the chance of disease. However, these substances only produce short-term profits because their intrusion into the surrounding environment leads to its deterioration and abandonment after a couple years (Flaherty *et al.,* 1999). According to Flaherty *et al.* (1999), most of intensive inland shrimp farmers discharge nutrients (waste and fecal matter, uneaten food and inorganic fertilizers) directly into irrigation canals. Farmers owning rice fields and orchards surrounding shrimp farm areas are very concerned about the possible negative impacts caused by discharge of untreated wastewater and salinity intrusion into their paddies, generating land-use conflict between the two types of farmers (Lebel *et al.,* 2002; Flaherty *et al.*, 1999). As explained by Lebel *et al.* (2002, p.319), "*... as a result of media coverage, the National Environment Board recommended in June 1998 a complete ban on inland shrimp farming in freshwater areas of 10 central plain provinces*". However, the shrimp farmers protested saying that the Department of Fisheries promoted it. Finally, the National Environment Board officially banned the activity and allowed 120 days for the farmers to harvest their last crop. The conflict continues today because of the "*... inability to enforce and regulate the ban*" (Lebel et al., 2002, p.319). Strict regulations concerning the techniques used by the farmers, as well as regular and accurate investigation methods evaluating the farm operations need to be established, in order to control the growth of the industry and its environmental and social impacts.

2.4 Environmental Impacts

The rapidly growing shrimp farming industry in Thailand has had a very significant environmental impact. Coastal shrimp farming involves the destruction of mangrove forests and other coastal wetlands, as well as a greater presence of pollution and algae in coastal waters (Huitric *et al.*, 2002). It can also lead to an over-exploitation of wild stocks, the destruction of natural seed resources, and the introduction of non-native species. In Thailand, the growth of shrimp cultivation has consumed a large portion of coastal land. In 1961 the area under mangrove forest in Thailand was estimated to be around 370,000 ha, but since then, 50% of it has been destroyed as a result of shrimp farming (Patmasiriwat, 1998; Menasveta, 1996; Primavera, 1994). Between 1981 and 1995, the total land area used for shrimp farming increased from 27,459 ha to almost 75,000 ha (table 2.1), at the cost of rice paddies, mangrove forests and other types of coastal land use (Royal Thai Department of Fisheries, 1997).

According to many researchers (Menasveta and Fast, 1998; Patmasiriwat *et al.*, 1998; FAO, 1997; Menasveta, 1996) the intensification of shrimp farming, if done properly in appropriate areas with suitable systems, can prevent environmental and resource management problems. Indeed, extensive systems require very large areas of land and water close to the ocean, contributing to the degradation and even destruction of natural habitats such as mangrove forests, compared to intensive farms that can be established further inland in smaller areas producing better yields (FAO, 1997). However, if the intensification of coastal or inland farms is not done correctly, for instance through the abusive and incorrect use of chemicals, it leads to environmental degradation such as

deterioration of the water quality and acidification of the soil (Flaherty *et al.*, 2000; Menasveta and Fast, 1998; Patmasiriwat *et al.*, 1998).

Examples of negative environmental impacts caused by intensive inland shrimp farming are: sediment deposit, saltwater intrusion, and abandoned shrimp farms (Patmasiriwat *et al.*, 1998; Dierberg and Kiattisimkul, 1996). The chemicals used by the farmers at various stages of the culture, such as nutrients (nitrogen and phosphorus), antibiotics and other drugs, can all have negative impacts on the surrounding environment (Flaherty *et al.*, 2000; Patmasiriwat *et al.*, 1998). Water pollution can occur during the three different crop stages: the culturing stage, the harvesting stage and the pond preparation stage. According to Patmasiriwat *et al.* (1998), it is during the culturing stage that the environmental impacts are lowest, and during the pond preparation stage that the impacts are most detrimental. At this stage, the farmers clean the bottoms of the ponds to remove the pond mud and sediments from the previous crop cycle. These sediments have very high concentrations of toxic organic and inorganic substances. Many of the small farmers do not have space for these dangerous residues so they dispose of them in public canals, streams or other areas situated close to their farms. (Patmasiriwat *et al.*, 1998).

The real negative environmental impacts of intensive inland shrimp farming are not very well known as yet since this type of aquaculture is still too recent. Nevertheless, according to Lebel *et al.* (2002, p320) and Flaherty *et al.* (1999), water and soil pollution from inland farms is greater than from coastal ones, because of the "*difference in volumes of water available for exchange and dilution of organic and salinity loadings*". The consumption of freshwater by inland shrimp farmers is the same as that used by rice farmers for the irrigation of their fields (Lebel et al., 202; Braaten and Flaherty, 2000).

Also, rice farmers and orchardists using the same public canals as shrimp farmers can suffer the consequences of this major amount of polluted freshwater (Lebel *et al.*, 2002).

2.5 Socio-Economic Impacts

Intensive inland shrimp farming has produced an economic boom in various regions of Thailand. Indeed, this type of aquaculture generates higher benefits than do rice paddies or fish farms in the shorter term. However, it may cause very important long-term unfavourable socio-economic and environmental impacts because of its unsustainability. (Flaherty *et al.*, 2000; Patmasiriwat, 1998). The majority of the farms are run by small-scale farmers who are not educated in management techniques, environmental sustainability, and economic sustainability. For example, Flaherty *et al.*, (2000) mentioned that many farmers use higher than advisable production densities resulting in disease due to overpopulation. In these cases, farmers can lose their whole yield and since they do not know how to manage their aquaculture, they are forced eventually to abandon their land because the soil and the water are too polluted for future use.

In rural communities, low-salinity shrimp farming improved the health and prosperity of the people by promoting their employment and direct participation in the economy. Nevertheless, because of all the negative impacts of the industry on the environment, low-salinity farming results in more marginalization and exclusion (Flaherty *et al.,* 1999). As explained by Flaherty *et al.* (1999, p.2056), "*the underlying conditions of low-incomes for rice farming households, indebtedness, limited off-farm employment opportunities, and the high profit potential associated with shrimp farming*", increase the pressure on farmers to choose short-term exploitation because of its higher

profits instead of the long-term benefits, even if most of the time small-scale farmers do not have the necessary skills to operate an intensive production properly (Patmasiriwat, 1998).

Shrimp farming was banned in freshwater areas in 1998. However, is this enough to stop the water and soil destruction of the Central Plain of Thailand? According to Flaherty *et al.* (1999, p.2057), many factors contribute to an inevitable disaster: "*constructions of ponds without regard to surrounding land uses or competing water requirements, rudimentary ponds design, lack of effluent treatment, and limited technical skills of new farm operators*". Even if it seems to be a very long and hard task, it is possible to render this industry sustainable. The support of international and local NGOs, as well as environmental activists, is paramount (Flaherty *et al.,* 1999 and Flaherty and Vandergeest, 1998). Already, in 1998, a *Code of Conduct for Responsible Fisheries* was published by the Food and Agriculture Organization (FAO, 1998) in order to help Thai aquaculture management. Also in 2000, the Thai government hosted a conference organized by NACA (Network of Aquaculture Centres in Asia-Pacific) and FAO on policy-making and planning for sustainable aquaculture (NACA/FAO, 2000; NACA, 1994). These groups, with their conferences and reports, put pressure on the Thai government and show the importance of a sustainable administration of aquaculture in general, but also low-salinity shrimp farming in particular. This industry can be very profitable if well supervised. Organizations need to inform and train small-scale farmers who commonly do not possess the knowledge to run intensive farming activities. The government needs to monitor shrimp farms and all reliable pertinent information about them in order to manage this growing industry properly and help it to become sustainable economically, environmentally and socio-economically.

2.6 Summary

In 1991, Thailand's share of the world's export shrimp market was 20%, and since then it has been considered the world's largest producer of black tiger shrimp. In 1994, 85% of the shrimp production was from intensive farms, 10% from semi-intensive and 5% from extensive ones (Patmasiriwat, 1998; Menasveta, 1996). Thailand produced a total of 258,000 tonnes cultured shrimp in 1997 (Table 2.1). The introduction of intensive low-salinity culture systems, using trucked salt water, totally changed the industry creating the expansion of inland shrimp farming in freshwater environments (Flaherty and Vandergeest, 1998). Many factors encouraged the establishment of ponds away from the coast; the rise of the coastal land prices, because of the tourism industry and industrial developments, but also the better profits that rice farmers could make in converting their paddies into shrimp ponds (Flaherty *et al.*, 1999). Nevertheless, farmers who use this new intensive low-salinity technique should be aware of how to manage it in order to not cause major negative environmental, social and economic effects. If the Thai shrimp industry does not effectively manage these challenges, northern consumer movements, concerned for their own health and that of the environment, could also put serious pressure on it and compromise the future of the industry. (Patmasiriwat, 1998).

CHAPTER THREE

POTENTIAL OF REMOTE SENSING AS A TOOL IN MONITORING SHRIMP FARMING

3.1 Remote Sensing

Remote sensing is the science of detecting and classifying objects, areas, or phenomena, as well as obtaining information on their physical properties, through the analyses of data acquired by a sensor that is not in direct contact with the target of the investigation (CCRS, 2002; Okamoto, 2001; Ritchie and Rango, 1996). The greatest advantage of remote sensing systems, particularly those on satellites, is to provide an augmented view of spatial and temporal variability of the earth system and the effect of humans on it, which can not be identified by any other conventional measuring techniques (Schowengerdt, 1997).

There are two types of satellite sensors (Short, 1999a). A passive sensor, such as that used by optical satellites, needs energy from an external source like the sun. With this type of sensor, the spectral reflectance characteristics of the earth surface (the pigmentation present in the vegetation, the sediment load, the biochemical properties of water, etc) can be studied (Forster, 1996). The active sensor, used by radar (acronym for *Radio Detection And Ranging*) generates its energy from within the sensor system (Sabins, 1997; Lillesand and Kiefer, 1987). The sensor sends a ray to the earth surface and the fraction that returns to the sensor is measured (Short, 1999b, Bonn and Rochon, 1996, p.209). Radar sensors use the microwave part of the electromagnetic spectrum (Sabins, 1997). Microwave imagery is captured with long-wavelength microwave energy

(Steinberg, 1991). Remote sensing using microwaves is related to two major factors: the moisture content of the objects studied and their physical geometry. Usually, as mentioned by Forster (1996), research using microwave remote sensing is concerned with the effects of the terrain, the roughness of the surface, the moisture content of the surface or volume and the sensitivity of earth surface features to polarisation differences, wavelength differences and differences in look angle.

3.2 SAR data

SAR, Synthetic Aperture Radar, is an active radar sensor producing imagery of the earth's surface in almost all weather conditions (it can penetrate cloud cover, haze, smoke and dust) at all times (in darkness), by generating its own illumination of the scene to be viewed (CCRS, 2002; CSA, 2000). In order to generate high-resolution remote sensing imagery, the SAR system uses a short antenna (15m long by 1.5m wide) and simulates the utilization of a larger antenna by combining the signals received by the radar as it moves along its flight track (CCRS, 2002; CSA, 2000; Ghedira, 2000). This system energy is transmitted in microwave frequencies on the electromagnetic spectrum (Henderson and Lewis, 1998; Raney, 1998; Forster, 1996). The images produced are monochrome (black and white), and usually only one data set is used at any time (each image only has 1 band). However, it is possible to generate a false-colour multitemporal image when superimposing multiple images of the same scene taken at different times.

As mentioned by Ghedira (2000), radar operates based on three principles. First, it emits a microwave signal (energy) to a scene. Second, the signal interacts with the scene and a part of the energy is reflected back towards the radar antenna (backscattering phenomena). Third, the radar measures the intensity as well as the delay (time it takes to

the signal to return to the antenna) of the signal. As shown on Figure 3.1, the roughness and geometry characteristics of the surface define how the signal is reflected. However, only the signal that is reflected back towards the radar antenna is recorded (Lillesand and Kiefer, 1987).

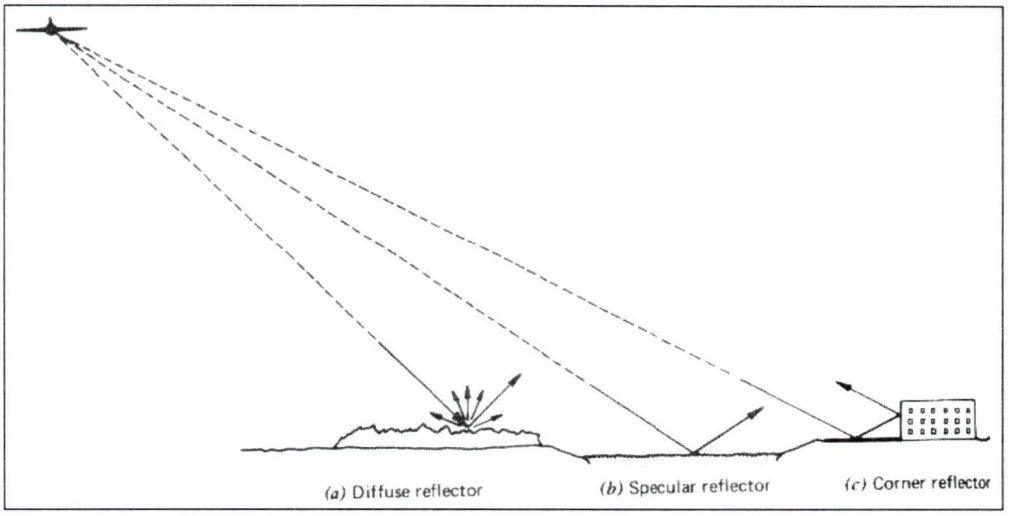

Figure 3.1 Radar reflection from various surfaces (Lillesand and Kiefer, 1987, p.496)

A rough surface, such as trees, will act as a diffuse reflector. On the resulting image, these rough surfaces will usually have a confused noncoherent backscatter pattern, like orchard plantations. Fruit trees are relatively heterogeneous reflectors. Surfaces considered as smooth, like calm water, will act as a specular reflector and result in very dark areas on the image because most of the signal is reflected away. Finally, a corner reflector, such as a building, will produce a very high response to the sensor. A double reflection produced by the adjacent smooth surface of the corner structure will send the signal back to the sensor, creating very bright pixels on the image.

Two other factors can determinate the intensity of the signal that will be returned to the sensor (Lillesand and Kiefer, 1987). These components are the electrical

characteristics of the features, as well as the slope of the surface. Regarding the electrical characteristics of features, a material having a high dielectric constant, for example moist vegetation or a wet surface, augments the reflectivity of the signal back towards the sensor and diminishes the penetration of the wave into the ground (Fung and Ulaby, 1983; Simonett and Davis, 1983). The dielectric constant is the "*electrical property of matter that influences radar returns*" (CCRS, 2002). Conversely, with a dry soil the penetration of the wave into the material will be higher and the reflectivity of the signal towards the sensor will be lower (Simonett and Davis, 1983). Also, as mentioned by Sabins (1997) and Simonett and Davis (1983), backscattered signals react differently to a horizontal or inclined surface. For flat surfaces, the backscattered signal is very low, and for a slope facing the sensor, the backscattering signal is very high (Lillesand and Kiefer, 1978).

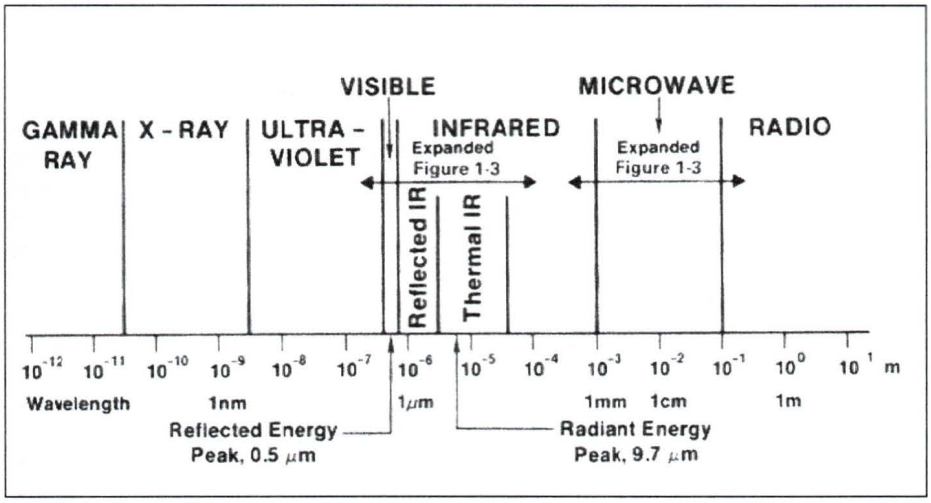

Figure 3.2 Electromagnetic spectrum (Sabins, 1997, p.4).

Because they are active energy sensors and provide their own imaging, SAR systems can acquire data at any time in any conditions (CSA, 2000). Also, radar wavelengths (microwave frequencies) are longer than the visible and infrared ones,

allowing this system to acquire images through clouds, fog and dust (CSA, 2000; Sabins, 1997) (Figure 3.2 and 3.3).

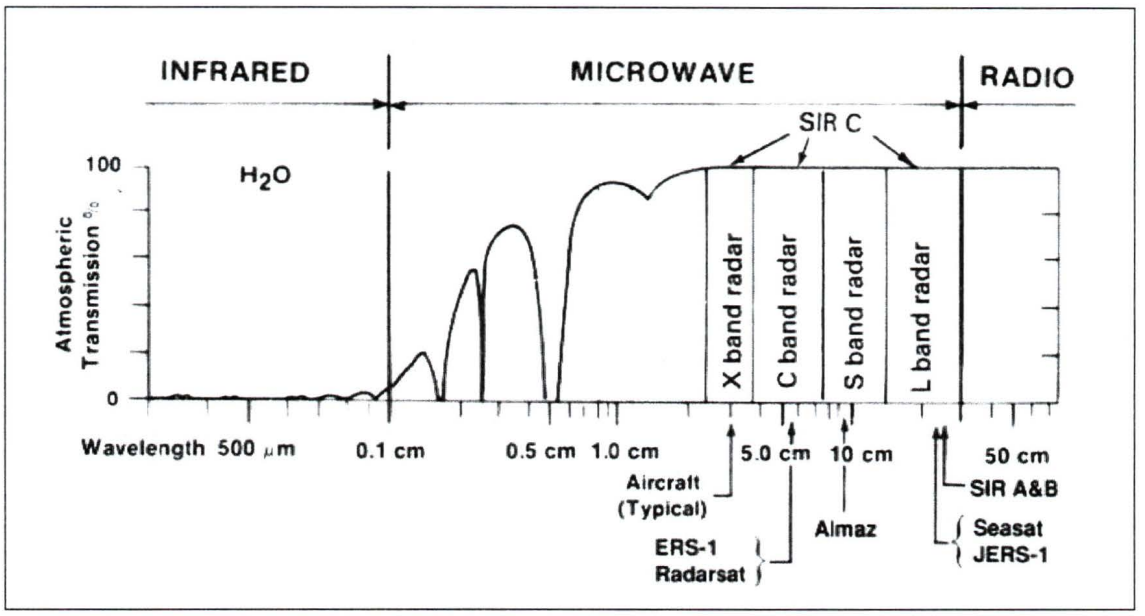

Figure 3.3 Expanded diagram of the microwave regions for transmission through the atmosphere (Sabins, 1997, p.5)

The RADARSAT-1 satellite, carrying a SAR system, was launched on Nov. 4, 1995 by the Canadian Space Agency (Figure 3.4). The Canada Centre for Remote Sensing (2002) describes RADARSAT-1 as an "*advanced Earth observation satellite project developed by Canada to monitor environmental change and to support resource sustainability*". This satellite was developed to provide a total coverage of the earth. It covers the Arctic (North of 70 degrees N) every day, areas situated North of 48 degrees N every four days (Canada every three days, depending on the swath selected) and equatorial latitudes (North of 80 degrees S) every 6 days (CSA, 2000). Compared to the other satellites, RADARSAT-1 offers superior regularity of image capture, circling the earth 14 times a day and repeating its orbit path every 24 days (CSA, 2000).

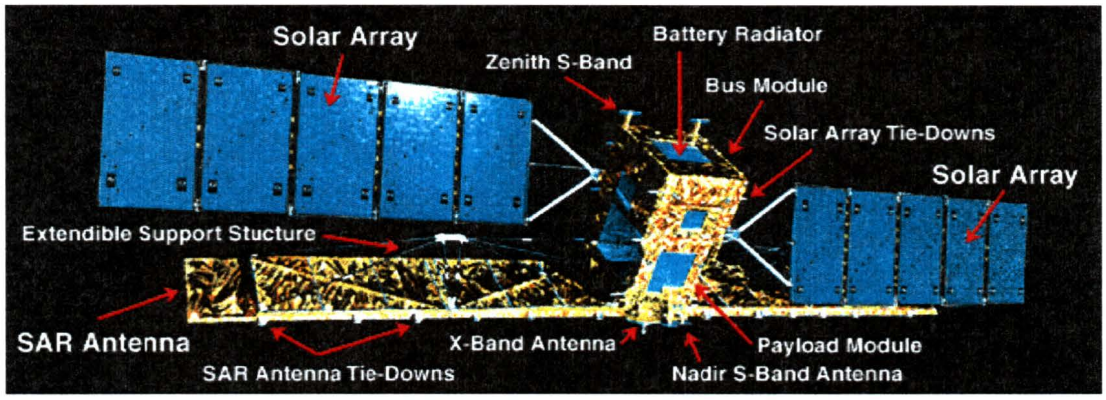

Figure 3.4 RADARSAT-1 characteristics (CSA, 2000)

RADARSAT-1 can be operated in 7 beam modes (swaths) with a beam selection of nominal areas (image size) from 50 to 500 kilometres and resolutions from 8 to 100 metres. The incidence angles of the satellite range from 20 degrees to more than 50 degrees (Figure 3.5 and Table 3.1).

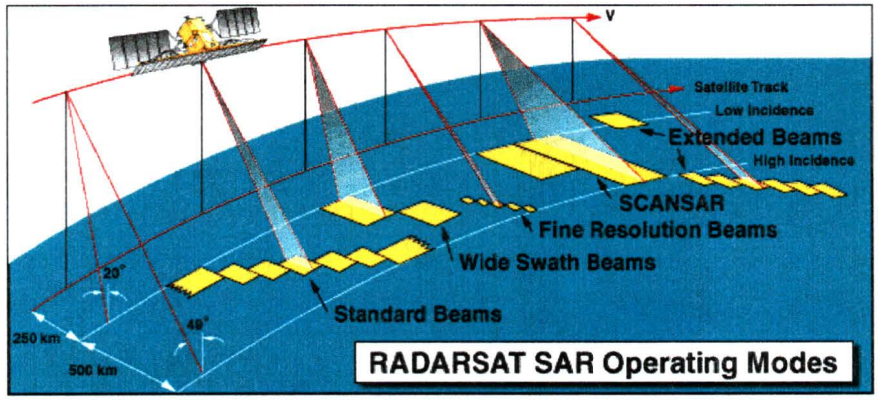

Figure 3.5 RADARSAT-1 beam modes (CSA, 2000)

Each RADARSAT-1 beam mode image can differentiate specific types of land cover because of its various resolutions and incidence angles. These characteristics of the satellite allow a large range of image acquisition, providing users with a great flexibility in interpretation (CCRS, 2002). This explains the advantage of using RADARSAT-1 instead of other SAR satellites, which can only acquire images in one mode with a

specific incidence angle and swath (Costa, 2000). In this project, only images taken with the fine beam mode have been used. Two were in fine 4, two in fine 1 and one in fine 5 (Table 3.1).

Table 3.1. RADARSAT-1 beam mode characteristics (CSA, 2000)

Beam Mode	Beam Position	Incidence Angle Range (°)	Approximate Resolution (m)	Nominal Area (km)
Fine	***F1***	***36.9-40.1***	***8 x 8***	***50 x 50***
	F2	39.2-42.3		
	F3	41.6-44.2		
	F4	***43.6-46.0***		
	F5	***45.3-47.8***		
Standard	S1	20-27	25 x 25	100 x 100
	S2	24-31		
	S3	30-37		
	S4	34-40		
	S5	36-42		
	S6	41-46		
	S7	45-49		
Wide	W1	20-31	30 x 30	165 x 165
	W2	31-39		150 x 150
	W3 (for tape recorded)	39-45		138 x 150
ScanSAR Narrow	SN1	20-40	50 x 50	300 x 300
	SN2	31-46		
ScanSAR Wide	SW1	20-49	100 x 100	500 x 500
Extended High	H1	49-52	25 x 25	75 x 75
	H2	50-53		
	H3	52-55		
	H4	54-57		
	H5	56-58		
	H6	57-59		
Extended Low	L1	10-23	35 x 35	170 x 170

3.2.1 Wavelength

A radar wave can either be reported in wavelength (cm) or in frequency (GHz). There are six different radar bands, each with a different wavelength and frequency (Table 3.2).

Table 3.2 Radar wavelengths and frequencies used in remote sensing (Sabins, 1997, p.180)

Band Designation	Wavelength (λ), cm	Frequency (ν), GHz
K	0.8 to 2.4	40.0 to 12.5
X	2.4 to 3.8	12.5 to 8.0
C	3.8 to 7.5	8.0 to 4.0
S	7.5 to 15.0	4.0 to 2.0
L	15.0 to 30.0	2.0 to 1.0
P	30.0 to 100.0	1.0 to 0.3

The backscattered signal of different radar wavelength is directly influenced by surface roughness and dielectric constant (Simonett and Davis, 1983) (Table 3.3). With a longer wavelength, the potential penetration of the radar wave into the ground increases (Ghedira, 2000; Bonn and Rochon, 1996; Simonett and Davis, 1983; Ulaby et al., 1982). Bands with longer wavelengths are thus more appropriate for studying ground humidity (Simonett and Davis, 1983). The penetration of a wavelength into the ground depends on its dielectric constant: in general, the higher the moisture content (high dielectric constant), the lower the penetration (Fung and Ulaby, 1983; Simonett and Davis, 1983). Shorter wavelengths are more sensitive to the geometry of the ground surface such as the roughness (Ghedira, 2000; Simonett and Davis, 1983; Ulaby et al., 1982; Ulaby et al., 1981). Consequently, they are usually more appropriate for studying differences in vegetation density (Simonett and Davis, 1983). RADARSAT-1 is a C band radar with a frequency of 5.3 GHz, corresponding to a wavelength of 5.6 cm. This length has the characteristic of being able to furnish information on both the surface geometry and the surface moisture conditions (Costa, 2000; Shao, 2000; Ribbes, 1999; D'Orio *et al.,* 1995; Brown *et al.*, 1993).

Table 3.3 Variations in the radar backscatter signal attributable to wavelength (λ) (adapted from Simonett and Davis, 1983).

Wavelength (λ)	Roughness	Dielectric Constant	Study Example
Short (for example band K, 1cm)	Most surfaces appear rough (diffuse backscatter signal).	Penetration is negligible.	More appropriate for detection of difference in vegetation density. Less appropriate for detection of variation in soil moisture properties.
Long (for example band P,1m)	Few surfaces appear rough (specular backscatter signal).	Penetration from 0.3m in wet soil (high dielectric constant) to 1m or more in dry soil (low dielectric constant).	More appropriate for detection of variation in soil moisture properties. Less appropriate for detection of difference in vegetation density

3.2.2 Polarization

Polarization is the orientation of the electromagnetic wave transmitted and received by the sensor (Ghedira, 2000). The polarization of an image is identified by two letters, which can either be H for horizontal or V for vertical orientation. The first letter refers to the transmission orientation and the second to the reception orientation. There are four possible polarization combinations: HH (such as RADARSAT-1) and VV are like-polarized imagery because the two polarizations are identical, and HV and VH are cross-polarized imagery because the transmission and reception orientations are different (CCRS, 2002; Bonn and Rochon, 1996; Fung and Ulaby, 1983). As mentioned by Lillesand and Kiefer (1987, p.494), "*the mode of signal polarization influences how the objects look on the resulting imagery*". If the object has a similar orientation to the polarization, the backscattering values will be lower. For example, a vertical plantation will appear darker on a HH image (more backscattered signal) than on a VV image (less backscattered signal). According to Bonn et Rochon (1996) and Fung and Ulaby (1983),

like-polarized imagery generally return more signal towards the sensor than cross-polarized one, and the tonal contrasts caused by wet soil surfaces are stronger on HH imagery.

3.2.3 Incidence Angle

RADARSAT-1 has a number of possible incidence angles, as well as resolutions and ground swath coverage (Figure 3.5 and Table 3.1). The images can be acquired with different resolution and incidence angles, and can be combined in order to take advantage of multiple mode processing. The difference between each beam mode (Fine, Standard, Scansar, etc) is their incidence angle. As shown in Figure 3.6, the incidence angle is the angle between the radar beam signal, and a line (*vertical axis*) perpendicular to the surface (Sabins, 1997; De Loor, 1993, p.204). According to Bonn and Rochon (1996, p.218), "*the incidence angle, of the radar signal received by the surface, has a major influence on the penetration of the wave in the ground, on the backscattered value according to the surface's roughness and on the effect of the relief*". In this project, only the fine resolution beam mode was used, with both steep angle (F1) and shallow angle (F4 and F5). Each incidence angle has different properties that make it more suitable for the identification of specific land cover or land use.

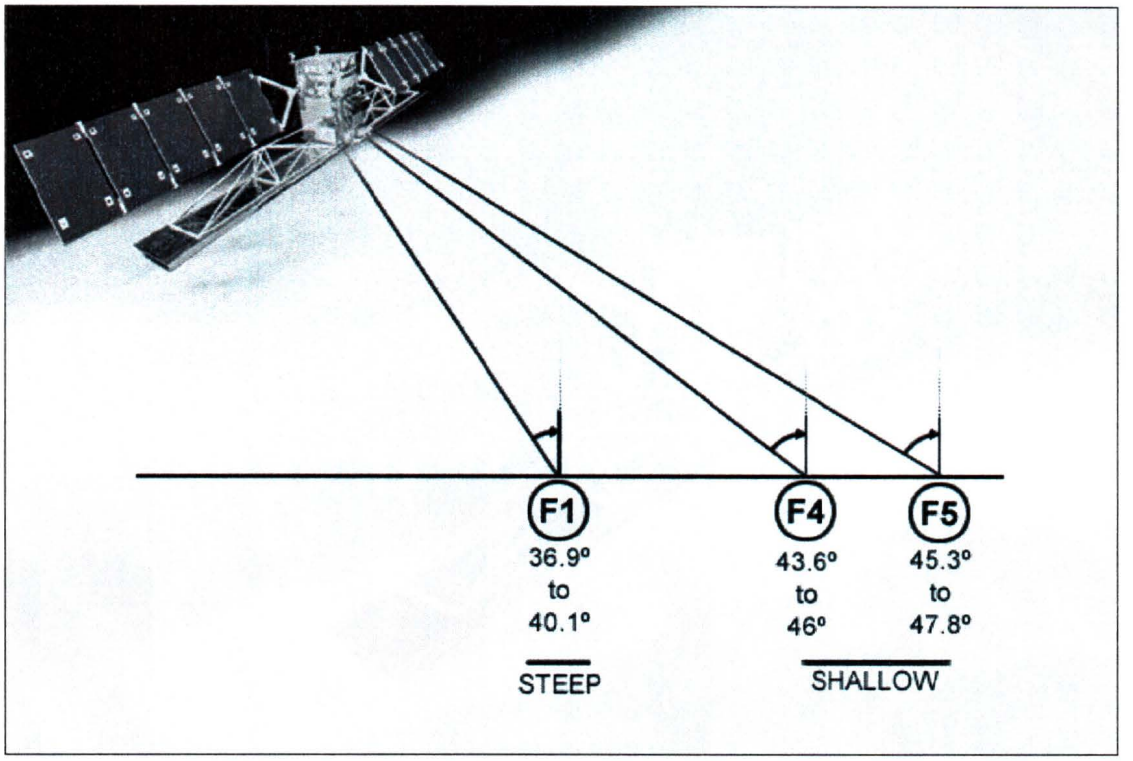

Figure 3.6 Difference between shallow and steep incidence angle, horizontal surface (example with RADARSAT-1 fine beam mode F1, F4 and F5)

Simonett and Davis (1983) and Fung and Ulaby (1983) describe the basic principles of incidence angle with radar sensors such as the fact that the total amount of backscattering signal increases as the incidence angle decreases (steeper angle). Usually, imagery with a steeper angle will be brighter than imagery with a shallower angle because a greater amount of the radar signal is returned to the sensor. Thus, in Figure 3.7, the F1 image is brighter (higher backscattering) than the F4 image because it has a steeper angle. Another important principle, mentioned by Simonnet and Davis (1983), is that as the incidence angle increases (shallower angle), the dependence of the like-polarized (with RADARSAT images it is HH) backscattering signal on the dielectric constant increases, and its dependence on the surface roughness decreases. As shown in Figure 3.7, the backscatter in the area within the red circle (image on the left with the shallower angle,

F4), is not influenced by the waves on the water (roughness) and consequently does not reflect the signal back to the sensor, resulting in only black pixels. However, on the steeper angle image (image on the right, F1), the signal is influenced by the roughness of the water and is reflected back to the sensor, resulting in brighter pixels in the water (see inside the grey circle, Figure 3.7). With a shallower angle, the sensor detects more the moisture of the objects and reflects a higher signal. However, this signal is reflected away from the sensor because water is a specular reflector, resulting in black pixels on the image.

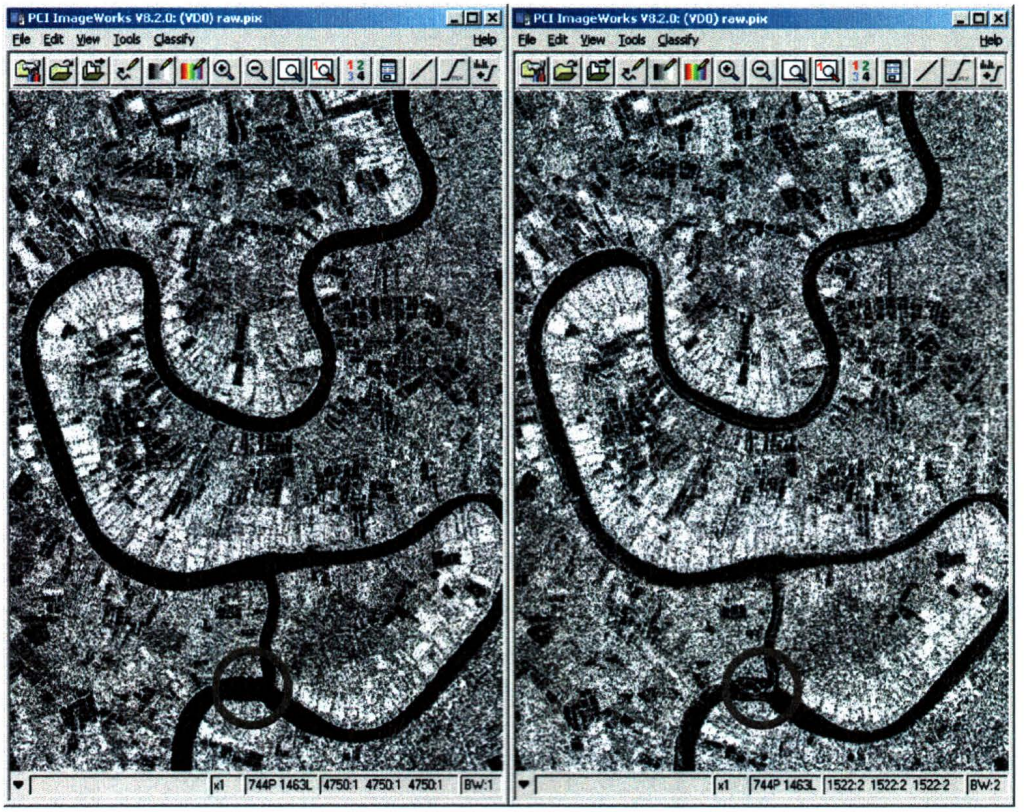

Figure 3.7 Comparison of the water backscattered between an image taken with a shallower angle (F4, left) and one taken with a steeper angle (F1, right).

3.3 RADARSAT-1 and Shrimp Farming monitoring

In 1998, the Thai Department of Land Development conducted a survey of inland shrimp farms in 23 provinces located in the Central Plain region (Ministry of Science, Technology and Environment, 1998). The survey used LANDSAT-5TM (level 8) images that were taken on March 10 and March 17, 1998. Shrimp ponds were identified manually and plotted on 1:50,000 base maps. The accuracy of these interpretations was field checked during the summer and fall of 1998. In December of the same year, the survey information was published as part of an environmental assessment of inland shrimp farming prepared by the Ministry of Science, Environment and Technology (1998). This survey did not involve any image processing or land cover classification but simply identified the presence or absence of inland shrimp farms. However, the frequent presence of cloud rendered regular acquisition of this type of data impossible.

Certain meteorological and physical aspects are important to consider when acquiring appropriate images of South East Asian countries for land mapping and land management. The tropical weather of this area, as well as the size of the land use and land cover are paramount. In general, the size of the agricultural plots in this part of the world is very small compared to those usual in Canada, Australia or the USA. Thus, high spatial resolution images are required so as to be able to identify them. Aquaculture crops, such as inland shrimp ponds for example, are smaller than 1 ha (Patmasiriwat *et al.*, 1998). Also, the crops (shrimp and rice) usually have many annual cycles, necessitating frequent image acquisitions spanning the different seasons, including the rainy one when there are clouds in the sky (Forster, 1996). RADARSAT-1 SAR has the capability to furnish high-resolution images on a regular basis for tropical areas.

RADARSAT-1 SAR has four major characteristics in the type of data it acquires and how these data are collected which makes it more appropriate than optical sensors for this specific project of monitoring inland shrimp farms in a tropical environment. The main great characteristic of this active sensor, as mentioned above, is its ability to penetrate heavy clouds, fog, and dust. It allows researchers to record detailed land and water characteristics in almost all weather, day or night (CSA, 2000; Kasischke and Bourgeau-Chavez, 1997). SAR data are therefore unique for mapping shrimp farms and rice paddies, normally situated in tropical and sub-tropical areas, because of this all weather capability. The second advantage is the unique microwave signature of water surfaces on SAR images compared to any other land cover types. The water-covered surfaces are easy to identify because of their very low backscatter resulting in very dark grey pixel levels on the image (Travaglia *et al.*, 1999). The third advantage of SAR data, according to research done by Travaglia et al. (1999), is the potential to distinguish shrimp ponds from all other water-covered surfaces because of the backscatter signal from the surrounding dykes (Figure 3.8).

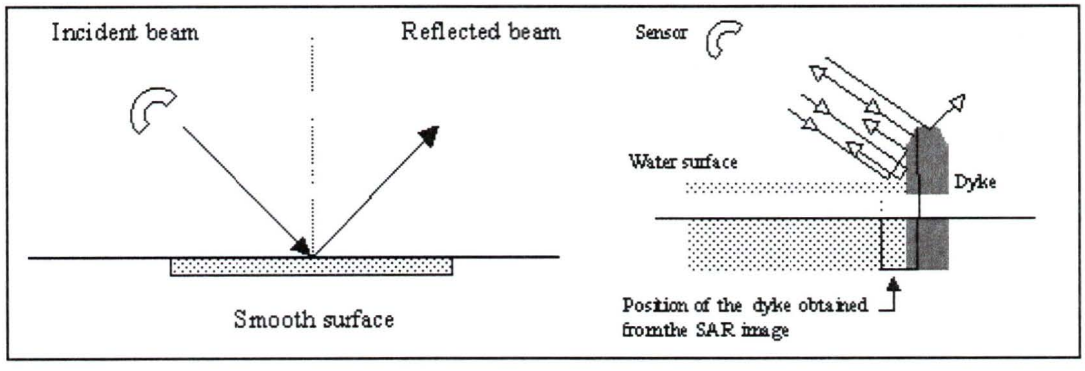

Figure 3.8 Differentiation between the radar backscattered with a smooth surface versus a dyke (Travaglia *et al.*, 1999).

The dykes that surround shrimp ponds normally vary in thickness between 0.5 and several metres. Their height is at most one metre above the water surface. These characteristics all influence the nature of the backscattered radiation (Travaglia *et al.*, 1999). The different positions of the dykes relative to the radar beam (perpendicular or parallel) impact the backscattered signal, which is an important consideration in image analysis (Travaglia *et al.*, 1999).

Finally, the fourth advantage of RADARSAT-1 is the possibility of multiple mode use. In the processing step, the satellite images can either be combined with other satellite images (multiple polarisation or multiple wavelength) or only with images from the same satellite but acquired in different modes (multiple incidence angles or multiple dates).

There are many advantages in the use of multiple mode images. Usually, multiple date images allow the recognition of seasonally variable land cover and multiple angle images allow the differentiation of vegetation cover and the study of surface moisture. With RADARSAT-1, each possible beam mode image can differentiate specific types of land cover because of the various resolutions and incidence angles available. In this project, the fine resolution beam mode was considered to be the best for studying small areas, such as inland shrimp farms and rice paddies. The different incidence angles available in each beam mode facilitated the identification of various types of land cover

3.4 Summary

Remote sensing is a tool well suited to monitoring different land cover and land use types, as well as their spatial and temporal evolution. This technology allows for the study of a large range of subjects, like objects or areas situated in remote locations, or large scale phenomena that would be difficult using conventional measuring techniques.

The aim of this project is to assess remote sensing, particularly using RADARSAT-1, as a tool for monitoring inland shrimp farms in Thailand as well as other water bodies, rice paddies, orchards and human settlements. RADARSAT-1 is a Synthetic Aperture Radar (SAR) that images the earth's surface by generating its own illumination of the scene, (CSA, 2000). This principle allows SAR system to record data at any time of day through heavy clouds, dusk, haze, and fog. Since the study area of this project is in Thailand, RADARSAT-1 is more appropriate than passive sensor for recording quality and regular data because of the effect of tropical climate. Also, water surfaces, such as shrimp ponds, are easy to identify because of their dark grey pixel levels on SAR images. The dykes surrounding the ponds are also potentially identifiable because of their steep angle, which could help in differentiating farms from other water bodies. Finally, the use of multiple modes is an advantage of RADARSAT-1 allowing the best results to be obtained by testing different combinations of multi-angle and multi-temporal data. According to the literature, it seems that RADARSAT-1 SAR imagery could be a useful tool for identifying and mapping inland shrimp farms and other land cover / land use in Thailand.

CHAPTER FOUR

STUDY AREA AND DATA SOURCE

4.1 Description of the Study Area

Thailand, with a total area covering 514 000 square kilometres, is situated in the centre of Southeast Asia, bordering the Andaman Sea and the Gulf of Thailand (Smith et al., 1968). As illustrated on the Figure 4.1, Thailand also shares frontiers with Laos on the north and east, Burma on the north and west, Cambodia on the south and east and Malaysia on the south.

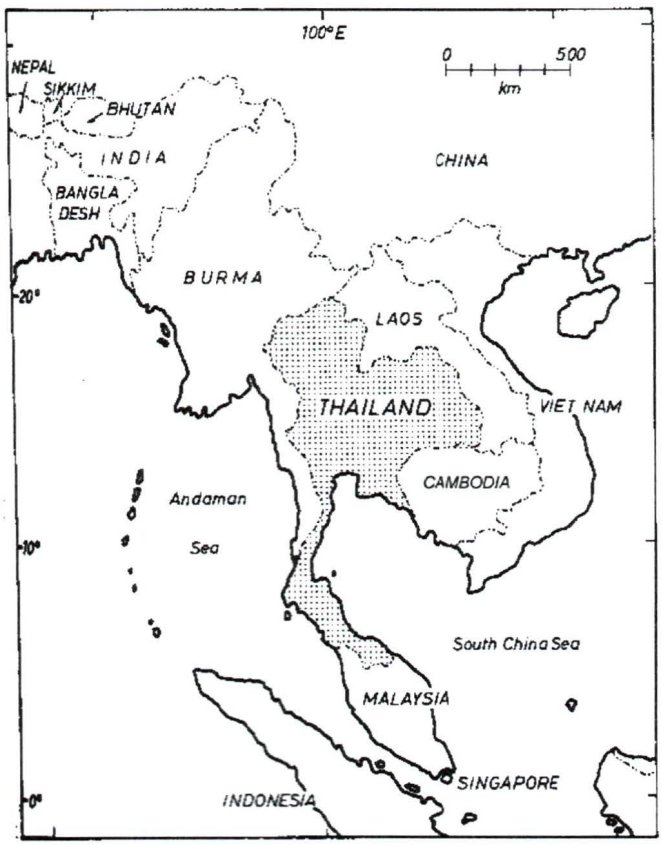

Figure 4.1 Thailand as a state in Southeast Asia (Donner, 1978, p.3)

Thailand has different agricultural regions (Figure 4.2), however, this study has been conducted in the most productive one, the Central Plain, where the richest farmlands of Thailand growing rice are situated (Flaherty *et al.*, 2000; 1999; Flaherty and Vandergeest, 1998; Donner, 1978). This central region can also be called the Chao Praya Delta or the basin of the Chao Praya River (Smith *et al.*, 1968).

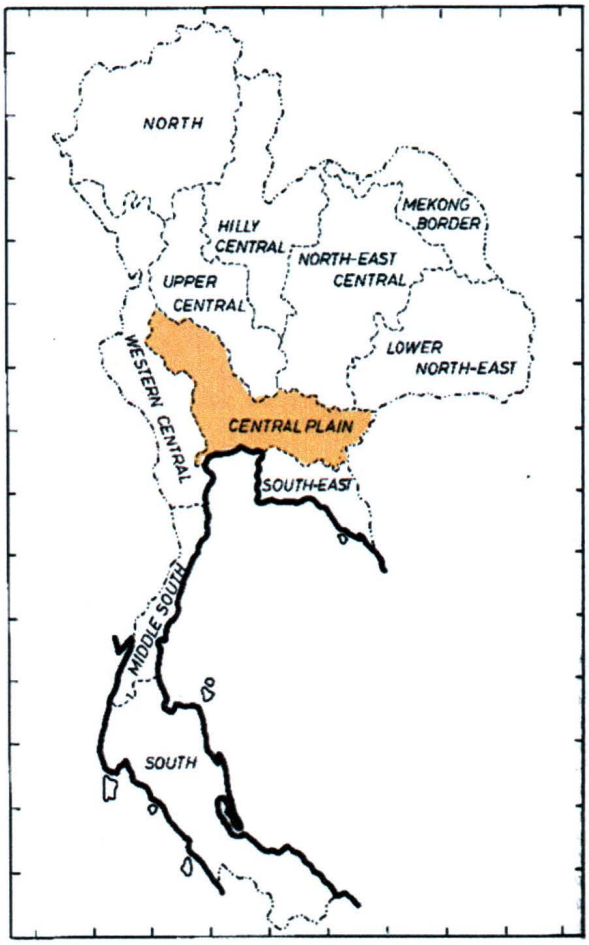

Figure 4.2 Agricultural regions of Thailand (Donner, 1978, p.78)

The central part of Thailand is characterized by a wet tropical savannah climate that is strongly influenced by monsoon winds, creating a wet season with heavy precipitation and a distinct dry season during the winter (Donner, 1978). Within a year, there are three dominant seasons in Thailand (Miller *et al.*, 1999; Arbhabhirama *et al.*,

1988). From approximately November until February, there is a Cool Season (also called Dry Season). This season is characterized by a dry and cool air mass from the interior of Asia (northeast monsoon) and it dominates the central, but also the northern region of Thailand. Then, approximately from March until May, just after the cool and dry northeast monsoon finishes and before the wet southwest monsoon starts, there is a second period called the Hot Season. Finally, the third period is usually taking place from June until October. This Wet Season is characterized by the strong southwest monsoon, loaded with moisture, moving towards the north to cover the entire country.

The soil of the Central Plain is characterized by very heavy clay, as well as marine and river alluvium, which makes it appropriate for agricultural activities (Donner, 1978). The altitude of the plain is low, averaging less than10 meters (Donner, 1978). The Bang Pakong River is also present in this region, situated in the Changwat Chachoengsao (Figure 4.3). Rice paddies, inland shrimp farms as well as fishponds and crop cultivation such as banana, mango, coconut and eucalyptus orchards, are the main agricultural crops of the Bang Pakong basin.

The five satellite images acquired for this project cover a small portion of the whole Central Plain (see figure 4.3). They cover three Changwat (Thai primary administrative division) of Eastern Thailand situated along the Bang Pakong river: Changwat Nakhon Nayok in the north, Changwat Prachinburi, including the Amphoe (Thai secondary administrative division) of Ban Sang, in the middle, and Changwat Chachoengsao in the south (Figure 4.3). The whole area covered by the five superimposed images is around 50km by 50km (2500 km^2). Each image does not cover exactly the same area, however they are all situated within this region. The upper left

coordinates of this region are 14°15'00''N (latitude) and 101°00'00''E (longitude) and the lower right coordinates are 13°30'00''N (latitude) and 101°30'00''E (longitude).

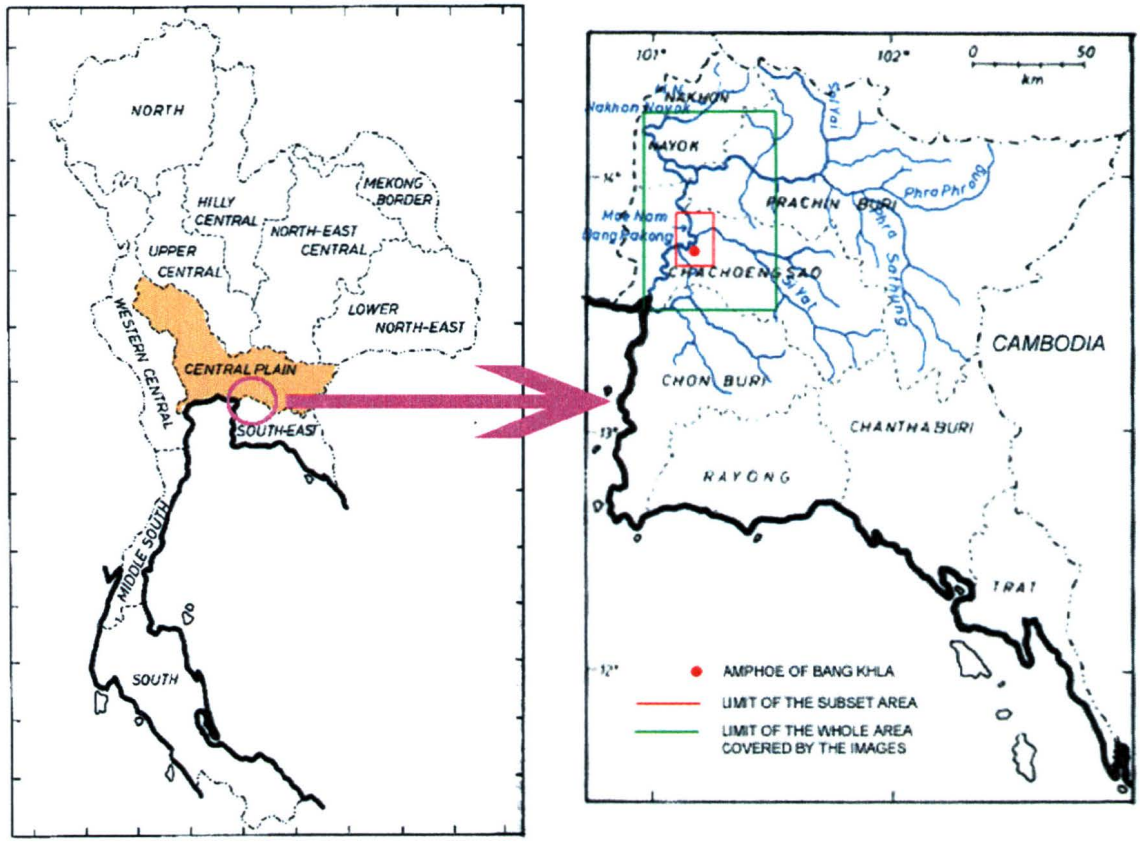

Figure 4.3 The Three provinces covered by the satellite images: Changwat Nakhon Nayok, Changwat Prachinburi and Changwat Chachoengsao (Adapted from Bonner, 1978)

Because of the large size of the whole image, the analysis was carried out on a subset of the image area, situated in the Changwat Chachoengsao, including the Amphoe and Ban (village) of Bang Khla (around 101°12'00''E, 13°44'00''N) located along the shore of the Bang Pakong River (Figure 4.3). The image subset size is 1126 pixels by 1735 lines, with a resolution of 10 m, in other words 195 361 000 m² or 195 km², which is around 8% of the whole area covered by the images. The upper left and lower right corner coordinates for this subset area are respectively 13°52'29.97" N (latitude) and

101°07'29.35" E (longitude), and 13°43'02.24" N (latitude) and 101°13'38.94" E (longitude). This area has been chosen for its high concentration of shrimp farms, as well as for the different land cover types present in the district, such as orchards, rice paddies, human settlements, transportation routes and irrigation areas (Figure 4.4).

LEGEND		
Land cover	**Colour**	**Date (Under water)**
All water bodies	Black	All dates
Orchard	Mix coloured	None
Human	White	None
	Light Yellow	None
Rice	Red	July18 / Sept19
	Blue	May7 / July18
	Green	May7 / Sept19
	Turquoise	May7
	Purple	July18
	Dark Yellow	Sept19

Figure 4.4 Subset area: False colour (RGB) combination of 3 RADARSAT-1 images F4 and F5 beam mode (Red: May 7, 2001 (F4); Green: July 18, 2001 (F4); Blue: September 19, 2001 (F5))

4.2 Data Source

This project is based on the use of remotely sensed data; multi-temporal and multi-angle RADARSAT-1 imagery, as well as hardcopy topographic maps (1:50 000 and 1:250 000) of the study area and data collected in the field. The five satellite images were geometrically corrected using the topographic maps. These maps also served to

orient the field campaign, delimiting the study area and helping to identify the different types of land use and land cover present. Pictures and notes of land cover and land use observed on the field were taken and the geographic coordinates recorded using a GPS. This information was then used in the imaging process in order to automatically identify and classify the types of land of the whole area.

4.2.1 Acquisition of RADARSAT-1 SAR Data

In this project, five RADARSAT-1 images taken during the wet and the hot seasons have been used. They are all in a fine resolution beam mode with three different incidence angles, namely F1, F4 and F5 (Table 4.1). For fine beam mode imagery, the nominal range resolution is 8x8 meters for F4 and F5 images, or 9x9 meters for F1, F2 and F3 images, and the azimuth resolution is 9x9 meters (CCRS, 2002). Weissel (2002) states, "*...the spatial resolution in the range direction is determined by the pulse length of the transmitted microwave energy*". On the other hand, the azimuth resolution is the spatial resolution in the azimuth direction, in other words, the flight direction of the satellite, calculated in degrees clockwise from geographic north (Weissel, 2002). Spatial resolution is, as defined by Weissel (2002), "*the ability to separate closely spaced objects of an image or a photograph*". Thus, the spatial resolution indicates the size of an object that can be distinguished on the ground by the satellite in a specific mode. However, on the image, the pixel sizes are resampled to 6.25x6.25 meters in the radiometric correction pre-processing step. If a certain object is smaller than the spatial resolution size (8x8 or 9x9 meters) but exhibits a very high reflectance (backscattering ratio), it can saturate the pixel, masking off all other features.

For the images used in this study, the pixel size was resampled during geometric correction, the second pre-processing step, to a resolution of 10x10 meters. This resolution was chosen for convenience, because it is a round number really close to the original spatial resolution. Also, this spatial resampling smooths the images a little, losing some noise present on the image, without losing important information about the land cover to be identified. The smallest features in the images to be monitored are shrimp ponds (approximately 80x80m), which are larger than the new pixel size. As a result, this new resolution will not lose important information contained in the original data set.

Table 4.1. Acquisition of SAR Images in fine resolution beams (CSA, 2000)

Acquisition Dates (2001)	Thai Season	Beam Type	Nominal Range Resolution (m)	Azimuth Resolution (m)	Incidence Angle (°)	Orbit
May 7	Hot	Fine 4	8x8	9x9	43.6 to 46.0	Descending
May 24	Hot	Fine 1	9x9	9x9	36.9 to 40.1	Descending
July 11	Wet	Fine 1	9x9	9x9	36.9 to 40.1	Descending
July 18	Wet	Fine 4	8x8	9x9	43.6 to 46.0	Descending
Sept. 19	Wet	Fine 5	8x8	9x9	45.3 to 47.8	Ascending

Two of the land cover types, monitored in this research, shrimp and rice crops, change during the year: (Miller *et al.*, 1999; Arbhabhirama *et al.*, 1988). These two crops have different growth stages and are therefore seasonally dependent. As mentioned in the Introduction to this thesis, inland low salinity shrimp farmers harvest between one and three crops per year. Four images were acquired during the second crop period (April/May to August): two during the hot season, May 7, 2001 (F4) and May 24, 2001 (F1), and two at the beginning of the wet season, July 11, 2001 (F1) and July 18, 2001 (F4).

On the other hand, rice farmers of non-irrigated areas (central and eastern Thailand) grow only one rice crop per year during the wet season (from June to October). Crops are planted when there is enough water available during the monsoon rains in May. The harvest time for these crops depends on the type of rice grown. The growing period for light rice is three months and five months for heavy rice, which causes the harvest time to vary from September to November. One image was acquired during this time, on September 19, 2001 (F5). Rice farmers of irrigated areas (central and eastern Thailand) have additional water supplies that allow a second dry season crop, generally planted in December and harvested in April or May (Miller *et al.*, 1999; Arbhabhirama *et al.*, 1988).

4.2.2 Topographic Maps of the Study Area

For this study, eight 1991 topographic maps were used. Two were at 1:250 000 scale and six were at 1:50 000 scale, covering the whole study area (Table 4.2, Figure 4.4). These maps were used during the fieldwork in order to orient and plan the data recording campaign. Also, these maps were used in order to correct the first of the five images geometrically because no other database, vector files or corrected images existed for this specific area.

Table 4.2 Topographic map information (Product of the Royal Thai Survey Department; Bangkok, Thailand, 1991)

	Projection	Title	Series	Sheet	Edition	Latitude	Longitude
1:250,000	Transverse Mercator	Bangkok Metropolis	1501 S	ND 47-12	2-RTSD	13°00' to 14°00'	100°30' to 102°00'
	Transverse Mercator	Changwat Phra Nakhon Si Ayutthaya	1501 S	ND 47-8	2-RTSD	14°00' to 15°00'	100°30' to 102°00'
1:50,000	NA	Changwat Chachoengsao	L7017S	5236 III	1-RTSD	13°30' to 13°45'	101°00' to 101°15'
	NA	Amphoe Phanom Sarakham	L7017S	5236 II	1-RTSD	13°30' to 13°45'	101°15' to 101°30'
	NA	Amphoe Bang Nam Prieo	L7017S	5236 IV	3-RTSD	13°45' to 14°00'	101°00' to 101°15'
	NA	Amphoe Khok Pip	L7017S	5236 I	1-RTSD	13°45' to 14°00'	101°15' to 101°30'
	NA	Changwat Nakhon Nayok	L7017S	5237 III	1-RTSD	14°00' to 14°15'	101°00' to 101°15'
	NA	Changwat Prachin Buri	L7017S	5237 II	1-RTSD	14°00' to 14°15'	101°15' to 101°30'

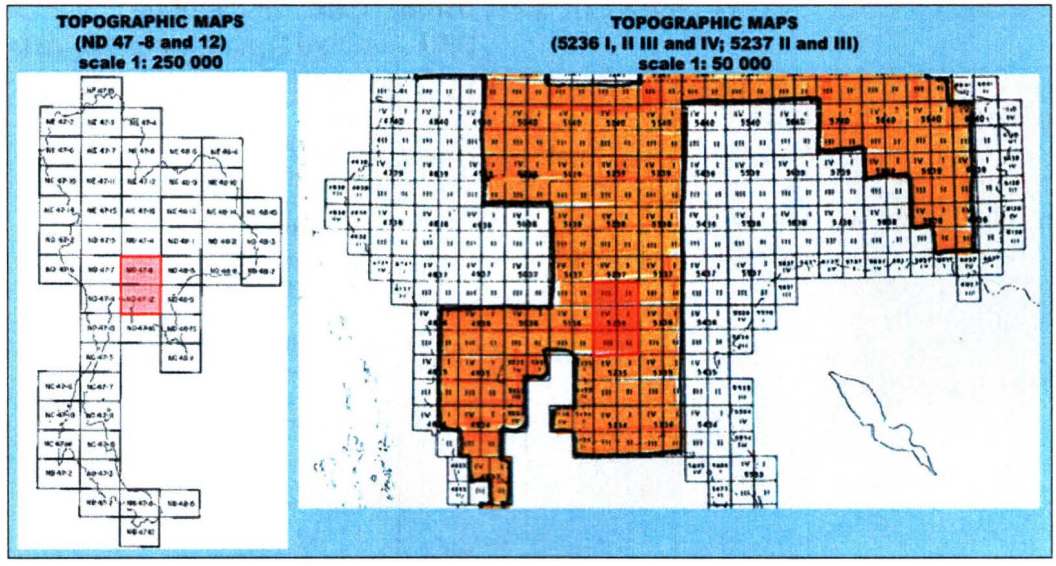

Figure 4.5 Topographic maps used for this project (Omniresources, 2002).

According to Table 4.2, all the maps covered the entire area. However, only maps three and five precisely covered the subset area (upper left corner: 13°52'00''N / 101°06'00''E; lower right corner: 13°43'00''N / 101°15'00''E), where all the image processing steps were performed.

4.3 Field Methodology

A field campaign was conducted from July 18 to July 28 2001 covering the whole area represented on the imagery. The fieldwork consisted of taking pictures, notes and coordinates of the different land cover and land use studied with a GPS (Global Positioning System). The GPS used was a Garmin III Plus with sightings accurate to within ± 15 meters (49 feet). The land cover and land use identified included various types of orchards (coconut, banana, mango, eucalyptus, etc.), human settlements (houses, roads, buildings, etc), rice paddies (paddies at different growing stages), water bodies (water reservoirs, fish ponds, rivers, etc) and shrimp farms (shrimp ponds and dykes) (Figures 4.6, 4.7, 4.8, 4.9 and 4.10).

Figure 4.6 Mixed orchard (mango and banana) with coconut trees delimiting the orchard territory, Amphoe Bang Nam Prieo, July 2001

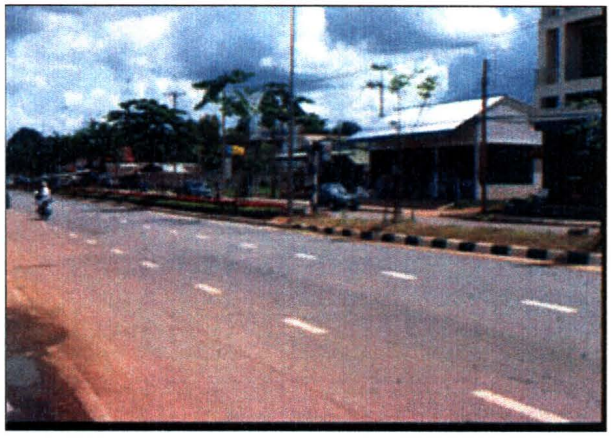

Figure 4.7 Human Settlements, Amphoe Bang Khla, July 2001

Figure 4.8 Rice paddies in a middle growing stage, Amphoe Phanom Sarakham, July 2001

Figure 4.9 Water bodies, such as a fish pond (left) and a water reservoir (right), Amphoe Khok Pip, July 2001

Figure 4.10 Shrimp farms with aerators and dykes, Amphoe Bang Nam Prieo, July 2001

4.4 Summary

In this research, five multi-temporal and multiple angle RADARSAT-1 images of Thailand's Central Plain were acquired in order to classify different types of land cover and land use present in this area. The first two images were taken in May 2001 during the hot season in Fine 4 and Fine 1 RADARSAT beam mode. The three other images were taken during the wet season; two in July in Fine 1 and Fine 4 beam mode as well, and one in September in Fine 5 beam mode. The whole area covered by the images includes three Thai provinces (Changwat) around the Bang Pakong River: Changwat Nakhon Nayok in the north, Changwat Prachinburi in the middle and Changwat Chachoengsao in the south. However, this study was restricted to a subset of this whole area situated in the Chachoengsao province, including the town of Amphoe Bang Khla (around 101°12'00''E, 13°44'00''N). This area was chosen because of its concentration of inland shrimp farms, but also because of the presence of other water bodies (reservoirs and fish farms for example), rice paddies, orchards and human settlements.

As an accurate inventory of land use / land cover is necessary to produce and assess a viable classification, a field mapping campaign was planned and executed during the summer of 2001. The classification methodology was then based on training sites traced according to the data recorded during this 2001 field campaign.

CHAPTER FIVE

METHODOLOGY

This section is a review of radar image pre-processing techniques (radiometric and geometric correction, principal component analysis, speckle filtering and texture analysis) used in this project. These techniques were employed to facilitate an accurate classification, and/or segmentation, of the land use and land cover of Changwat Chachoengsao, Thailand. The objectives of this section are thus to explain the methodology of the project, to define the technical terms and the imagery processing techniques, and to examine previous studies using RADARSAT-1, and other SAR data, for similar discrimination of tropical land use and land cover. An emphasis is placed on case studies in tropical regions, mainly South East Asia, although studies from other parts of the world are also summarized as they relate to image processing techniques used in this project. The review of previous work in the methodological part of a study project is important as it allows a logical continuation of the research based on the researchers' knowledge; it also prevents the researchers from repeating their predecessors' mistakes and helps to understand the important concepts.

5.1 Image Pre-Processing

The goal of image rectification and restoration is to correct the inherent distortion and/or the degradation of the original image (Lillesand and Kiefer, 1994; Gerbrands, 1993). Firstly, radiometric and geometric corrections are applied to compensate for geometric and instrument related issues (Richards, 1986). Once corrected, filters can be applied to the images, texture analysis can be applied, as well as a principal component

analysis. All these pre-processing techniques were applied with the aim of increasing the accuracy of image classification or segmentation. In this project, all the images were pre-processed using the PCI programs *OrthoEngine*, *Xpace* and *Image works* supplied as part of the PCI Geomatica V8.0 software.

5.1.1 Radiometric Correction

The first type of correction applied on the raw data is only applicable to the intensity of the signal received by the sensor (Bonn and Rochon, 1996). On a satellite image acquired by a SAR sensor, the pixel values (DN, digital number) are related to the local area illuminated by the beam (Small *et al.*, 1997). These values are calibrated by the supplier RADARSAT International (Ghedira, 2000). The calibration establishes a physical link between the numerical value of each pixel and the characteristics of the surface of the corresponding area. The numerical pixel values of an image can be converted into intensity (power), amplitude, or decibel (Ghedira, 2000). A radiometric calibration of the images is necessary to compensate for the effects of the local illuminated area, of the incidence angle, and of the antenna pattern on the local backscatter (Ghedira, 2000; Toutin, 1998; Small *et al.*, 1997). These parameters have a significant effect on the quantity of energy captured by the satellite and can produce noise (Bonn and Rochon, 1996). The objective of the radiometric correction is to recover the signal backscatter and eliminate part of the noise (Ghedira, 2000; Bonn et Rochon, 1996). The numerical values are usually first converted into intensity (power) or amplitude, values because these types of value allow more flexibility in subsequent processing, such as during the filtering and the texture analysis. The intensity equals the radar brightness (backscatter) and the amplitude is the square root of the intensity. Once the pre-

processing and processing steps are applied, the intensity or amplitude values are then converted into decibel values to quantitatively assess the resulting data (Ghedira, 2000). In most of the publications, radar images are generally presented in decibel values for convenience (Freeman, 1992). Decibels have a range of real negative and positive numbers on a logarithmic scale. This format allows a proportional scaling of the parameters' variations that influence the backscattering values, such as the incidence angle, the dielectric property and the state of the observed surface (Ghedira, 2000 and Ulaby *et al.*, 1982). There are three steps for radiometric correction when using the PCI Geomatica software. The first, CDSAR, reads all the layers available on the compact disk and then automatically creates a PCIDSK file of one layer. The second function, SARINCD, produces a table of incidence angles corresponding to the table of gain scaling values produced with the first function. Then, the image file contains the orbit segment (ORBIT) and the array segment (A0SEG), both required as inputs for the third function, the SARSIGM. This last one generates a calibrated layer containing the radar backscatter. The function produces the output backscatter coefficient (sigma-0) for the entire image (PCI Geomatic, 2000). The choice of the range of pixel values, intensity (power), amplitude or decibels, is chosen as part of this last step (Equations 5.1, 5.2, 5.3).

Intensity (power) = $$Sigmaij = \frac{DN * DN + A0}{Aj} * \sin(ij)$$ Equation 5.1

Amplitude = $$Sigmaij = \sqrt{\frac{DN * DN + A0}{Aj} * \sin(ij)}$$ Equation 5.2

Decibel = $$Sigmaij = 10 * \log_{10}\left(\frac{DN * DN + A0}{Aj} * \sin(ij)\right)$$ Equation 5.3

Where:

$Sigmaij$:	output backscatter coefficient for scanline i, pixel j.
$\log_{10}(\ )$:	logarithm base 10 function
$\sqrt{(\ )}$:	square root function
DN:	input image value for scanline I, pixel j
A0:	gain offset from the first member of A0SEG
Aj:	expanded gain scaling table value for column j.
Sin():	sine trigonometric function
ij:	expanded incidence angle table value for column j.

Once registered as PCIDSK files with the radiometric correction, each channel is in 32 bit real with power values. Prior to geometric correction, the images are converted from 32 bit real to 16 bit unsigned channels since larger sizes can corrupt files during the correcti on process (Equation 5.4). The differences between these two types of channel are the size of the file and the range of pixel values: 32 bit real channels allow a range of real numbers from -10 exp38 to + 10 exp38, while with 16 bit unsigned channels, the range is positive (possible range from 0 to 65, 535) (PCI Geomatics, 2000; Penny, 1994). The use of 16 bit unsigned also allows the application of mathematical operations to the pixels (filter, texture, etc.) (PCI Geomatics, 2000). Thus, after the radiometric correction, the images are first automatically placed in 32 bit real channels with power backscatter values. Then, they are converted into 16 bit unsigned channels for all the following image pre-processing and processing applications. Finally, for the interpretation and the presentation of the results, they are reconverted into decibel backscatter values, in order to compare the results with other research results (Equation 5.5). To convert intensities

(power) values into decibels, a logarithmic transformation needs to be applied (Ghedira, 2000).

$$POW_{16} = (POW_{32}) * 10{,}000 \qquad \text{Equation 5.4}$$

$$dB_{32} = 10 * \log_{10}\left(\frac{POW_{16}}{10{,}000}\right) \qquad \text{Equation 5.5}$$

Where:

POW_{16}: Power (intensity) values in 16 bit unsigned channel

POW_{32} Power values in 32 bit real channel

dB_{32}: Decibel values in 32 bit real channel

For the original (not geometrically corrected) image of May 7, 2001, the maximum value of the data set in intensity (16 bit unsigned) is 59,949, the mean is 1219.429, and the standard deviation is 1955.251. In order to convert intensity values into decibel, equation 5.5 needs to be applied to the data. Once applied to the intensity values, the decibel maximum is then 7.77782, the mean -9.138 and the standard deviation -7.088. The original range of the data set is changed by the multiplication of the original 32 bit values by 10 000 (equation 5.4), which retain only the four first decimals of the intensity values. But, in order to fit into a 16 bit unsigned channel (max 65,535), 10 000 is the maximum number possible to use for the transformation of the intensity values. The maximum number of the original data set in 32 bit real (intensity values) was 5.994916, so that multiplication by 10,000 eliminated all the decimals after the fourth, and resulted in a maximum value of 59,949 for the 16 bit unsigned data set. The minimum, maximum,

mean and standard deviation of the grey level values (in intensity) of the whole image (May 7, 2001), as well as the subset image, before and after geometric correction on 16 bit unsigned as well as on 32 bit real channel are demonstrated in the Table 5.1.

5.1.2 Geometric Correction

A geometric correction rectifies the image from its distortion by warping it in order to fit a map projection (Verbyla, 1995). The distortion of the raw images, when compared to a geo-referenced (spatially corrected) map or image, is readily apparent. A raw and unprocessed image is not linked to a specific referencing system (UTM or latitude/longitude). Instead, it has an arbitrary reference system based on pixel coordinates (Niemann, 2001). Geo-referencing is a procedure that spatially refers an image to its known position on the ground (Niemann, 2001). Since the images need to be almost perfectly superimposed, the precision of this step is critical. It has an important influence on further processing analysis steps (Ghedira, 2000). As described by Ghedira (2000) and Richards (1986), when the satellite collects image data, it is distorted by three main sources of error. Firstly, the error can come from the observed environment, such as the rotation of the earth during the image acquisition, the curvature of the earth, the variation in the ground altitude and topography effects. Secondly, the distortion can be produced by an error in the measurement system, such as wide or finite scan sensors, and the effect of the incidence angle on the pixel size. Finally, platform movement, such as variations in altitude, latitude or speed, during image acquisition can also be a source of error.

The choice of an appropriate geometric correction method depends on the future uses of the corrected images and on the information available from the study area. There

are two techniques that can be used to correct the geometric distortion present in digital image data, depending on its source and origin. The first approach, *mathematical modeling*, addresses the nature and the magnitude of the sources of distortion. It uses models to establish geometrical correction formulae (Ghedira, 2000 and Richards, 1986). This technique is effective when the types of distortion are well characterized, such as those caused by earth rotation or by the incidence angle (Ghedira, 2000). The second approach, the *mapping polynomial*, depends upon establishing mathematical relationships between the addresses of the pixels in an image, and the real corresponding coordinates of those points on the ground (Ghedira, 2000 and Richards, 1993). These coordinates can be obtained from a topographic map or from a geo-referenced satellite image of the same area.

In this research, the OrthoEngine program of PCI Geomatica V8.0 was used to geometrically correct the five RADARSAT-1 images registered in intensity (power) backscatter values in 16 bit unsigned channels. The mathematical modelling method used for the correction of all five images was the polynomial transformation, and the output images were resampled to a pixel spacing of 10.00m using the bilinear technique. The polynomial transformation is a 1^{st} to 5^{th} order polynomial that creates a new geocoded image with interpolated pixel values. In this project, the second order was used for the first corrected image. For that image, the GCPs (Geographic Control Points) were collected manually from topographic maps of the area (1:50 000 and 1:250 000). This order gave the lowest root mean square (RMS) errors without introducing other significant errors in the part of the image situated far away from the GCPs. The first order was then used for the other four images, which were corrected using the image-to-image method, resulting in a small RMS because of the better precision of this type of GCPs

collection. The bilinear technique was chosen, instead of the nearest neighbour (Bernier et al., 2003; Ghedira et al, 2001) or the cubic convolution (Moisan et al., 1999), because as it corrects the image, it also removes some of the effects of speckle (grey level of one pixel according to the average of the four closest pixels) and it does not introduce artefact (Bernier et al., 2003; PCI Geomatics, 2000; Bernier et al., 1999). This method smoothes the image but also can result in a loss of detail. However, in this project, the smallest features such as shrimp ponds and the surrounding dykes, were still visible after using the bilinear method. The mean and standard deviation of the data set were not significantly affected using this resampling method (Table 5.1).

Table 5.1 Grey level values of the whole image (May7, 2001), as well as the subset image, before and after the geometric correction.

	BEFORE geometric correction		**AFTER geometric correction, using the bilinear resampling method**			
	WHOLE IMAGE		**WHOLE IMAGE**		**SUBSET AREA**	
	Intensity (16 bit unsigned)	Decibel* (32 bit real)	Intensity (16 bit unsigned)	Decibel* (32 bit real)	Intensity (16 bit unsigned)	Decibel* (32 bit real)
Min.	0	-40** (low backscatter e.g. water)	0	-40* (low backscatter e.g. water)	0	-40* (low backscatter e.g. water)
Max.	59,949	7.77782 (high backscatter e.g. dry land)	59,931	7.77652 (high backscatter e.g. dry land)	57,331	7.58389 (high backscatter e.g. dry land)
Mean	1219.429	-9.138	869.421	-10.608	1085.674	-9.643
Std. Dev.	1955.251	7.088	1453.318	8.376	1609.093	7.934

The conversion is done (from intensity to decibel) using this equation:* ***10 *LOG10 (16bitUns/10,000)*

Table 5.2 Geometric correction results

DATE (2001)	Ground Control Points (GCPs) Collection Method	Accepted GCPs	Polynomial Order	RMS (Root Mean Square error)	xRMS	yRMS
May 7	Manually (From the topographic maps)	23	2	1.37	0.88	1.37
May 24	Image to image (From the May 7 image)	19	1	1.35	0.93	0.98
July 11	Image to image (From the May 7 image)	18	1	1.15	0.86	0.76
July 18	Image to image (From the May 7 image)	20	1	1.27	0.97	0.82
Sept. 19	Image to image (From the May 7 image)	18	1	1.30	0.99	0.84

The project area is situated in the UTM (Universal Transverse Mercator) zone 47 and row P, with the surface of the earth represented by the horizontal Datum earth model D078 (Indian 1975, Thailand).

The GCPs used for the first image, May 7, 2001, were collected manually from the available 1:50 000 topographic maps of the study area. The other fourth images were corrected based on the first corrected image (Table 5.2.).

5.1.3 Principal Component Analysis

A principal component analysis is a linear transformation converting a number of variables, for example multiple radar images, into the same number of new uncorrelated variables (also known as principal components or synthetic bands) through rotating the axes of the initial variables (Torma and Koskinen, 1997; Bonn and Rochon, 1996; Buiten, 1993; Lillesand and Kiefer, 1987; Mather, 1987; Richards, 1986). Lillesand and Kiefer (1987, p.656) describe "*...principal component data values as simply linear combinations of the original data values*". The main goal of this analysis is to decrease the number of variables by preserving, as much as possible, the information they contain; in other words, it is to attain a data reduction by decorrelating the data set for classification

purposes (Sabins, 1997; Lillesand and Kiefer, 1987). Each component explains a certain percentage of the variance between the images, and is expressed by its eigenvalue. The first principal component (eigenvector) is centered on the axis of maximum data variance and contains most of the information, while the second component is perpendicular to the first axis. The first component explains the greatest variance (Torma and Koskinen, 1997; Bonn et Rochon, 1996; Holecz *et al.,* 1993). The second describes the axis with the second highest variance. The same holds true for all the other components; they all explain a part of the variance but always less than the preceding one. The result of a PCA is a new set of images, the first containing relevant information, such as the maximum variance of data, and the last image contains random noise components, such as speckle (Sabins, 1997; Torma and Koskinen, 1997; Bonn and Rochon, 1996).

Researchers use this technique in order to differentiate features or identify changes between multiple images. Hoogeboom (1993) used the PCA for crop discrimination on radar images. According to him, the integration of these components reduced the amount of information and the classification became simpler and clearer. Torma and Koskinen (1997) used median filtering to reduce the speckle in an image and a principal component analysis to select and extract the relevant features in the 14 ERS-1 SAR images. These two steps, speckle removal as well as the selection and extraction of the important features, have a profound influence on the accuracy of a classification. Researchers have used the median filter because this technique removes the low and high valued pixels. The results of their research show a classification accuracy of 55-60%, which is quite low. In further research, they proposed to continue using the PCA but with images of other frequencies or polarizations and to run some texture measures. Verhoeye and De Wulf (1999) also used a PCA on four ERS-1 SAR images to classify different land cover

types in Costa Rica. They applied a filter to the images, then they ran a PCA and image segmentation, and they finally did a supervised classification of multi-temporal radar images. In their research, they tried multiple ways to achieve the best classification. They found that the PCA was not the best way to increase the accuracy of the model. With their chosen procedure, they obtained a map with an overall accuracy of 76%.

In this project, two principal component analyses were applied to the images. The first included all five multi-temporal and multi-angle RADARSAT-1 images. Once the PCA was completed, a classification was run on the first three components. The second was applied to the three shallower angle images (F4 and F5). Then, a classification was run on the three resulting components.

5.1.4 Speckle Filtering

A SAR image is formed when the signal is backscattered from the ground back to the sensor. Every pixel on an image has its own backscattering value. One important disadvantage of SAR images is the speckle effect on the resulting images. Speckle is the result of coherent interference of the reflection off the surfaces, because the physical properties of the ground modify the radiation (Arvelyna, *et al.*, 2001; Costa, 2000; Touzi, 1999b; Oliver and Quegan, 1997; Bonn and Rochon, 1996; Touzi and St-Jean, 1995; Richards, 1993; Richards, 1986). Therefore, as explained by Costa (2000, p.100-101), when "*...the radiation reaches a resolution cell on the ground, it interacts with all the scatters within the resolution cell*", and "*...for similar targets the backscattered signal might be different due to the differences between scatter within a resolution cell*". The effect of speckle is a degradation of the radiometric information of the image (Costa, 2000; Ghedira, 2000; Touzi, 1999b; Oliver and Quegan, 1997), which makes visual

interpretation difficult, because of the grainy appearance of unfiltered SAR images (Costa, 2000). Also, on radar images, the speckle noise is multiplicative, which means that it augments with the backscatter value (Bonn and Rochon, 1996; Schwan *et al.,* 1995). In other words, the greater the backscattered signal of the surface towards the sensor, the greater the speckle effect on this area on the image.

Classification or image segmentation, with the presence of speckle, is highly ineffective and will complicate the image interpretation (Arvelyna *et al.,* 2001; Costa, 2000; Oliver and Quegan, 1998; Touzi and St-Jean, 1995). Prior to classification or image segmentation, it is critical to apply an appropriate filter to facilitate the detection of the fine features. To reduce speckle noise, some satellites use an average of several numbers of looks before forming an image (Li, 1988). However, in particular cases, such as the fine beam mode of RADARSAT-1 used in this project, the data are a product of only one look. As a result, the speckle noise is quite marked. Some posterior filter treatments, therefore, need to be applied to the image to reduce the speckle effect without losing the edges and textural information (Arvelyna *et al.,* 2001; Oliver and Quegan, 1997; Smith, 1996).

Several algorithms, used as filters, have been developed to reduce the speckle effect in SAR images (Ghedira, 2000; Touzi, 1999b; Travaglia *et al.*, 1999). A filter is a moving window (usually 3x3, 5x5 or 7x7) that passes over each pixel on the image, replacing the value of the central pixel by a value derived from all the pixels within the window (Smith, 1996). It estimates the backscatter of the central pixel of the window, according to its own intensity as well as the intensities of the neighbouring pixels (Fjortoft, 2000; Touzi, 1999b). As a result, an entire image is built up with new pixel values. However, the noise reduction generally produces a loss of detail. According to

Oliver and Quegan (1997) and Travaglia (1999), it is important to choose an appropriate filter, by considering the characteristics of the image and the type of analysis planed, with the aim of optimizing the results. There are four criteria to evaluate the appropriateness of a filter (Arvelyna *et al.,* 2001; Costa, 2000; Touzi, 1999b; Lopes et al., 1990). While reducing the speckle effect on the image, the filter should also preserve the radiometric information (backscattering coefficient value), increase the equivalent number of looks (decreasing the local variance), and preserve the information about texture and edges. Eight commonly used filters, Mean and Median, Lee and Enhanced Lee, Frost and Enhanced Frost, Kuan, and finally Gamma, are fully explained in the following sections. However, only the six most common were tested in this project: the Lee and Enhanced Lee filters, the Frost and Enhanced Frost filters, the Kuan filter and the Gamma filter. For many years, these filters have been used to suppress speckle noise on SAR images and they have proven their accuracy (Arvelyna et al., 2001; Ristau and Moon, 2001).

5.1.4.1 Mean and Median Filters

The mean and the median filters change the value of the central pixel of a given window by respectively calculating the mean and the median of all the neighbouring pixels present in this window (Li, 1988). The median filter is normally applied with a 3x3 window size, since a larger window size produces an increased smoothing effect on the image (Holecz, 1993). This filter removes the anomalous pixels, which do not fit in with neighbouring pixel pattern. For example, isolated noise is removed with a median filter (Schowengerdt, 1997). The mean filter will also eliminate pixels with very different values. These filters are not normally appropriate for SAR images as they smooth the

edges and the features as well as removing speckle noise, resulting in a loss of detail (Smith, 1996).

5.1.4.2 Minimum Mean Square Error and Non-stationary Mean and Non-stationary Variance Filters

Touzi (1999a and b) and Lopes *et al.* (1993) proposed to classify most of the filters appropriate for SAR images into two groups: the minimum mean square error (MMSE) and the non-stationary mean and non-stationary variance (NMNV). MMSE filters do not take into consideration the statistical distribution of the underlying scene, for example the Lee, the Frost and the Kuan filters. On the other hand, NMNV filters apply an a priori statistical model to the underlying scene signal, such as the Bayesian filters (Gamma-Gamma MAP). For the NMNV group of filters, the term non-stationary mean describes the raw structure of the image and the non-stationary variance characterizes the edges and the elementary texture information (Holecz *et al.* 1993). These filters use a small-sized moving window, usually 7x7 or smaller, "*which should provide a satisfactory compromise between speckle reduction and preservation of small structures within a tolerable computing time*" (Touzi, 1999a, p.1).

5.1.4.2.1 Lee and Enhanced Lee Filter (MMSE)

The Lee Filter, with a possible window size up to 33x33, removes the multiplicative noise contained in a radar image (PCI Geomatics, 2000; Lee, 1981). It is essentially used to eliminate speckle and to conserve edges and sharp features. As described by Ristau and Moon (2001), the Lee Filter uses a linear approximation to calculate and minimize the mean square error by least square estimation. The Enhanced

Lee filter is a variation of the original Lee filter. Lopes *et al.* (1990) improved the filter by making it divide the data set into areas of three classes (Ristau and Moon, 2001, PCI Geomatics, 2000). The first class groups homogeneous areas, where a low-pass filter can eliminate the noise. A spatial low-pass filter only preserves the large homogeneous regions without keeping the details of their structure (Ghedira, 2000; Bonn and Rochon, 1996; Gerbrands, 1993). The second class contains the heterogeneous areas, where the eliminated noise preserves the information provided by the texture. The third class corresponds to the "*isolated point targets where the filter should preserve the observed value*" (Ristau and Moon, 2001; Costa, 2000).

5.1.4.2.2 Frost and Enhanced Frost Filter (MMSE)

The Frost filter, proposed by Frost et al. (1982), uses an *exponentially damped convolution kernel*. The algorithm is based on a circular symmetrical filter, and for each pixel, there is a possible set of weighted values. The kernel of this adjustable filter adapts to the features by using local statistics (PCI Geomatics, 2000). This filter can have a window size up to 33x33. The Enhanced Frost filter, improved by Lopes *et al.* (1990), works similarly to the Enhanced Lee filter, by differentiating homogeneous, heterogeneous, and homogeneous areas with isolated points. However, this filter uses the Frost Filter basic equation instead of the Lee Filter's. The same window sizes as the Lee filter can also be used.

5.1.4.2.3 Kuan Filter (MMSE)

A Kuan Filter (Fjortoft *et al.,* 2000; Kuan *et al*, 1985) is a linear minimum square error estimator (LMMSE). In the first step, it transforms the "*multiplicative noise model*

into a signal-dependent additive noise model" (Ristau and Moon, 2001, p.344). In the second step, a minimum mean square error is applied. The resulting filter is similar to the Lee filter, with a different weighting function and with no approximation made on the original model (Ristau and Moon, 2001).

5.1.4.2.4 Gamma Filter (NMNV)

The Gamma Filter, developed by the Centre d'Études Spatiales des Rayonnements (CESR), Toulouse, France, and by the Canada Centre for Remote Sensing (CCRS), assumes that the unspeckled intensity of the underlying scene is Gamma distributed (Arvelyna *et al.*, 2001; PCI Geomatics, 2000; Touzi and St-Jean, 1995). This filter uses the Bayesian approach because it takes into account the statistical properties of the underlying scene, as well as the speckle statistics (Touzi, 1999b; Touzi and St-Jean, 1995). The Gamma filter, in geological application, can preserve the sharpness of faint ridges (Touzi and St-Jean, 1995), and in hydrological applications, can preserve linear features like drainage and filled boundary (Touzi and St-Jean, 1995), or an oil slick (Arvelyna *et al.*, 2001). With this filter, low radiometric contrasts (uniform vegetation) are smoother and strong radiometric contrasts (creeks, roads, etc) are enhanced. As noticed by Touzi and St-Jean (1995, p.2), when using the Gamma filter, "*strong reflectors are preserved and do not alter the radiometry of neighbouring pixels*". The possible window size is up to 11x11.

5.1.5 Texture Analysis

One of the most important classes of information in SAR images is contained in its structural component (Oliver and Quegan, 1997). The texture, a structural element of

SAR images, represents the natural spatial variability of neighbouring pixels (CRISP, 2001; Costa, 2000). In other words, the texture is a spatial distribution of the local tonal variation and it determines the smoothness or coarseness of the image features (Holecz *et al.*, 1993; Lillesand and Kiefer, 1987). The texture component of an image "*is produced by an aggregation of unit features that may be too small to be discerned individually, such as tree leaves or leaf shadows; it is a product of their individual shape, size, pattern, shadow, and tone*" (Lillesand and Kiefer, 1987, p.114). This image component contains significant information about the structural arrangement of the surfaces, as well as their relationship with the neighbouring environment (Holecz *et al.*, 1993).

The radar backscatter is mostly influenced by the roughness (geometry) and the moisture content (dielectric constant) of an object. Thus, differences in surface roughness can have an important impact on the backscatter characteristics and therefore, on the image texture (Kuntz *et al.,* 1994). A texture region in an image can be large areas such as fields or forests, but can also be discrete objects, such as individual trees, roads and buildings. (Oliver and Quegan, 1997). Texture features have proven to be an important component of an SAR image interpretation, characterization and classification (Rajesh *et al.* 2001; Prasad and Gupta, 1998; Soares *et al.*, 1997; Anys and He, 1995; Buchroithner, 1993; Sali and Wolfon, 1992). In many cases, different types of land cover may have similar backscattering coefficients and can be classified as the same type of land cover. A texture analysis can help to differentiate the various cover types. In an example, given by Costa (2000), some vegetated areas with uniform canopies (homogeneous area) may present very little backscattering variation and other areas with short and tall trees (heterogeneous area) may present higher backscattering variation. A texture analysis of these two vegetated areas could facilitate their separation.

When a texture analysis is applied, it is important that no speckle suppression filter has previously been applied. The purpose of this analysis is to establish the original textural information contained in the original image, by determining the spatial relationship of the original grey level values of neighbouring pixels (Bonn and Rochon, 1996). The filtering of the raw image modifies the pixel values. The raw image is processed by the texture analysis, prior to a classification. An image texture analysis is based on the brightness values (grey levels, GL, or digital numbers, DN) of the pixels. The Grey Level Co-occurrence Matrix (GLCM) is the most popular method applied to SAR images for the purpose of texture analysis (Hall-Beyer, 2000; Soares, 1997). As explained by Hall-Meyer (2000), the GLCM is a tabulation of how often combinations of pixel brightness values occur in an image. The GLCM uses second order statistics, which "*describe the relation between pixels in addition to the statistical description of the grey-level distribution*" (Sali and Wolfson, 1992, p. 3396). Second order statistics are used because they detect many properties of texture and they are not sensitive to noise. They also take into account information about the different pixels' relationship, not only about the neighbourhood of a single pixel such as in the case of first order statistics (Sali and Wolfson, 1992). The two pixels studied in a second order GCLM texture analysis are the reference pixel and its neighbour.

There are many possible features that can be computed from the co-occurrence matrix: the Homogeneity, the Contrast, the Dissimilarity, the Mean, the Standard Deviation, the Entropy, the Angular Second Moment, the Correlation, the GLDV Angular Second Moment, the GLDV Entropy, the GLDV Mean (equivalent to Dissimilarity) and the GLDV Contrast (equivalent to Contrast) (Ghedira, 2000; Hall-Beyer, 2000; PCI Geomatic, 2000; Conners, 1980; Haralick 1979; Haralick *et al.*, 1973). The four GLDV

measures are computed from the Grey Level Difference Vectors, derived from a grey level co-occurrence matrix. In this project, only the eight GLCM texture components were tested on the RADARSAT-1 imagery.

1. Homogeneity $\sum_{i,j=0}^{N-1} \frac{(i,j)}{1+(i-j)^2}$ Equation 5.6

2. Contrast $\sum_{i,j=0}^{N-1} P(i,j)*(i-j)^2$ Equation 5.7

3. Dissimilarity $\sum_{i,j=0}^{N-1} P(i,j)*\left|IR(i)-IC(j)\right|$ Equation 5.8

4. Mean $\sum_{i,j=0}^{N-1} P(i,j)=\mu_i$ Equation 5.9

5. Standard Deviation $\sum_{i,j=0}^{N-1} P(i,j)*(1-\mu_i)^2=\sigma_i^2$ Equation 5.10

6. Entropy $\sum_{i,j=0}^{N-1} P(i,j)*\log P(i,j)$ Equation 5.11

(Assuming that 0*log (0) = 0)

7. Angular second moment $\sum_{i,j=0}^{N-1} P(i,j)^2$ Equation 5.12

8. Correlation $\sum_{i,j=0}^{N-1} \frac{P(i,j)*(1-\mu_i)*(j-\mu_i)}{\sigma_i*\sigma_j}$ Equation 5.13

Where:

N = number of grey levels

P = normalized symmetric GLCM of dimension N x N

P (ij) = normalized co-occurrence matrix

The Contrast component "*creates a weight that increases as distance from the diagonal increases*" (Hall-Beyer, 2000, p.13). The values situated on the GLCM diagonal do not show any contrast. However, the ones situated away from the diagonal show a high contrast. The resulting window has increased contrast because the numbers, produced by this equation, are larger. With the Dissimilarity feature, the weighting increases linearly (1,2,3,4, etc), instead of exponentially (1,4,9, etc), as the values are far away from the diagonal. Just like the Contrast component, the resulting window has large numbers for more contrast (Hall-Beyer, 2000). The Homogeneity feature calculates the inverse of the Contrast feature, which means it "*weights values by the inverse of the Contrast weight, with weight decreasing exponentially away from the diagonal*" (Hall-Beyer, 2000, p.15). The weighting is high when the values are concentrated along the diagonal. The Mean feature does not only calculate the average of all the pixels values within a window size. Each pixel value is weighted in relation to "*its occurrence in combination with a certain neighbour pixel value...*" (Hall-Beyer, 2000, p.20). The Standard Deviation, measures the values dispersion around the mean value, and it is similar to the Contrast and the Dissimilarity components. The Entropy component result is a probability between 0 and 1. The smaller the Pij value (equation 5.11), the higher the weighting. When the values in the window are uniform, the weighting is low. The Angular Second Moment is the opposite of the Entropy. This component measures local homogeneity. When the values are uniform within the window, the weight is high. The Correlation measures the grey levels linear dependency between neighbouring pixels. If the correlation is high, it means that there is a high predictability of pixel relationships.

The result of a texture calculation, such as the speckle filtering principle, is a single number representing the entire window and replacing the value of the central pixel

(Hall-Beyer, 2000). The choice of texture window size is very important. As explained by Ulaby et al. (1986), the window size should not be bigger than the size of the smallest feature included in the classification. This operation is repeated for all the pixels before producing an entire new image. Depending on which type of data is treated, some texture calculations will be more appropriate than others. It is very important to choose the ones that will give relevant results and help obtain a better image classification.

In this project, three window sizes were tested, 3x3, 5x5 and 7x7. These sizes were chosen according to the smallest feature of interest, shrimp ponds (approximately 80x80 meters (Flaherty *et al.,* 2000)), in order not to generate a loss of information. The eight GLCM texture components were evaluated according to the separability of the signatures of the different land use classes.

5.2 Image Processing

Several pixel-based, or segmentation-based, classification techniques can be used in order to separate different tropical land cover and land use, using RADARSAT-1 imagery. The overall objective of the classification is to categorize all the pixels of an image into cover classes using each pixel's unique backscatter response patterns, for pixel-based classifiers, and spatial pattern for segmentation-based classifiers. In this paper, three image processing techniques will be described and a literature review of each one will be done. Unsupervised and supervised classifications, as well as segmentation-based classification, will be explained in the three main following sections. In this present project, the unsupervised and supervised classifications were applied to the radiometrically and geometrically corrected raw images, and then applied to the pre-

processed images where a filter, a texture analysis or a principal component analysis was run. The segmentation-based classification was then run on texture images.

5.2.1 Unsupervised Classification

Unsupervised classification is a pixel-based classifier that groups pixels with similar backscatter values. Each group of pixels is characteristically called a backscatter class (Verbyla, 1995). Groups with similar backscatter values are created automatically using a clustering algorithm, such as the k-means algorithm, also called sequential clustering. The task of the analyst is to label the different classes resulting from the procedure corresponding to the specific cover type classes studied in the research, and also to some other cover types present on the image (Schowengerdt, 1997). Unsupervised classification procedures generally require no knowledge of the existing cover types. This is a considerable advantage when the researcher does not know all the cover types in an area. According to Verbyla (1995), another advantage of the unsupervised classification is the identification of areas that have unusual backscatter values. Even if they are rare, this type of classification will categorize them. Therefore, this first classification will help to define the general types of land cover. Moreover, it will also help to find the rare and small ones, which are usually hard to classify using a supervised classification.

There are many unsupervised clustering methods. However, for this project, the very common K-means-minimum-distance algorithm was used (Schowengerdt, 1997; Verbyla, 1995; Lillesand and Kiefer, 1994; Schowengerdt, 1983; Duda and Hart, 1973). This algorithm samples each pixel and assigns it to the nearest class mean, consequently separating the data set into a given number of distinct clusters (D'Iorio *et al.*, 1995; Verbyla, 1995). For each cluster identified with this algorithm, an initial mean vector is

specified. The centre of each cluster is determined by iteration. In each iteration, as explained by Schowengerdt (1983, p.147), "*each pixel of the training set is assigned to the class whose mean vector is closest to the pixel vector (the minimum-distance classifier) forming the first set of decision boundaries*". The number of iterations is chosen to maximize the classification result. It is then preferable to choose the highest number of iterations as possible in order to augment the precision of the classification. The other parameters that need to be identified are the number of classes, the sample size and the minimum threshold. The threshold is the range of backscattered values outside which a pixel has a very low probability to be included in a certain class; consequently it is excluded. In the unsupervised classification using PCI Geomatica, only the minimum threshold boundary needs to be identified.

In this project, the K-means unsupervised classification method was used prior to the supervised one. It was a first approximation intended to see how well the different features of the image were being discriminated.

5.2.2 Supervised Classification

The goal of a supervised classification is "*to sample areas of known cover types to determine representative spectral values of each cover type*" (Verbyla, 1995, p.134). However, in this research, we were dealing with backscatter values instead of spectral values, since we were working with a SAR sensor. There are several steps in a supervised classification, including the identification of the classes, which is the main difference from an unsupervised classification (Niemann, 2001; Gorte, 1999; Bonn and Rochon, 1996; Richards, 1993). With the supervised technique, prior to classification, representative examples (training sites) need to be outlined for each type of land cover

and land use. Each class needs to have a backscatter response different from all others with the aim of obtaining a good result in the classification step. When a separability analysis has been run to make sure all the cover types have a representative backscatter value, every pixel of the image can then be classified into a specific class using an appropriate classifier. All these steps are explained in the following sections.

5.2.2.1 Creation of the Classes

To create the classes necessary for a pixel-based classification of an area, it is necessary to locate training sites for each cover type of interest. The training sites are "*sample areas for estimating representative spectral statistics of a certain cover type*" (Verbyla, 1995, p.134). In this project, the sample areas were not estimating representative spectral statistics but backscatter statistics of the cover type because RADARSAT-1 SAR imagery was used. This step is usually based on a prior field session to identify the current nature of the land cover; the use of recent maps of the region is also recommended (Gorte, 2000). Once the training sites have been established, the analyst has to assign a unique identifier to each cover type by digitizing polygons around each training site on the satellite image. Every pixel, from all the different training sites, is then analysed and compiled to produce a signature for each cover type. Two sets of training sites were created in order to verify which one was best (best separability, best classification).

Table 5.3 Mean, standard deviation and colours of the training sites for each type of land use illustrated in Figure 6.3 (First set of training sites). See Appendix II for training site histograms.

		07-May-01		24-May-01		11-Jul-01		18-Jul-01		19-Sep-01	
Land Types	**Colour**	**Mean**	***Std.Dev.***	**Mean**	***Std.Dev.***	**Mean**	***Std.Dev.***	**Mean**	***Std.Dev.***	**Mean**	***Std.Dev.***
Rice	Red	-9.87	*10.04*	-8.11	*8.66*	-7.28	*7.78*	-7.00	*7.34*	-8.15	*8.38*
Human	Green	-7.93	*5.48*	-6.74	*3.46*	-5.96	*2.92*	-7.79	*5.00*	-7.77	*6.19*
Orchard	Blue	-7.68	*6.69*	-7.12	*6.11*	-6.84	*7.08*	-7.47	*6.63*	-7.01	*5.79*
Water	Pink	-23.58	*20.10*	-19.60	*19.04*	-20.48	*18.41*	-21.70	*18.09*	-20.76	*17.68*
Farm	Turquoise	-11.61	*8.44*	-11.11	*8.68*	-10.17	*8.37*	-11.90	*9.19*	-10.85	*7.68*
Shrimp	Yellow	-16.31	*14.21*	-14.41	*10.81*	-14.03	*11.04*	-15.98	*10.47*	-14.19	*12.10*

For the first set of training sites, six types of land cover and land use types were identified in the field (Figure 5.1a) and (Table 5.3). The rice class includes many growing stages. The rice stages identified are from flooded to harvested paddies. This is because all the fields situated in the subset area are not simultaneously at the same growing stage. The rice training sites thus group pixels representing rice fields at all their different growing stages. The human settlement land cover encompassed all human features, such as buildings, roads, houses, bridges, etc. The orchard class included the various different types of plantation present in the study area, such as mango, banana, coconut, corn, etc. The water cover type included all water bodies such as reservoirs, canals, rivers, fishponds, etc. At last, in order to test the separation of the shrimp farms from other land cover, two different types of training sites were used: shrimp ponds, where only the ponds were included in the training sites, and shrimp farms, where the ponds as well as the dykes were included in the training sites.

Table 5.4 Mean, standard deviation and colours of the training sites for each type of land use illustrated in Figure 6.3 (Second set of training sites) See Appendix II for training site histograms.

		07-May-01		24-May-01		11-Jul-01		18-Jul-01		19-Sep-01	
Land Types	**Colour**	**Mean**	***Std.Dev.***	**Mean**	***Std.Dev.***	**Mean**	***Std.Dev.***	**Mean**	***Std.Dev.***	**Mean**	***Std.Dev.***
Rice	Red	-9.46	*9.30*	-8.79	*-7.96*	-8.62	*-7.64*	-8.23	*-7.39*	-7.67	*-6.84*
Human	Green	-4.50	*3.88*	-4.16	*-3.88*	-4.53	*-4.33*	-4.67	*-4.30*	-4.29	*-4.15*
Orchard	Blue	-8.57	*8.88*	-7.82	*-8.02*	-7.11	*-7.49*	-8.34	*-8.80*	-8.12	*-8.83*
Water	Pink	-23.87	*24.92*	-18.22	*-14.92*	-16.73	*-15.67*	-23.47	*-24.21*	-22.48	*-23.98*
Farm	Turquoise	-12.45	*9.91*	-11.45	*-8.03*	-10.28	*-7.21*	-12.55	*-9.76*	-11.54	*-8.33*
Shrimp	Yellow	-21.64	*20.80*	-18.97	*-17.34*	-18.28	*-16.46*	-21.94	*-21.57*	-19.90	*-17.46*
AllWater	White	-22.88	*21.64*	-17.86	*-14.99*	-16.68	*-15.36*	-22.77	*-21.67*	-22.77	*-21.67*

The second set of training sites was based on the exact same criterion of the six features to be identified. They were traced on different areas of the image, not overlapping the first set (Figure 5.1 b) and (Table 5.4).

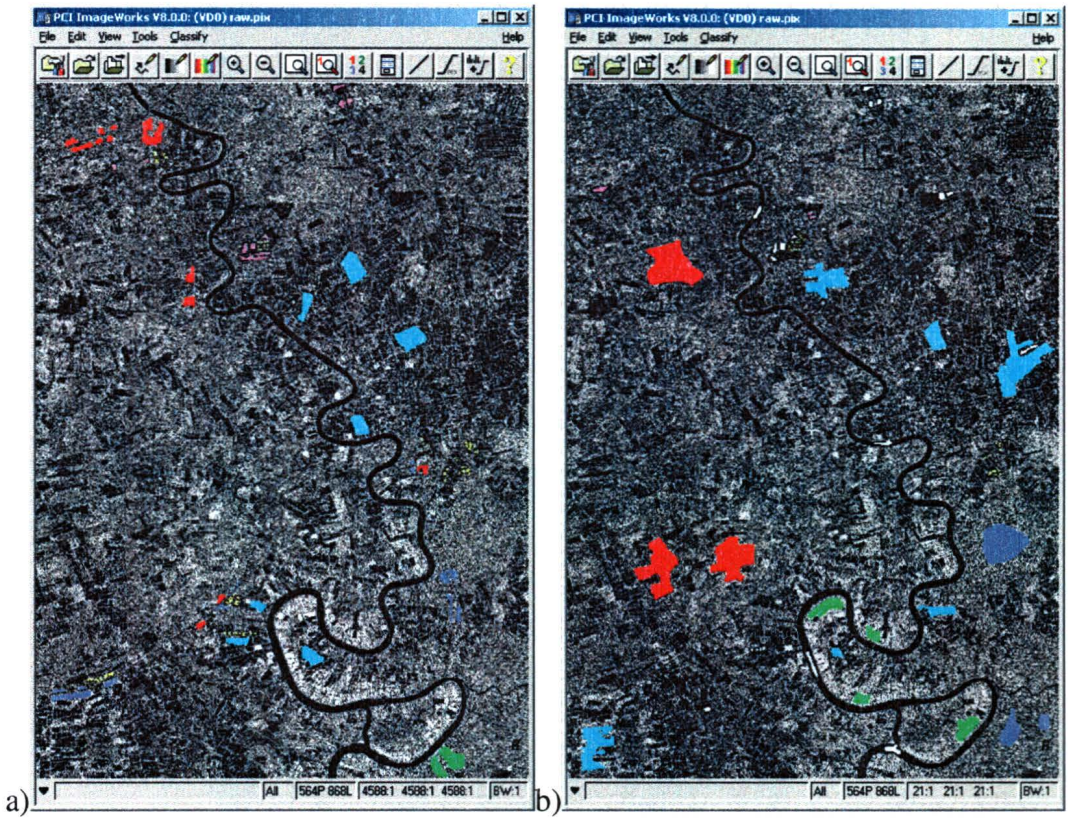

Figure 5.1 a) First set of training sites identifying land use present in the study area, image of May 7, 2001 in mode F4 b) Second set of training sites identifying the land use present in the study area, image of May 7, 2001 in mode F4

All the training sites (water, shrimp farms, shrimp ponds, human settlement, orchards, and rice), of the two sets are not characterized by normal distributions. They are all left-skewed, but they are not bimodal (see Appendix II). In order to apply a maximum likelihood classification, the theory says that the distribution of the training sites needs to be normal (Estes et al., 1983; Schowengerdt, 1983). However, in chapter 6 presenting the results, it is demonstrated that the mix of training sites yields good classification results.

5.2.2.2 Separability Between Classes

As mentioned in the previous section, training sites are representative samples of all the different features to be classified (Schowengerdt, 1997). Because every class will

not necessarily be distinguished from the others, a separability analysis between the training data is usually performed prior to a classification (Estes *et al.,* 1983). There are two separability methods possible: the Transformed Divergence and the Bhattacharya Distance.

5.2.2.2.1 Transformed Divergence

The Transformed Divergence (TD) is a popular empirical measure, which is computationally simpler than the Bhattacharya Distance (BD). While this measure is computationally less intensive the BD, the results are usually less rigorous. The results of this test fall between zero and two. If the result is zero, there is a total confusion between the two classes evaluated, while a result of two, represents a total separation between the two classes. Equation 5.14 explains the formula of the Transformed Divergence (Richards, 1986).

$$TD(i,j) = 2 * \left[1 - \left(\frac{-D(i,j)}{8} \right) \right]$$ Equation 5.14

Where:

TD (i,j) = Transformed Divergence between i and j

D (i,j) = 0.5 * T [M(i) – M(j)] * [InvS(i,) + InvS(j)] * [M(i) – M(j)]

+ 0.5 * Trace [InvS(i,) * S(j) + InvS(j) * S(i) –2*I]

Where:

M (i) = mean vector of class I, where the vector has N channel elements (N channel is the number of channels used)

S (i) = covariance matrix for class I, which has N channels by N channel elements

InvS (i) = inverse of matrix S (i)

Trace [ ] = trace of matrix (sum of diagonal elements)

T[ ] = transposition of matrix

I = identity matrix

5.2.2.2.2 Bhattacharya Distance

The Bhattacharya (or Jeffries-Matusita) Distance (BD) measures the separability between two classes (Haralick and Fu, 1983). It is theoretically a sounder method than the Transformed Divergence because it is directly related to the upper bound of the probabilities of errors of the classification. The results vary between zero and two, as in the Transformed Divergence method, and are evaluated the same way.

$$BD(i,j) = 2 * \left[1^{-(-a(i,j))}\right]$$ Equation 5.15

Where:

BD (i,j) = Bhattacharya Distance between i and j

A (i,j) = 0.125 * T [M(i) – M(j)] * Inv[A(i,j)] * [M(i) – M(j)]

+ 0.5 * ln{det (A(i,j))/$\sqrt{}$ [det(S(i)) * det(S(j))]}

Where:

M (i) = mean vector of class I, where the vector has N channel elements (Ncanell is the number of channel used)

S (i) = covariance matrix for class I, which has N channels by N channel elements

Inv [ ] = inverse of matrix

T [ ] = transposition of matrix

A (i,j) = 0.5 * [S(i) + S(j)]

Det () = determinant of a matrix

Ln {} = natural logarithm of scalar value

$\sqrt{\ }$ [ ] = square root of scalar value

The Bhattacharya Distance, demonstrated in equation 5.15, was used in this project because it resulted in more precise results (Richards, 1986). The separability analysis of the two sets of training sites is presented in Figures 5.2 and 5.3. There are two major differences between the first and second set. Firstly, the separability is better between the human settlement and the orchards classes in the second set. This can be explained by the new training sites representing human settlement. In the first set, the human training sites included some orchards pixels, confusing the signature separability of the two classes. The second set of training sites included only very bright pixels representing human settlement. Secondly, the shrimp class (including only the ponds) varies in the same way in the two sets, but the values are higher in the first. The shrimp signature is separate from the water signature in the first set because some dyke pixels, with higher backscattered values, were accidentally included in the pond training sites. Also, a new training site was added in the second set, called "*allwater*", including all the various water features such as rivers, reservoirs, fishponds, but also shrimp ponds. This explains why the second set of training sites should demonstrate more accurate results. These sites were mapped out more precisely in accordance with fieldwork and knowledge of the area.

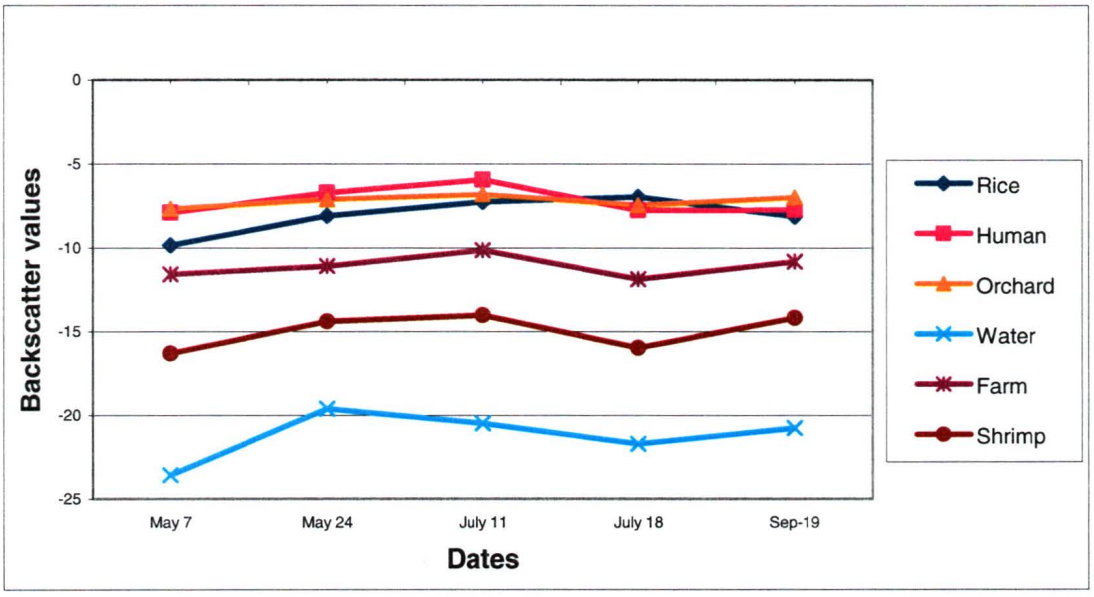

Figure 5.2 Signature separability of the land use classes of the first set of training sites (decibel values).

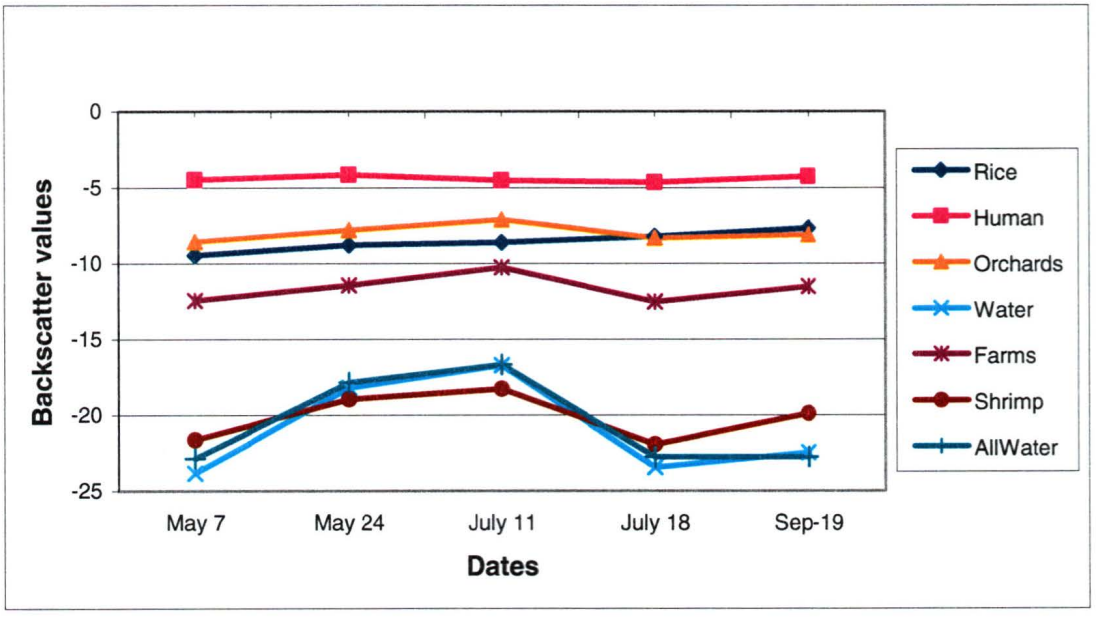

Figure 5.3 Signature separability of the land use classes of the second set of training sites (decibel values).

5.2.2.3 Pixel-Based Supervised Classifiers

Once all the categories of clusters are finalized, the entire image is classified by considering each pixel and by comparing its particular signature with each of the known signatures. The pixel-based classifiers used in this thesis assume that the distribution of values for each training site is normal. The software will assign each pixel to a cluster. Each pixel can only be assigned to one class. The pixels in an image that cannot be assigned in any of the trained classes will be attributed the label *unknown* and will not be classified (Gorte, 2000; D'Iorio *et al.*, 1995). There are different statistical techniques, such as the minimum-distance-to-means, the parallelepiped and the maximum-likelihood classifiers, which are used to analyse the image in order to make decisions on how similar signatures are to each other (Niemann, 2001; Lillesand and Kiefer, 1994). In this project, the maximum-likelihood classifier was used to obtain the most accurate classification of land cover and land use types. The minimum-distance–to-means, as well as the parallelepiped method, are described in the following sections in order to justify the choice of the maximum-likelihood method.

5.2.2.3.1 Minimum-Distance-to-Means

Primarily, with a minimum-distance-to-means classifier, the backscatter value average of each class is established. The classifier compares the distances between each pixel value with the centre of all the classes. Finally, as shown in Figure 5.4, each pixel is assigned to the class that has its centre closest to it (Hodgson, 1998; Schowengerdt, 1983; Estes *et al.,* 1983). In Figure 5.4, point 1 will be classified as "C" because the centre of this cluster is the closest to that point.

The minimum distance classifier is one of the simplest classification methods (Verbyla, 1995; Estes *et al.,* 1983). However, it is not the most commonly used because of its restrictions causing confusion in the classification result when classes are too similar to each other (Hodgson, 1998; Lillesand and Kiefer, 1987). As demonstrated in Figure 5.4, point 2 would be associated to the "S" class, even if it would be more appropriate to associate it to the "U" class.

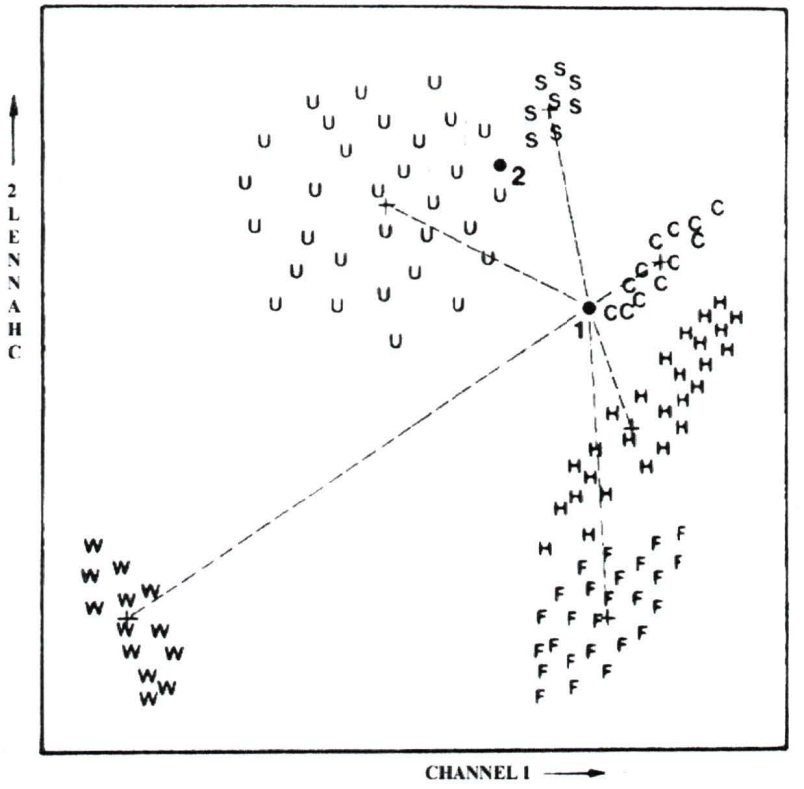

Figure 5.4 Minimum-distance-to-means classifier (Estes *et al.,* 1983; Lillesand and Kiefer, 1979)

5.2.2.3.2 Parallelepiped

The parallelepiped technique is very sensitive to the variance between pixels, but has difficulty dealing with the covariance (correlation) among them. This method uses the threshold of each class' signature to determine where all the pixels belong (Estes *et al.,*

1983). The threshold specifies the dimensions of the parallelepiped neighbouring the mean of each class. As shown in Figure 5.5, "a *parallelepiped is a multi-dimensional rectangle*" (Verbyla, 1995. p.140). This rectangle is built using the maximum and minimum backscatter values of each cover class to be classified (Verbyla, 1995).

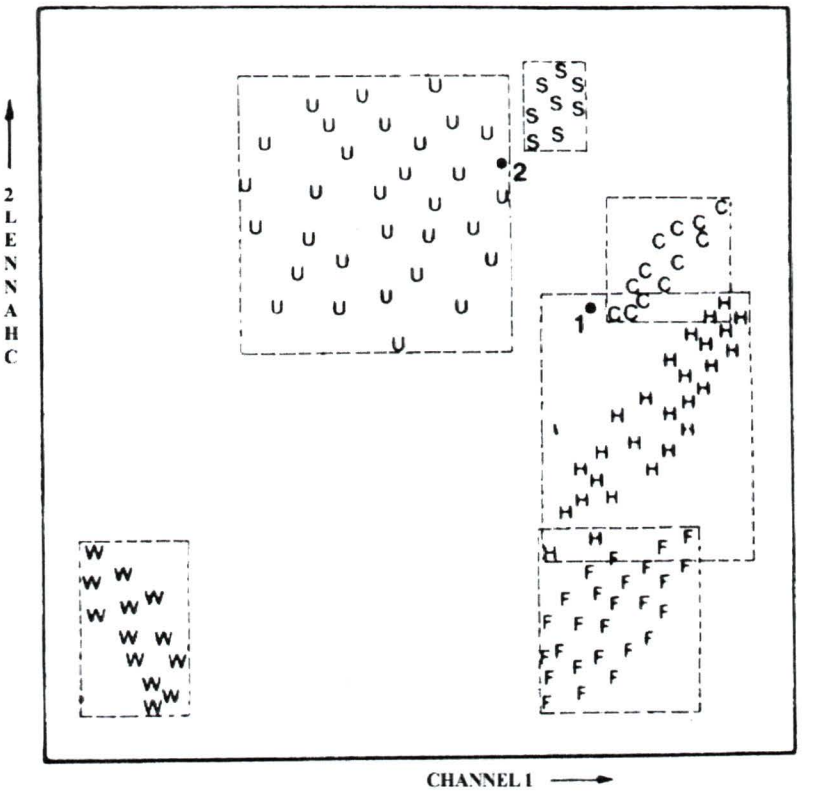

Figure 5.5 Parallelepiped classification strategy (Estes et al., 1983; Lillesand and Kiefer, 1979)

This method is efficient only for non-precise and quick image interpretations (Schowengerdt, 1983). The result is usually poor in accuracy because a large number of pixels are not properly classified; either they fall into more than one parallelepiped, or they fall into none. These pixels are either unclassified or, with a minimum-distance-to-means method, classified in the closest class (Verbyla, 1995; Estes *et al.,* 1983).

5.2.2.3.3 Maximum-Likelihood

The maximum-likelihood classification (MLC) technique is more computationally complex, but it is the most commonly used, because of its greater accuracy (Estes *et al.*, 1983; Schowengerdt, 1983; Duda and Hart, 1973). The equation 5.16 demonstrates the algorithm used to perform a pixel-based maximum likelihood classification (PCI Geomatics, 2000):

$$Gi(X) = -\frac{1}{2}(X - U_i)^t Ci^{-1}(X - Ui) - \left(\frac{d}{2}\right)\log(2TT) - \left(\frac{1}{2}\right)\log(|Ci|) + \log(Pi) \qquad \text{Equation 5.16}$$

Where:

Gi (X):	is the result for class i on pixel X
d:	is the number of layers in the classification
X=(x1, ..., xd):	is the (d by 1) pixel vector of grey-levels
Ui:	is the (d by 1) mean vector for class i
Ci:	is the (d by d) covariance matrix for class i
TT:	is pi = 3.1415...
|Ci|:	is the determinant of the covariance matrix
Pi=Bi/ Σ(Bi):	is the a priori probability for class i
Bi:	is the BIAS for class i
Σ(Bi):	is the sum of BIASes for all classes used
t:	as a superscript denotes transpose
-1:	as a superscript denotes inverse
Ti:	is the threshold value THRS for class i

The values d, Ui, Bi, Ti, Ci^{-1} and |Ci| are obtained from the class signature layer

It is a pixel-based methodology that assigns each pixel to one of the classes previously determined by the analyst (D'Iorio *et al*, 1995). The value of each pixel is compared with all the class signatures, with the purpose of determining to which cluster each pixel statistically belongs (D'Iorio *et al*, 1995). Thus, the classifier quantitatively evaluates the variance and the covariance (correlation) of the backscatter values of all the classes when it classifies a pixel (Estes *et al.,* 1983). As such, "*it is assumes that the distribution of the pixels of each category training-data is Gaussian (normally distributed)*" (Estes et al., 1983, p.1045). The classifier assumes that the training areas are homogeneous (Schowengerdt, 1983). With this classifier, "*a pixel is classified when it is within a statistical distance of less than one standard deviation from the class centre"* (D'Iorio *et al*, 1995, p.169). As shown in Figure 5.6, the maximum-likelihood classifier delineates "*ellipsoidal equiprobability contours*" in the diagram to determine each "*decision region*" (Estes *et al.,* 1983, p.1045).

The maximum-likelihood classifier has been chosen to run all the classifications in this project because of its high accuracy compared to the two other well known classifiers described above.

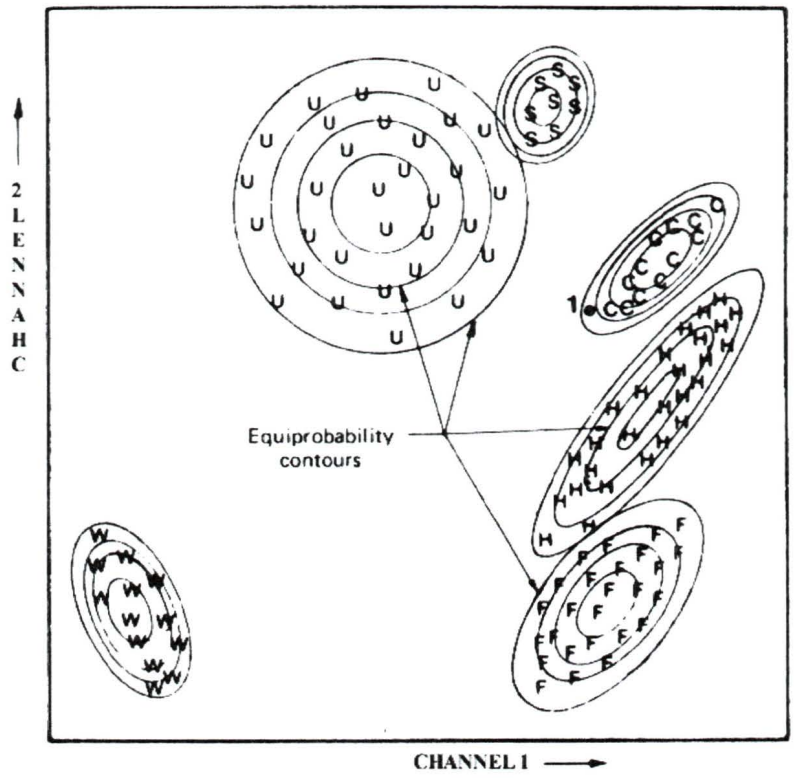

Figure 5.6 Equiprobability contours defined by the maximum-likelihood classifier (Estes et al., 1983; Lillesand and Kiefer, 1979)

In this research, the shrimp farm signature does not respond to the parametric assumption of the maximum-likelihood classifier. The training sites include shrimp pond pixels (water, low backscattering values) and dyke pixels (dry surface with angle, high backscattering values). The distribution of the pixels in this category is not perfectly normal (see Appendix II), but is not bimodal. The classification results using that signature are better than using the homogeneous training sites (shrimp ponds only). All the results are demonstrated in the Chapter 6 of this document.

5.2.2.4 Accuracy Assessment of the Classification Result

Once the classification has been run on an image, the accuracy of the classification results needs to be evaluated. The accuracy assessment "*determines the*

quality of the information derived from remotely sensed data and this can be done qualitatively or quantitatively" (Congalton and Green, 1999, p.4). In this project, the accuracy of the different classification results has been assessed qualitatively and quantitatively. A qualitative accuracy is a visual evaluation of the classification precision. Verification is done to make sure the land cover and the land use types in the classification's results were identified in accordance with reality, consistent with the information collected during the field campaign. A quantitative accuracy is the analysis of the different map errors identified by the confusion matrix, which is provided by the PCI software after a supervised maximum likelihood classification is run.

The PCI Geomatica software produces a confusion matrix when it quantitatively evaluates the accuracy of the classification. With the confusion matrix, an overall and average accuracy, as well as a mapping accuracy, are obtained. Table 5.5 presents an independent data set showing the different accuracy results obtained with a confusion matrix. The overall accuracy is the percentage of well-classified pixels in the whole image. The percentage is acquired by dividing the total number of well-classified pixels by the total number of pixels (Equations 5.16 and 5.17). The average accuracy is the total percentage of well-classified pixels divided by the number of classes (Equations 5.18 and 5.19). The mapping accuracy for each class can also be acquired with the matrix. This equation gives the percentage of correctly identified pixels for each class, by dividing the total number of well identified pixels by the addition of the total number of well identified pixels to the non correctly classified pixels of omissions and commissions (Short, 1999b) (Equations 5.20 and 5.21).

Table 5.5 Example of the overall and average accuracy calculations, as well as the mapping accuracy calculation (Short, 1999c; Lillesand and Kiefer, 1979).

Ground Classes	Radarsat Classes				Number of pixels	% well classified	Omissions	Commissions	Mapping accuracy * (MA)
	Water	Vegetation	Human	Others					
Water	**25**	5	10	3	43	58%	18 / 43 = 42%	7 / 43 = 16%	25 / (25+18+7) = 50%
Vegetation.	2	**50**	6	5	63	79%	13 / 63 = 21%	11 / 63 = 17%	50 / (50+13+11) = 68%
Human	3	4	**60**	5	72	83%	12 / 72 = 17%	18 / 72 = 25%	60 / (60+12+18) = 67%
Others	2	2	2	**100**	106	94%	6 / 106 = 6%	13 / 106 = 12%	100 / (100+6+13) = 84%
Total	32	61	78	113	**284**	**79%**			

OVERALL ACCURACY:

$$\text{Overall accuracy} = \frac{\text{Total of Pixels correctly classified } (25 + 50 + 60 + 100)}{\text{Total of Pixels } (284)} = 83\% \qquad \text{Equation 5.17}$$

AVERAGE ACCURACY:

$$\text{Average accuracy} = \frac{\text{Total of \% correctly classified } (58 + 79 + 83 + 94)}{\text{Number of classes } (4)} = 79\% \qquad \text{Equation 5.18}$$

MAPPING ACCURACY (MA) FOR ANY CLASS X:

$$\text{MA for any class X (Example for the water class)} = \frac{\text{Pixels of X (correctly classified) } (25)}{\text{Pixels of X (correctly classified)} + \text{Pixels of X (omission)} + \text{Pixels of X (commission)} \; (25 + 18 + 7)} \qquad \text{Equation 5.19}$$

Where:

Pixels of X (omission) = All other pixels in X row

Pixels of X (commission) = All other pixels in X column

In this research, all the classification accuracy results were compared to each other and with the overall accuracy (equation 5.18). This percentage take into account all the pixels of the classification.

In this project, the best classification results, identified in the following chapter, were also assessed with a set of accuracy sites. These sites were different from the set used for the classification. The resulting matrix produced by this accuracy analysis identifies the percentage of pixels (of the accuracy sites) overlapping the class it should belong to. The average accuracy could then be calculated considering the accuracy percentage of each class.

5.2.3 Segmentation-Based Classifier

Unsupervised and supervised classifications only take into account backscatter characteristics and do not consider the shapes, patterns and other spatial associations, as image segmentation does, to subdivide an image into regions that are homogeneous (Baztz and Schäpe, 2000; Gorte, 2000). Thus, the segmentation gives a simple label, like a number, to each region. An example given by Gorte (2000) is the fact that a number of pixels organized in a linear position do not help to classify them as a road. The pixels that have a pattern are usually mixed, this means that they include different types of land cover, and they are difficult to classify as to their true nature. Recently, image segmentation algorithms have grown in sophistication (Smith, 1996; Cook *et al.*, 1994; Bénié and Thompson, 1992). The goal of segmentation is to classify the images into homogeneous regions, or components, based on the spatial pattern of the pixels (Lillesand and Keifer, 1994; Gerbrands, 1993; Gonzalez, 1977). This processing technique can be very useful for the classification of ground land cover or land use categories.

Segmentation is accomplished employing criteria different from the pixel-based classifiers. It uses the backscatter value pattern of the pixel, such as the pattern and the form of the object to be classified. Thus, according to Gorte (2000), an image classification, where segmentation was previously performed, can be complementary and effective. According to Smith (1996), SAR image segmentation into regions having similar characteristics is helpful for the recognition of different features present in the image, it also helps to detect changes between different images (multi-temporal and multi-angle images) and it improves classification accuracy. However, as explained by Li *et al.* (1999), it is of paramount importance to pay attention to the presence of strong speckle while a segmentation of the SAR image is performed. The speckle can make visual interpretation more hazardous and create interclass confusion.

Researchers have developed several segmentation tools useful with SAR images. Watershed transformation, developed by Li *et al.* (1999), is a hierarchical segmentation algorithm appropriate for land use applications, particularly when the land cover types are made up of individual plots. Benié and Thompson (1992) demonstrated a modified approach to hierarchical image segmentation by step-wise optimization. In order to distinguish the homogeneous objects of the image, this method uses local similarity rules. These rules are based on neighbouring pixels or segments and allow the creation of new entities. The results show that this technique is appropriate for the discrimination of crops on the images. In 2001, Allen *et al.* conducted a research on the geometric snakes method. Their paper demonstrated the applicability of level-based snakes for contour segmentation in SAR images. The detection of edges is usually a problem in SAR images and this level-based snakes technique is an attractive alternative.

According to Tilton (2000), there are three approaches to image segmentation. The first, *characteristic feature thresholding or clustering,* does not consider spatial information. Therefore, it is usually not effective for segmentation. The second, *boundary and detection*, incorporates spatial information into the analysis. This approach examines the edges present in the image. This technique is good if there is no noise on the image. If there is noise, some edges will be missing and extra edges will be detected. This will produce a set of non-connected curves around the connected region. The last, *region growing*, is the one of the most popular approaches because it takes into account spatial information and it guarantees that the set of curves around the region will be connected. However, even this type of image segmentation has some problems, such as when the regions have similar backscatter values but, being spatially disjointed, are not associated. Another approach has been developed to resolve the problem, *hybrid region growing and spectral clustering* (Tilton, 2000; Tilton and Lawrence, 2000; Tilton, 1998); in this research, using radar images, it would be *backscatter clustering*. This approach takes into consideration regions with similar backscatter values that are spatially disjointed, and detects the natural convergence points. The segmentation result contains the combination of each region labelling maps that have been produced at each natural convergence point.

In this project, the segmentation-based classification was performed using eCognition software (Definiens Imaging, 2003). With this program, input images are "*...classified based on parcels of pixels known as objects that are created using a segmentation routine...*" (Kaya et al., 2002, p.2). This segmentation routine extracts homogeneous regions, like water bodies or urban areas, which have similar brightness values and shape (Definiens Imaging, 2003; Kaya, 2002). This technique allows a

weighting between brightness and shape heterogeneity of the features to be segmented, minimizing the average heterogeneity of the image objects (Definiens Imaging, 2003).

5.3 Summary

This chapter is based on a literature review, and describes the methodology followed in the project to obtain a good classification result of the major land cover types of interest, inland shrimp ponds, and other land use activities. Radiometric and geometric correction were first explained, followed by each of the pre-processing techniques applied to the images: principal component analysis, speckle filtering analysis and a texture analysis. Secondly, the different classification techniques were explicated, according to the pixel-based and segmentation-based classifiers. All the classes were also mentioned and situated on one of the RADARSAT-1 images used for the classification. The next chapter will present and discuss the results of this project.

CHAPTER SIX

RESULTS AND DISCUSSION

6.1 Analysis of Raw Imagery

The first step of the analysis was to look at the raw images, radiometrically and geometrically corrected, individually and in false colour combination (RGB: Red, Green and Blue). Then, unsupervised classification, using the k-means method, was run in order to give a rough idea of which image combinations, multi-temporal or multi-angle, might produce better results.

6.1.1 RGB Combination

Looking at the images individually, it appeared that images with a shallower incidence angle, F4 (May 7, July 18) and F5 (September 19), had a greater potential for identifying water bodies. These images showed better contrast between water bodies and land features (Figure 6.1 a). At these angles, the water surface became more specular and less signal was returned to the sensor, resulting in black areas (CSA, 2000). The images with a steeper angle (F1), May 24 and July 11, were more influenced by the roughness of the water and reflected more signals back to the sensor. This explains why the brighter pixels are situated in water areas (noise), such as the Pang Pakong River, water reservoirs and shrimp farms.

RGB combination of multi-temporal images with a shallow angle (F4 and F5) allow for a very good identification of water bodies because of their low backscattering

signal and their very small variation within the time of acquisition, resulting in black regions even on false colour image combinations (Figure 6.1 and Table 6.1).

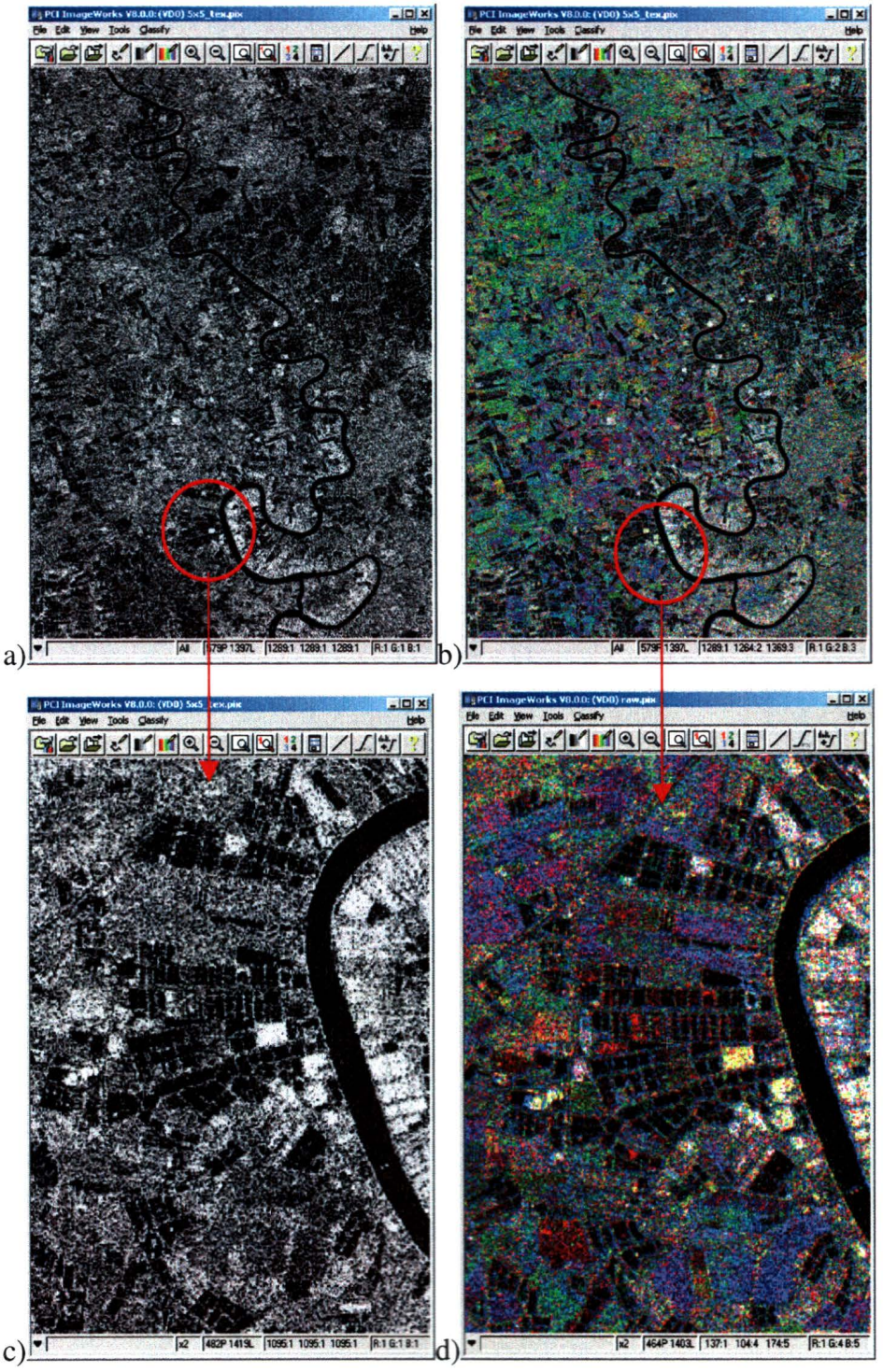

Figure 6.1 a) Raw image May 7, 2001, F4 b) RBG combination of 3 images F4 and F5 (Red: May 7 (F4), Green: July 18 (F4), and Blue: September 19 (F5) c) Zoom of the raw image May 7, 2001, F4 d) Zoom of the RGB combination

The human settlement areas have a very high backscattering signal in all of the images, so they are represented on the RGB combination as very bright pixels (white and light yellow). The orchard plantations have confused and no coherent backscatter patterns, and result in a mixed colour tone (area in the lower right of the image, Figure 6.1b). Fruit trees seem to be heterogeneous reflectors. The rice fields are represented by different bright colours on the RGB image. This can be explained by the fact that rice fields change over the period of time the image was taken. The fields are the colour of the channel (red, green or blue) of when they are dry (late growing stage). For example, the red areas on the image represent dry rice fields (harvested, or late growing stage) on May 7 (Image load on the first channel: Red composite), and flooded on July 18 and September 19. If the field is dry on two images, then the resulting colour on the RGB is a mix of these two images in false colour. For example, if a field is dry on May 7 and September 19, and flooded on July 18, then the resulting colour of the field in the RGB combination will be purple (mix of red: false colour for May 7, and Blue: false colour for September 19). See Table 6.1 for the complete legend of the RGB combinations of Figure 6.1.

Table 6.1 Colours for land use in the RGB image combination of the F4 and F5 images illustrated in Figure 6.1

Land Types	Colour	Date (Under water)
All water bodies	Black	All dates
Orchard	Mixed colour	None
Human	White	None
	Light Yellow	None
Rice	Red	July18 / Sept19
	Blue	May7 / July18
	Green	May7 / Sept19
	Turquoise	May7
	Purple	July18
	Dark Yellow	Sept19

6.1.2 Unsupervised Classifications (k-means)

In order to compare the information contained in different images, unsupervised classifications were run on multi-date and multi-angle image combinations. The multi-date image combinations were only composed of images with shallow incidence angle (F4: May 7 and July 18, and F5: September 19), or with steep incidence angle (F1: May 24 and July 11). The multi-angle combination combined images taken on dates very close together, but with different incidence angles (F1: July11 and F4: July 18). In this preliminary analysis, the F4 and F5 multi-temporal combination demonstrated their potential to classify the features present in the image. It also demonstrated that these three images could give results similar to an analysis run with all five images, reaching the goal of the best classification using few images as possible.

It is important to compare the results of the unsupervised classification with the same number of classes. Because no speckle filtering or texture analysis has been performed on the images at this stage, a larger number of classes are necessary in order to identify the desired feature. When there is less speckle and noise present on the images, fewer classes are necessary and it is possible to obtain enhanced results. What is important, is to compare different image combinations with the same number of classes. The first unsupervised classification was run on the five images, in order to see all the information contained in all the images. Using the same number of classes (16) and the same number of iterations (16), the unsupervised classification was run on the multi-date images with shallow and steep angle, and then on the multi-angle images. The visual results demonstrated that the multi-date combination of images with shallow angle is very similar to the classification runs with all the images (Figure 6.2 a and b). The two other

multi-date (F1) and multi-angle (F1 and F4) combinations did not generate usable visual results (Figure 62 c and d).

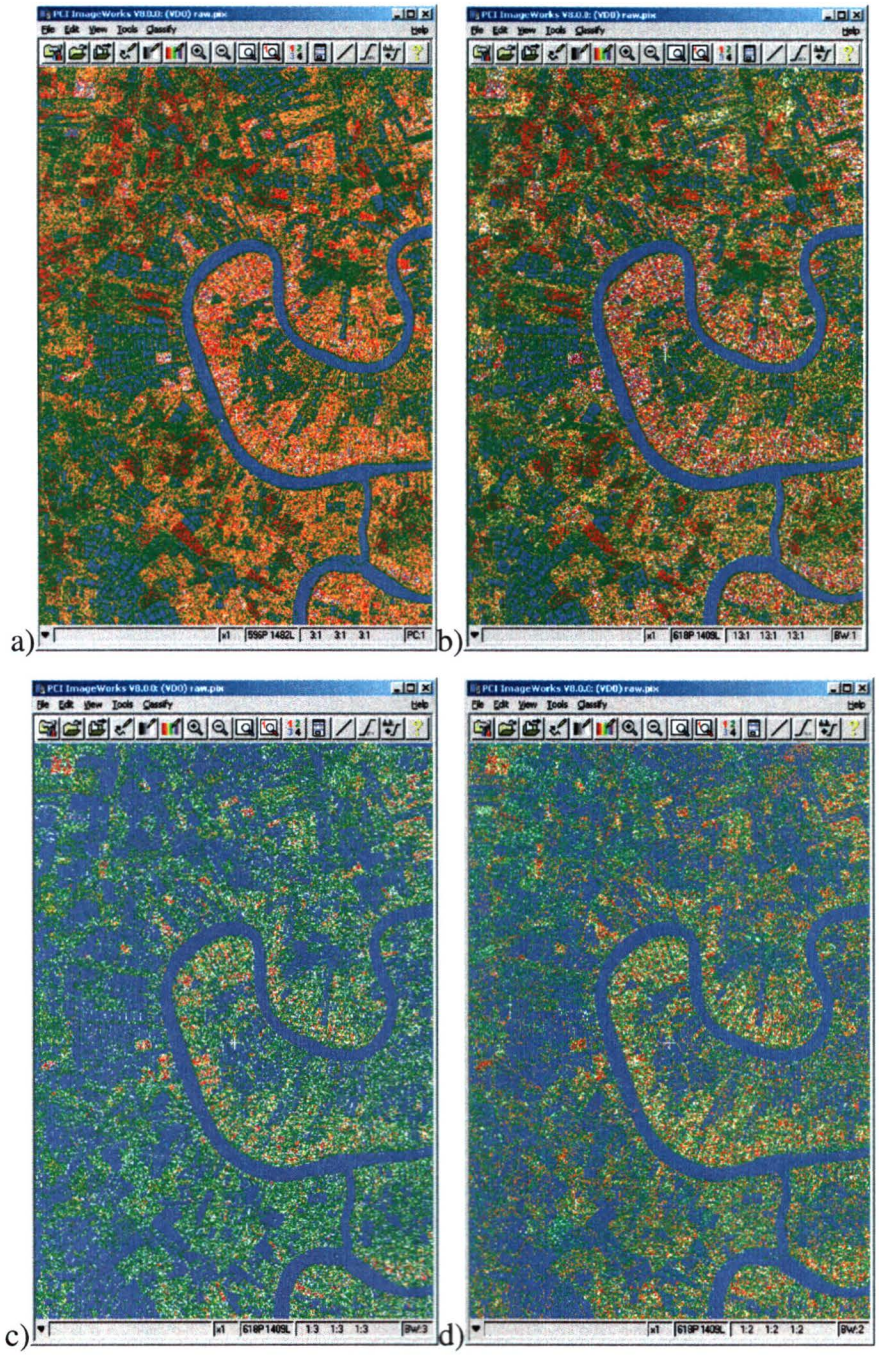

Figure 6.2 a) Unsupervised classification a) of all 5 images b) of multi-temporal combination (3 images F4 and F5, 16 classes) c) of multi-angle combination (2 images F1, July 11, and F4, July 18, 16 classes) d) of multi-temporal combination (2 images F1, 16 classes)

In the classification result of the F4 and F5 images, the shrimp ponds are well defined, as well as other water bodies like the Bang Pakong River (Figure 6.3 and Table 6.2). The dykes surrounding the shrimp ponds are also well defined. They are identified as rice paddies (green pixels) because of their higher backscattered signal. The rice paddies appear in either red or green, and are distinct from the orchards, and human settlements. These last two classes are however, a little run together; the orchards are represented by mostly pink and orange pixels, and the human settlements are represented by an amalgam of pink, white, orange, purple, etc pixels. In general, the orchard plantations seem to be represented by a more orange tone, and the human settlement areas by a pinker tone.

Figure 6.3 a) Zoom of the RGB combination of the 3 F4 and F5 images b) Zoom of the unsupervised classification of MULTIDATE combination (3 images F4 and F5, 16 classes)

Table 6.2 Colours of the land use of the three unsupervised classifications with 16 classes (principal four classes identified in the legend) illustrated in Figure 6.1.

Land Types	b) *Multi-angle* F1 (July 11) & F4 (July 18)	c) *Multi-temporal* F1 (May 24 & July 11)	d) *Multi-temporal* F4 (May 7), F4 (July 18) & F5 (September 19)
Water	Blue	Blue	Blue
Rice	Blue and mixed greens	Blue and mixed greens	Red or green
Orchard	Mixed greens	Mixed greens	Mixed green, orange, yellow and red (orange tone)
Human	Mixed green and yellow (green tone)	Mixed green and yellow (yellow tone)	Mixed white, purple and red (pink tone)

6.1.3 Summary

The results of the visual evaluation of the radiometrically and geometrically corrected images can be summarized as follows:

- The RGB combination of the multi-temporal images May7 (F4), July 18 (F4) and September 19 (F5), clearly show the features present in the area, which are rice paddies, orchard plantations, human settlements, shrimp farms and water bodies (river, water reservoirs, etc).
- This false colour image clearly shows the extent of shrimp farms in this region.
- The unsupervised classification using the k-means clustering method demonstrates the efficacy of the multi-temporal F4 and F5 images compared to the other multi-temporal F1 or multi-angle F1 and F4 image combinations
- The results of this classification visibly illustrate the water bodies and the rice paddies. However, the orchard plantations and the human settlements were confused together.

- This preliminary analysis demonstrates that the use of multi-temporal F4 and F5 image combinations can substitute for the use of all 5 images for k-means classifications.

6.2 Pixel-Based Classifications

In order to apply a pixel-based classification, like MLC (Maximum Likelihood Classification), three types of pre-processing were applied separately on the radiometrically and geometrically corrected images. The following sections will thus review all the methods used in order to obtain the best average and overall accuracy in a classification. The image combinations used for the MLC were the same as the ones used for the unsupervised classification k-means used in the previous section, which are:

- Multi-temporal (same incidence angle, different dates), 2 possibilities:
  -Shallow incidence angle:
  May 7 (F4), July 18 (F4) and September 19 (F5).
  -Steep incidence angle:
  May 24 (F1) and July 11 (F1)

- Multi-angle (different incidence angles, similar dates), 1 possibility:
  -Steep and shallow incidence angles together with similar dates:
  July11 (F1) and July 18 (F4)

The purpose of this section is to demonstrate the results, presenting the pre-processing techniques that generate the best classification accuracy with particular image combinations, and to discuss each of the methods used. The research methodology is illustrated with a schematic model in Appendix 1.

6.2.1 Assessment of Principal Components Analysis (PCA)

A principal component analysis was first applied on all five images in order to see if there was any temporal change over the whole period when the images were taken during the summer of 2001. Then, only the multi-temporal combination of images F4 (May 7 and July 18) and F5 (September 19) were used. The resulting components of this last PCA were then used as input channels to a MLC employing the first set of training sites.

6.2.1.1 Results of the Principal Component Analysis (PCA)

The first PCA was run using all five RADARSAT-1 images available for this project. Figure 6.4 displays the first three resulting components and Table 6.3 explains the statistics of the results. The first component illustrates the features with a low backscattering signal that did not change over the whole period of time like water reservoirs, shrimp ponds and the Bang Pakong River in white. The black pixels represent features with a high backscattering signal, such as human settlements, that did not change over time either. Rice paddies are represented by salt and pepper pixels signifying their change over time. The orchard plantations are also represented by salt and pepper pixels probably because of their variable backscattering signals on each image. This grainy pixel colour could also correspond to noise present in the input images. In the second principal component, white pixels seem to still symbolize the areas (water bodies) that did not change over time. However, looking at each input image, even the new shrimp ponds that occur at later dates are included in this colour category, while they should be included in the black colour pixel category, representing in this component the areas that change over time, like rice paddies. The orchards still correspond to salt and pepper areas, which could

still include noise. Darker grey pixels appear to represent the human areas, but also some rice paddies. In the third component, as well as in the fourth and the fifth, the information is less significant than in the previous components. These components are showing a larger number of grey pixels, at this point representing areas that did not change over time (some shrimp ponds), but also areas that did change (rice paddies) as well as noise.

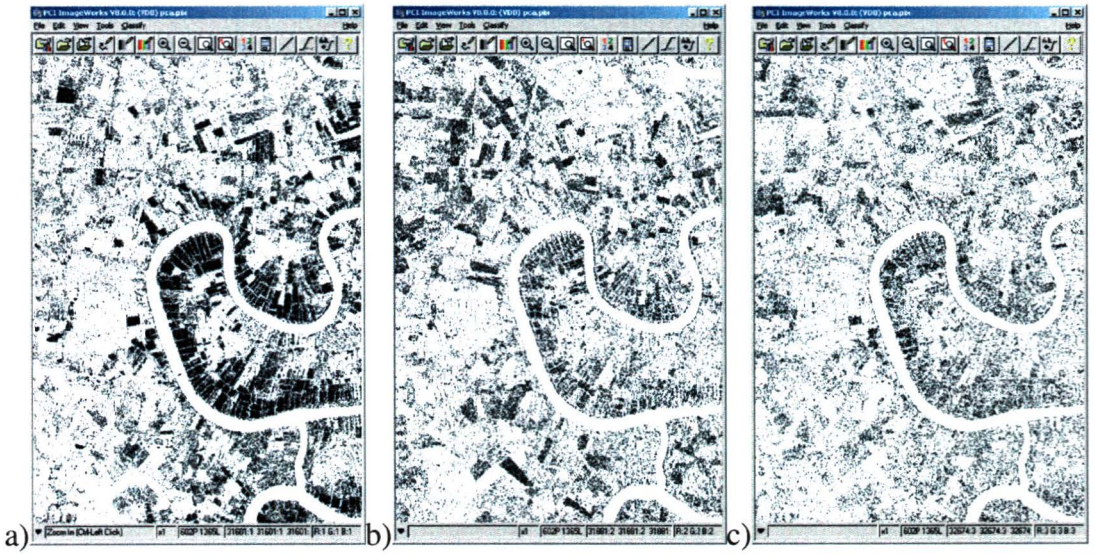

Figure 6.4 The first three components of the Principal Component Analysis (PCA) for the five original images.

The first eigenchannel only explains 43.88% of the variance, meaning that the images are not highly correlated. According to the theory, highly correlated images usually explain more than 70% of the variance (Torma and Koskinen, 1997; Bonn and Rochon, 1996; Holecz *et al.,* 1993). The PCA using all five images does not demonstrate a very useful result for further processing steps. This analysis is useful for eliminating redundancy in highly correlated images, that *"... appear similar and convey essentially the same information*" (Lillesand and Kiefer, 1987, p.655).

Table 6.3 Statistics from the first PCA with all five images (see first three components in figure 6.4)

Eigenchannel	Eigenvalue	Deviation	%Variance
1	0.8121937E+07	0.2849901E+04	**43.88%**
2	0.3693464E+07	0.1921839E+04	19.95%
3	0.2630090E+07	0.1621755E+04	14.21%
4	0.2400362E+07	0.1549310E+04	12.97%
5	0.1663934E+07	0.1289936E+04	8.99%

In the case of this project, the images seem not to be highly correlated (low variance explained by the first component), so this could mean that it would be better to use the original images, instead of the principal components. However, a second PCA was performed using only the multi-temporal combination of three F4 and F5 images, in order to apply a supervised classification and verify the accuracy of the results. This combination was chosen for three specific reasons. Firstly, because the other multi-temporal (F1) and multi-angle (F1 and F4) combinations were only combining two images, and a larger number of images is better in a PCA to extract the most information possible from the input images and to explain a greater percentage of the variance in the resulting components. Secondly, this mutli-temporal group of images covers the whole period of time (earliest image: May7 and latest image: September 19) when all five images were taken, so it is a good representation of the overall temporal change. Finally, this combination was chosen because, in the previous section, the preliminary analysis on the raw imagery proved that the use of the F4 and F5 images only could replace all five images. Figure 6.5 presents the three resulting components of the PCA performed on the three F4 and F5 images, and Table 6.4 explains the statistics of the results.

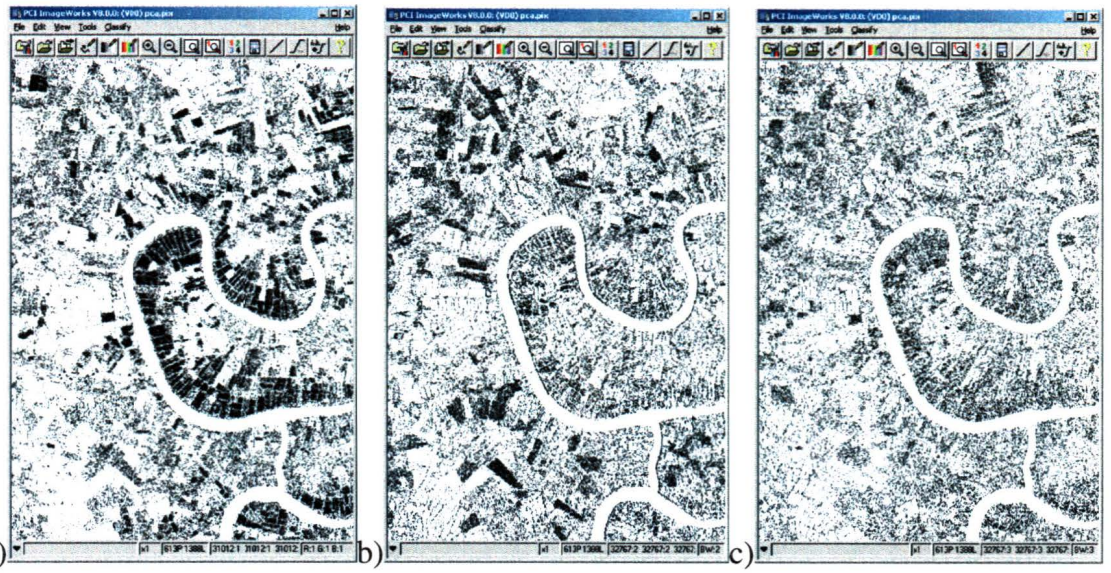

Figure 6.5 The three resulting components of the principal component analysis (PCA) of the three F4 and F5 input images.

The resulting components of this second principal component analysis demonstrated a result similar to the analysis run on all the RADARSAT-1 imagery. The first and second component pixel colour represents the same features as in the first PCA, and the third also mostly represents noise. This analysis explained 48.85% of the variance compare to 43.88% in the first PCA, which is almost the same but a little bit higher, probably because fewer input images include less noise but are also less useful for temporal information. This is another reason why these three images are a good compromise between using all the images or only two (multi-temporal with F1 or multi-angle with F1 and F4).

Table 6.4 Statistics from the second PCA with three F4 and F5 input images (see 3 components in figure 6.5)

Eigenchannel	Eigenvalue	Deviation	%Variance
1	0.4861951E+07	0.2204983E+04	**48.85%**
2	0.3391296E+07	0.1841547E+04	34.07%
3	0.1700099E+07	0.1303878E+04	17.08%

6.2.1.2 Supervised Maximum Likelihood Classification (MLC) with Principal Component Analysis (PCA) Results

Only the three components of the PCA using the three F4 and F5 images as input were employed to perform supervised maximum likelihood classifications. Two classifications were performed using the first set of training sites. The first employed the shrimp pond class with the classes of rice, human, orchard and water; and the second employed the shrimp farm class instead of the shrimp pond one. The results of both classifications were poor, with respective overall accuracy of 37.91% and 40.40% (Table 6.5).

Table 6.5 Confusion matrix of the MLC using three PCA from F4 and F5 images a) 1st set of training sites with shrimp pond class b) 2nd set of training sites with shrimp farm class

a)

Name	Code	Pixels	NULL	Water	Shrimp	Rice	Human	Orchards
Water	1	2100	0	**96.48**	3.05	0.48	0	0
Shrimp	2	2263	0.22	63.01	**30.14**	5.83	0.04	0.75
Rice	3	5989	1.65	0.45	30.86	**56.4**	2.22	8.42
Human	4	3222	3.72	2.02	33.64	43.6	**4.53**	12.45
Orchards	5	4749	3.92	0.19	24.3	52	4.53	**15.06**
Average accuracy = 40.52 %								
Overall accuracy = 37.91 %								

b)

Name	Code	Pixels	NULL	Water	Farm	Rice	Human	Orchards
Water	1	2100	0	**96.48**	3.38	0.14	0	0
Farm	2	11983	1.08	32.45	**53.43**	9.15	0.98	2.92
Rice	3	5989	1.65	0.45	42.81	**45.8**	2.22	7.08
Human	4	3222	3.72	2.02	55.09	24.3	**4.53**	10.37
Orchards	5	4749	3.92	0.19	46.26	33	4.53	**12.11**
Average accuracy = 42.46 %								
Overall accuracy = 42.40 %								

In both classifications, the resulting images of shrimp farms and shrimp ponds, rice paddies, orchard plantations, as well as human settlements were totally confused together

statistically and visually. However, the water class was well identified, showing the shrimp ponds, the water reservoirs and the Bang Pakong River. In both classification results, the shrimp farm and shrimp pond classes were visually confused with the water class, probably because both of these training site groups included some water pixels, and statistically confused with rice paddies, because they both included some land pixels.

6.2.1.3 Summary

The results of the principal component analysis (PCA) on the radiometrically and geometrically corrected images prior to a supervised maximum likelihood classification (MLC), can be summarized as follows:

- PCA using as input a multi-temporal combination of F4 (May 7 and July 18) and F5 (September 19) images produces similar resulting principal components as the PCA using all five available images as input.
- The resulting principal components of the multi-temporal image combination do not demonstrate useful information concerning the different features present in the study area.
- The overall and the average accuracies of the two classifications run on the resulting components of the multi-temporal image combination, using the first set of training sites, are not significant (overall accuracies of 37.91% with the shrimp ponds class, and 42.40% with the shrimp farm class)
- Principal component analysis does not seem to be a useful technique applied to raw images in order to perform a supervised maximum likelihood classification and obtain accurate results.

6.2.2 Adaptive Filtering

It is important to apply proper speckle filtering onto the raw images in order to augment the accuracy of the classification results. To choose the most suitable one, different filters have to be visually and statistically compared and evaluated. In this section, it is demonstrated why the Frost filter was applied onto the raw images as a pre-processing step prior to further analysis. Then, unsupervised classifications, using the k-means method, were performed on multi-angle and multi-temporal filtered image combinations, in order to verify which combinations generate a classified image with superior feature differentiation. Finally, supervised maximum likelihood classifications were applied on the same multi-angle and multi-temporal image combinations as the unsupervised classification. The first set of training sites was tested, as well as the second set. For each set of training sites, classifications were run using either the shrimp pond or the shrimp farm classes, and for the second set, the class representing all the water bodies (*allwater*) was also tested.

6.2.2.1 Choice of the Appropriate Filter

With the aim of choosing the most appropriate speckle filter to apply on the raw images, six typical radar images filters were tested: Frost, Enhanced Frost, Lee, Enhanced Lee, Gamma and Kuan. All the filters were applied on one image, May7, 2001 (F4), and the mean, as well as the standard deviation, were compared with the one of the raw image (Table 6.6 and Figure 6.6). The objective of the filter is to keep the mean as close as possible of the raw image mean, and to have the lowest standard deviation value.

The Frost filter was chosen over the other filters because of three reasons. Firstly, according to the statistics (Table 6.6), the mean of the Frost filtered image is the second

lowest after the Kuan filter. A third decimal was added to the mean values of the Frost and enhanced Frost filter to show that the Frost mean is actually lower than the enhanced Frost mean. However, the Kuan filter has a very high standard deviation value compared to the Frost filter, which is second lowest after the enhanced Lee filter. The Frost filter was chosen because statistically, its mean is the second closest to that of the raw image, and its standard deviation is the second lowest.

Table 6.6 Mean and Standard Deviation of the raw and filtered images of May7, 2001

	Values in Intensity (16 bit unsigned)		Values in Decibels (32 bit real)	
Image of May7, 2001	**Mean**	**Standard Deviation**	**Mean**	**Standard Deviation**
Raw image	**1085.67**	**1551.70**	**-9.64**	**8.09**
FROST	1069.12	1084.53	***-9.710***	***9.65***
ENHANCED FROST	1066.94	1044.16	-9.72	9.81
LEE	1068.80	1042.38	***-9.711***	9.82
ENHANCED LEE	1062.21	1096.87	-9.74	***9.60***
GAMMA	1040.20	1058.28	-9.83	9.75
KUAN	1077.01	996.81	***-9.68***	10.01

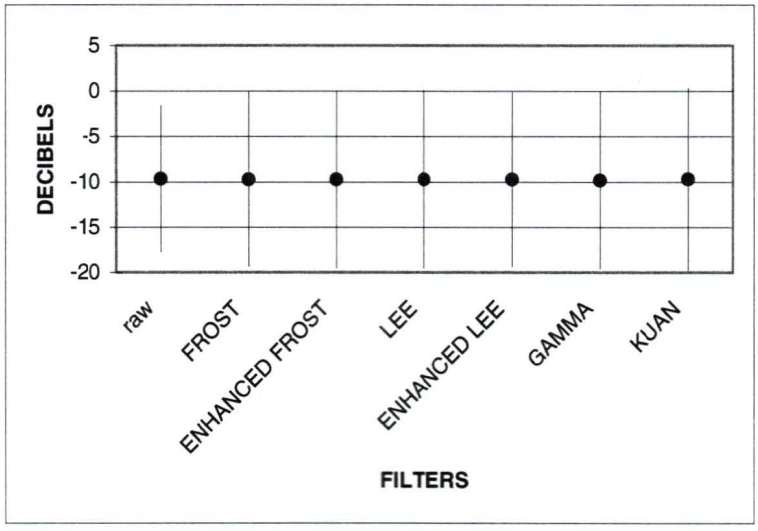

Figure 6.6 Mean and Standard Deviation in decibels of the filtered image of May7, 2001

Secondly, according to the visual evaluation of all the resulting images where speckle filters were applied, the Frost filter seems to generate the best result (Figure 6.7). This filter appears to retain more details in smoothing the edge of the shrimp ponds (the smallest features in the image) without losing the presence of the dykes surrounding each pond, in other words, without merging the ponds together. Visually, the shrimp pond edges seem to be better preserved with this filter than with the others.

a) b)

Figure 6.7 a) Original F4 image of May 7, 2001 b) One application of Frost filter 3x3

Finally, this filter was selected because of the results of significant previous research done by Travaglia *et al.* (1999). In their research, they tested Frost and Lee filters on SAR images to detect shrimp farms in Sri Lanka. They chose the Frost filter with the smallest window size "*because the smallest shrimp ponds were visible only after the passage of that filter*" (part 3, p.2). In this present study, the smallest window size (3x3) was used as well, in order to preserve as much information as possible regarding the shrimp farm and dykes pixels. According to Travaglia *et al* (1999), the Frost filter "*...adapts the local statistics of the image to preserve edges and small features...*" (part

3, p.1), which is the filter application's goal in the present case study about inland shrimp farms.

6.2.2.2 Unsupervised Classifications (k-means)

Unsupervised classifications were performed on multi-temporal image combinations, with shallow (F4 and F5) or steep (F1) angles, as well as on multi-angle image combinations (F1 and F4). A large number of classes were still required even if a filter had been previously applied to the input images. The three resulting classifications, each of 16 classes, were compared to each other and happened to be similar. However, the best seemed to be the multi-temporal one using the three images with shallower angle (F4 and F5). In that one, display of Figure 6.8 b), the water bodies (blue pixels), particularly the shrimp ponds were very clearly identified. In that classification result, the rice paddies (green pixels) and orchard plantations (orange pixels) were confused together, and the human settlements were represented by a blend of many classes (red, orange and pink pixels). A second unsupervised classification was run on the same multi-temporal combination but using eight classes (Figure 6.8 c)). The result demonstrates that the shrimp ponds were well identified (even showing the dykes between them), and the human settlement areas as well. However, the rice paddies and orchards were confused.

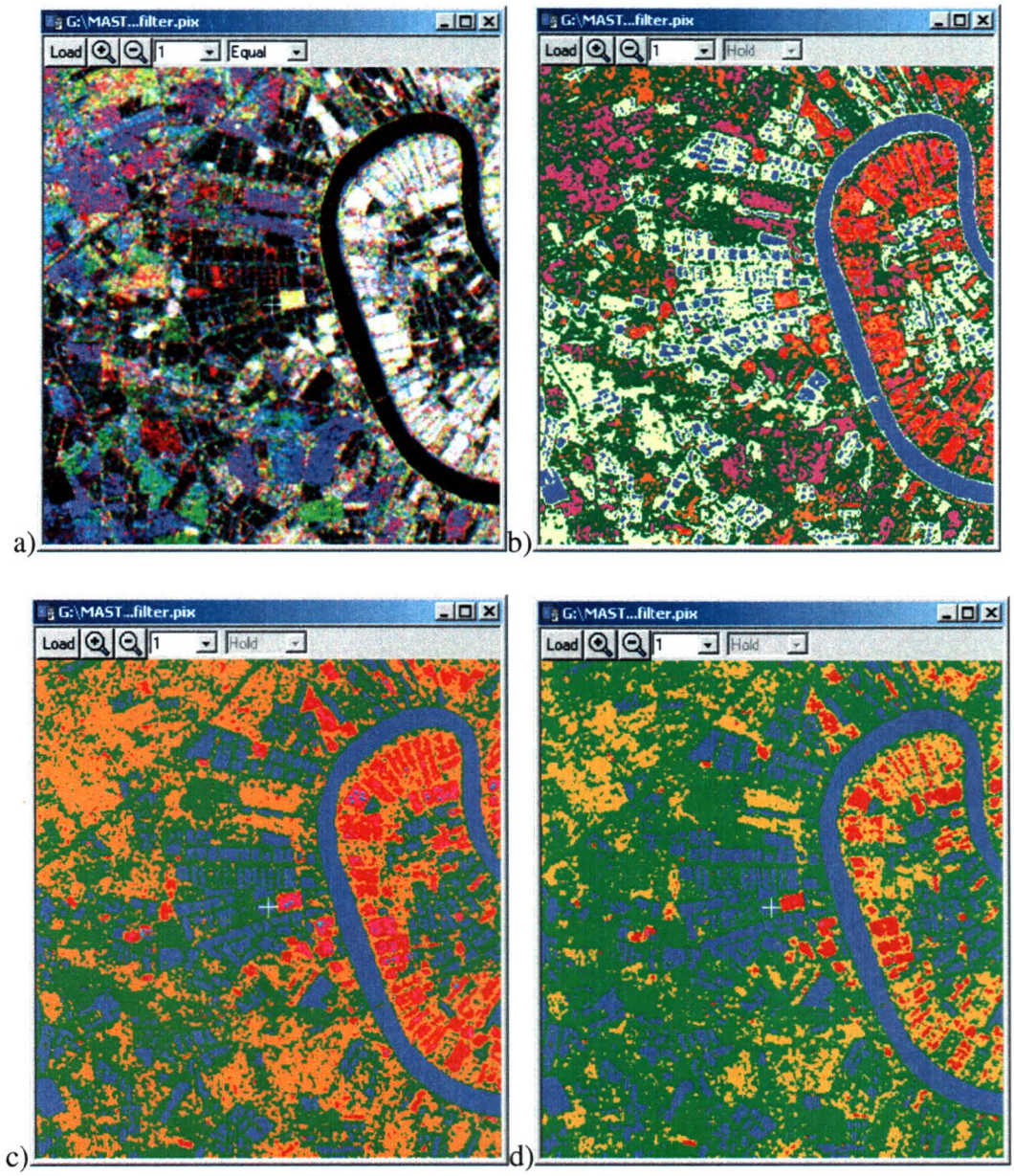

Figure 6.8 a) RGB combination of the 3 Frost filtered F4F5 images b) unsupervised classification with 3 multi-temporal Frost F4 and F5 images (May 7, July 18, and September 19) using 16 classes c) using 8 classes d) using 5 classes

Table 6.7 Legend of Figure 6.8

Land Types	a) RGB multitemporal F4 and F5	b) k-means with multitemporal F4 and F5 (16 classes)	c) k-means with multitemporal F4 and F5 (8 classes)	d) k-means with multitemporal F4 and F5 (5classes)
Water (reservoirs, Shrimp ponds, river)	Black	Blue	Blue	Blue
Dykes (also dry soil)	Green or mixed pixels	Beige	Green	Green
Orchards Plantations	Pinkish amalgam of pixels	Green	Orange and Green	Orange and Green
Rice paddies	Purple, Blue, Red and green square areas	Pink, orange, and also green in some areas (depending on when the field is under water in which image)	Green and Orange	Green and Orange
Human settlements	White and light yellow	Areas with a mix of pink, red and orange	Red, Pink and light turquoise	Red and Orange

A last unsupervised classification was performed with only five classes (Figure 6.8d). The shrimp ponds were still very well identified, the orchard and rice paddies were confused, and the orchard class was also present in human settlement areas. The RGB combination of the Frost filtered F4 and F5 images, as well as the classifications using the same images with 16, eight and five classes, are illustrated in Figure 6.8 and the classification legends are presented in Table 6.7.

6.2.2.3 Supervised Maximum Likelihood Classifications (MLC)

Supervised maximum likelihood classifications (MLC) were performed on the same multi-temporal and multi-angle image combinations as for the unsupervised k-

means classifications. Two sets of training sites were used. In the first, all the classifications (Tables 6.8 and 6.9) were not very significant with a maximum overall accuracy of 55.35%. This result was obtained with the farm class using the multi-temporal combination of shallower angle images as input for the classification (Figure 6.9 and Table 6.9). All the other classifications using the shrimp class or other image combinations had lower overall accuracy results.

Table 6.8 Confusion matrix of the MLC using Frost images with the shrimp pond (shrimp) class of the 1st set of training sites a) Multi-temporal combination of F4 and F5 images b) Multi-temporal combination of F1 images c) Multi-angle combination of F1 and F4 images

a)

Name	Code	Pixels	NULL	Shrimp	Water	Rice	Human	Orchard
Shrimp	1	2263	0.13	**45.78**	48.08	4.95	0.57	0.49
Water	2	2100	0	3.24	**96.43**	0.33	0	0
Rice	3	5989	0.13	9.78	0	**81.02**	2.35	6.71
Human	4	3222	3.72	12.1	0.19	59.87	**6.58**	17.54
Orchard	5	4749	2.36	3.26	0	69.59	4.61	**20.17**
Average accuracy = 50.00 % Overall accuracy = 49.57 %								

b)

Name	Code	Pixels	NULL	Shrimp	Water	Rice	Human	Orchard
Shrimp	1	2263	0.13	**40.96**	54.79	3.09	0.53	0.49
Water	2	2100	0	3.29	**96.43**	0.19	0	0.1
Rice	3	5989	0.1	11.39	0	**78.03**	2.74	7.75
Human	4	3222	3.04	16.98	0.37	61.92	**7.01**	10.68
Orchard	5	4749	1.07	8.82	0	72.16	5.5	**12.44**
Average accuracy = 46.98 % Overall accuracy = 46.07 %								

c)

Name	Code	Pixels	NULL	Shrimp	Water	Rice	Human	Orchard
Shrimp	1	2263	0.31	**35.09**	61.38	1.15	0.31	1.77
Water	2	2100	0	4.81	**94.95**	0.1	0	0.14
Rice	3	5989	0.13	12.12	0.02	**69.58**	3.92	14.23
Human	4	3222	2.89	23.87	0.37	45.78	**7.7**	19.4
Orchard	5	4749	1.03	15.1	0	62.39	5.07	**16.4**
Average accuracy = 44.74 % Overall accuracy = 43.56 %								

Table 6.9 Confusion matrix of the MLC using Frost images with the shrimp farm (farm) class of the 1st set of training sites a) Multi-temporal combination of F4 and F5 images b) Multi-temporal combination of F1 images c) Multi-angle combination of F1 and F4 images

a)

Name	Code	Pixels	NULL	Farm	Water	Rice	Human	Orchard
Farm	1	11983	1.15	**65.96**	19.09	10.52	1.24	2.04
Water	2	2100	0	5.19	**94.81**	0	0	0
Rice	3	5989	1.14	12.67	0.05	**78.76**	1.65	5.73
Human	4	3222	3.63	34.61	0.09	44.91	**4.66**	12.1
Orchard	5	4749	3.37	19.81	0	56.58	4.21	**16.02**
Average accuracy = 52.04 % Overall accuracy = 55.35 %								

b)

Name	Code	Pixels	NULL	Farm	Water	Rice	Human	Orchard
Farm	1	11983	0.25	**58.08**	21.13	17.76	1.31	1.47
Water	2	2100	0	2.9	**96.95**	0.1	0	0.05
Rice	3	5989	0.1	17.26	0	**72.22**	2.74	7.68
Human	4	3222	3.04	21.69	0.56	57.11	**7.01**	10.58
Orchard	5	4749	1.07	13.64	0	67.45	5.5	**12.34**
Average accuracy = 49.32 % Overall accuracy = 50.40 %								

c)

Name	Code	Pixels	NULL	Farm	Water	Rice	Human	Orchard
Farm	1	11983	0.25	**64.22**	24.31	6.43	1.4	3.4
Water	2	2100	0	4.33	**95.67**	0	0	0
Rice	3	5989	0.13	23.79	0.03	**59.89**	3.92	12.22
Human	4	3222	2.89	42.95	0.5	32.59	**7.7**	13.38
Orchard	5	4749	1.03	34.28	0	46.89	5.07	**12.72**
Average accuracy = 48.04 % Overall accuracy = 50.43 %								

The classifications run with the second set of training sites, on the same image combinations and using the shrimp pond class give much better results with a maximum overall accuracy of 62.32% and 63.34%, obtained respectively with multi-temporal combinations of F4 and F5 images and F1 images ((Figure 6.9 and Table 6.12; Table 6.10).

Table 6.10 Confusion matrix of the MLC using Frost images with the shrimp pond (shrimp) class of the 2nd set of training sites a) Multi-temporal combination of F4 and F5 images b) Multi-temporal combination of F1 images c) Multi-angle combination of F1 and F4 images

a)

Name	Code	Pixels	NULL	Rice	Orchard	Human	Water	Shrimp
Rice	1	24307	1.41	**47.11**	45.69	5.79	0	0
Orchard	2	11708	0.17	8.35	**89.67**	1.81	0	0
Human	3	5794	6.8	9.04	25.08	**59.08**	0	0
Water	4	2891	0	0.55	0	0	**94.71**	4.74
Shrimp	5	1571	0	3.56	2.86	0	47.23	**46.34**
Average accuracy = 67.38 %								
Overall accuracy = 62.32 %								

b)

Name	Code	Pixels	NULL	Rice	Orchard	Human	Water	Shrimp
Rice	1	24307	0.37	**58.73**	29.82	4.43	3.61	3.04
Orchard	2	11708	0.23	10.46	**84.34**	4.53	0.4	0.03
Human	3	5794	4.06	3.23	41.03	**51.64**	0.05	0
Water	4	2891	0	3.67	0	0	**28.4**	67.93
Shrimp	5	1571	0	2.86	0.06	0	11.58	**85.49**
Average accuracy = 61.72 %								
Overall accuracy = 63.34 %								

c)

Name	Code	Pixels	NULL	Rice	Orchard	Human	Water	Shrimp
Rice	1	24307	0.19	**43.61**	36.24	9.55	2.62	7.8
Orchard	2	11708	0.21	10.33	**85.96**	3.43	0	0.08
Human	3	5794	4	13.86	35.36	**46.77**	0	0
Water	4	2891	0	1.56	0	0	**91.11**	7.33
Shrimp	5	1571	0	3.63	0	0	66.45	**29.92**
Average accuracy = 59.47 %								
Overall accuracy = 57.22 %								

The classifications run with the shrimp farm class as well give better results, higher than the ones using the shrimp pond class, with an overall accuracy of 66.70%, obtained with the multi-temporal combinations of F4 and F5 images (Figure 6.9 and Table 6.12; Table 6.11).

Table 6.11 Confusion matrix of the MLC using Frost images with the shrimp farm (farm) class of the 2nd set of training sites a) Multi-temporal combination of F4 and F5 images b) Multi-temporal combination of F1 images c) Multi-angle combination of F1 and F4 images

a)

Name	Code	Pixels	NULL	Rice	Orchard	Human	Water	Farm
Rice	1	24307	1.41	**44.89**	32.89	5.79	0	15.02
Orchard	2	11708	0.17	8.24	**81.17**	1.81	0	8.61
Human	3	5794	6.8	9.03	24.68	**59.08**	0	0.41
Water	4	2891	0	0	0	0	**95.5**	4.5
Farm	5	25663	0.38	3.11	8.3	0.8	8.18	**79.22**
Average accuracy = 71.97 %								
Overall accuracy = 66.70 %								

b)

Name	Code	Pixels	NULL	Rice	Orchard	Human	Water	Farm
Rice	1	24307	0.37	**40.21**	24.93	4.43	5.49	24.59
Orchard	2	11708	0.23	7.22	**79.11**	4.53	0.33	8.58
Human	3	5794	4.06	2.99	40.71	**51.64**	0.03	0.57
Water	4	2891	0	1.59	0	0	**95.57**	2.84
Farm	5	25663	0.39	5.74	11.25	1.26	49.92	**31.45**
Average accuracy = 59.60 %								
Overall accuracy = 46.70 %								

c)

Name	Code	Pixels	NULL	Rice	Orchard	Human	Water	Farm
Rice	1	24307	0.19	**19.87**	30.85	9.53	5.09	34.47
Orchard	2	11708	0.21	7.34	**75.5**	3.43	0.01	13.51
Human	3	5794	4	13.51	34.21	**46.77**	0	1.5
Water	4	2891	0	0	0	0	**97.09**	2.91
Farm	5	25663	0.3	1.4	10.6	1.26	22.86	**63.57**
Average accuracy = 60.56 %								
Overall accuracy = 50.46 %								

In this classified image, the human settlement class accuracy increased from 5 to 59%, the orchard plantation class increased from 16 to 81%, the rice class accuracy diminished from 79 to 45%, the water bodies class stayed the same at around 95%, and the farm class accuracy increased from 66 to 79%.

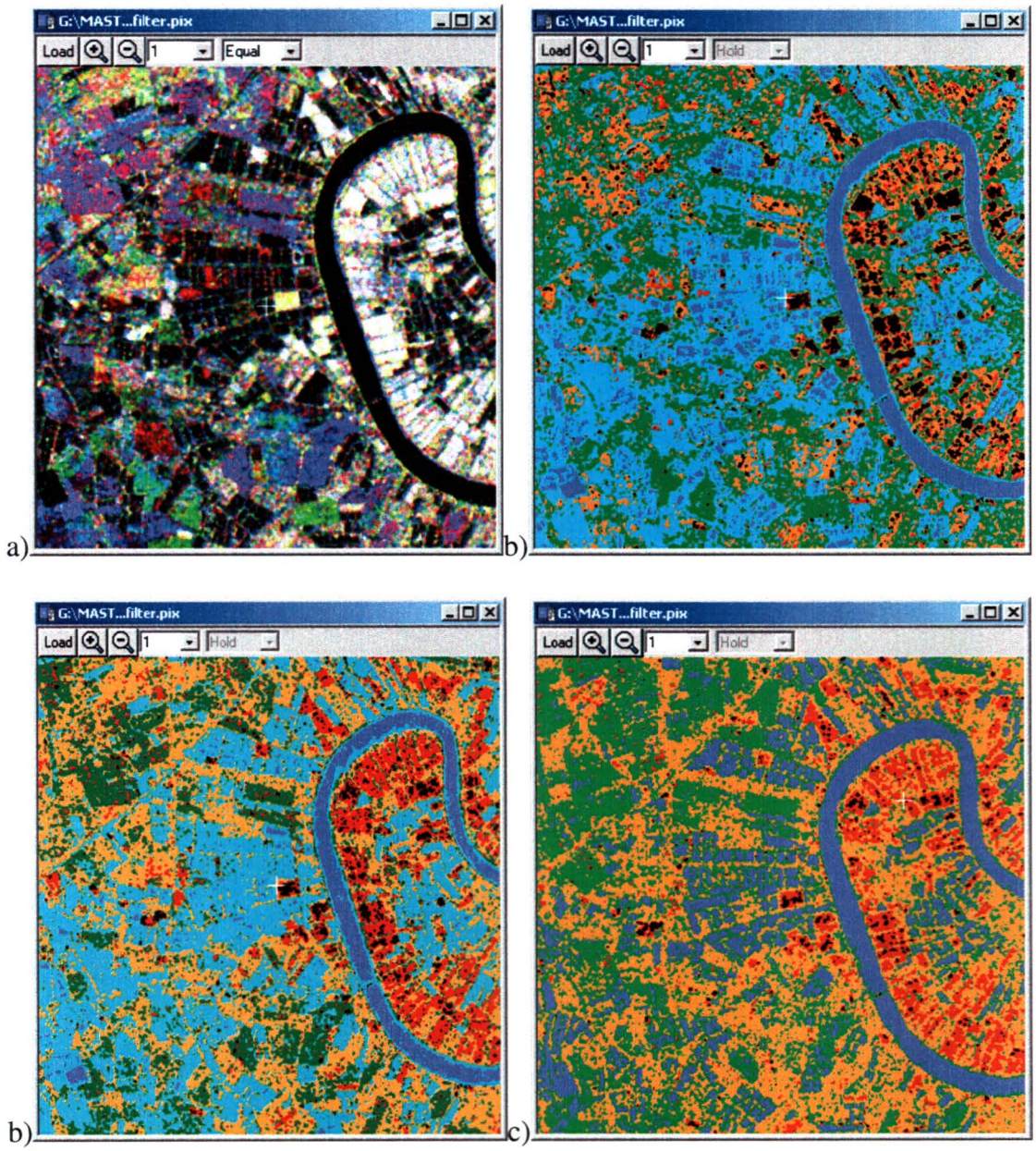

Figure 6.9 A) RGB combination of the 3 Frost filtered F4 and F5 images b) MLC with multi-temporal F4 and F5 images using the first set of training sites with shrimp farm class (farm) c) second set of training sites with shrimp farm class (farm) d) second set of training sites with *allwater* class

This second classification using the second set of training sites was more precise statistically. Except for the rice that was a little more confused with the orchard areas, and also with the shrimp farms (because of the dykes). Also, with this classification the

shrimp ponds were merged together and were representing the area covered by the whole farms area.

Table 6.12 Legend of the Figure 6.9

Land Types	a) RGB multi-temporal F4 and F5	b) MLC with multi-temporal F4 and F5 (1st set: farm class)	c) MLC with multi-temporal F4 and F5 (2nd set: farm class)	d) MLC with multi-temporal F4 and F5 (2nd set: *allwater* class)
Water (reservoirs, shrimp ponds, river)	Black	Blue	Blue	Blue
Shrimp Farm (ponds and dykes)	-	Turquoise	Turquoise	-
Orchards plantations	Pinkish amalgam of pixels	Orange	Orange	Orange
Rice paddies	Purple, Blue, Red and green square areas	Green	Green (and a little bit of orange)	Green
Human settlements	White and light yellow	Red	Red	Red

A third series of classifications was then run using only four classes, without trying to separate the shrimp farms from the other water bodies, but instead grouping all the water bodies together (*allwater class*) (Figures 6.9 and 6.10).

Table 6.13 Confusion matrix of the MLC using Frost images with the *allwater* class of the 2nd set of training sites a) Multi-temporal combination of F4 and F5 images b) Multi-temporal combination of F1 images c) Multi-angle combination of F1 and F4 images

a)

Name	Code	Pixels	NULL	Rice	Orchard	Human	*Allwater*
Rice	1	24307	1.41	**47.11**	45.69	5.79	0
Orchard	2	11708	0.17	8.35	**89.67**	1.81	0
Human	3	5794	6.8	9.04	25.08	**59.08**	0
Allwater	4	4268	0	3.02	3.07	0	**93.91**
Average accuracy = 72.44 %							
Overall accuracy = 63.76 %							

b)

Name	Code	Pixels	NULL	Rice	Orchard	Human	*Allwater*
Rice	1	24307	0.37	**59.1**	29.82	4.43	6.29
Orchard	2	11708	0.23	10.44	**84.34**	4.53	0.46
Human	3	5794	4.06	3.23	41.03	**51.64**	0.05
Allwater	4	4268	0	3.51	0.09	0	**96.39**
Average accuracy = 72.87 % Overall accuracy = 68.03 %							

c)

Name	Code	Pixels	NULL	Rice	Orchard	Human	*Allwater*
Rice	1	24307	0.19	**44.79**	36.24	9.55	9.24
Orchard	2	11708	0.21	10.37	**85.96**	3.43	0.03
Human	3	5794	4	13.86	35.36	**46.77**	0
Allwater	4	4268	0	3.44	0.05	0.02	**96.49**
Average accuracy = 68.50 % Overall accuracy = 60.29 %							

With this classification, 96% of the water pixels and 84% of the orchard plantations pixels were correctly classified. However, the rice paddies pixels, as well as the human settlements ones, were both confused with the orchard plantations pixels. Visually, it is also possible to see that the dykes surrounding the shrimp ponds are considered as rice paddies using this classification. Classifications using these four classes (rice, orchard, human and all water bodies) were performed on the three multi-date and multi-angle image combinations. The best result occurred with the use of multi-temporal combination of images with steeper angle (F1), with an overall accuracy of 68.03% (Figure 6.10 and Table 6.14; Table 6.13).

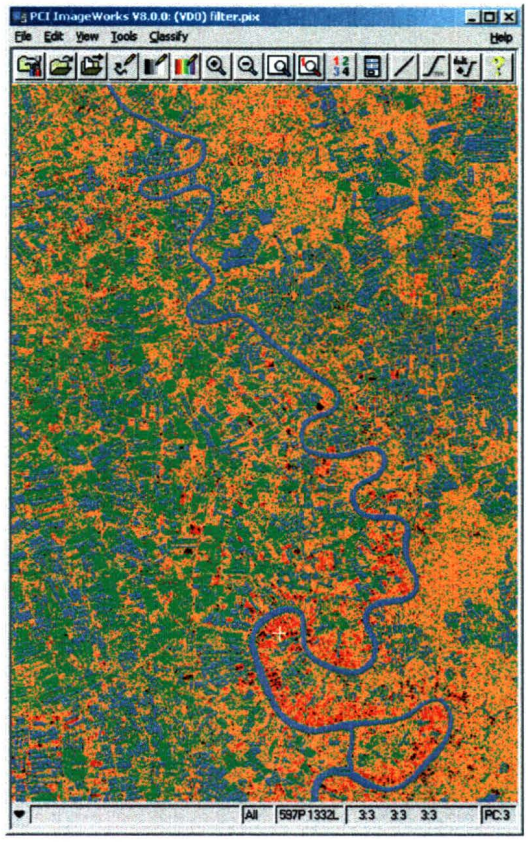

Figure 6.10 MLC with multi-temporal F1 images using the second set of training sites with *allwater* class

Table 6.14 Legend of MLC with multi-temporal F1 images using the second set of training sites with *allwater* class, Figure 6.10

Land Types	MLC with two Three Frost F4 and F5 images (2^{nd} set of training sites with *allwater*)
All water	Blue
Rice	Green
Orchard	Orange
Human	Red

6.2.2.4 Summary

The results of the speckle filtering on the radiometrically and geometrically corrected images, prior to an unsupervised classification (k-means) and supervised maximum likelihood classification (MLC), with two sets of training sites, can be summarized as follows:

- The Frost filter with a 3x3 window size is the best filter to use.
- **Unsupervised classification (k-means):**
    - Best results obtained with the multi-temporal image combination of shallower incidence angle (F4 and F5)
    - Better results than an unsupervised classification run on the raw images.
- **Supervised classification (MLC) using the first set of training sites:**
    - Good results obtained with the multi-temporal image combination of shallower incidence angle (F4 and F5), using the rice, orchard, human, water, and shrimp farm classes.
        - Overall accuracy: 55.35% (but still with lots of confusion)
- **Supervised classification (MLC) using the second set of training sites:**
    - Good results obtained with the multi-temporal image combination of shallower incidence angle (F4 and F5), using the rice, orchard, human, water, and shrimp farm classes.
        - Overall accuracy: 66.70% (good identification of the shrimp farm areas)
    - Best results of the speckle filtering analysis obtained with the multi-temporal image combination of steeper incidence angle (F1), using the rice, orchard, human, and *allwater* classes.
        - Overall accuracy: 68.03% (good identification of water bodies, and all other classes
- Summary Table of the average and overall accuracy of the MLC run on the Frost images (Table 6.15)

Table 6.15 Summary table of the average and overall accuracy of the MLC on Multi-temporal and Multi-angle Frost filtered image combinations (%)

Image Combinations	MLC with first set of training sites				MLC with second set of training sites					
	Shrimp		Farm		Shrimp		Farm		*Allwater*	
	Av. Acc.	Over. Acc.	Av. Acc.	Over. Acc.	Av. Acc.	Over. Acc.	Av. Acc.	Over. Acc.	Av. Acc.	Over. Acc.
Multi-temporal All F4 & F5	50.00	49.57	52.04	55.35	67.38	62.32	71.97	66.70	72.44	63.76
Multi-temporal All F1	46.98	46.07	49.32	50.40	61.72	63.34	59.60	46.70	72.87	68.03
Multi-angles July11 F1 & July18 F4	44.74	43.74	48.04	50.43	59.47	57.22	60.56	50.46	68.50	60.29

- The classification results using Frost filtered images are good, but further analyses, such as texture analysis, needed to be done in order to obtain better overall accuracy in results.

6.2.3 Texture Analysis

A texture analysis was executed on the radiometrically and geometrically corrected images. Firstly, the appropriate window size was determined testing the 3x3, 5x5 and 7x7 dimensions. Then, the correlation between all the texture components was evaluated in order to find which were the least correlated. Finally, a separability analysis of the signatures (first set of training sites), on all the texture components run on all the images, was performed in order to choose the components where the signatures were well separated, and which of the shrimp farm or shrimp pond signatures was the most appropriate to use.

Once these preliminary tests were performed on the texture components, k-means unsupervised classifications were run on the best mix of texture components but also on each best component (multi-date and multi-angle). Then, MLC were run with the same component combinations, only using the shrimp pond class, which was showing a greater potential of separability with the other classes in general. A second group of MLC was subsequently performed using the second set of training sites, testing the shrimp ponds class, as well as the ones for shrimp farm and the all water bodies, but only on the combinations that generated the best results with the first group of classifications. Finally, the reliability of the best classification results was tested using a set of accuracy sites.

6.2.3.1 Evaluation of the Texture Components

The evaluation of the texture components is dependent upon the choice of the window size, the evaluation of the correlation between all the texture components, and a separability analysis of the first set of training sites on all the texture components (generated from all the imagery available).

6.2.3.1.1 Choice of the Window Size

In order to choose the best window size for texture analysis, all eight GLCM texture components were generated from the F4 image of May 7, 2001, with these three window size: 3x3, 5x5 and 7x7. Then, the signatures of the first set of training sites were created on all these 24 components (8 texture components with 3 sizes of windows). The classes used were rice, human, orchard, water, shrimp farm and shrimp pond. The mean and the standard deviation of each signature for each of the texture components, with each window size, were compiled in a summary table (Appendix 4). Graphs for the

signatures' mean, as well as for their standard deviation, were then generated in order to compare how the signatures varied for each texture component with each different window size.

The standard deviation of each signature seems to be more influenced by the increase in window size: the bigger the window, the lower the standard deviation. On the other hand, the mean does not seem to be influenced by the variation of window size. So, according to this analysis, the biggest window size would be the best, keeping the same mean and reducing the standard deviation of all the classes. However, taking into account the smallest feature of the study area to be identified, shrimp farms, the smallest window needed to be used. As mentioned in the previous section of this chapter dealing with the choice of filter window, shrimp ponds are approximately 0.64 ha in size (6,400m², i.e. 80x80 meters and 8x8 pixels) (Flaherty *et al.*, 2000), so the window chosen needed to be as small as possible, in order to retain as much detail as possible concerning the farms and their surrounding dykes. As a compromise, the 5x5 window size was chosen as the most appropriate one, reducing the standard deviation while preserving the maximum amount of information on the shrimp farms.

6.2.3.1.2 Correlation Analysis of all the Texture Components

The purpose of this analysis is to compare each texture component to the others to find out which ones are the most correlated, and thus to establish which ones should be used together, to capture different information. For this analysis, the signatures of the first set of training sites were used on all the texture components generated for all the available imagery. For each signature, a report was created comparing the eight GLCM texture components created from one image a the time, to evaluate the correlated information

furnished by each component, for each signature on each date (Appendix 4). Highly correlated components obtain values close to 1, and components with low correlation return values that are close to 0.

According to this analysis, the Correlation component seemed definitely to be the least correlated with all the other texture components with a value generally lower than -0.20 or +0.20. The two other components with which the Correlation was least correlated seemed to be Homogeneity (-0.01) and Dissimilarity (0.07) (Table 6.12). The Mean component also seemed to be less correlated with the other texture components. The values were never much lower than 0.40, and so definitely higher than the Correlation component, but still lower than all the other components (Table 6.16).

Table 6.16 Summary table of all the GLCM texture components, for all images (dates) and signatures

	Homogeneity	Contrast	Dissimilarity	Mean	Standard Deviation	Entropy	Angular 2nd moment	Correlation
Homogeneity	1.00							
Contrast	-0.75	1.00						
Dissimilarity	-0.90	0.95	1.00					
Mean	-0.61	0.65	0.69	1.00				
Standard Deviation	-0.72	0.92	0.90	0.66	1.00			
Entropy	-0.88	0.71	0.82	0.62	0.76	1.00		
Angular 2nd moment	0.83	-0.55	-0.70	-0.47	-0.60	-0.91	1.00	
Correlation	-0.01	0.09	0.07	0.20	0.41	0.25	-0.17	1.00

The other components have different correlation values, depending on the date and on the signatures, so there is no observed trend. It is possible to note that the Angular 2nd Moment, the Contrast and the Standard Deviation also seem to be less correlated with each other. However, the separability analysis identified the components where the signatures had the greatest separation. The images with the greatest separation and the lowest correlation were retained for further analysis.

6.2.3.1.3 Separability Analysis

The aim of the separability analysis is to determine which texture component allows for a better separability of all the classes. It was also determined with this analysis which of the shrimp pond class or shrimp farm class was going to be used for the supervised classifications. In other words, this analysis identified which classes (shrimp pond or shrimp farm) should be used, with which images (which incidence angle and which date), with which texture component. However, the choice of the texture component also needed to take into account the correlation analysis done previously, in order not to use two highly correlated components in conjunction.

The graphs (Appendix 4) showing the signature separability of the texture components demonstrate that the best were Contrast, Mean and Standard Deviation. The Contrast component seemed to separate greatly all the signatures on all the images, but the best image seems to be the F1 of May 24. The Mean component seemed to separate the different signatures on the image with steeper incidence angle F4 (May7 and July18) well. Finally, the other texture component demonstrating a good separability analysis is the Standard Deviation applied on the F1 image of May 24.

Looking at this separability analysis in parallel with the correlation analysis, the Mean component was retained because its correlation to the other components was relatively low (0.65 and 0.66). Figure 6.11 displays a comparison of the raw image of May 7, 2001, and the Mean texture component applied on the same image. Comparing the two other components, only the Standard Deviation applied on the F1 image of May 24 was retained, and not the Contrast. Only one was kept because even if the separability

analysis was good on both, they were too correlated with each other, usually around 0.90 (Table 6.16, see Appendix 4 for all the correlation analysis).

a) 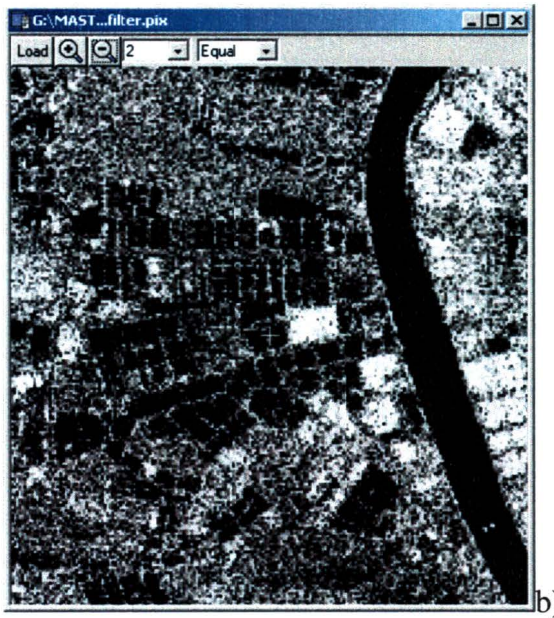

b) 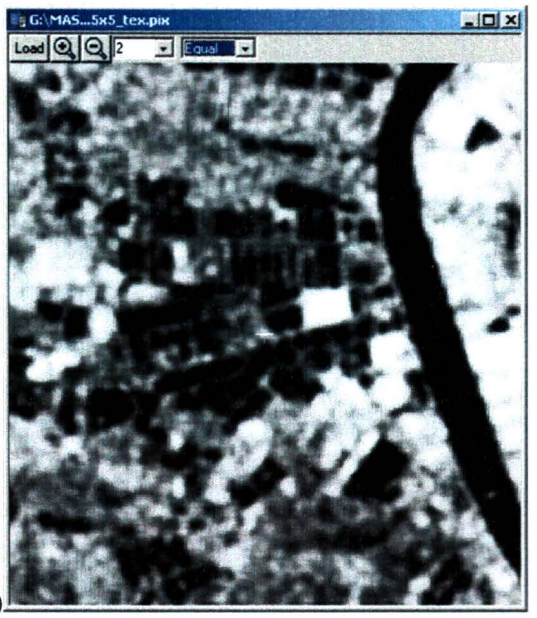

Figure 6.11 a) Original F4 image of May 7, 2001 b) 5x5 Mean Texture image of May 7, 2001

The Contrast was statistically correlated with the Mean in the same way as the Standard Deviation, as mentioned before 0.65 and 0.66 respectively. So, visually evaluating the RGB combination of the two Mean F4 images with either the Standard deviation or the Contrast F1 image, the Standard Deviation was chosen because it showed the edge of the shrimp ponds more clearly than the Contrast (Figure 6.12).

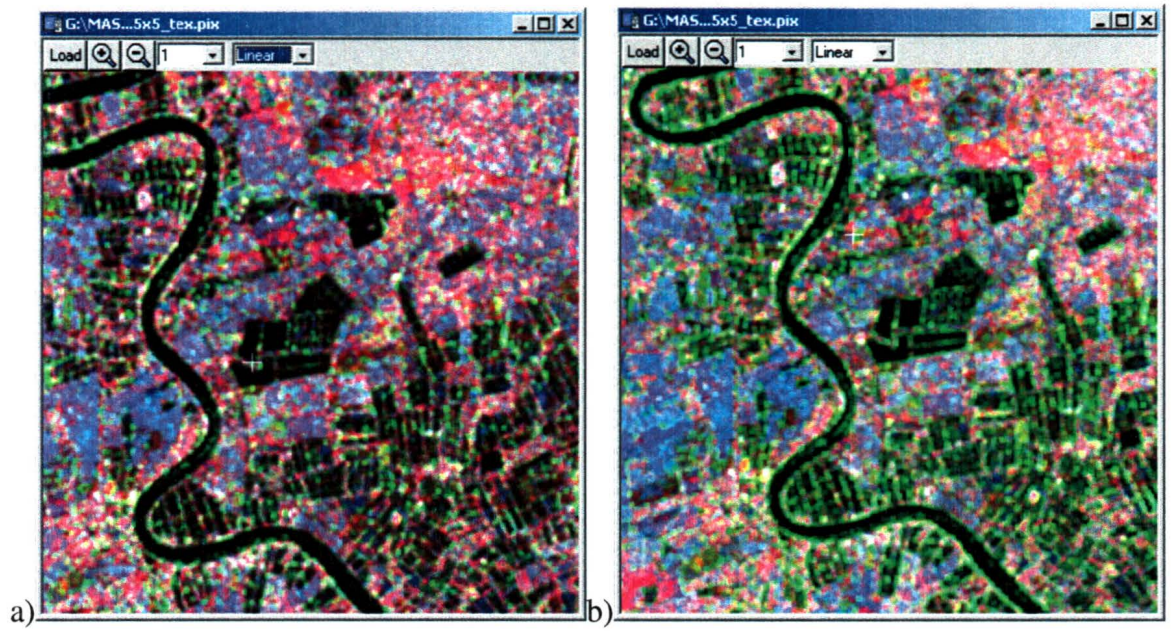

Figure 6.12 a) Red: Mean (F4, May 7); Green: Contrast (F1, May 24); Blue: Mean (F4, July 18) b) Red: Mean (F4, May 7); Green: Standard Deviation (F1, May 24); Blue: Mean (F4, July 18)

With this separability analysis, it was proven that the shrimp class was more separate from the other classes than the shrimp farm class. The shrimp farm signature was confused with the one for rice because the pixels of both classes include land and water pixels. The rice pixels were covering areas occupied by fields from the earliest stage (flooded) to their latest stages (harvested), and the shrimp farm pixels were including dykes and shrimp ponds.

The classifications of the following sections were performed on two types of texture combinations:

a) Combinations using the two best texture components:
   -Mean (May 7, F4; July 18, F4) and Standard Deviation (May 24, F1)
b) Multi-angle (F1 and F4 images) or Multi-temporal (F4 and F5 or F1 images) combinations using one of the three best texture components:
   -Mean

-Standard Deviation

-Contrast

Only the shrimp farm class was used with the first set of training sites. However, with the supervised classification run with the second set of training sites, the shrimp but also the farm and the *allwater* classes were tested as well because no previous separability analysis had been performed with these training sites on the texture components.

6.2.3.2 Unsupervised Classifications (k-means)

Unsupervised classifications were run on two types of texture combinations. The first type was a combination of two best texture components together (Mean and Standard Deviation). The second type was the multi-angle (F1 and F4) and multi-temporal (F1, or F4 and F5) combinations, but performed on only the Mean texture component because it is the best one according to the components evaluation of the previous section.

6.2.3.2.1 Best Texture Components

According to the correlation and separability analyses (Appendix 4) of the previous section, the Mean component for the images of May 7 (F4) and July 18 (F4), and the Standard Deviation component for the images of May 24 (F1), demonstrate the best results. These three components were combined together for an unsupervised classification.

Figure 6.13 RGB combination of the best texture component: Mean for May7 and July18, and the Standard Deviation for May24

The three input components for the classification were the Mean texture of the F4 images of May 7 and July 18, and the Standard Deviation texture of the F1 image of May 24, demonstrated in a RGB combination in the Figure 6.13. On this image, the dykes are clearly visible, they are the green edges surrounding the shrimp ponds. The two mean components are smoothing the images and the standard deviation component is accentuating the pond dykes.

The unsupervised classification was first run using 16 classes, but only a few were actually grouping most of the pixels into classes representing land use features. This

number of classes was too high and was separating the pixels in too many different categories. A second classification was then run using only 8 classes (Figure 6.14 and Table 6.17). The result was more significant than the previous one. The water bodies are very well identified (blue), as well as the surrounding dykes (turquoise).

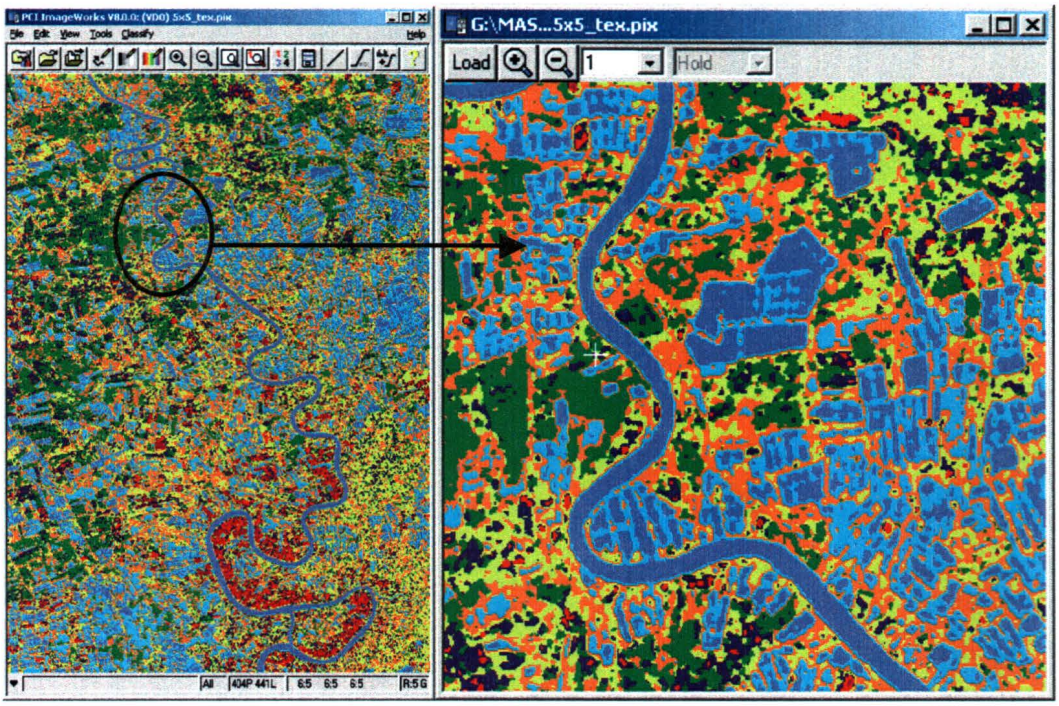

Figure 6.14 k-means classification with the best texture component: Mean for May7 and July18, and the Standard deviation for May 24 (with eight classes)

Table 6.17 Legend of k-means classification with the best texture component: Mean for May 7 and July 18, and the Standard deviation for May 24 with eight classes (principal five classes are in the legend), Figure 6.14

Land Types	k-means with Best Texture Components (8 classes)
Water (river, ponds, etc)	Blue
Dykes	Turquoise
Rice	Green, Purple and Orange
Orchard	Yellow and Orange
Human	Red

The rice paddies are represented by the green, purple and orange pixels, and the orchards are represented by the yellow and orange pixels. The rice and orchard plantations are a little bit confused together. The human settlements were pretty well identified by the red pixels, but a bit confused with the rice paddies.

6.2.3.2.2 Multi-temporal Combinations

The supervised classifications done with multi-date combinations had the same incidence angle, either F1 or F4 and F5.

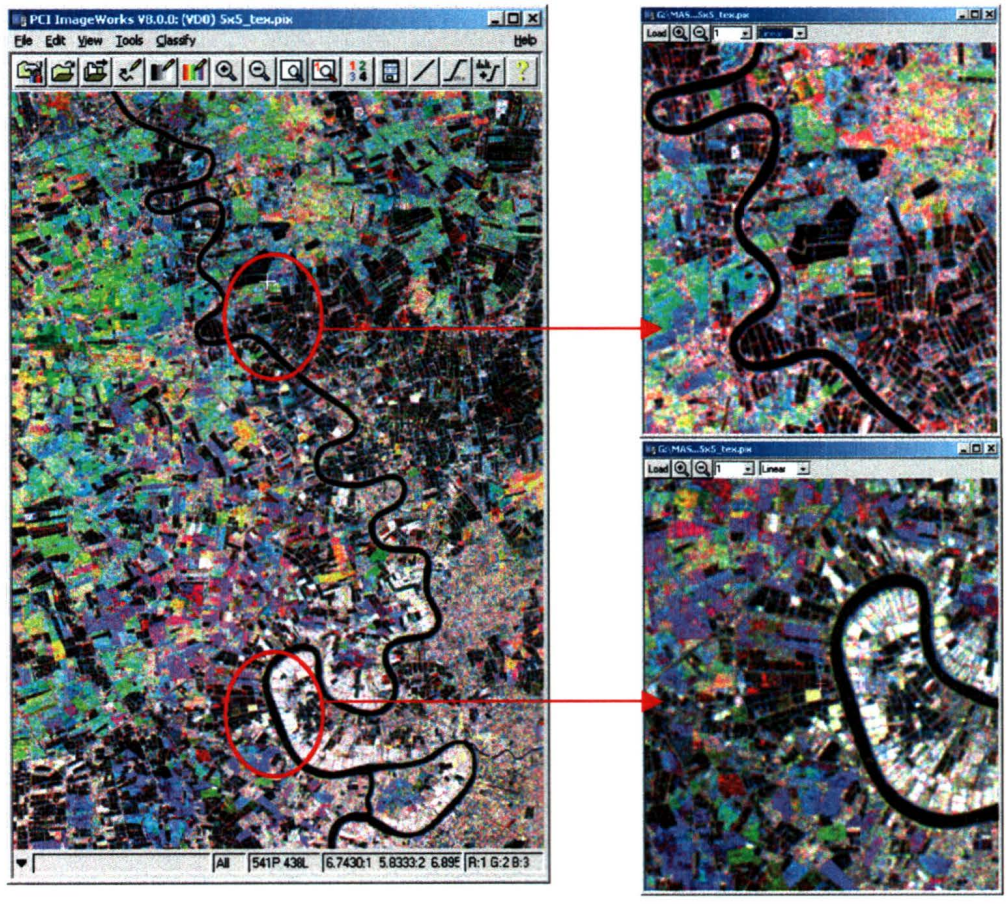

Figure 6.15 Multi-date F4 and F5 RGB combination of the Mean texture component: May 7 (F4), July 18 (F4), and September 19 (F5)

The Mean component was chosen because it was the one having the best signature separability for all the different classes. Figure 6.15 is an RGB combination of the Mean F4 and F5 images. It illustrates very well the different features present in the area. The same legend as the raw image (see table 6.1) is used here because it is the same image combination, except the feature definitions are smoother.

The result of the unsupervised classification on Mean F1 images with 16 classes was not very good. All the classes were mixed together, principally the water and the dykes, as well as the rice, the orchards and the human settlement. However, the one using 16 classes as well but on the Mean component of F4 and F5 images was better. The rice was well identified and the water bodies too. The human settlements were still confused with the orchard plantations. Two more unsupervised classifications using the same image combination but with fewer classes were tested. The first one, used eight classes and produced a better resulting image. In Figure 6.16 a) (Table 6.18), the rice is very well visible in green and orange, the water bodies are in blue, and the purple pixels are representing the dykes. The human areas are confused (white areas) as well as the orchards (red areas). The use of fewer classes, in this case five, clearly augments the quality of the resulting image of the unsupervised classification (Figure 6.16 b) and Table 6.18). All the classes were well distinguished from each other, and well situated on the image. Only the rice (which should be in green) was not very well identified, half of the entire rice area was considered to be orchard (orange on the west side of the river).

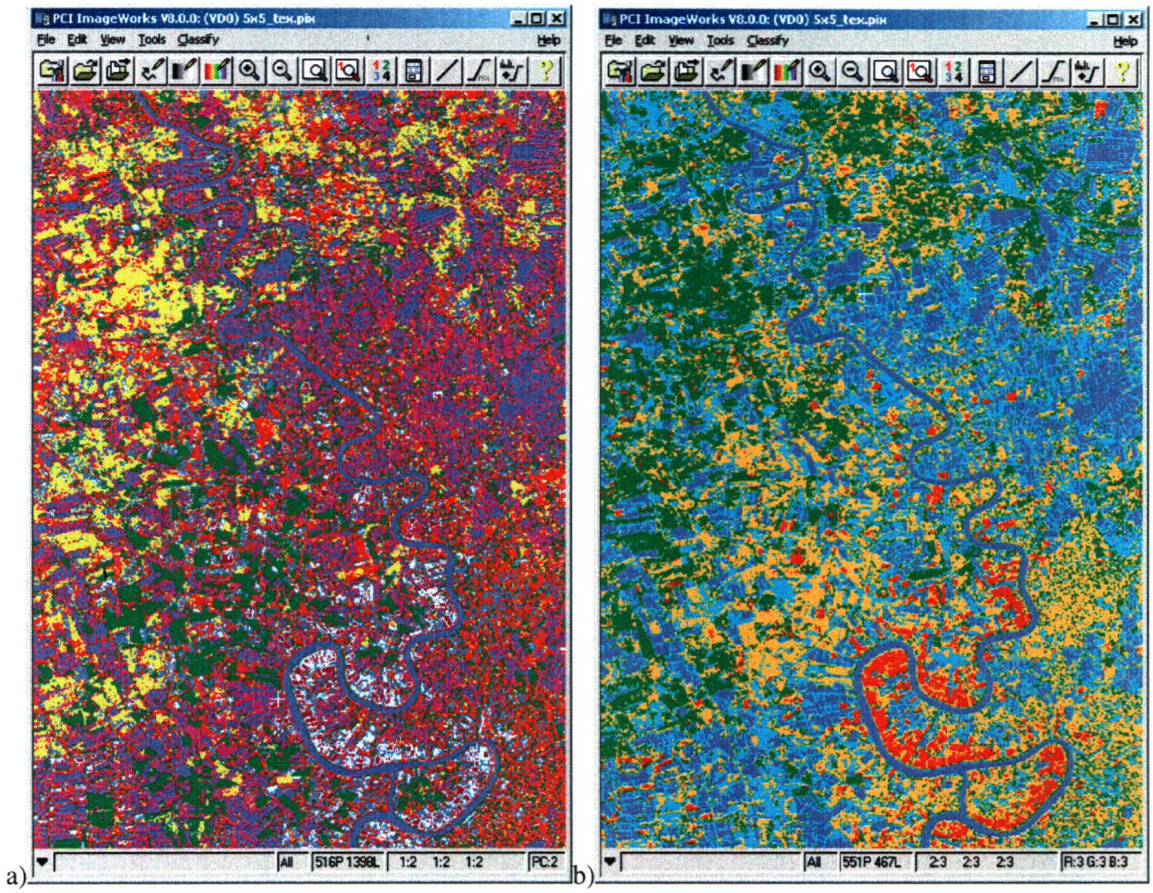

a) b)

Figure 6.16 a) Unsupervised classification k-means using Mean texture F4 and F5 images with 8 classes b) using 5 classes

Table 6.18 Legend of k-means classification using Mean texture F4 and F5 images with a) 8 classes (principal five classes are in the legend) and b) 5 classes, Figure 6.16

Land Types	k-means with three Frost F4 and F5 images (8 classes)	k-means with three Frost F4 and F5 images (5 classes)
Water (river, ponds, etc)	Blue	Blue
Dykes	Purple	Turquoise
Rice	Green and Orange	Green
Orchard	Red areas	Orange
Human	White areas	Red

6.2.3.2.3 Multi-angle Combination

In order to test the reliability of the multi-angle (July 11, F1 and July 18, F4) combination of Mean texture images, an unsupervised classification was performed on them using 16 classes, then eight and finally five. The best result was obtained with the one run with only five classes. The resulting image is similar to the one run with the F4 and F5 images done previously using five classes as well (Figure 6.17 and Table 6.19).

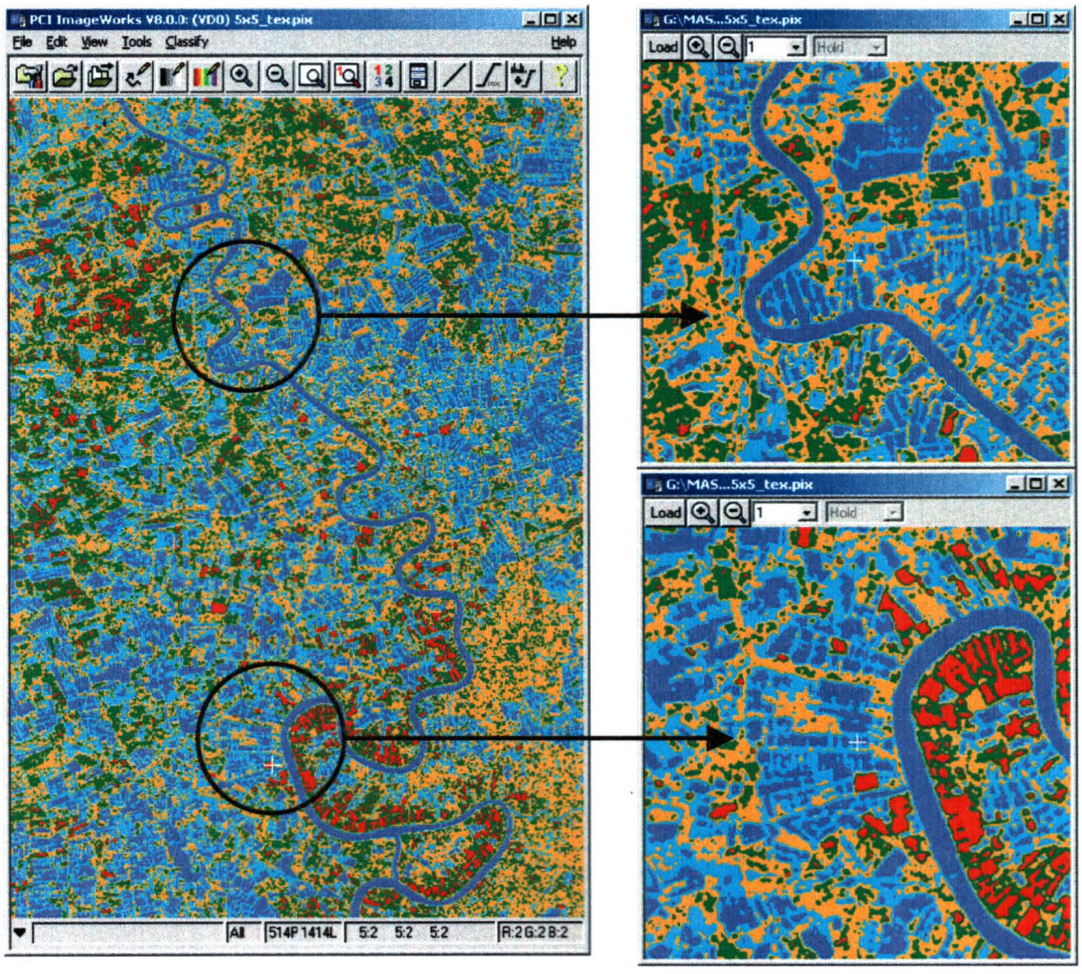

Figure 6.17 Unsupervised Classification with multi-angle combination of Mean F1 and F4 images with 5 classes

Table 6.19 Legend of k-means classification with multi-angle combination of Mean F1 and F4 images with 5 classes, Figure 6.17

Land Types	k-means with three Mean F4 and F5 images (8 classes)
Water (river, ponds, etc)	Blue
Dykes	Turquoise
Rice	Green, Red and Orange
Orchard	Orange
Human	Red

However, the rice paddies are almost unidentifiable on the resulting classified image of this multi-angle combination because they are included in the orchard plantations class. The human settlements, the water bodies, and the dykes surrounding the shrimp ponds are well identified, but these features seem to be more merged together in this classification result, than in the classification results of the multi-temporal combination of the Mean F4 and F5 components.

6.2.3.3 Supervised Maximum Likelihood Classifications (MLC)

The supervised maximum likelihood classifications (MLC) were performed on three types of texture components combination:

- Best Texture Component Combination
  - First set of training sites (only with shrimp) and second set of training sites (shrimp/farm/*allwater*) were tested.
    - -F4 May 7 and July 11 Mean
    - -F1 May 24 Mean
- Multi-temporal Combinations
  - First set of training sites (only with shrimp)
    - F1 Mean / Contrast / Standard Deviation
    - F4 and F5 Mean / Contrast / Standard Deviation

- Second set of training sites (shrimp/farm/*allwater*)
  - -F1 Mean
  - -F4 and F5 Mean

- Multi-angle Combination
  - First set of training sites (only with shrimp)
    - -F1 and F4 Mean / Contrast / Standard Deviation
  - Second set of training sites (shrimp/farm/*allwater*)
    - -F1 and F4 Mean

This section is followed by an accuracy assessment of the best results obtained with MLC.

6.2.3.3.1 Best Texture Components

The same texture component combination used for the k-means unsupervised classification of the previous section was used for the MLC supervised classification. The classification had as input texture components Mean, image of May 7 and July 18, and Standard Deviation image of May 24. For the classification using the first set of training sites, only the class shrimp pond (only the pond) was used because of the separability analysis done with all the classes. For the classification using the second set of training sites, the shrimp ponds, shrimp farms, as well as the class including all the water bodies (*allwater*) were compared.

The classifications using the shrimp class with the first and second set of training sites obtained respectively overall accuracies of 59.28% and 78.92% (Table 6.20).

Table 6.20 Confusion matrix of the MLC run on the best texture components a) 1st set of training sites with the shrimp class b) 2nd set of training sites with shrimp class c) 2nd set of training sites with farm class d) 2nd set of training sites with *allwater* class

a)

Name	Code	Pixels	NULL	Rice	Human	Orchard	Water	Shrimp
Rice	1	5989	1.85	**61.93**	17.98	17.85	0	0.38
Human	2	3222	2.51	8.19	**60.49**	24.83	0	3.97
Orchard	3	4749	3.37	16.57	38.2	**41.82**	0	0.04
Water	4	2100	1.62	0	0.33	0	**88.67**	9.38
Shrimp	5	2263	3.71	0.22	3.31	0.13	32.7	**59.92**
Average accuracy = 62.57 % Overall accuracy = 59.28 %								

b)

Name	Code	Pixels	NULL	Rice	Orchard	Human	Water	Shrimp
Rice	1	24307	2.16	**74.71**	19.2	3.93	0	0
Orchard	2	11708	0.09	9.08	**84.71**	6.12	0	0
Human	3	5794	2.8	1.04	12.43	**83.74**	0	0
Water	4	2891	3.77	0	0	0	**90.28**	5.95
Shrimp	5	1571	3.88	2.16	0	0	31.64	**62.32**
Average accuracy = 79.15 % Overall accuracy = 78.92 %								

c)

Name	Code	Pixels	NULL	Rice	Orchard	Human	Water	Farm
Rice	1	24307	2.14	**65.63**	18.92	3.9	0	9.41
Orchard	2	11708	0.09	6.47	**84.43**	6.04	0	2.97
Human	3	5794	2.78	0.85	12.41	**83.67**	0	0.29
Water	4	2891	3.6	0	0	0	**92.77**	3.63
Farm	5	25663	2.02	5.57	4.48	0.46	5.2	**82.27**
Average accuracy = 81.75 % Overall accuracy = 77.43 %								

d)

Name	Code	Pixels	NULL	*Allwater*	Rice	Orchard	Human
Allwater	1	2891	7.19	**92.77**	0.03	0	0
Rice	2	24307	2.16	0	**74.71**	19.2	3.93
Orchard	3	11708	0.09	0	9.08	**84.71**	6.12
Human	4	5794	2.8	0	1.04	12.43	**83.74**
Average accuracy = 83.98 % Overall accuracy = 79.67 %							

Both classifications had a large numbers of pixels classified in the null class. The land use classes were also confused with each other. With the MLC using the shrimp pond

signature of the first set, the classes had mostly less then 60% of the pixels correctly classified, except for the water class. With the same class (shrimp pond), but with the second set of sites, the rice class took over the shrimp farms area (water ponds and dykes). Also, even if the pixels of each class seemed to be correctly classified in the confusion matrix, looking at the output image of the classification, the identification of the land uses was not right. The classification using the second set of training sites, but with the shrimp farm class, creates a resulting image with an overall accuracy of 77.43% (Figure 6.18, and Table 6.21).

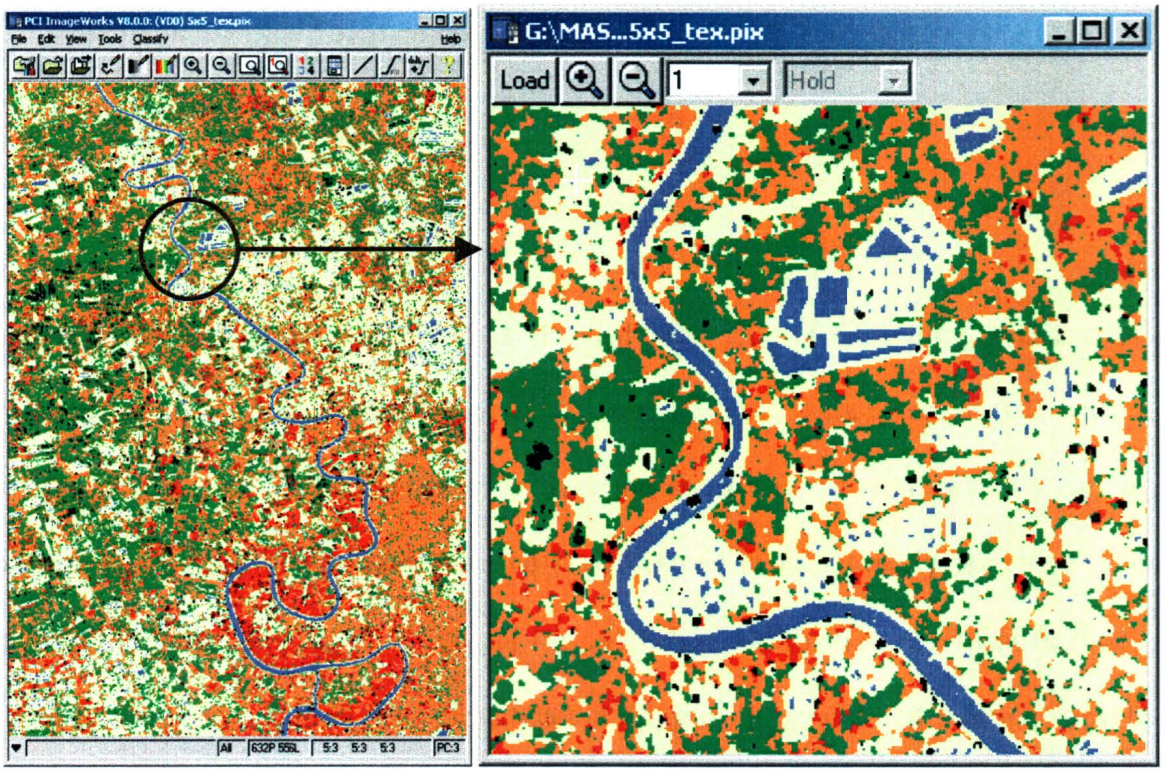

Figure 6.18 Supervised classification MLC using the best texture components Mean (May7 and July18), and Standard Deviation (May24) (with the farm class of the second set of training sites)

Table 6.21 Legend Supervised classification MLC using the best texture components, Mean (May 7 and July 18), and Standard Deviation (May24) a) with the farm class of the second set of training sites, Figure 6.18 b) with the *allwater* class or the second set of training sites, Figure 6.19

Land Types	a) MLC with Best Texture Components (2^{nd} set of training sites with Farm)	b) MLC with Best Texture Components (2^{nd} set of training sites with *allwater*)
Water (river, ponds, etc)	Blue	Blue, Black and Green
Farm (ponds and dykes)	Beige and Blue	-
Rice	Green	Green
Orchard	Orange	Orange
Human	Red	Red

The dykes (beige areas in Figure 6.18 and Table 6.21) surrounding the shrimp ponds were confused with other classes, including too many pixels that should be representing shrimp ponds (water), orchard plantations or rice paddies.

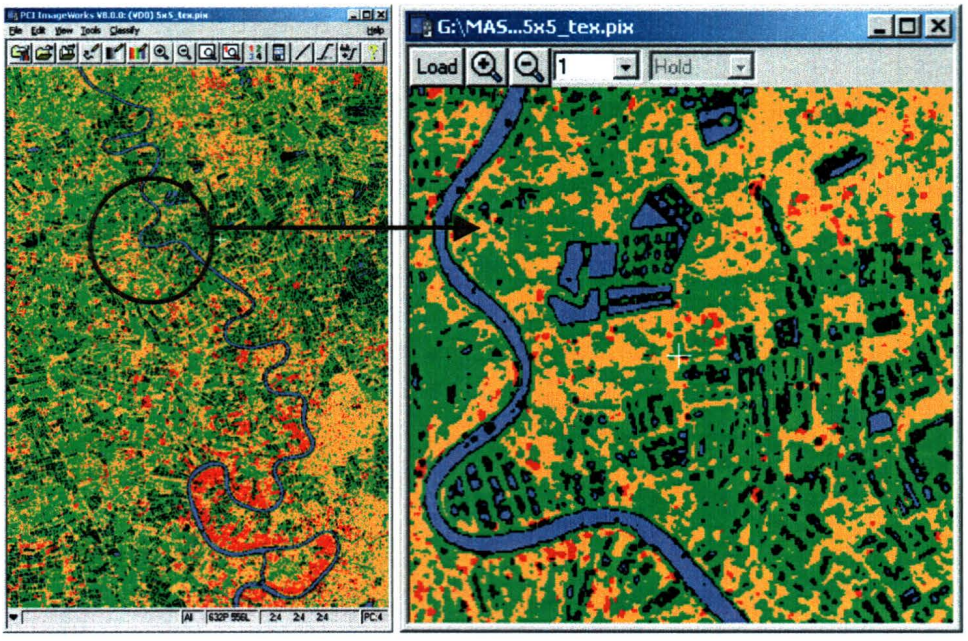

Figure 6.19 Supervised classification MLC using the best texture components, Mean (May 7 and July 18), and Standard Deviation (May24) (with the *allwater* class or the second set of training sites)

The MLC run with the same training sites using the *allwater* class produced a resulting classified image where the *allwater* class was confused with the rice paddies (Figure 6.19, and Table 6.21). Also, many pixels that were supposed to be identified as water areas were classified as null pixels. This classification did not produce a good output classified image.

Table 6.22 Summary table of the average and overall accuracy of the MLC on the textured image combination with the best separability (%)

Image Combinations	MLC with first set of training sites		MLC with second set of training sites					
	Shrimp		Shrimp		Farm		*Allwater*	
	Av. Acc.	Over. Acc.	Av. Acc.	Over. Acc.	Av. Acc.	Over. Acc.	Av. Acc.	Over. Acc.
Mean (May7/F4, July18/F4) & Std. Dev. (May24/F1)	62.57	59.28	79.15	78.92	81.75	77.43	83.98	79.67

The best of all the classifications using the best components Mean, image of May 7 and July 18, and Standard Deviation image of May 24, was the one using the second set of training sites with the shrimp farm class (Table 6.22).

6.2.3.3.2 Multi-temporal Combinations

The first set of classifications was performed using the first set of training sites with the shrimp pond class. Each classification was run on multi-temporal combinations of three different texture components run on images with either shallow (F4 and F5) or steep (F1) incidence angles. Table 6.23 is a summary table of the average and overall accuracy all the supervised classifications performed on the multi-temporal combinations of texture images.

Table 6.23 Summary table of the average and overall accuracy of the MLC on the multi-date combinations of texture images (%)

Texture	Image Combinations	MLC with first set of training sites		MLC with second set of training sites					
		Shrimp		Shrimp		Farm		*Allwater*	
		Av. Acc.	Over. Acc.	Av. Acc.	Over. Acc.	Av. Acc.	Over. Acc.	Av. Acc.	Over. Acc.
Contrast	All F4 & F5	53.89	52.31						
	All F1	49.44	46.26						
Mean	All F4 & F5	62.33	58.08	85.13	82.30	86.76	83.71	87.12	82.49
	All F1	55.55	51.41	75.68	77.98	77.66	70.91	84.32	80.12
Standard Deviation	All F4 & F5	54.82	53.97						
	All F1	50.66	48.69						

The results using the first set of training sites were not very significant. With the Contrast texture component, the overall accuracy of the classification using steep angle was 46.26% and with shallow angle the accuracy was 52.31%. On the output classified image, all the classes were confused with each other. The results were pretty much the same with the Standard Deviation texture components, since they are highly correlated (demonstrated in section 6.4.3.1.2). The overall accuracy of the classifications, run on shallow and steeper angle multi-temporal combinations were respectively 48.69% and 53.97%. Using the Mean texture component (Table 6.25), the resulting classified image using the multi-temporal combination with shallower angle (F4 and F5) demonstrates a greater recognition of the different land uses (Figure 6.20 and Table 6.24), with an overall accuracy of 58.08%.

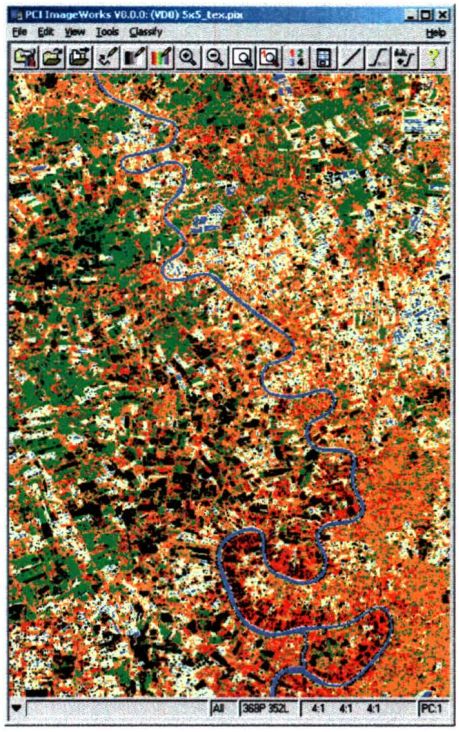

Figure 6.20 Supervised classification MLC using the Mean F4 and F5 components (May 7 and July 18 and September 19), using the first set of training class with the shrimp pond class.

Table 6.24 Legend of the MLC using the Mean F4 and F5 components (May 7 and July 18 and Sept 19), using the first set of training class with the shrimp pond class, Figure 6.20.

Land Types	MLC with Mean F4 and F5 (1st set of training sites with Shrimp)
Water (river, ponds, etc)	Blue
Shrimp (but representing the farm areas)	Beige
Rice	Green
Orchard	Orange
Human	Red

However, like the classifications with Contrast and Standard Deviation components, using the shrimp class, the null class was important and was including a lot of pixels that should have been classified as rice paddies or human settlements. The overall accuracy of the classification using the steeper angle was lower, 51.41% (Table 6.25). The shrimp

class does not recognize the ponds themselves. It groups the pixels surrounding the ponds, as well as the ponds. So the shrimp class seems to act in the same way as the farm class.

Table 6.25 Confusion matrix of the MLC using Mean component with the shrimp pond (shrimp) class of the 1st set of training sites a) Multi-temporal combination of F4 and F5 images b) Multi-temporal combination of F1 images

a)

Name	Code	Pixels	NULL	Rice	Human	Orchard	Water	Shrimp
Rice	1	5989	1.77	**60.53**	24.98	12.26	0	0.47
Human	2	3222	1.55	9.4	**67.78**	18.4	0	2.86
Orchard	3	4749	4.23	14.02	48.39	**33.31**	0	0.04
Water	4	2100	1.29	0	0.24	0	**88.29**	10.19
Shrimp	5	2263	3.62	0.35	3.54	0	30.76	**61.73**
Average accuracy = 62.33 % Overall accuracy = 58.08 %								

b)

Name	Code	Pixels	NULL	Rice	Human	Orchard	Water	Shrimp
Rice	1	5989	0.73	**66.76**	18.93	12.67	0	0.9
Human	2	3222	1.52	51.02	**29.64**	14.84	0	2.98
Orchard	3	4749	2.59	58.58	18.11	**20.49**	0	0.23
Water	4	2100	0	0.05	0.1	0	**89.86**	10
Shrimp	5	2263	0.88	1.33	2.52	0.44	23.82	**71.01**
Average accuracy = 55.55 % Overall accuracy = 51.41 %								

For the second set of classifications, only the multi-temporal combinations with steep (F4 and F5) and shallow (F1) incidence angles were tested on the Mean texture component. This texture component was chosen to run further MLC because it was the one that obtained the higher overall accuracy using the first set of training sites. Furthermore, in the separability analysis executed in section 6.4.3.1.3, the Mean component demonstrated a better signature separability for all classes in all the available images. Each signature was well separated from the others (See Appendix IV, p.245). With this second set of classifications, three different ways were tried in order to recognise the shrimp ponds (or farms) and the other land covers on the images.

Table 6.26 Confusion matrix of the MLC using Mean component with the shrimp pond (shrimp) class of the 2nd set of training sites a) Multi-temporal combination of F4 and F5 images b) Multi-temporal combination of F1 images

a)

Name	Code	Pixels	NULL	Rice	Orchard	Human	Water	Shrimp
Rice	1	24307	3.5	**76.18**	18.48	1.83	0	0
Orchard	2	11708	0	7.43	**89.99**	2.58	0	0
Human	3	5794	1.57	1.43	9.27	**87.73**	0	0
Water	4	2891	0.38	0	0	0	**94.4**	5.22
Shrimp	5	1571	5.41	0.13	0	0	17.12	**77.34**
Average accuracy = 85.13 %								
Overall accuracy = 82.30 %								

b)

Name	Code	Pixels	NULL	Rice	Orchard	Human	Water	Shrimp
Rice	1	24307	0.21	**74.59**	19.65	2.23	0.75	2.57
Orchard	2	11708	0	7.93	**85.57**	6.49	0	0
Human	3	5794	1.19	0.66	17.54	**80.62**	0	0
Water	4	2891	0	2.73	0	0	**82.6**	14.67
Shrimp	5	1571	0	2.93	0	0	42.08	**55**
Average accuracy = 75.68 %								
Overall accuracy = 77.96 %								

Each of the two multi-temporal combinations (with shallow or steep incidence angle image) were run using three different groups of training sites in order to identify the shrimp: the same shrimp pond (Table 6.26) and shrimp farm (Table 6.27) classes were used (new training sites), but also a new class grouping all the water bodies (*allwater)* (Table 6.28) was tested.

Table 6.27 Confusion matrix of the MLC using Mean component with the shrimp farm (farm) class of the 2nd set of training sites a) Multi-temporal combination of F4 and F5 images b) Multi-temporal combination of F1 images

a)

Name	Code	Pixels	NULL	Rice	Orchard	Human	Water	Farm
Rice	1	24307	3.48	**74.23**	18.13	1.83	0	2.32
Orchard	2	11708	0	5.79	**89.21**	2.58	0	2.42
Human	3	5794	1.57	1.43	9.27	**87.73**	0	0
Water	4	2891	0	0	0	0	**94.57**	5.43
Farm	5	25663	1.48	4.13	4.06	0.08	2.21	**88.05**
Average accuracy = 86.76 %								
Overall accuracy = 83.71 %								

b)

Name	Code	Pixels	NULL	Rice	Orchard	Human	Water	Farm
Rice	1	24307	0.21	**66.08**	19.59	2.23	0.7	11.21
Orchard	2	11708	0	5.29	**85.45**	6.49	0	2.78
Human	3	5794	1.19	0.6	17.54	**80.62**	0	0.05
Water	4	2891	0	2.21	0	0	**91.87**	5.91
Farm	5	25663	0.06	8.1	5.69	0.27	21.57	**64.31**
Average accuracy = 77.66 %								
Overall accuracy = 70.91 %								

Table 6.28 Confusion matrix of the MLC using Mean component with the *allwater* class of the 2nd set of training sites a) Multi-temporal combination of F4 and F5 images b) Multi-temporal combination of F1 images

a)

Name	Code	Pixels	NULL	*Allwater*	Rice	Orchard	Human
Allwater	1	2891	5.43	94.57	0	0	0
Rice	2	24307	3.5	0	76.18	18.48	1.83
Orchard	3	11708	0	0	7.43	89.99	2.58
Human	4	5794	1.57	0	1.43	9.27	87.73
Average accuracy = 87.12 %							
Overall accuracy = 82.49 %							

b)

Name	Code	Pixels	NULL	*Allwater*	Rice	Orchard	Human
Allwater	1	2891	0	95.54	4.46	0	0
Rice	2	24307	0.21	2.37	75.54	19.65	2.23
Orchard	3	11708	0	0	7.93	85.57	6.49
Human	4	5794	1.19	0	0.66	17.54	80.62
Average accuracy = 84.32 %							
Overall accuracy = 80.12 %							

The output classification obtained a high overall accuracy of respectively, 82.13%, 83.71% and 82.49%, but the visual interpretation of the results was not very conclusive (Figure 6.21 and Table 6.29). In the first classification using the shrimp class, the resulting image does not represent the shrimp farms, but includes them in the rice paddies class. In the second one, the farm areas are very well identified and represented on the resulting image by the beige pixels. There are however, some areas that were not classified as anything (null class) that were represented by black pixels, and also some

reservoirs that are identified as shrimp farms. The third classification, grouping all the water bodies together in one class, produced a very bad resulting image, including a lot of null pixels (black) that should have been classified as water bodies or rice paddies.

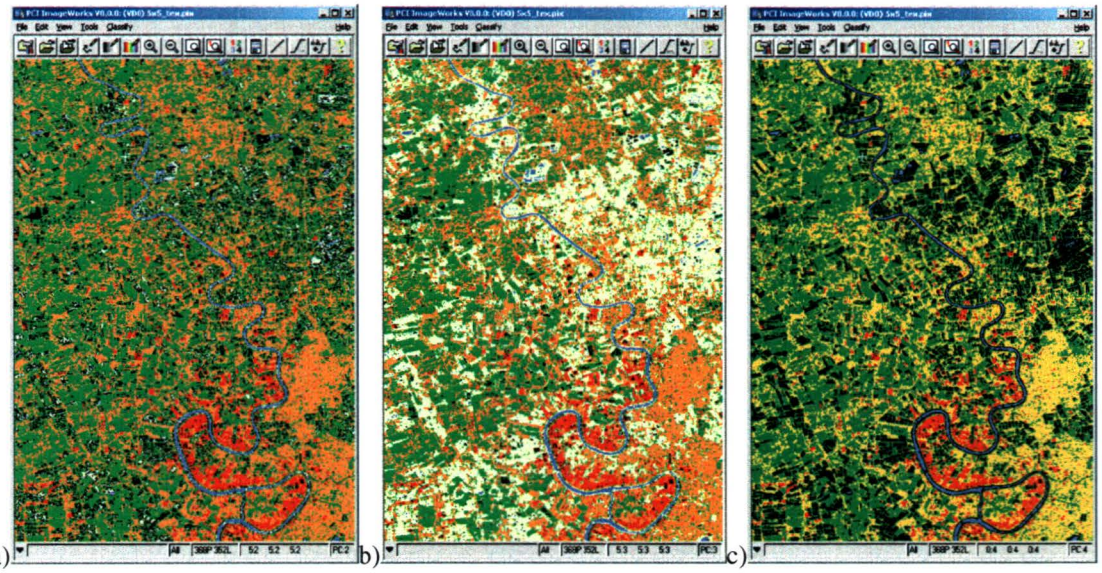

Figure 6.21 a) MLC using the Mean F4 and F5 components (May7, July18 and September 19) with the second set of training sites: shrimp b) farm c) *allwater*

Table 6.29 Legend of MLC using the Mean F4 and F5 components (May 7, July 18 and September 19) with the second set of training sites: shrimp b) farm c) allwater; Figure 6.18

Land Types	MLC with Mean F4 and F5 (2nd set of training sites with shrimp)	MLC with Mean F4 and F5 (2nd set of training sites with farm)	MLC with Mean F4 and F5 (2nd set of training sites with *allwater*)
Water (river, ponds, etc)	Blue	Blue	Blue, Black and Blue
Shrimp (pond only)	Green, Beige and Blue	-	-
Farm (pond and dykes)	-	Beige and Blue	-
Rice	Green	Green	Green
Orchard	Orange	Orange	Orange
Human	Red	Red	Red

The following classifications were applied on the Mean textured image with steeper incidence angle (F1). The classification using the shrimp pond class produced a bad classified image. Even if the overall accuracy was quite high (77.98%) the rice and shrimp ponds were confused together visually. However, the classifications with either the shrimp farm or the *allwater* classes were very good visually and statistically compared to the previous one using the F4 and F5 combination, even if their overall accuracy results were lower (Table 6.27). The MLC that used the shrimp farm clearly distinguished the ponds from the dykes, the human areas, as well as the rice paddies and the orchard plantations (Figure 6.22 and Table 6.30). The overall accuracy of this classification is 70.91%.

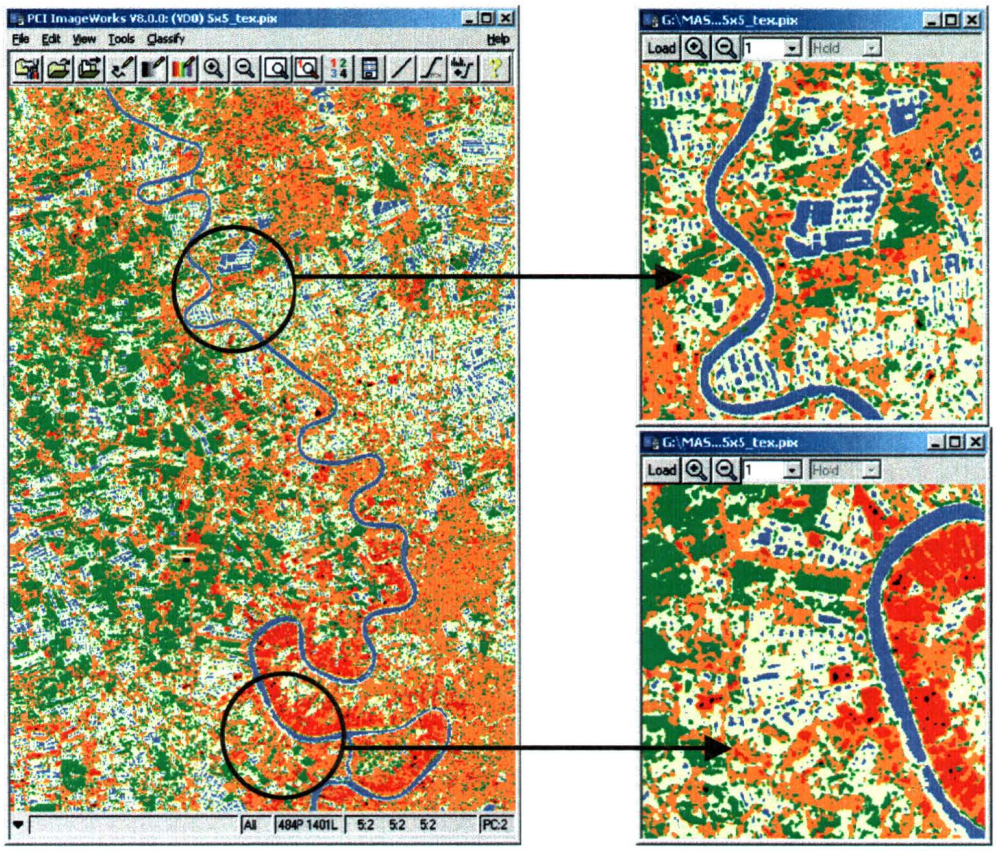

Figure 6.22 Supervised classification MLC using the Mean F1 components (May 24 and July 11) with the second set of training sites (farm)

Table 6.30 Legend of MLC using the Mean F1 components (May 24 and July 11) with the second set of training sites a) farm; Figure 6.18 b) *allwater*; Figure 6.19

Land Types	MLC with Mean F1 (2^{nd} set of training sites with farm)	MLC with Mean F1 (2^{nd} set of training sites with *allwater*)
Water (river, ponds, etc)	Blue	Blue
Shrimp Farms (ponds and dykes)	Blue and Beige	-
Rice	Green	Green
Orchard	Orange	Orange
Human	Red	Red

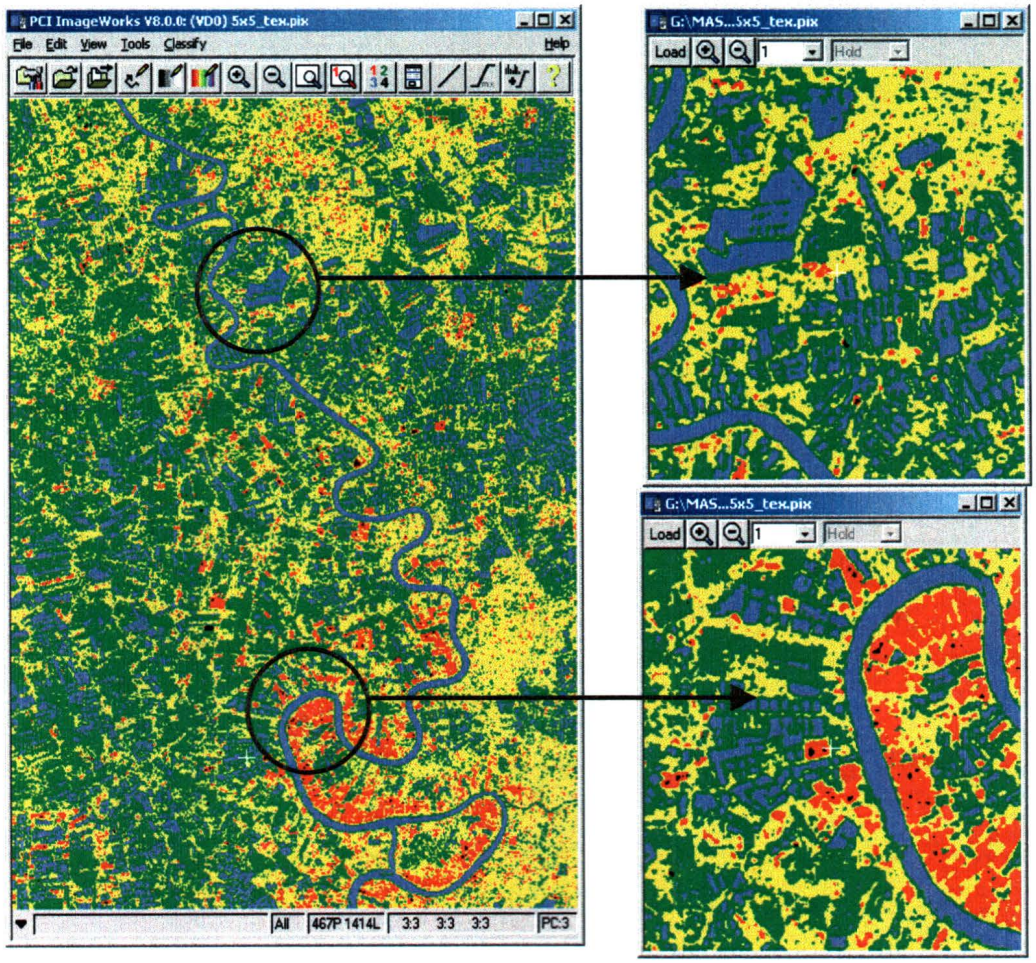

Figure 6.23 Supervised classification MLC using the Mean F1 components (May 7 and July 18 and September 19) with the second set of training sites (*allwater*)

The other MLC using the allwater class, grouping all the water bodies together, generated an excellent classified image (Figure 6.23 and Table 6.30). All four classes were very clearly delineated, and the overall accuracy of the classification was 80.12%.

6.2.3.3.3 Multi-angle Combination

The classifications run with the first set of training sites with the shrimp pond class created similar results when performed on the multi-angle combination of textured images (F1 July 11 and F4 July 18), as the one performed on multi-temporal combination of steeper (F1 only) incidence angle images. The overall accuracy of the multi-angle classifications using the Contrast component was 45.33%, using the Standard Deviation component 47.10% and 52.91% (Table 6.32) when run with the Mean component (Table 6.31).

Table 6.31 Summary table of the average and overall accuracy of the MLC on the multi-angle combination (July 11 (F1) and July 18 (F4)) of texture images (%)

Texture	MLC with first set of training sites		MLC with second set of training sites					
	Shrimp		Shrimp		Farm		*Allwater*	
	Av. Acc.	Over. Acc.	Av. Acc.	Over. Acc.	Av. Acc.	Over. Acc.	Av. Acc.	Over. Acc.
Contrast	49.08	45.33						
Mean	59.96	52.91	73.82	64.24	75.01	65.81	79.19	68.87
Standard Deviation	49.94	47.10						

The result was slightly higher using this last component. Since the confusion was marked on these classification results, further analyses were executed using the second set of training sites on the Mean textured images. This particular component was chosen for the same reason as explained in the previous sections: it generated the best results using the

first set of training sites and the separability analysis demonstrated that it was the texture component presenting the best separability between all the signatures on all dates.

MLC were run on multi-angle combination of Mean textures images (F1 July 11 and F4 July 18), using these three classes separately: shrimp ponds, shrimp farms and *allwater* (all water bodies) (Table 6.32).

Table 6.32 Confusion matrix of the MLC on Multi-angle (F1 and F4) combination of Mean components a) 1st set of training sites with shrimp pond class b) 2nd set of training sites with shrimp pond class c) 2nd set of training sites with shrimp farm class d) 2nd set of training sites with *allwater* class

a)

Name	Code	Pixels	NULL	Rice	Human	Orchard	Water	Shrimp
Rice	1	5989	0.33	**44.9**	27.33	27.02	0	0.42
Human	2	3222	1.86	10.15	**61.27**	23.4	0	3.32
Orchard	3	4749	2.3	19.23	46.35	**32.01**	0	0.13
Water	4	2100	1.19	0	0.19	0	**89.33**	9.29
Shrimp	5	2263	0.4	0.4	3.54	0.09	23.29	**72.29**
Average accuracy = 59.96 % Overall accuracy = 52.91 %								

b)

Name	Code	Pixels	NULL	Rice	Orchard	Human	Water	Shrimp
Rice	1	24307	0.7	**46.54**	23.5	17.91	1.61	9.74
Orchard	2	11708	0.05	6.76	**87.03**	6.15	0	0
Human	3	5794	0.86	2.59	18.81	**77.74**	0	0
Water	4	2891	0	0.86	0	0	**93.77**	5.36
Shrimp	5	1571	0	2.93	0	0	33.04	**64.04**
Average accuracy = 73.82 % Overall accuracy = 64.24 %								

c)

Name	Code	Pixels	NULL	Rice	Orchard	Human	Water	Farm
Rice	1	24307	0.7	**33.54**	23.01	17.91	2.72	22.12
Orchard	2	11708	0.05	4.47	**86.04**	6.15	0	3.3
Human	3	5794	0.86	2.4	18.81	**77.74**	0	0.19
Water	4	2891	0	0.52	0	0	**96.78**	2.7
Farm	5	25663	0	5.45	6.23	0.19	7.16	**80.96**
Average accuracy = 75.01 % Overall accuracy = 65.81 %								

d)

Name	Code	Pixels	NULL	*Allwater*	Rice	Orchard	Human
Allwater	1	2891	0	97.37	2.63	0	0
Rice	2	24307	0.7	3.26	54.63	23.5	17.91
Orchard	3	11708	0.05	0	6.76	87.03	6.15
Human	4	5794	0.86	0	2.59	18.81	77.74
Average accuracy = 79.19 % Overall accuracy = 68.87 %							

With the shrimp pond class, the rice class included too many areas that should have been identified as shrimp farms or as orchard plantations. The two classifications using the shrimp farm and the *allwater* classes generated similar classified images as the previous classifications done with multi-temporal F1 Mean textured images. However, the results of both classifications run with the multi-angle images were less accurate than the one with the multi-temporal combinations.

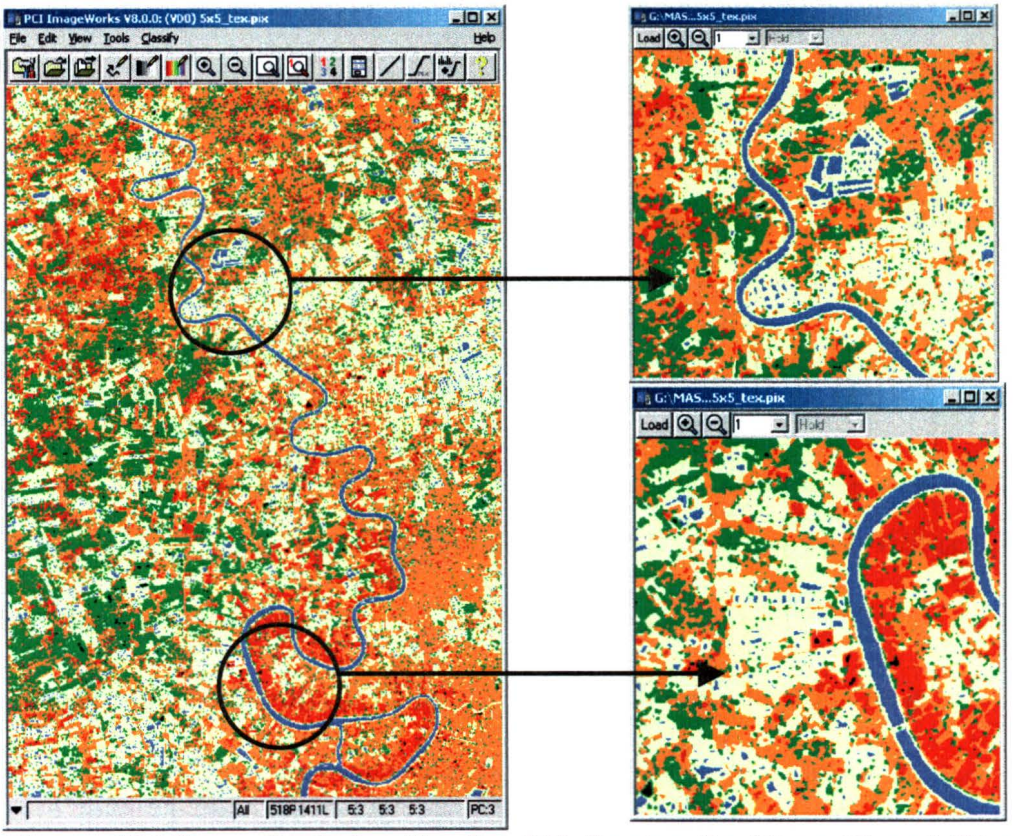

Figure 6.24 Supervised classification MLC using the Mean F1 and F4 components (July 11 and July 18) with the second set of training sites (farm)

Table 6.33 a) Legend of MLC using the Mean F1 (July 11) and F4 components (July 18) with the second set of training sites farm; Figure 6.20 b) *allwater*; Figure 6.21

Land Types	MLC with Mean F1 and F4 (2nd set of training sites with Farm)	MLC with Mean F1 and F4 (2nd set of training sites with *allwater*)
Water (river, ponds, etc)	Blue	Blue
Shrimp Farms (ponds and dykes)	Blue and Beige	-
Rice	Green	Green
Orchard	Orange	Orange
Human	Red	Red

On Figure 6.24 (Table 6.33), it is possible to see that fewer pixels were identified as water, and a large area of the classified image (top left) was identified as human settlements when it should have been classified as rice paddies. The overall accuracy of this classification was around 5% less then the one run on the F1 multi-temporal images (Table 6.32).

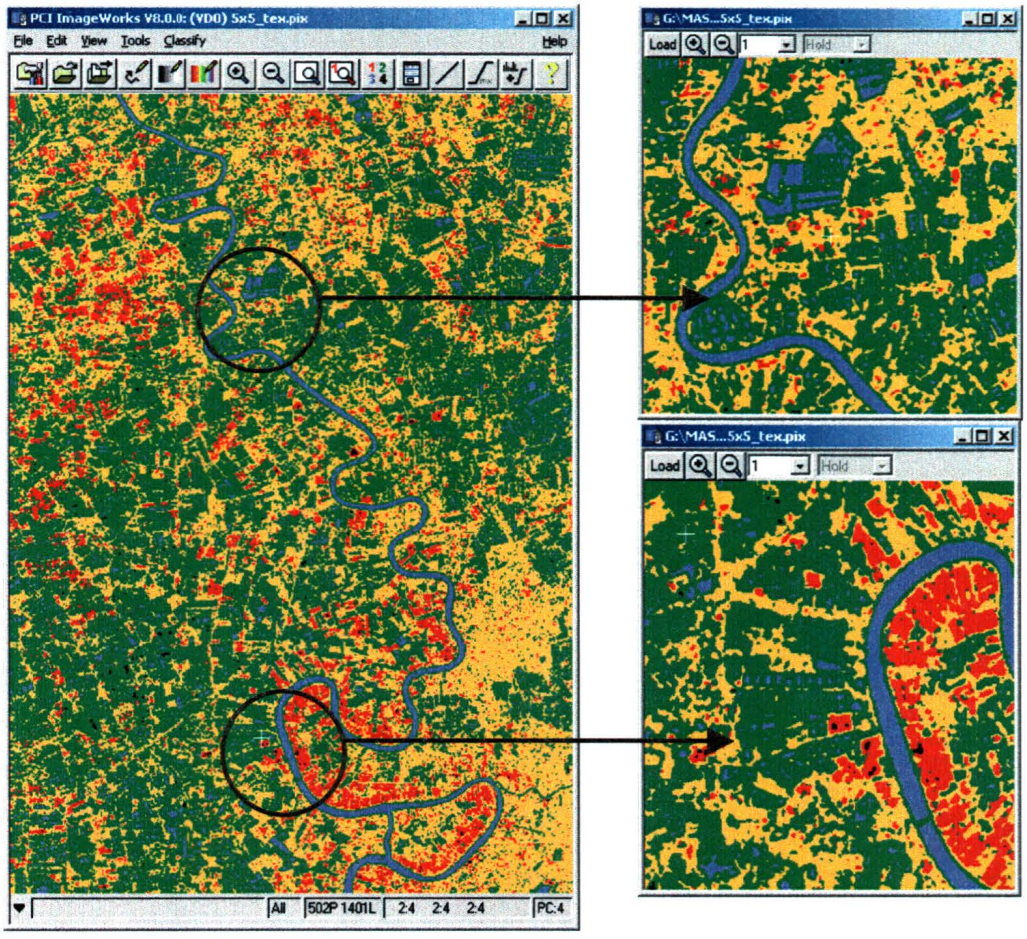

Figure 6.25 Supervised classification MLC using the Mean F1 (July 11) and F4 (July 18) components with the second set of training sites (allwater)

With the *allwater* class, the classification was not as good as the one run with the F1 images only. The rice class took over the water areas, and the human class took over the rice areas (Figure 6.25 and Table 6.33). The overall accuracy of this classification was around 10% less then the one run with the F1 images (Table 6.32).

The classifications based on the multi-angle imagery were less accurate than the ones based on the multi-temporal combinations possibly because the image with the shallow incidence angle, F4, presented more contrast between the land and the water, and the image with a steeper incidence angle, F1, was usually more sensitive to the roughness of the features, and reflected a greater proportion of signal back to the sensor. These

different characteristics in both images yielded different reflectance characteristics for the same features, resulting in more confusion between them. The use of a multi-temporal combination resulted in similar reflectance characteristics from land features.

6.2.3.4 Accuracy Assessment

The accuracy assessment was run with only the two better classification results, which were the MLC using F1 Mean texture components with the second set of training sites (Figure 6.26 and Table 6.34). The first classification was run with 5 classes, using the shrimp farm class, and the second with 4 classes, using the class grouping all the water bodies together (*allwater*).

a) d) g)

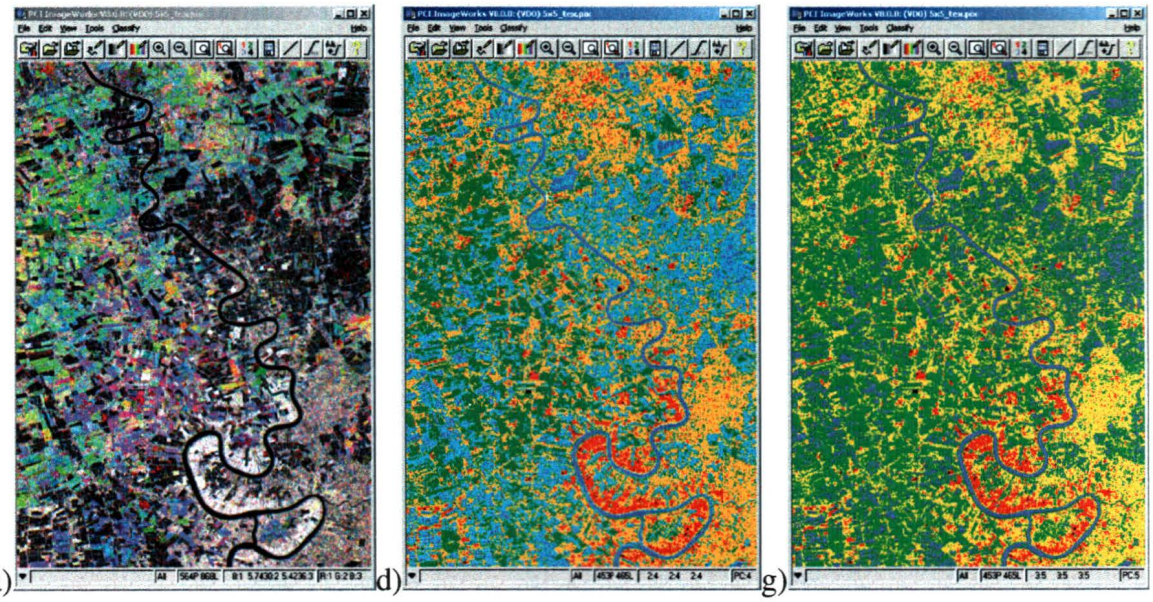

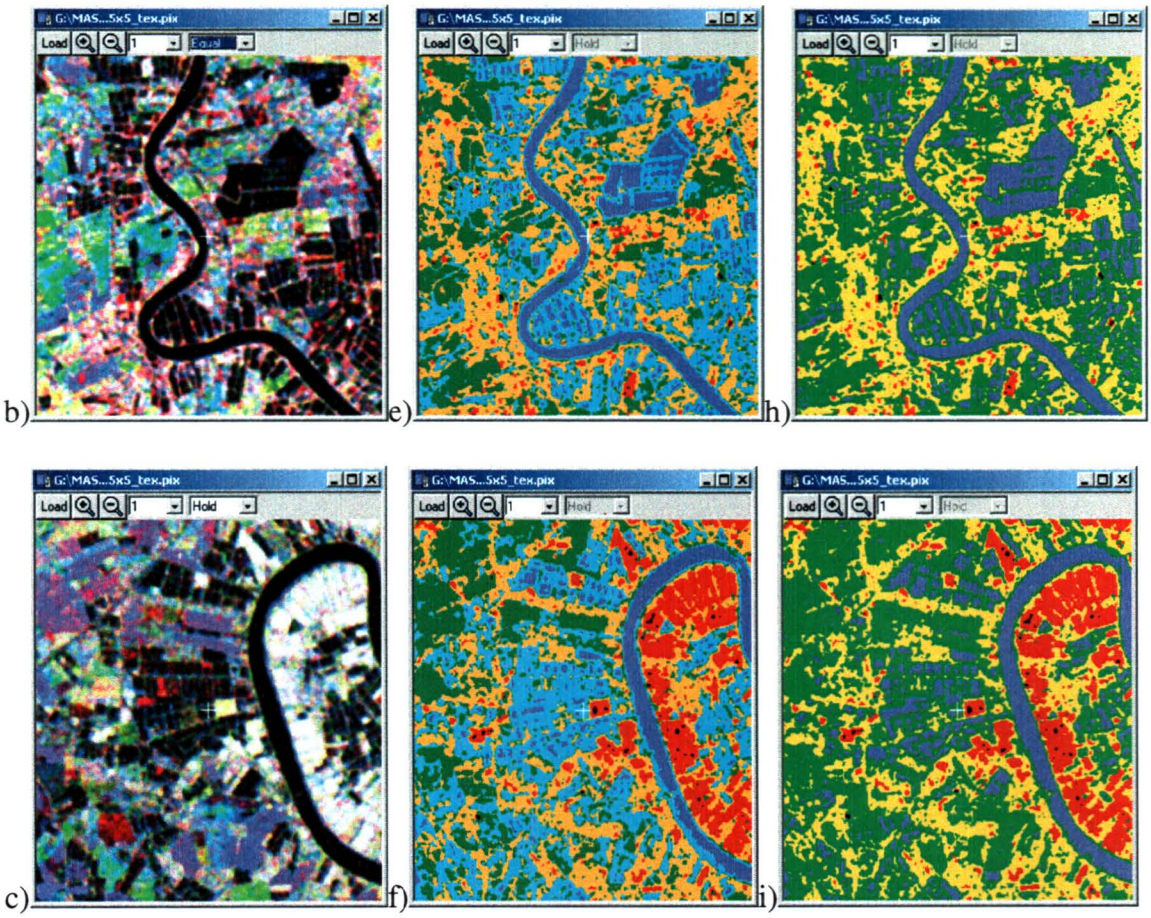

Figure 6.26 a-b-c) RGB combination of F4 and F5 Mean components d-e-f) MLC using the Mean F1 components (May 24 and July 18) with the second set of training sites (farm) g-h-i) MLC using the Mean F1 components (May 24 and July 18) with the second set of training sites (*allwater*)

Table 6.34 a) Legend of (Figure 6.22) a) RGB combination of F4 and F5 Mean components b) MLC using the Mean F1 components (May 24 and July 11) with the second set of training sites (farm) c) *allwater*

Land Types	a) RGB combination of Mean F4 and F5 images	b) MLC with Mean F1 (2nd set of training sites with Farm)	c) MLC with Mean F1 (2nd set of training sites with *allwater*)
Water (river, ponds, etc)	Black	Blue	Blue
Shrimp Farms (ponds and dykes)	Black	Turquoise and Blue	-
Rice	Red, Blue, Green, Turquoise, purple, dark yellow	Green	Green
Orchard	Mix colours	Orange	Orange
Human	White and light yellow	Red	Red

A third set of training sites, called accuracy sites, were created in order to verify the identification of the land covers by the supervised MLC using the second set of training sites. The accuracy sites needed to be different from the training sites used for the classification. Six new training sites were created in order to assess the classification results: rice paddies, orchard plantations, human settlements, water (river, reservoir, but not shrimp ponds), shrimp farms and a class representing all the water bodies (river, reservoir and also shrimp ponds). Table 6.35 presents the mean and standard deviation of the training sites (second set of training sites used for this classification) and the accuracy sites (third set of training sites) for all the classes to be verified.

Table 6.35 Mean and standard deviation of the training and accuracy sites (F1 images).

	Training Sites		Accuracy sites		Training sites		Accuracy sites	
	24-May-01		24-May-01		11-Jul-01		11-Jul-01	
Land Types	**Mean**	***Std.Dev.***	**Mean**	***Std.Dev.***	**Mean**	***Std.Dev.***	**Mean**	***Std.Dev.***
Rice	-8.79	*-7.96*	-8.56	*8.48*	-8.62	*-7.64*	*-9.40*	*8.59*
Human	-4.16	*-3.88*	-3.46	*2.92*	-4.53	*-4.33*	*-4.25*	*4.30*
Orchard	-7.82	*-8.02*	-8.17	*8.87*	-7.11	*-7.49*	*-7.42*	*7.97*
Water	-18.22	*-14.92*	-18.48	*17.27*	-16.73	*-15.67*	*-16.86*	*15.01*
Farm	-11.45	*-8.03*	-14.16	*12.46*	-10.28	*-7.21*	-12.61	*10.51*
Allwater	-17.86	*-14.99*	-18.67	*16.50*	-16.68	*-15.36*	*-16.86*	*14.73*

The reason that the shrimp farm class is not exactly the same in the two sets is probably because these sites include different types of pixels, land for dykes and water for ponds, so it is possible that the mean and standard deviation will vary a little (Table 6.35 and Figure 6.27).

a)

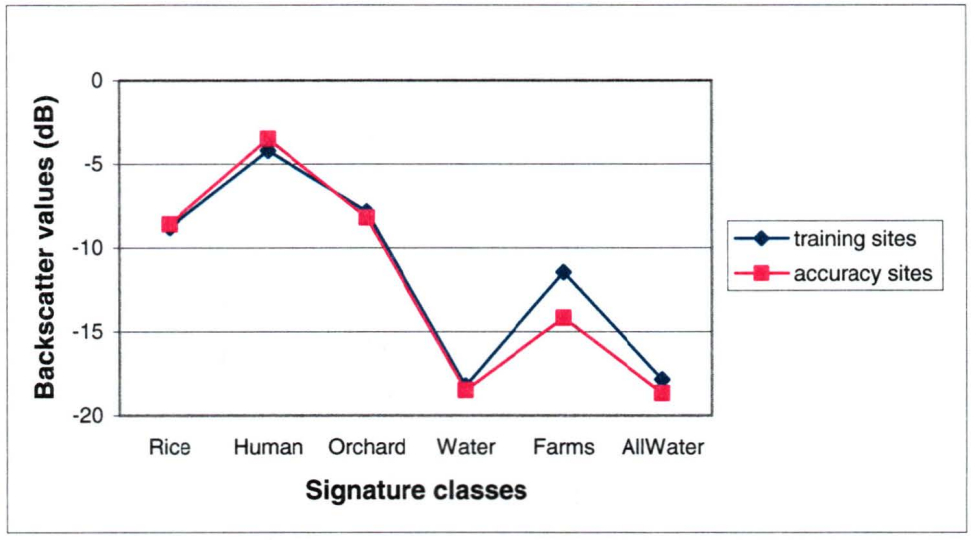

b)

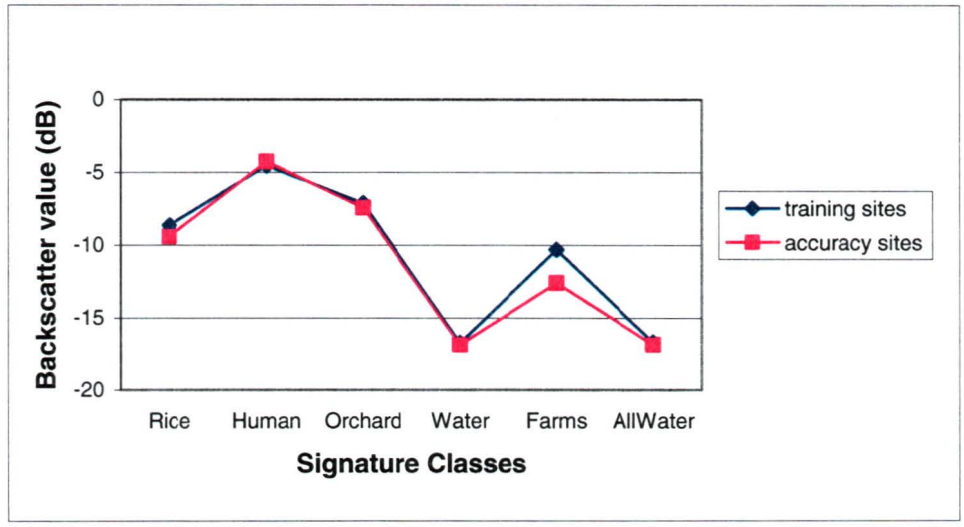

Figure 6.27 Signature comparison of the training and accuracy sites (F1 images) a) for May 24, 2001 b) July 11, 2001

Both matrix analyses were created with the MAT function (matrix analysis) of the XPACE program with PCI Geomatica. Each of the classifications was assessed using this function, entering both classification and accuracy sites as input channels. This function computes the percentage of pixels of the accuracy sites that are well identified in the classification channel.

Table 6.36 Accuracy analysis of the classifications run with five classes (shrimp farm), using Mean texture F1 images.

	Accuracy Sites					
Training Sites	Rice	Orchard	Human	Water	Farm	TOTAL
Rice	68%	19%	3%	0%	10%	100%
Orchard	8%	84%	3%	0%	6%	101%
Human	2%	12%	83%	0%	1%	98%
Water	0%	0%	0%	85%	15%	100%
Farm	1%	0%	0%	46%	53%	100%
Average Accuracy: 75%						

Tables 6.36 and 6.37 demonstrate the accuracy of the classifications run with the Mean texture F1 images using the second set of training sites with either the shrimp farm class or the *allwater* class. It is important to note that MAT averages the results, so no decimals are shown in the results (full report in Appendix 3). That explains why the totals do not always come to 100%. The results of the matrix analysis can be read horizontally. Only the average accuracy was calculated in the accuracy analysis because the report produced by MAT does not give the number of pixels overlapping null areas, which is necessary in order to obtain overall accuracy. For the first classification results (Table 6.36), 68% of the rice accuracy sites were overlapping rice areas in the classification using the second set training sites. However, 19% were overlapping the orchard plantations, 3% the human settlements and 10% the shrimp farm areas. The rice is then slightly confused with the orchard plantations according to this analysis. The orchard, human, as well as the water classes are accurate, and almost not confused with other classes. The overall accuracy of the accuracy analysis is 75%, which is high. However, the shrimp farm class demonstrates confusion with the rice and the water pixels. Even if the classification looks good visually, showing the dykes of the ponds, the farm class was actually supposed to enclose the whole area where farms were situated (ponds and dykes). Although, it did not work very well, and the dyke's pixels were classified as farm, plus the ones representing ponds were confused with the water class. In further analysis it would be recommended to test the dykes as a separate class, and the water should not be separated into different classes.

Table 6.37 Accuracy analysis of the classification run with four classes (*allwater*), using the Mean texture F1 images.

	Accuracy Sites				
Training Sites	*Allwater*	Rice	Orchard	Human	TOTAL
Allwater	96%	4%	0%	0%	100%
Rice	0%	78%	19%	3%	100%
Orchard	0%	13%	84%	3%	100%
Human	0%	3%	12%	83%	98%
Average Accuracy: 85%					

With the classification run with the Mean F1 images using the *allwater* class, the accuracy results are very good (Table 6.37). The accuracy sites were almost all overlapping the right classified areas. The average accuracy of this analysis is 85%, demonstrating very good accuracy results. All the classes were very well identified. The only issue was with the dykes surrounding the shrimp ponds. They were identified as rice paddies because of their high backscattering signal, which was similar to the rice class. This demonstrates once more the usefulness of a further analysis testing the separation of the dykes themselves as an independent class.

6.2.3.5 Summary

The results of the texture analysis on the radiometrically and geometrically corrected images, prior to unsupervised classification (k-means) and supervised maximum likelihood classification (MLC), with two sets of training sites, can be summarized as follows:

- **Evaluation of the texture components:**
  - Best window size is 5x5
  - Least correlated texture components: Principally Correlation and Mean; but also Angular 2nd Moment, Contrast and Standard Deviation.

- Texture components with best separability analysis (tested with 1st set of training sites): Mean (May 7, F4 and July 18, F4), Standard Deviation (May 24, F1), and Contrast (May 24, F1).

- **RGB combination:**
  - Best texture components together (Mean for May 7 and July 18, and Standard Deviation for May 24) show the linear perimeter of the shrimp ponds.

- **Unsupervised classification (k-means):**
  - Best results obtain with the multi-temporal Mean textured image combination of shallower incidence angle (F4 and F5) with 8 and 5 classes.
  - Results of this classification are more accurate than the unsupervised classification run on the raw images and Frost speckle filtered images.

- **Supervised classification (MLC) using the first set of training sites:**
  - Good results obtained with this mix of the best texture components (Mean for May 7 and July 18, and Standard Deviation for May 24), using the rice, orchard, human, water and shrimp pond classes.
    - Overall accuracy: 59.28% (still lots of confusion)
  - Good results obtained with the multi-temporal Mean textured image combination of shallower incidence angle (F4 and F5), using the rice, orchard, human, water and shrimp pond classes.
    - Overall accuracy: 58.08% (still lots of confusion)

- **Supervised classification (MLC) using the second set of training sites:**
  - Best results obtained with the multi-temporal Mean texture image combination of steeper incidence angle (F1), using the rice, orchard, human, water, and shrimp farm classes.
    - Overall accuracy: 70.91%
  - Best results obtained with the multi-temporal Mean texture image combination of steeper incidence angle (F1), using the rice, orchard, human, and *allwater* classes.

- Overall accuracy: 80.12% (very good identification of the water bodies, and all the other classes)

- The accuracy assessment demonstrated that the two MLC using Mean F1 images produced accurate results at 75% with the shrimp farm class, and 85% with the *allwater* class.
- The MLC and accuracy analysis results using multi-temporal Mean F1 images demonstrated the potential of RADARSAT-1 imagery for monitoring and mapping shrimp farms and other land use types present on the area of study.

6.3 Image Segmentation

Image segmentation could be a better way to obtain accurate classification results. Compared to the pixel-based classifications, the segmentation-based method agglomerates similar pixels into rough or very precise regions prior to classification. In this way, a heterogeneous class can be turned into a homogenous region. With the use of eCognition software, the segmentation application first groups the pixels into regions, and then the analyst can program a supervised classification based on the information of these regions, such as their neighbouring regions, their shape, texture, colours, etc. The analyst can specify many parameters in order to create a supervised classification representing the specific features [s]he wants.

In the present analysis, the shrimp farms have a special shape and pattern. Each farm is constituted by many water ponds (small with square shape), characterized by low backscattering values, which are surrounded by linear dykes having high backscattering values. These shrimp farms are areas constituted by heterogeneous pixels, which could be grouped together using a segmentation procedure, and then identified as homogenous regions, prior to classification.

This method was tested briefly on a multi-temporal combination of Mean textured RADARSAT-1 images with shallow incidence angles, using eCognition 3.0 software.

6.3.1 Segmentation-Based Classification

The Mean texture images with shallow incidence angles F4 and F5 were chosen because their combination generated the best unsupervised classification results. The results obtained from the k-means classifications were the ones that mattered because they were performed without major intervention by the analyst that might corrupt the information contained in the raw images. Also, this multi-date combination covered the whole temporal period of the study and presented a good RGB resulting image. The visual quality of the input image is important with segmentation based classification.

A subset area of the image used for all the previous analysis had to be done because the demo version of eCognition 3.0 only allowed a maximum area of 1024 pixels and 1024 lines. The upper left coordinates of the subset were 101d08'51.55"E (longitude), 13d46'57.08"N (latitude), and the lowest right coordinates were 101d12'27.69"E (longitude), 13d43'34.76"N (latitude). The total area covers 655 pixels by 616 lines. This area was chosen because it afforded a good representation of all the features present in the whole study area: rice paddies, orchard plantations, human settlements, shrimp farm and water bodies, like the Bang Pakong river (Figure 6.28).

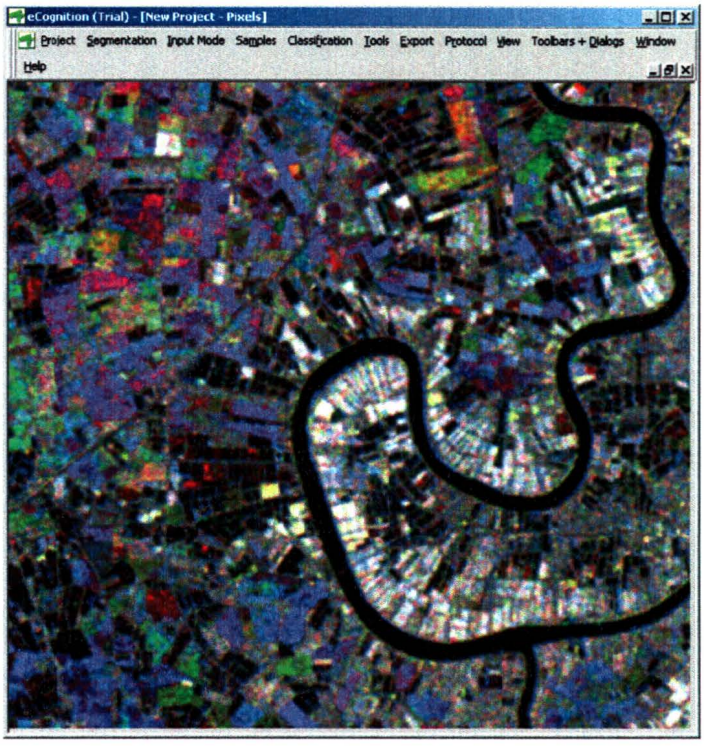

Figure 6.28 Subset area used for segmentation-based classification, RGB of F4 and F5 Mean images.

Once the subset had been defined, a multi-resolution segmentation was applied to it. At this step, the analyst specifies the scale parameter and the homogeneity criterion (colour, shape, smoothness and compactness) in order to create appropriate regions grouping the right pixels together. Different values were tested on the subset area in order to establish the most suitable criteria. After changing the weighting for each of the four possible criteria (colour, shape, smoothness and compactness), the best segmentation result was obtained using the colour for principal criteria. The colour criteria gave good results, probably because a RGB combination of three images was used as input. If only two images were used as input, the important criterion may have been different, since the false colour composite of two images is not as great as three images. The shape criterion should also be taken into consideration in order to classify the shrimp

farms. Further analyses are suggested. Polygons were traced around groups of pixels representing the same land use types. Rice paddies, orchard plantations, human settlements and water (river) were all recognized as regions. The most important was that the shrimp farm areas were also recognized as a homogeneous area, including the dyke and the shrimp pond pixels (Figure 6.29 and Table 6.38). Figure 6.29 points out an example of a shrimp farm region using a red arrow.

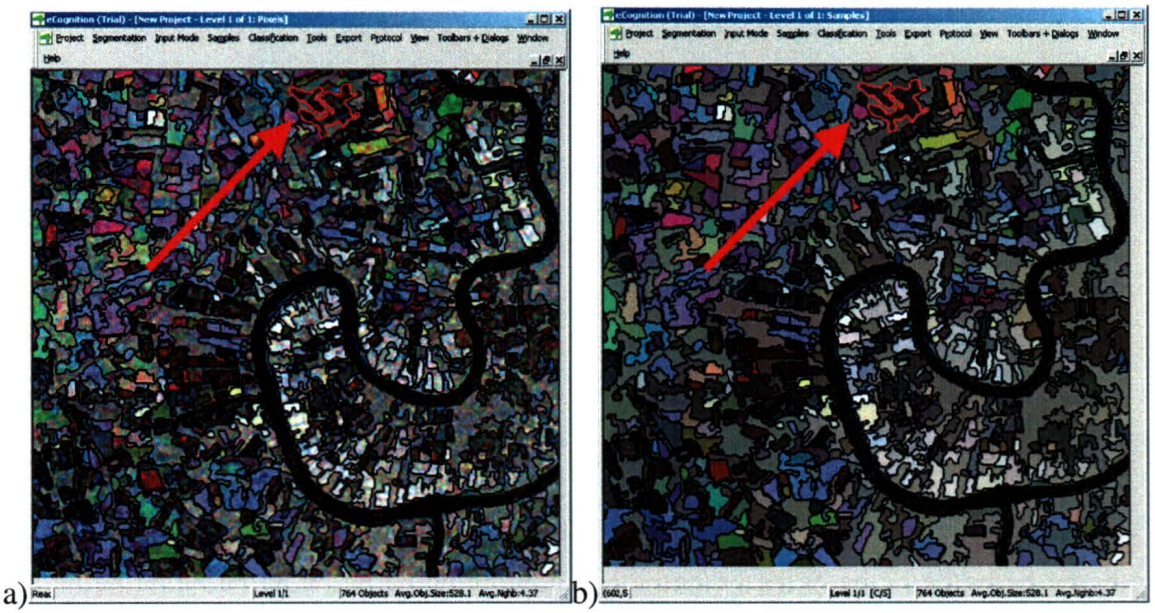

Figure 6.29 Segmentation of the F4 and F5 Mean texture images a) transparent view (keeping the original pixel values) b) object mean.

Table 6.38 Legend of the segmentation of the F4 and F5 Mean texture images.

Land Types	Colour
Rice paddies	Purple, green, red, yellow
Orchards	Mixed colour
Human settlements	White, light grey
Water (Bang Pakong River)	Black
Shrimp farms	Areas constituted of shrimp pond pixels (black), and dyke pixels (mixed colours): demonstrated by the area selected in red.

The classification was based on five classes demonstrated in Figure 6.29: rice paddies, human settlements, orchard plantations, water bodies, and shrimp farms. The training sites, Figure 6.30 a), were traced after segmentation. The only criterion selected for the classification was the standard nearest neighbour of each class for all the input images.

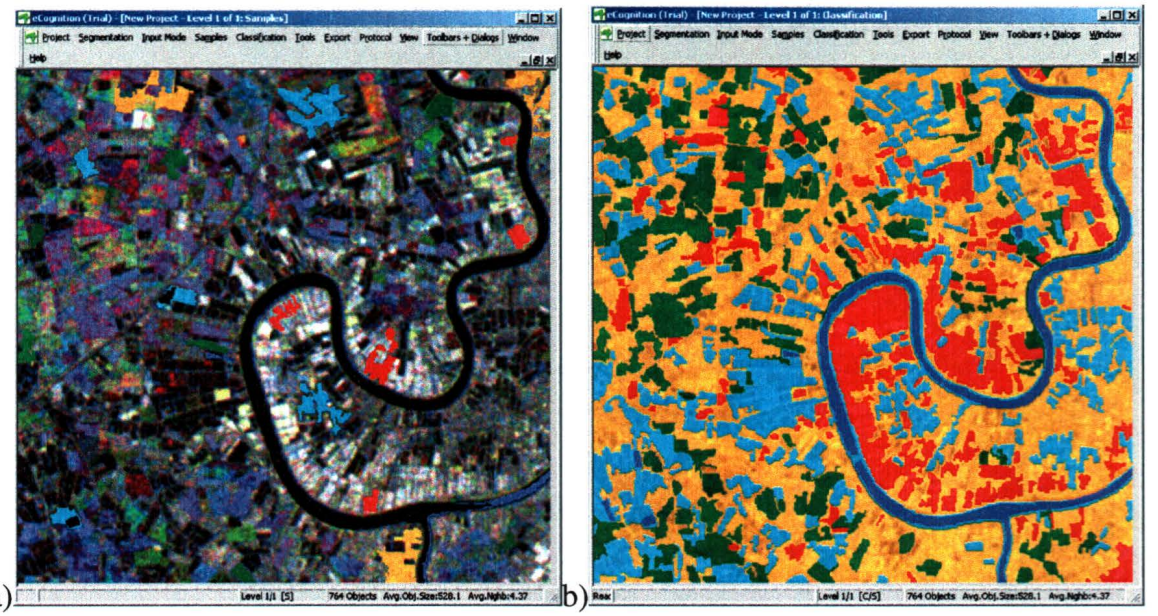

Figure 6.30 a) training sites (original F4 and F5 Mean texture image) b) segmentation-based classification result

Table 6.39 Classes identification

Classes (training sites)	Colour
Rice paddies	Green
Orchards	Orange
Human settlements	Red
Water	Blue
Shrimp farms	Turquoise

The resulting classification was very good Figure 6.30 b) and Table 6.39). The shrimp farms were actually the feature that was the best recognized by the process. The human settlement class was confused with the rice paddies that were in dryer stages and had lighter colours (high backscattering values). The water class identified the Bang Pakong

River, but did not see the water reservoirs. Finally, the orchard class is representing the area covered by this type of land use very well.

More analysis should be done in order to obtain better results and statistically verify their accuracy. The classification results seem good visually, but since the demo version of eCognition does not provide an accuracy assessment option, the results could not be verified statistically. The present analysis was done in order to prove the potential of this method using eCognititon software version 3.0.

6.3.2 Summary

The results of the segmentation on the Mean texture image with shallow incidence angle (F4 and F5), prior to a supervised classification, can be summarized as follow:

- Segmentation transformed heterogeneous areas like shrimp farms (water and land pixels) into homogenous regions.
- Segmentation-based classification, using the eCognition software 3.0 (demo version), seems to have great potential in identifying the land covers of the study area.
- Further analyses are suggested.

6.4 Results Summary

The synthesis of all the results obtained with the different pre-processing analyses, in order to reach accurate unsupervised and supervised classifications, can be summarized as follows:

- **Raw images:**
    - Good false colour composite (RGB) with the multi-temporal images F4 (May 7 and July 18) and F5 (September 19)
    - Best k-means: with multi-temporal images F4 (May 7 and July 18) and F5 (September 19) using 16 classes

- **Pixel-Based Classifications:**
  - Principal Component Analysis:
    - PCA on 5 images and on the multi-temporal F4 (May 7 and July 18) and F5 (September 19) images: not enough change over time, so results not significant.
    - MLC with the principal components of the multi-temporal images F4 (May 7 and July 18) and F5 (September 19): 42.40% of overall accuracy.
    - Not an appropriate analysis
  - Speckle Filtering:
    - Best filter: Frost, using the 3x3 window size
    - Good false colour composite (RGB) with the multi-temporal Frost images F4 (May 7 and July 18) and F5 (September 19)
    - Best k-means: with multi-temporal Frost images F4 (May 7 and July 18) and F5 (September 19) using 16 and 8 classes.
    - Two Best MLC:
      - Frost multi-temporal images F4 (May 7 and July 18) and F5 (September 19), with 5 classes (rice, orchard, human, water and shrimp farm): 66.70%
      - Frost multi-temporal images F1 (July 11 and July 18), with 4 classes (rice, orchard, human, and *allwater)*: 68.03%
  - Texture Analysis
    - Good texture components: Mean, Contrast and standard Deviation, using the 5x5 window size
    - Best texture components: Mean
    - Good false colour composite (RGB) with the Mean images F4 (May 7 and July 18) and F5 (September 19)
    - Best k-means: with F4 (May 7 and July 18) and F5 (September 19) using 8 and 5 classes.
    - Two Best MLC:

- Mean multi-temporal images F1 (July 11 and July 18), with 5 classes (rice, orchard, human, water and shrimp farm): 70.91%
- Mean multi-temporal images F1 (July 11 and July 18), with 4 classes (rice, orchard, human, and *allwater)*: 80.12%

- Accuracy analysis on the two best classifications with Mean texture components demonstrated the great significance of the two classifications with 75% (5 classes) and 80% (4 classes) correct identification of the features.

- **Segmentation-Based Classification:**
  - Segmentation group heterogeneous pixels, representing one land use, into one homogeneous region.
  - Demonstrate potential for classification of heterogeneous type of land use, like shrimp farms.
  - Further analysis suggested.

CHAPTER SEVEN

CONCLUSION

As mentioned in the introduction to this document, the goal of this study was to evaluate the potential of multi-temporal, and/or multi-angle, RADARSAT-1 imagery as a tool in monitoring and mapping shrimp farms, as well as other land cover and land use types, present in the Bang Pakong River basin situated in the Central Plain of southeastern Thailand.

The first main objective was to find the best RADARSAT-1 image classification procedure to identify shrimp farms and other land use present on the study area. The first step to reach that objective was to choose between principal components analysis (PCA), speckle filtering or texture analysis, to see which pre-processing approach was the better one to use and how to apply it. The second step was to evaluate if the classification results were better when performed with an unsupervised algorithm (k-means) or a supervised one (MLC). The greater part of the analysis was performed with pixel-based classifiers, but a segmentation-based classifier was tested as well. In order to evaluate if the results were more accurate using multi-temporal, and/or multi-angle images, all these experiments were executed using two different image combinations, with shallow and steeper angles (multi-angle), or using multi-temporal images. In combining multi-temporal images together, the purpose was not to see change over the time since there was almost no change (except in the rice paddies) as demonstrated by the PCA. The aim was to evaluate the different information from a combination of images with similar incidence angles, with different acquisition dates (F1 together, and F4 and F5 together),

compared to a combination of images with different incidence angles (F1 and F4) with similar acquisition dates.

The second main objective of this project was to verify if the shrimp farms could be differentiated from other water bodies in a supervised classification by assessing if polygons grouping pixels representing shrimp ponds only (water and possibly aerators, if detectable by the RADARSAT-1 satellite), or polygons grouping pixels representing shrimp farm areas (water and dykes surrounding the ponds, if detectable by the RADARSAT-1 satellite) could be differentiated from the water class in a resulting classification.

In order to look at the images without any post processing applied to them, different combinations of the different incidence angle images F1 or F4 and F5 were interpreted. The images with steep incidence angles (F1) are influenced by the roughness of the water, displaying high backscattering value pixels in water regions, where the majority of the pixels have very low backscattering pixel values. On the other hand, the images with shallower incidence angle images (F4 and F5) are not influenced by the roughness of the surface, and assume the water to be a very specular region, reflecting the backscattering signal away from the sensor and displaying the water bodies on the image as uniform black areas. So, for a false colour composite (RGB combination) that would clearly show the extent of shrimp farms in this region, the multi-temporal combination of F4 and F5 images, prove to be the best. The training sites used for the classifications were traced on this particular combination, since the features were very clearly distinguishable from one another, and the shrimp ponds in particular.

In order to classify the land covers in the area, training sites were drawn around examples of rice paddies, orchard plantations, human settlements and water bodies but

not shrimp ponds. With the purpose of differentiating the shrimp farms from the other water bodies two more classes were tested. The shrimp pond class, including pixels of the ponds only, and the shrimp farm class, representing farm areas and including shrimp ponds and dykes pixels. Two sets of training sites were outlined because some mistakes occurred when drawing the first set of polygons. In this first set, the shrimp pond class included too many surrounding pixels, representing the dykes, so that the backscattering signal for that class came in higher than desired. The other problem involved the human training sites since they included some orchard pixels causing confusion between the two classes in most of the classifications performed with them. The second set of training sites used the same classes (rice, orchard, human, water bodies, shrimp ponds and shrimp farms), but with training sites identifying land use more correctly. A sixth class was added to this second set of training sites in order to test if the water class could be well separated from all the other classes, without trying to separate out the shrimp farms from simply water. The new class was called the *allwater* class, representing all the water bodies (river, reservoirs, and shrimp ponds).

Since the ultimate objective of the thesis was to separate shrimp farm land use from other uses, the question to be answered was: which combination of techniques, images and appropriate classes would result in the best classification. In comparing the pre-processing techniques, it was demonstrated that the Frost filter and the Mean texture component were the best criteria to use for image classification. According to the analysis performed in order to find out which of the image combinations was the best with which classification techniques, the F4 and F5 images produced accurate results with k-means classification, using the Frost filtered images, and the Mean texture components. One of the best maximum likelihood classification results was with the *allwater* class

(classification using only four classes), not trying to separate the shrimp farms from the other water bodies, using the mean component of the steeper incidence angle (F1) images. The overall accuracy result was 80.12%. However, with this technique, the surrounding pixels of the farms were considered to be rice paddies. The other best maximum likelihood classification result was obtained when trying to separate the shrimp farms from the other water bodies. The results were still the best using the same input images, with an overall accuracy of 70.19%. The classification was reasonably good with the shrimp farms class (mixing water and dykes), creating a new mean, different from water and rice. However, the water in the ponds was still recognized in most of the classified images, so the "farm class" seemed mostly to include the surrounding pixels of the water ponds, the dykes, but also some of the pond. This would explain the low overall accuracy of results (mixed class), but the good visual interpretation of the results. An accuracy analysis was applied to the two best MLC results using the Mean texture images with a set of accuracy sites. The results of the analysis demonstrated an accuracy of 75% for the classification using the farm class, and 85% for the classification using the *allwater* class. These final results reveal the potential of RADARSAT-1 imagery using this classification procedure for the present project.

Here is the best approach, proposed by this study, to classify the shrimp farms, and other land use / land cover, and to monitor their evolution over time. The statistically and visually best pre-processing technique was the texture analysis. Within the eight texture components and the three window size tested, the mean component using a 5x5 window size was the best. With this component each land cover were well defined, removing the speckle (salt and pepper effect), smoothing the image while keeping the edges of the land features. All the image processing techniques give very high results,

depending which input images were used, with which training sites. The best pixel-based unsupervised classification k-means was obtained with the mean texture components, using a multi-temporal combination of shallow incidence angles, F4 and F5, using eight classes. The statistically and visually best pixel-based supervised maximum likelihood classification results were obtained with the mean texture component, using a multi-temporal combination of steep incidence angle, F1, and using 5 classes (with the shrimp farm class). In the resulting image, the shrimp farm class was grouping the dykes and the small shrimp ponds. However, the bigger shrimp ponds and the water reservoir were included in the water class. The difference between the bigger shrimp ponds and the water reservoir was the dyke areas surrounding them. For the water reservoir, the surrounding dyke area was smaller, and for the bigger shrimp ponds, the dyke area was bigger. This classification demonstrates that with a little bit of knowledge of the area, it is possible to obtain a sound interpretation of the resulting image. The results of this classification also proved that it is was possible to differentiate the shrimp farms from other water bodies in a supervised classification using the shrimp farm class (class including shrimp pond and dyke pixels), with a supervised maximum likelihood classification using steep incidence angle (F1) images as input. According to all the resulting classifications, the best images combinations were the multi-temporal ones.

Trying to identify the shrimp farms, as a distinct class from the water and the other land features, was a challenge with pixel-based classifiers. This class was considered to be heterogeneous, with pixels representing two types of land, according to the theory (Schowengerdt, 1983). However it happens to work well for shrimp farms, identifying the dyke areas surrounding the shrimp ponds with F1 images.

For further work, with the purpose of differentiating shrimp farms from other water bodies and other land uses, it would seem to be desirable to create a class representing dykes and to keep the one representing water, using a pixel-based classifier. Also, the use of a segmentation-based classifier, such as the eCognition software tested in section 6.3 of Chapter 6, could be recommended in order to transform the heterogeneous class of pixels, in this case shrimp farms, into a homogeneous region. The segmentation-based classification produce a good resulting classified image, using a multi-temporal combination of shallow incidence angle (F4 and F5), and using 5 classes with the shrimp farm class. The results demonstrated in that section were interesting, and suggest going further into this type of image analysis.

This study proposes a potential way to monitor and manage shrimp farming, this growing aquaculture sector of the global economy of Thailand. As Thailand has been the world's largest producer and exporter of cultured shrimp for over 10 years, and with total production increasing, an accurate methodology able to be used on a regular basis is highly necessary (Huitric *et al.*, 2002; Flaherty *et al.*, 2000; 1999; Patmasiriwat *et al*, 1998). The outcome of this project demonstrates the accuracy of a simple procedure to perform accurate supervised classifications on a regular basis in Thailand of the different types of land use, and of shrimp farms in particular.

REFERENCES

Allen, S., Gagnon, L. and Lesage, F. 2001. Hydrous Area Segmentation in Radar Imagery by Level Set-Based Snakes. *10e Congrès de l'Association Québecoise de Télédétection*, Ste-Foy, Québec.

Anderson, J.L. and Fong, Q.S.W. 1997. Aquaculture and International Trade. Aquaculture Economics and Management. 1(1):29-44.

Anys, H. and He, D.-C. 1995. Evaluation of Textural and Multi-polarization Radar Features for Crop Classification. *IEEE Transactions on Geoscience and Remote Sensing*. 33(5):1170-1181.

Arbhabhirama, A., Phantumvanit, D., Elkington, J., Ingasuwan, P. 1988. Thailand Natural Resource Profile. *Thailand Development Research Institute*, Singapore: Oxford University Press.

Aquasol, Inc. 2002a. Shrimp Farming: *The Market for Farm-Raised Shrimp*. (www.fishfarming.com)

Aquasol, Inc. 2002b. What is Aquaculture: *Aquaculture Involves the Managed Reproduction and Grow Out of Aquatic Animals Under Controlled Conditions*. (www.fishfarming.com)

Arvelyna, Y., Oshima, M., Kristijono, A. and Gunawan, I. 2001. Auto Segmentation of Oil Slick in RADARSAT SAR Image Data Around Rupat Island, Malacca Strait. *Proceedings of the 22nd Asian Conference on Remote Sensing,* Singapore.

Baatz, M. and Schäpe, A. 2000. Multiresolution Segmentation: an Optimization Approach for High Quality Multi-Scale Image Segmentation. *AGIT Symposium*. Salzburg, Austria.

Bénié, G.B. and Thompson, K.P.B. 1992. Hierarchical Image Segmentation Using Local and Adaptive Similarity Rules. *International Journal of Remote Sensing*. 13, 1559-1570.

Bernier, M., Ghedira, H., Gauthier, Y., Magadi, R., Filion, R., De Sève, D., Ouarda, T., Villeneuve, J.-P. and Buteau, P. 2003. Détection et Classification de Tourbières Ombrotrophes du Québec à partir d'Images RADARSAT-1. *Canadian Journal of Remote Sensing*. 29(1):88-98.

Bernier, M., Fortin, J.P., Gauthier, Y., Gauthier, R., Roy, R., and Vincent, P. 1999. Determination of Snow Water Equivalent using RADARSAT in Eastern Canada. *Hydrological Processes, John Wiley & sons*. 13(18): 3031-3042.

Bonn, F. and Rochon. G. 1996. *Precis de Télédétection : Principes et Méthodes*. Presses de l'Univesrité du Québec, Canada. Volume I. 485p.

Braaten, R.O. and Flaherty , M. 2000. Hydrology of Inland Brackishwater Shrimp Ponds in Chachoengsao, Thailand. *Aquaculture Engineering*. 23, 295-313.

Brown, R.J., Brisco, B., Leconte, R., Major, D.J., Fisher, J.A., Reichert, G., Korporal, K.D., Bullock, P.R., Pokrant, H., and Culley, J. 1993. Potential Applications of RADARSAT Data to Agriculture and Hydrology. Canadian Journal of Remote Sensing. 19(4):317-329.

Buchroithner, M. 1993. Chapter 15: Cartographic Information Extraction from SAR Images Using Filtering and Textural Analysis. (Schreier, G. Ed.), *SAR Geocoding: Data and Systems*. Wichmann. 435p.

Buiten, H.J. 1993. Supplement 10: Principal Components Transformation and Data Reduction. In: *Current Topics in Remote Sensing: Land Observation by Remote Sensing, Theory and Applications*. Buiten, H.J. and Clevers, J.G.P.W. Eds. Gordon and Breach Science Publishers. Volume 3. 642p.

CCRS, Canada Centre for Remote Sensing. 2002. *Imagery and Sensors: RADARSAT-1*. Natural Resources Canada. (www.ccrs.nrcan.gc.ca)

Congalton, R. and Green K. 1999. *Assessing the Accuracy of Remotely Sensed Data: Principles and Practices*. CRC/Lewis Press, Boca Raton, FL. 137 p.

Conners, R.W. and Harlow, C.A. 1980. A theoretical Comparison of Texture Algorithms. IEEE Tr. On Pattern Analysis and Machine Intelligence. Vol PAMI-2 (3).

Cook, R., McConnell, I., Oliver, C. and Welbourne, E. 1994. MUM (Merge Using Moments) Segmentation for SAR Images. *Proceedings of Europto SAR Data Processing for Remote Sensing*, SPIE-216, Rome, Italy, (Piscataway, NJ: IEEE). p92-103.

Costa, M. 2000. Net Primary Productivity of Aquatic Vegetation of the Amazon Floodplain: A Multi-SAR satellite Approach. *University of Victoria*, Ph.D. Thesis. 230p.

CRISP, Centre *for* Remote Imaging, Sensing *and* Processing. 2001. The National University *of* Singapore (www.crisp.nus.edu.sg)

CSA, Canadian Space Agency. 2000. Earth and Environment, RADARSAT-1. (www.space.gc.ca)

Definiens Imaging. 2003. *Product Overview, eCognition White Paper*. eCognition: Object Oriented Image Analysis Software.

De Loor, G.P. 1993. Chapter 10: Radar Backscatter of Crops. In: *Current Topics in Remote Sensing: Land Observation by Remote Sensing, Theory and Applications*. Buiten, H.J. and Clevers, J.G.P.W. Eds. Gordon and Breach Science Publishers. Volume 3. 642p.

Dierberg, F.E. and Kiattisimkul, W. 1996. Issues, Impacts and Implications of Shrimp Aquaculture in Thailand. *Environmental Management*. 20(5):649-666.

D'Iorio, M., Vibulsresth, S., Dowreang, D., Silapathong, C., Polngam, S. and Gordon, H. 1995. Identification of Agriculture and Land Use Practices in Southern Thailand from SAR Data. *Canadian Journal of Remote Sensing* 21(2):165-175.

Donner, W. 1978. *The Five Faces of Thailand; An Economic Geography*. C.Hurst and Co. Ltd. 930p.

Duda, R.D. and Hart, P.E. 1973. *Pattern Classification and Scene Analysis. New York.* John Wiley & Sons. 482p.

Estes, J.E., Hajic,E.J. and Tinney, L.R. 1983. Chapter 24: Fundamentals of Image Analysis: Analysis of Visible and Thermal Infrared Data. In: *Manual of Remote Sensing.* Colwell, N, Simonett, D.S. and Ulaby, F.T. eds. John Wiley & Sons, Inc. Volume 1. 866p.

FAO (Food and Agriculture Organization). 1990. Yearbook of fishery statistics. FAO, Rome.

FAO (Food and Agriculture Organization, Fisheries Department). 1997. Review of the State of World Aquaculture *FAO Fisheries Circular No. 886 FIRI/C886 (Rev.1).*

FAO (Food and Agriculture Organization), 1998. Report of the Ad-hoc Expert Meeting on Indicators and Criteria of Sustainable Shrimp Farming. *FAO Fisheries Report* No. 582, Rome, Italy, 28-30 April 1998.

FAO/SEAFDEC (Food and Agriculture Organization, Fisheries Department). 1997. Dramatic Change in Shrimp Culture in Thailand. Regional *Workshop on Fishery Statistics (FAO/SEAFDEC/97/12,Suppl.).* Bangkok, Thailand.

FAO (Food and Agriculture Organization). 2000. Thai Department of Fisheries, FAO FishStats.

Fjortoft, R., Lopes, A. and Adragna, F. 2000. Radiometric and Spatial Aspects of Speckle Filtering. *Proceeding of IGARSS'00*, Honolulu, Hawaii.

Flaherty, M., Szuster, B.W. and Miller, P. 2000. Low Salinity Inland Shrimp Farming in Thailand. *Ambio*. 29(3):174-179.

Flaherty, M., Vandergeest, P. and Miller, P. 1999. Rice Paddy or Shrimp Pond: Tough Decisions in Rural Thailand. *World Development*. 27(12):2045-2060.

Flaherty, M and Vandergeest, P. 1998. Low-Salt Shrimp Aquaculture in Thailand: Goodbye Coastline, Hello Khon Kaen! *Environmental Management.* 22(61):817-830.

Flaherty, M and Karnjanakesorn, C. 1995. Marine Shrimp Aquaculture and Natural Resource Degradation in Thailand. *Environmental Management.* 19(1):27-37.

Forster, B. 1996. Current Advances in Radar Remote Sensing Research and its Application in South East Asia. *Geocarto International.* 11(6):3-10.

Freeman, A. 1992. SAR calibration: an overview. *IEEE Transaction of Geoscience and Remote Sensing.* 30(6):1107-1121.

Frost, V. S. Stiles, J.A., Shanmugan, K.S., and Holtzman, J.C. 1982. A Model for Radar Images and its Application to Adaptive Digital Filtering of Multiplicative Noise. *IEEE Transaction on Pattern Analysis Machine Intelligence,* PAM-4, 157-165.

Fung, A.K. and Ulaby, F.T. 1983. Chapter 4: Matter-Energy Interaction in the Microwave Region. In: *Manual of Remote Sensing.* Colwell, N, Simonett, D.S. and Ulaby, F.T. eds. John Wiley & Sons, Inc. Volume 1. 866p.

Gonzalez, R.C. and Wintz, P. 1977. *Digital Image Processing.* Addison-Wesley. 431p.

Gerbrands, J.J. 1993. Chapter 14: Digital Image Processing. In: *Current Topics in Remote Sensing: Land Observation by Remote Sensing, Theory and Applications.* Buiten, H.J. and Clevers, J.G.P.W. Eds. Gordon and Breach Science Publishers. Volume 3. 642p.

Ghedira, H. 2000. Utilisation des Réseaux de Neurones pour la Cartographie des Milieux Humides à partir d'une Série Temporelle d'Images RADARSAT. Examen Doctoral. *Université du Québec, Institut National de la Recherche Scientifique* (INRS-Eau). 81p.

Ghedira, H., Bernier, M., Ouarda, T.B.M.J. 2001. Contribution of Textural Information on RADARSAT SAR Imagery Classification Accuracy Using Backpopagation Neural Networks. *Compte-Rendu du 23^{e} Symposium Canadien sur la Télédétection, 10^{e} Congrès de l'Association Québecoise de Télédétection.* 21-24 août, Sainte-Foy, Québec, Volume 2, pp.773-778.

Gorte, B.G.H. 2000. Chapter 7: Land-Use and Catchment Characteristics. In: *Remote Sensing in Hydrology and Water Management.* Schultz, G.A and Engman, E.T. eds. Springer. 483p.

Gorte, B.G.H. 1999. Chapter 9: Supervised Image Classification. In: *Spatial Statistics for Remote Sensing.* Stein, A. *et al.* eds. Klumer Academic Publishers. 284p.

Hall-Meyer, M. 2000. GLCM Texture: A Tutorial. *University of Calgary, Geography.* 27p.

Haralick, R.M. 1979. Statistical and Structural Approaches to Texture. *Proceedings of the IEEE*, 67(5):786-804.

Haralick, R.M. and Fu, K.-S., 1983. Chapter 18: Pattern Recognition and Classification. In: *Manual of Remote Sensing.* Colwell, N, Simonett, D.S. and Ulaby, F.T. eds. John Wiley & Sons, Inc. Volume 1. 866p.

Haralick, R.M., Shanmugan, K. and Dinstein, I. 1973. Textural Features for Image Classification. *IEEE Tr. On Systems, Man and Cybernetics*. Vol SMC-3 (6):610-621.

Henderson, F.M. and Lewis, A.J. 1998. Chapter 1: Introduction in Principles and Applications of Imaging Radar. In: *Manual of Remote Sensing, 3rd Edition*. Henderson, F.M. and Lewis, A.J. eds. John Wiley & Sons, Inc. Volume 2. 866p.

Hodgson, M.E. 1998. Reducing the Computational Requirements of the Minimum-Distance Classifier. *Remote Sensing of Environment*. Volume24.

Holecz, F. Meier, E. and Nuesch, D. 1993. Chapter 14: Postprocessing of Relief Induced Radiometric Distorted Spaceborne SAR Imagery. In: *SAR Geocoding: Data and Systems*. Schreier, G. Ed. Wichmann. 435p.

Hoogeboom,P. 1993. Chapter 19: Crop Classification with Radar Data. In: *Current Topics in Remote Sensing: Land Observation by Remote Sensing, Theory and Applications*. Buiten, H.J. and Clevers, J.G.P.W. Eds. Gordon and Breach Science Publishers. Volume 3. 642p.

Huitric, M., Folke, C. and Kautsky, N. 2002. Development and Government Policies of the Shrimp Farming Industry in Thailand in Relation to Mangrove Ecosystems. *Ecological Economics*. 40(2002)441-455.

Kaya, S., Pultz, T.J., Mbogo, C.M., Beier, J.C., and Mushinzimana, E. 2002. The Use of Radar Remote Sensing for Identifying Environmental Factors Associated with Malaria Risk in Coastal Kenya. *Proceedings of IGARSS'02,* Toronto.

Kasischke, E.S. and Bourgeau-Chavez, L.L. 1997. Monitoring South Florida Wetlands Using ERS-1 SAR Imagery. *Photogrammetric Engineering &Remote Sensing*. 63(3):281-291.

Khor, M. 1995. The Aquaculture Disaster: Third World Communities Fight the 'Blue Revolution' . *Third World Resurgence*. Issue #59.

Kuan, D.T., Sawchuk, A.A., Strand, T.C., and Chavel, P. 1985. Adaptive Noise Smoothing Filter for Images with Signal-Dependent Noise. *IEEE Transaction on Pattern Analysis Machine Intelligence,* PAM-7, 165-177.

Kuntz, S., Seigert, F. and Streck, C. 1994. Evaluation of ERS-1 SAR Data for Tropical Rain Forest Monitoring. *European Symposium on Satellite Remote Sensing*, CNR, Rome, Italy.

Lavallee, M. 1996. Thai Shrimp Export and Loss of Mangroves and Wetlands. *TED Case Studies (on-line Journal).* 5(1)

Laubier, A. 1990. Penaeid Prawns. In: *Aquaculture: Volume1.* G.Barnabe (ed.). Ellis Horwood, New York, pp. 405-500pp.

Lebel, L., Tri, N.H., Saengnoree, A., Pasong, S., Buatama, U. and Thoa, L.K. 2002. Industrial Transformation and Shrimp Aquaculture in Thailand and Vietnam: Pathways to Ecological, Social, and Economic Sustainability? *Ambio,* 31(4): 311-323.

Lee, J.S. 1981. Speckle Analysis and Smoothing of Synthetic Arpeture Radar. *Comp. Graph. Proceedings.* (17):24-32.

Li, C. 1988. Two Adaptive Filters for Speckle Reduction in SAR Images by Using the Variance Ratio *International Journal of Remote Sensing.* 9(4):641-653.

Li, W., Bénié, G.B., He, D.-C., Wang, S., Ziou,D. and Gwyn, Q. H. J. 1999. Watershed-Based Hierarchical SAR Image Segmentation. *International Journal of Remote Sensing.* 20(17):3377-3390.

Lillesand, T.M. and Kiefer, R.W. 1979. *Remote Sensing and Image Interpretation.* John Wiley & Sons Inc. 396p.

Lillesand, T.M. and Kiefer, R.W. 1987. *Remote Sensing and Image Interpretation, 2sd edition.* John Wiley & Sons Inc. 721p.

Lillesand, T.M. and Kiefer, R.W. 1994. *Remote sensing and image interpretation, 3rd edition.* John Wiley & Sons Inc., 750p.

Lopes, A., Nezry, E., Touzi, R. and Laur, H. 1993. Structure Detection and Statistical Adaptive Speckle Filtering in SAR Images. *International Journal of Remote Sensing.* 14(9):1735-1758.

Lopes, A. Touzi, R. and Nezry, E. 1990. Adaptive Speckle Filters and Scene Heterogeneity. *IEEE Transaction on Geoscience and Remote Sensing.* (28): 992-1000.

Mather, P.M. 1987. *Computer Processing of Remotely-Sensed Images; an Introduction.* John Wiley & Sons, Chichester, 352p.

Menasveta, P. 1996. Mangrove Destruction and Shrimp Culture Systems. *Thai Journal of Aquatic Science.* 2(2):72-82.

Menasveta, P. and Fast, A.W. 1998. The Evolution of Shrimp Culture and its Impact on Mangroves. *Infofish International*. 1/98:24-29.

Miller, P., Flaherty, M and Szuster, B.W. 1999. Inland Shrimp Farming in Thailand. *Aquaculture Asia*. 4(1):27-32.

Ministry of Science, Technology and Environment. 1998. Environmental Impact of Shrimp Farming in Freshwater Areas. *Committee on Inland Shrimp Farming*. Bangkok, Thailand. December, 1998. (In Thai).

Moisan, Y., Bernier, M., and Dubois, J.M. 1999. Détection des Changements dans une Série d'Images ERS-1 Multi-Dates à l'aide de l'Analyse en Composantes Principales. *International Journal of Remote Sensing*. 20(6):1149-1176.

NACA. 1994. Draft Project Proposal: Aquaculture and the Environment. *Overseas Development Administration (ODA) of the United Kingdom*. August 1994, Bangkok, Thailand.

NACA/FAO. 2000. Aquaculture Development Beyond 2000: The Bangkok Declaration and Strategy. *Conference on Aquaculture in the Third Millenium*. 20-25 February 2000, Bangkok, Thailand. NACA, Bangkok and FAO, Rome, 27pp.

Niemann, O. K. 2001. *Introduction to Digital Geomatics*. Class notes (geog228). University of Victoria, Geography.

Okamoto, K. 2001. Chapter 1: Overview of Remote Sensing. In: *Global Environment Remote Sensing*. Okamoto, K. ed. IOS Press. 308p.

Oliver, C. and Quegan, S. 1997.*Understanding Synthetic Aperture Radar Images*. 1st edition. Artech House, Inc. MA. 478p.

Omniresources. 2002. Map Catalogue. www.omnimap.com

Patmasiriwat, D, Kuik, O. and Pednekar, S. 1998. The Shrimp Aquaculture Sector in Thailand: A Review of Economic, Environmental and Trade Issue. *CREED Working Paper 19*. 31p.

PCI Geomatics. 2000. Radar Analysis. Technical specification. In: *EASI/PACE Imaging Pro*.

Pillay, T. 1990. *Aquaculture: Principles and Practices*. Fishing News Books, Oxford, 575pp.

Prasad, T.S. and Gupta, R.K. 1998. Texture Based Classification of Multidate SAR Images – A Case Study. *Geocarto International*. 13(3):53-62

Primavera, J.H. 1994. Shrimp Farming in the Asia-Pacific: Environmental and Trades Issues and Regional Cooperation. *Presented at the Nautilus Institute Workshop on Trade and Environment in Asia-Pacific: Prospects for Regional Cooperation*, 23-25 September 1994, East-West Center, Honolulu.

Rajesh, K., Jawahar, C.V., Senguptas S. and Sinha, S. 2001. Performance Analysis of Textural Features for Characterization and Classification of SAR Images. *International Journal of Remote Sensing*. 22(8):1555-1569.

Raney, R.K. 1998. Chapter 2: Radar Fundamentals: Technical Perspective in Principles and Applications of Imaging Radar. In: *Manual of Remote Sensing, 3rd Edition.* Henderson, F.M. and Lewis, A.J. eds. John Wiley & Sons, Inc. Volume 2. 866p.

Ribbes, F. and Le Toan, T. 1999. " Rice Field Mapping and Monitoring with RADARSAT data". *International Journal of Remote Sensing*, 20(4):745-765

Richards, J.A. 1993. *Remote Sensing Digital Analysis*. 2st edn. Springer-Verlag. 340p.

Richards, J.A. 1986. *Remote Sensing Digital Analysis*. 1st edn. Springer-Verlag. 281p

Ritchie, J.C. and Rango, A. 1996. Remote Sensing Applications to Hydrology: Introduction. *Hydrological Sciences Journal*. 41(4):429-431

Ristau, J.P. and Moon, M.W. 2001. Adaptive Filtering of Random Noise in 2-D Geophysical Data. *Geophysics*. 66(1):342-349.

Sabins, F.F. 1997. *Remote Sensing Principles and Interpretation*. 3rd edition. W.H. Freeman and Company. 494p.

Sali, E. and Wolfson, H. 1992. Texture Classification in Aerial Photographs and Satellite Data. *International Journal of Remote Sensing*. 13(18):3395-3408.

Shao, Y., Fan, X., Liu, H., Xiao, J., Ross, S., Brisco, B., Brown, R. and Staples, G. 2001. Rice Monitoring and Production Estimation Using Multitemporal RADARSAT. *Remote Sensing of Environment*, 76, 310-325.

Schowengerdt, R.A. 1983. *Techniques for Image Processing and Classification in Remote Sensing*. Academic Press. 249p.

Schowengerdt, R.A. 1997. *Remote Sensing, Models and Methods for Images Processing*. 2sd edition. Academic Press. 522p.

Schwan, H., Wunerle, S. and Denos, Y.-L. 1995. Evaluation of Speckle-Filtered ERS-1 SAR Images in Patagonia and Antarctica. *ESA EOQ* Nr. 49.

Short, N.M. 1999a. Introduction. The Remote Sensing Tutorial, hosted by the Earth Observing System (NASA) - Goddard Program Office.(http://rst.gsfc.nasa.gov/start.html)

Short, N.M. 1999b. Section 8: "Radar and Microwave Remote Sensing: Radar Defined". The Remote Sensing Tutorial, hosted by the Earth Observing System (NASA) - Goddard Program Office. (http://rst.gsfc.nasa.gov/start.html)

Short, N.M. 1999c. Section 13: "Collecting Data at Surface - Ground Truth: Accuracy Assessment". The Remote Sensing Tutorial, hosted by the Earth Observing System (NASA) - Goddard Program Office. (http://rst.gsfc.nasa.gov/start.html)

Simonett, D.S. and Davis, R.E. 1983. Chapter 25: Image Analysis-Active Microwave. In: *Manual of Remote Sensing.* Colwell, N, Simonett, D.S. and Ulaby, F.T. eds. John Wiley & Sons, Inc. Volume 1. 866p.

Small, D., Holecz, F., Meier, E., Nuesch, D. and Barmettler, A. 1997. RADARSAT Terrain Geocoding and Radiometric Correction over Switzerland. *Proceedings of Geomatics in the Era of RADARSAT*, Ottawa, Canada, May 24-30.

Smith, H.H., Bernier, D.W., Bunge, F.M., Rintz, F.C., Shin, R.-S., Teleki, S. 1968. *Area Handbook for Thailand.* American University-Washington, 558p.

Smith, D.M., 1996. Speckle Reduction and Segmentation of Synthetic Aperture Radar images. *International Journal of Remote Sensing*. 17, 2043-2057.

Soares, J.V., Renno, C.D., Formaggio, A.R., Yanasse, C. da C. F. Yanasse, and Frery, A.C. 1997. An Investigation of the Selection of Texture Features for Crop Discrimination Using SAR Imagery. *Remote Sensing of Environment.* (59):234-247.

Steinberg, B.D. and Subbaram, H.M. 1991. *Microwave Imaging Techniques*. John Wiley & Sons, Inc. 361p.

Tilton, C.J. 1998. Image Segmentation by Region Growing and Spectral Clustering with a Natural Convergence Criterion. *Proceedings of IGARSS'98*, Seattle, W.A.

Tilton, C.J 2000. Hierarchical Image Segmentation: as Applied to Remotely Sensed Multispectral or Hyperspectral Imagery. *NASA's Goddard Space Flight Centre*, Applied Information Science Branch.

Tilton, C.J. and Lawrence, W.T. 2000. Interactive Analysis of Hierarchical Image Segmentation. *Proceedings of IGARSS'00*, Honolulu, Hawaii.

Torma, M and Koskinen, J. 1997. Land-Use Classification Using Temporal SAR-Images. *Proceedings of IGARSS'97*, Singapore.

Toutin, T. 1998. Évaluation de la Précision Géométrique des Images de RADARSAT. *Canadian Journal of Remote Sensing*. 24(1):80-88.

Touzi, R. 1999a. Speckle Filtering of Stationary and Non-Stationary Scene Signals in SAR imagery. *Proceedings of IGARSS'99*, Hamburg, Germany.

Touzi, R. 1999b. Taking The Speckle Out of SAR: The Multi-Resolution Filter. *RSIC* (Remote Sensing In Canada, on-line). 27(1).

Touzi, R. and St-Jean, R. 1995. Taking The Speckle Out of SAR: The Gamma Filter. *RSIC* (Remote Sensing In Canada, on-line). 23(3).

Travaglia, C., Kapetsy, J.M. and Profeti, G. 1999. Inventory and monitoring of shrimp farms in Sri Lanka. Environmental and Natural Resources Service and Sustainable Development Department. *Working paper No.1. Food and Agriculture Organization of the United Nations (FAO)*. Rome. 34p.

Ulaby, F.T., Kouyate, B., Brisco, B. and Williams, L. 1986. Textural Information in SAR Images. *IEEE Transaction on Geoscience and Remote Sensing*. (24):235-245.

Ulaby, F.T., Moore, R.K. and Fung, A.K. 1982. *Microwave Remote Sensing: Active and Passive: Radar Remote Sensing and Surface Scattering and Emission Theory.* Addison-Wesley. US. Volume II. 1064p.

Ulaby, F.T., Moore, R.K. and Fung, A.K. 1981. *Microwave Remote Sensing: Active and Passive: Fundamentals and Radiometry*. Addison-Wesley. US. Volume I. 456p.

Verbyla, D. L., 1995. *Satellite Remote Sensing of Natural Resources, 1st edition.* Lewis Publishers. 198p.

Verhoeye, J. and De Wulf, R. 1999. An Image Processing Chain for Land-Cover Classification Using Multitemporal ERS-1 Data. *Photogrammetric Engineering &Remote Sensing*. 65(10):1179-1185.

Weissel, J. 2002. "Appendix D: Glossary". The Remote Sensing Tutorial, hosted by the Earth Observing System (NASA) - Goddard Program Office. (http://rst.gsfc.nasa.gov/start.html)

APPENDIX I

METHODOLOGY SCHEMATIC MODEL & SUMMARY TABLE OF MLC RESULTS

METHODOLOGY SCHEMATIC MODEL

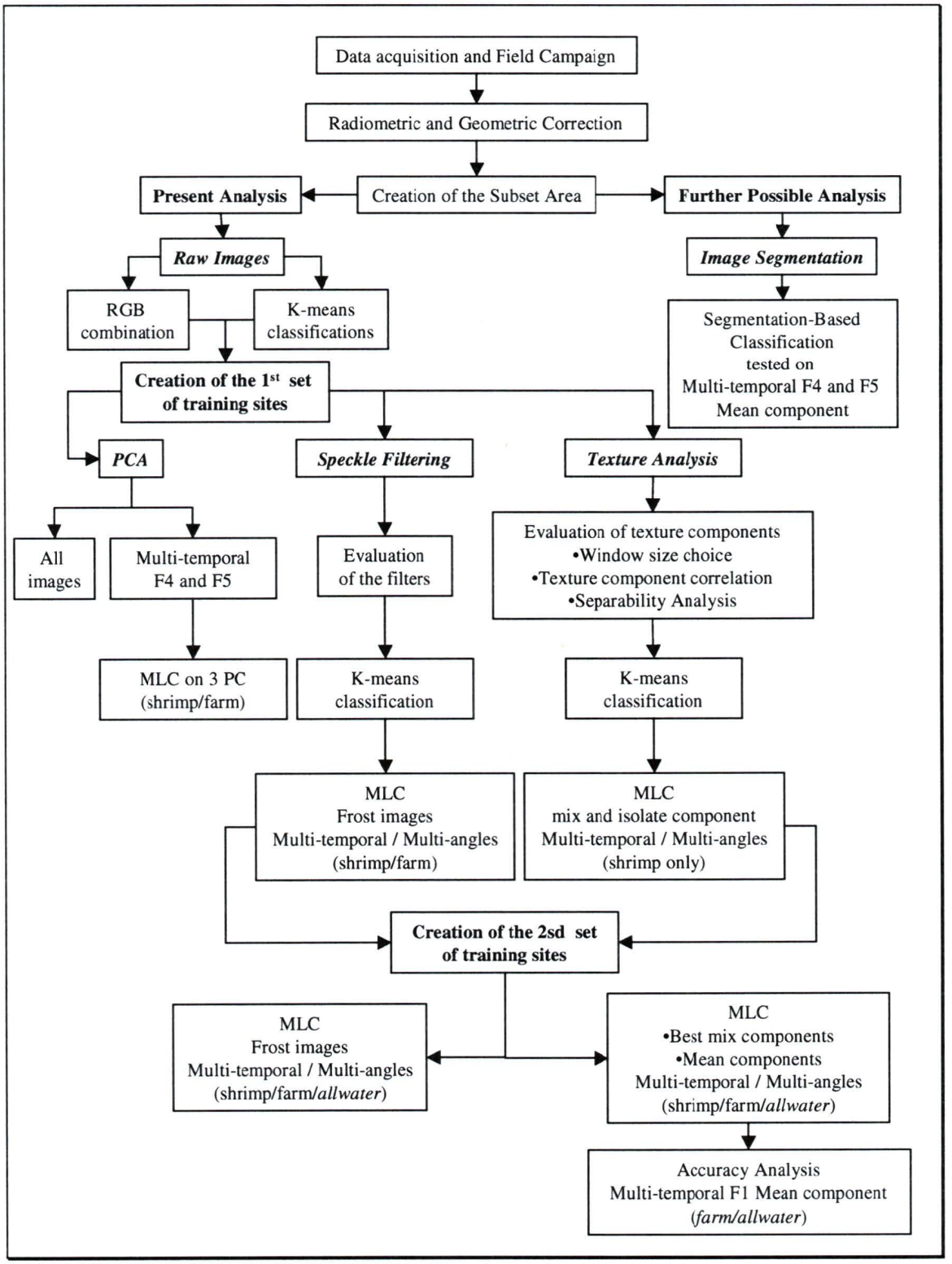

SUMMARY TABLE OF MLC RESULTS

Image Processing Techniques	Filter/ Texture Components	Multi -	Image Combinations	Maximum Likelihood Classification (MLC) in %									
				First set of training sites				Second set of training sites					
				Shrimp Ponds		Shrimp Farms		Shrimp Ponds		Shrimp Farms		*Allwater*	
				Av. Acc.	Over. Acc.	Av. Acc.	Over. Acc.	Av. Acc.	Over. Acc.	Av. Acc.	Over. Acc.	Av. Acc.	Over. Acc.
PCA	---	Dates	All F4 & F5	40.52	37.91	42.46	42.40						
Speckle Filtering (3x3)	Frost	Dates	All F4 & F5	50.00	49.57	52.04	55.35	67.38	62.32	71.97	66.70	72.44	63.76
		Dates	All F1	46.98	46.07	49.32	50.40	61.72	63.34	59.60	46.70	72.87	68.03
		Angles	F1 (July11) & F4 (July 18)	44.74	43.74	48.04	50.43	59.47	57.22	60.56	50.46	68.50	60.29
Texture Analysis (5x5)	Mix	Best	Mean: May7(F4) & July18(F4) Std. Dev.: May24(F1)	62.57	59.28			79.15	78.92	81.75	77.43	83.98	79.67
	Contrast	Dates	All F4 & F5	53.89	52.31								
		Dates	All F1	49.44	46.26								
		Angles	F1 (July11) & F4 (July 18)	49.08	45.33								
	Mean	Dates	All F4 & F5	62.33	58.08			85.13	82.30	86.76	83.71	87.12	82.49
		Dates	All F1	55.55	51.41			75.68	77.98	77.66	70.91	84.32	80.12
		Angles	F1 (July11) & F4 (July 18)	59.96	52.91			73.82	64.24	75.01	65.81	79.19	68.87
	Standard Deviation	Dates	All F4 & F5	54.82	53.97								
		Dates	All F1	50.66	48.69								
		Angles	F1 (July11) & F4 (July 18)	49.94	47.10								

APPENDIX II

PIXEL DISTRIBUTION FOR TRAINING SITES AND ACCURACY SITES

PIXEL DISTRIBUTION FOR TRAINING SITES (1st SET):

1) Rice: (0-5000)

May7, 2001

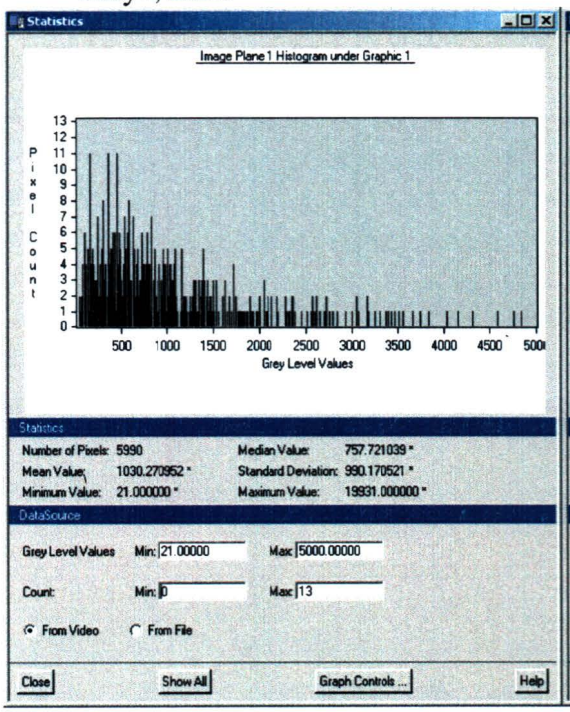

May 24, 2001

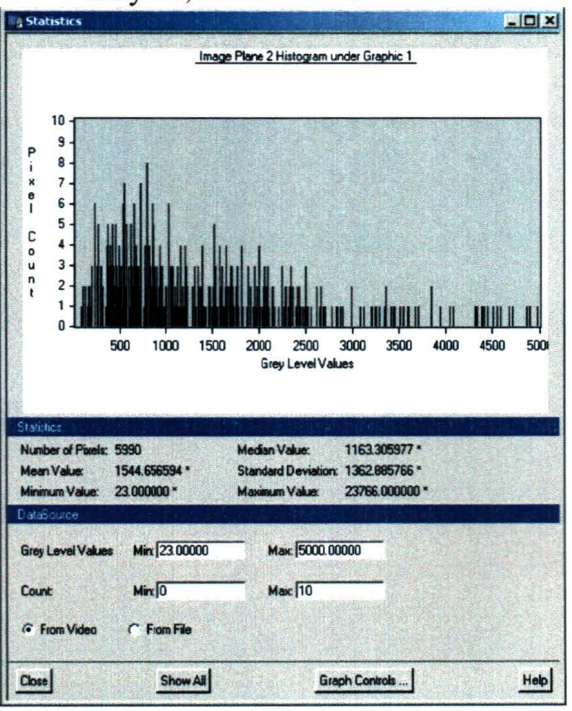

July 11, 2001:

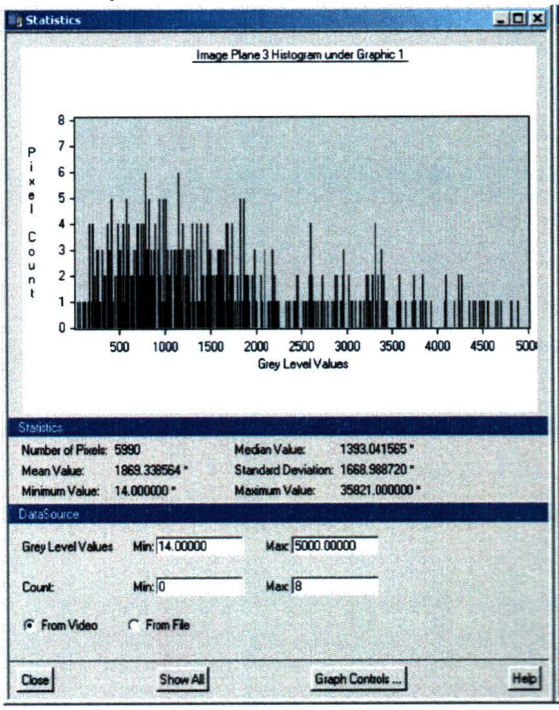

July 18, 2001:

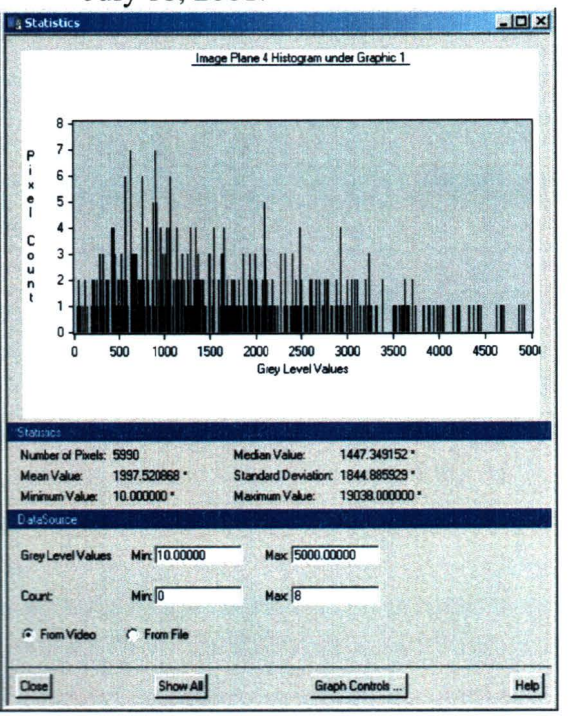

September 19, 2001:

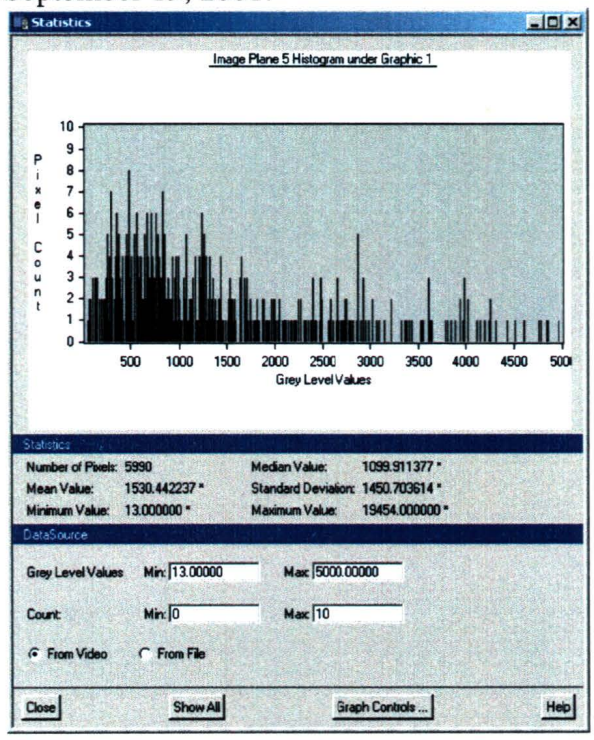

2) Human Settlement: (0-5000)

May7, 2001

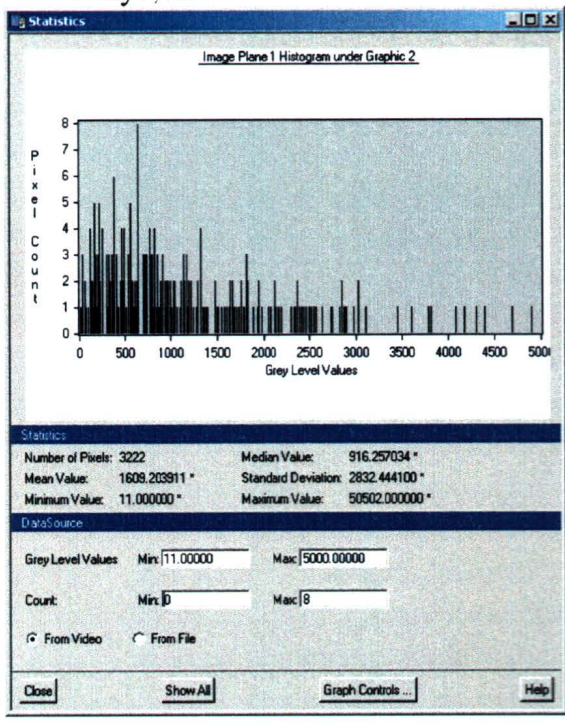

May 24, 2001

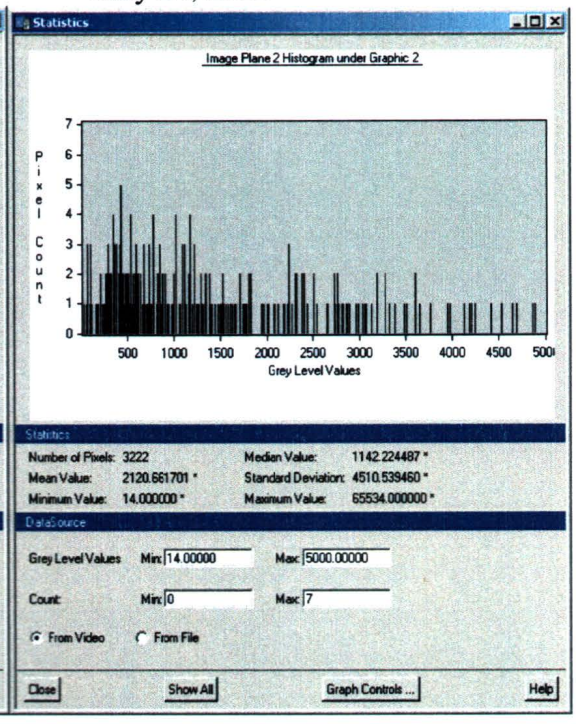

July 11, 2001:

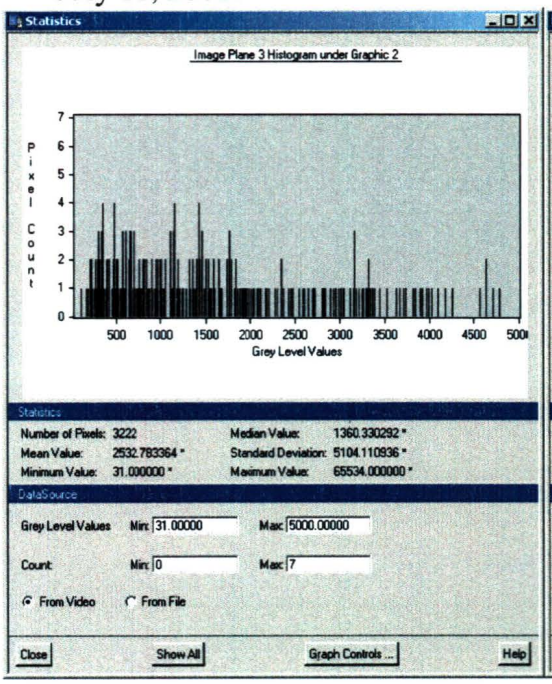

July 18, 2001:

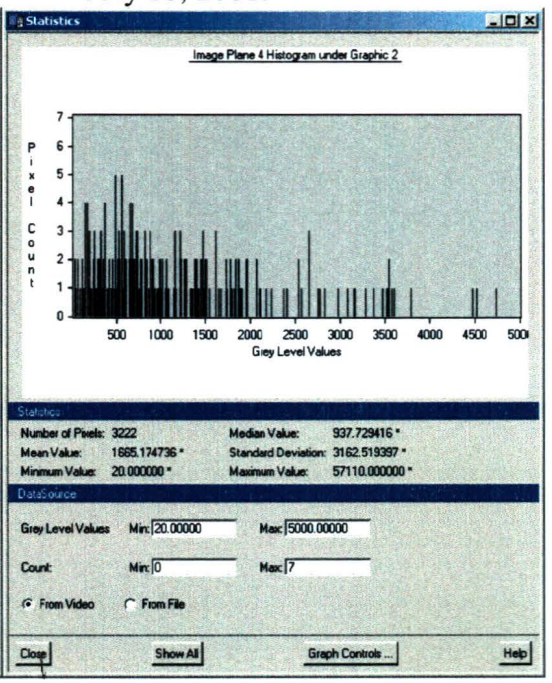

September 19, 2001:

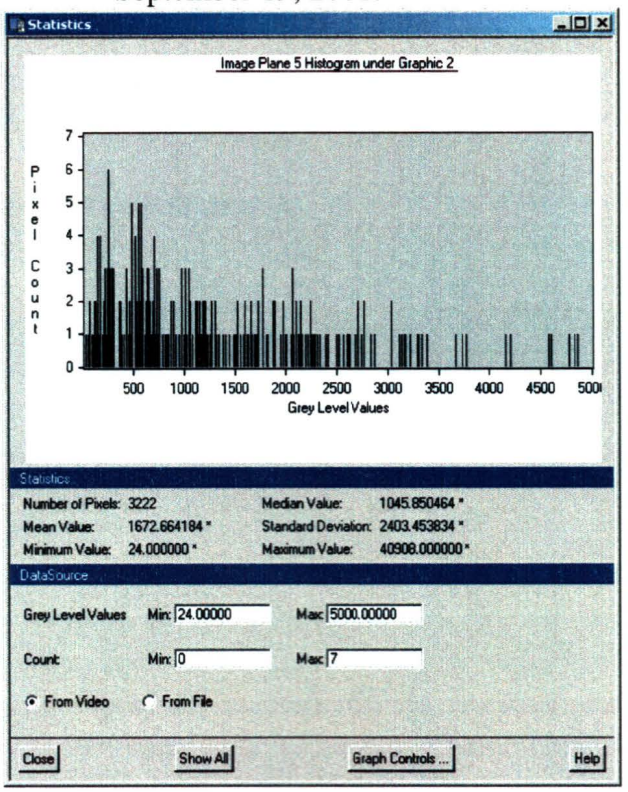

3) Orchards: (0-5000)

May7, 2001

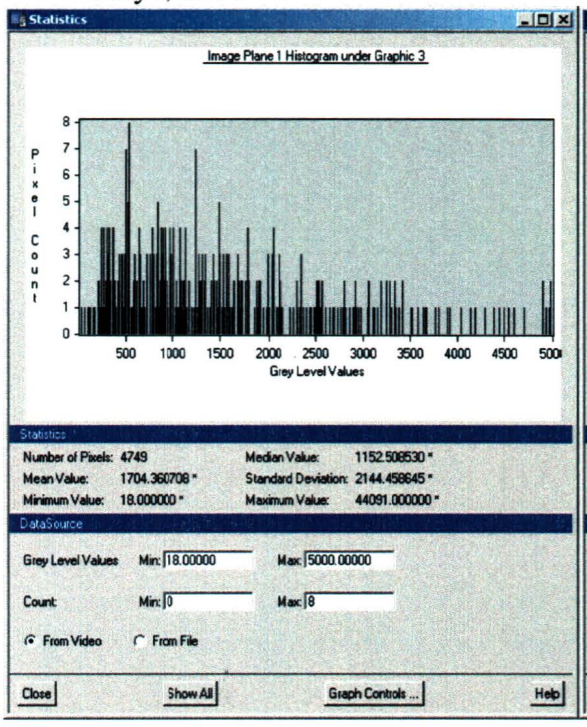

May 24, 2001

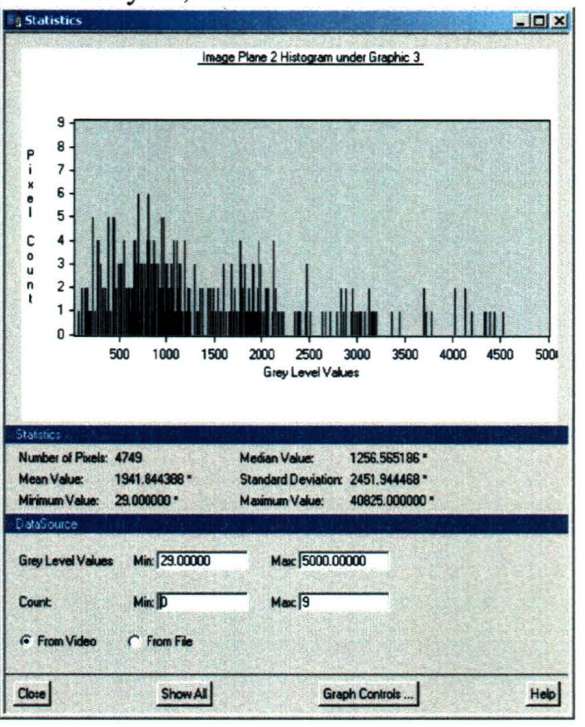

July 11, 2001:

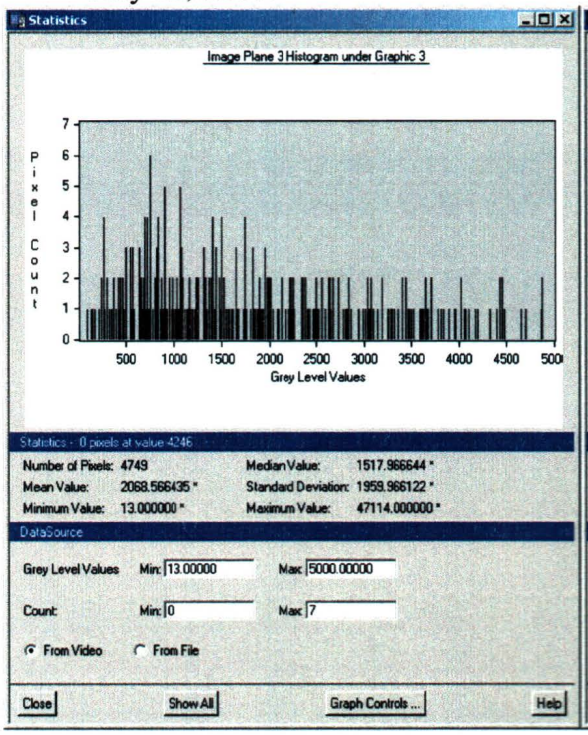

July 18, 2001:

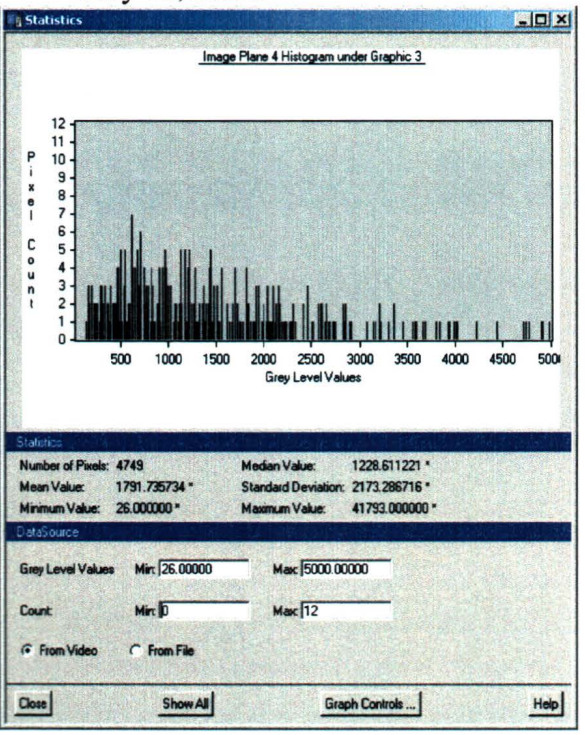

September 19, 2001:

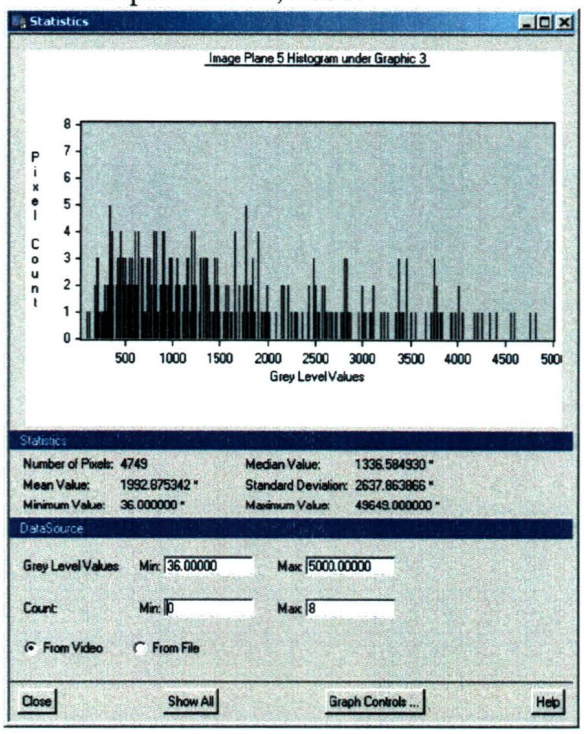

4) Water: (0-200)

May7, 2001

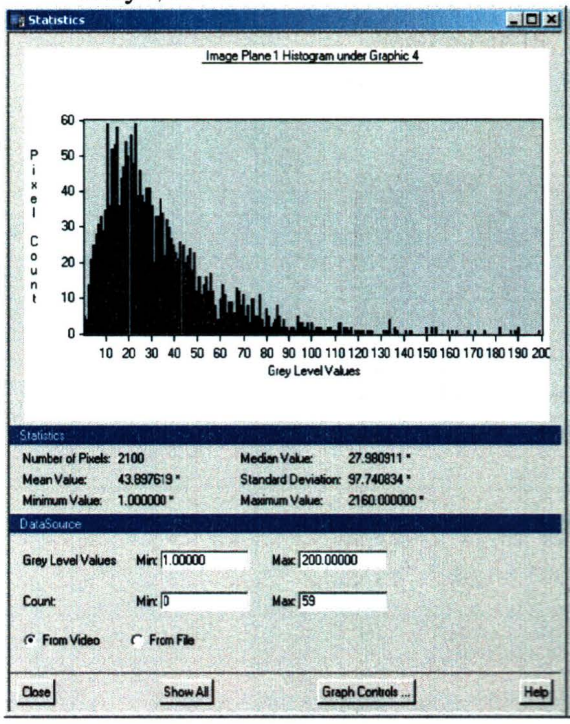

May 24, 2001

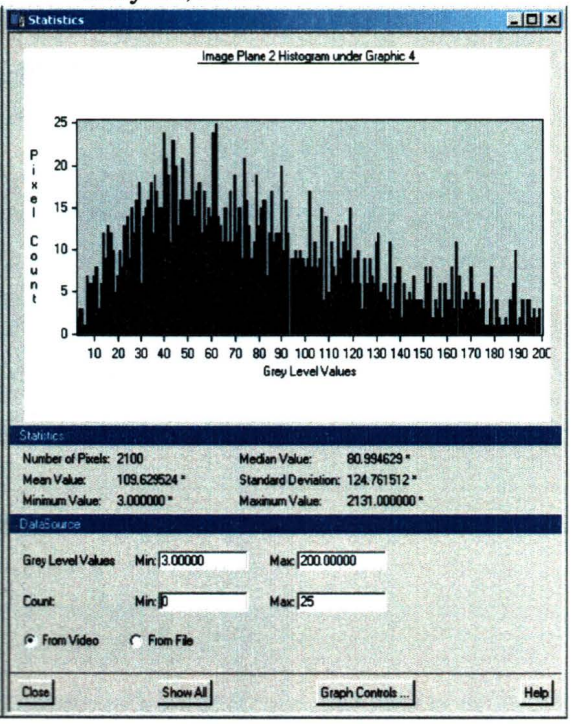

July 11, 2001:

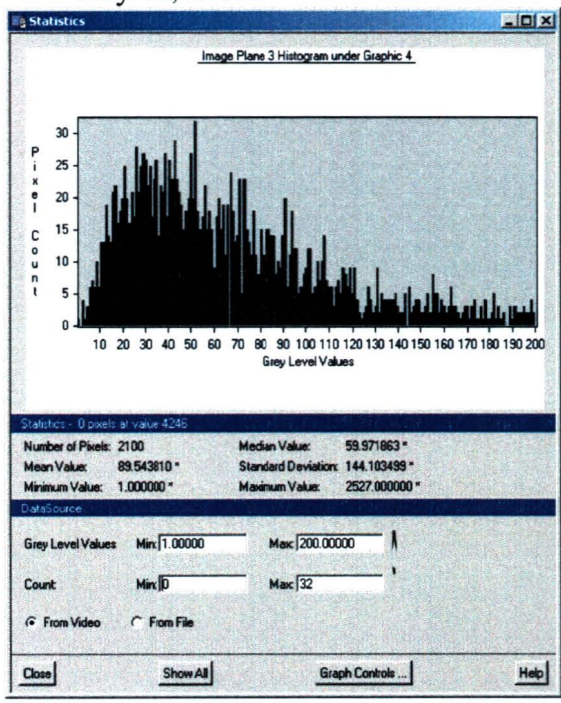

July 18, 2001:

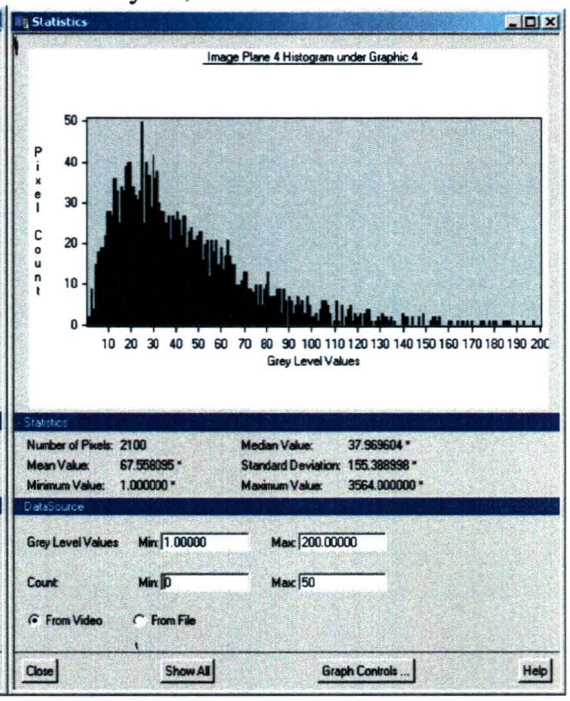

September 19, 2001:

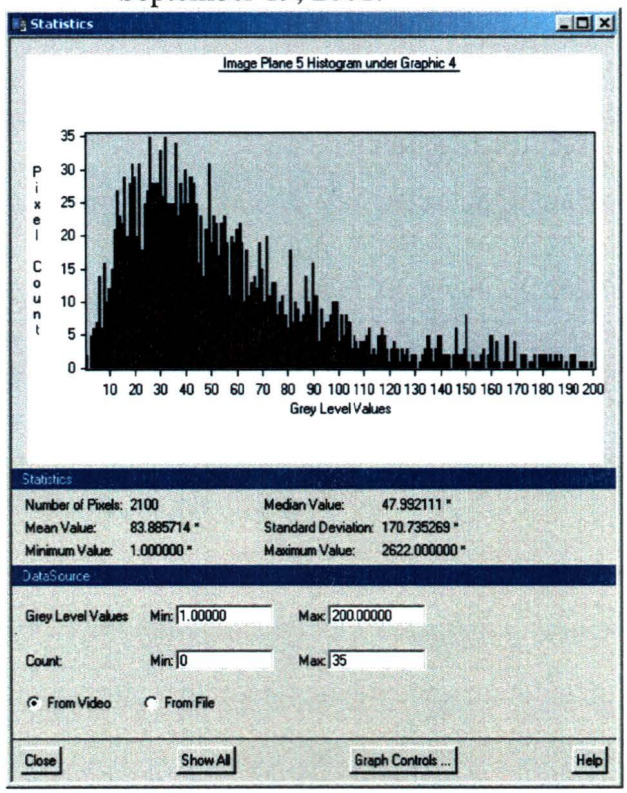

5) Shrimp pond: (0-500)

May7, 2001

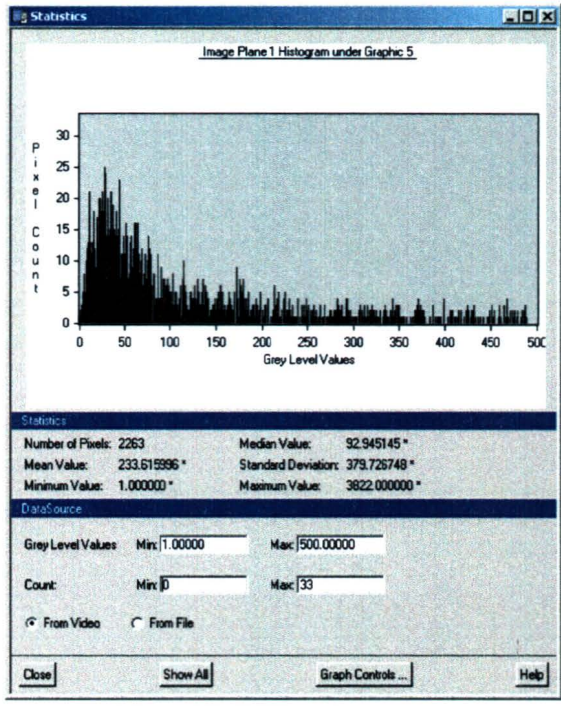

May 24, 2001

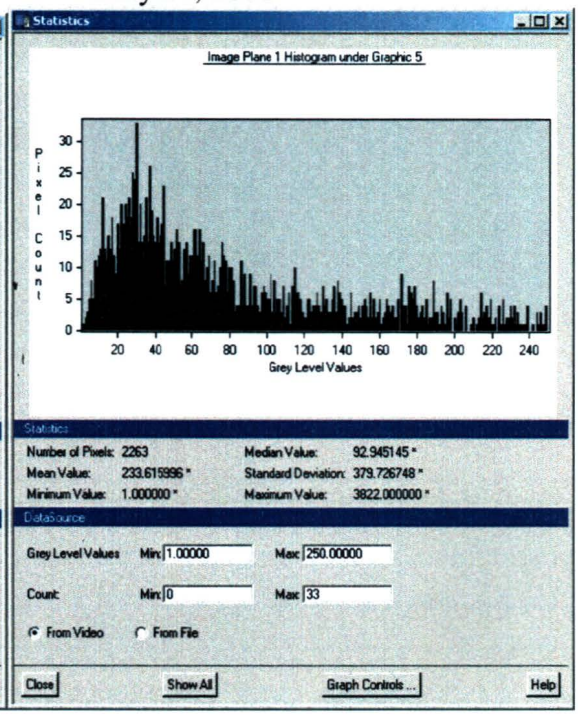

July 11, 2001:

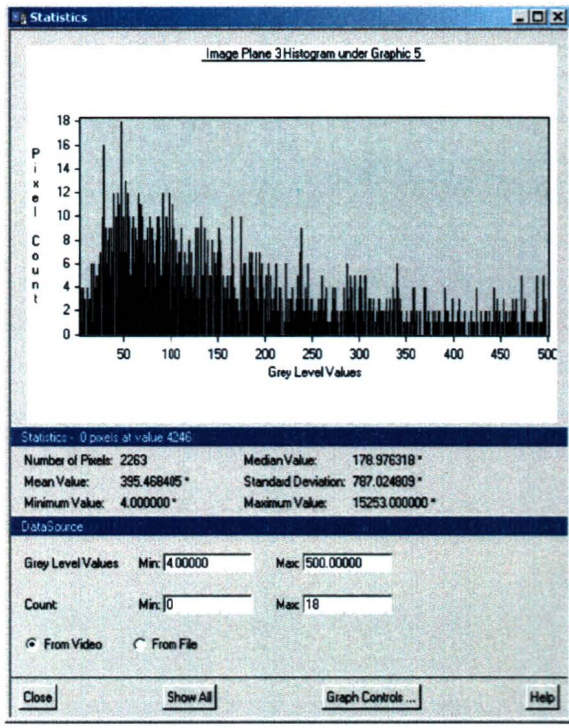

July 18, 2001:

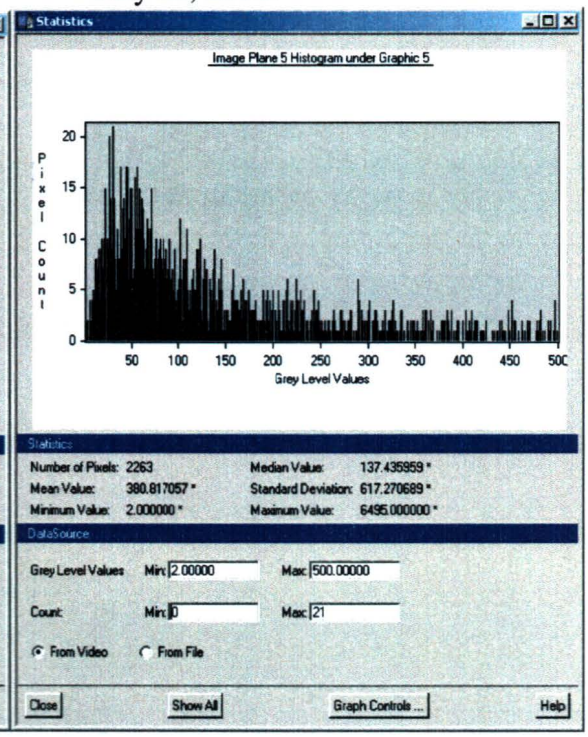

September 19, 2001:

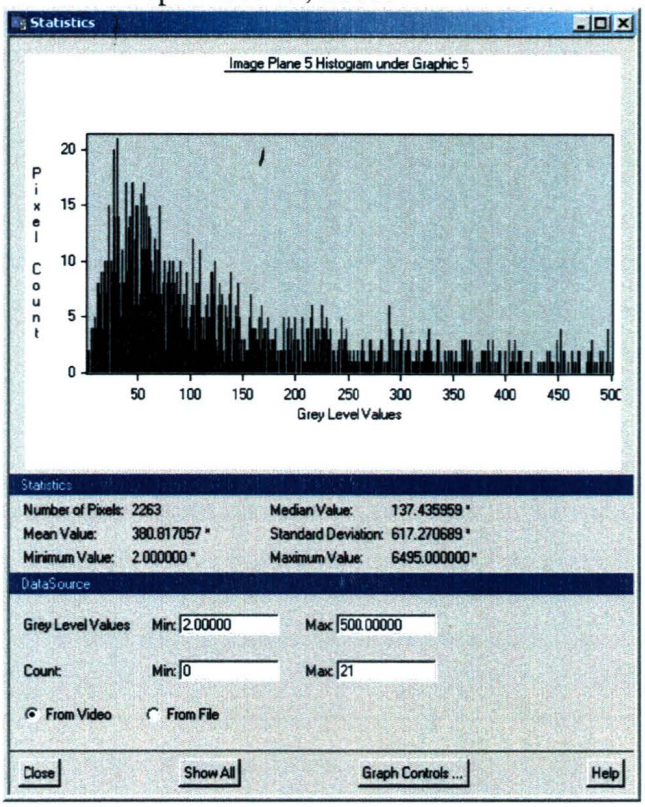

6) Shrimp farm: (0-1000)

May7, 2001

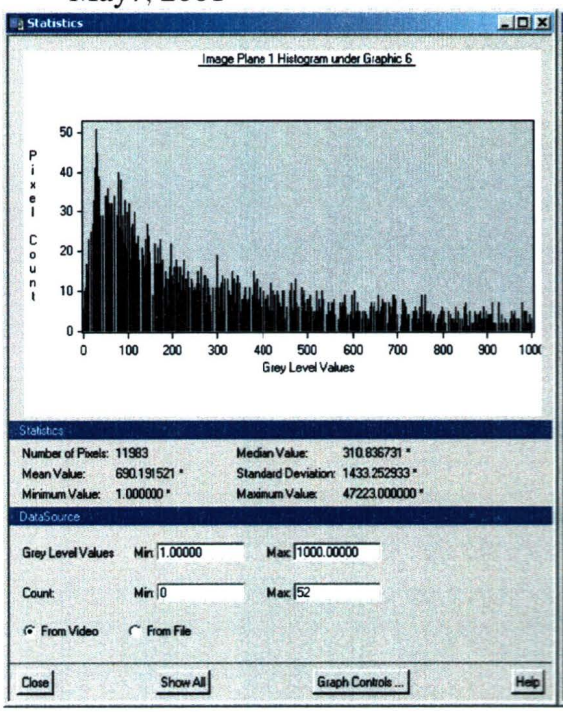

May 24, 2001

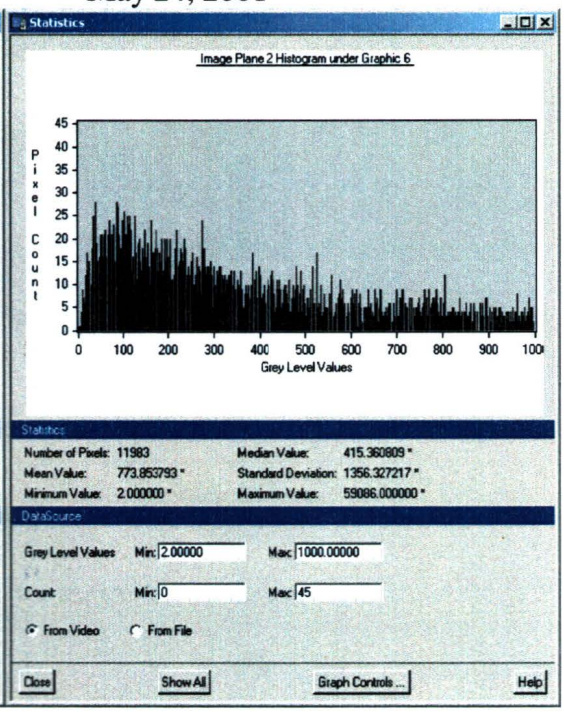

July 11, 2001:

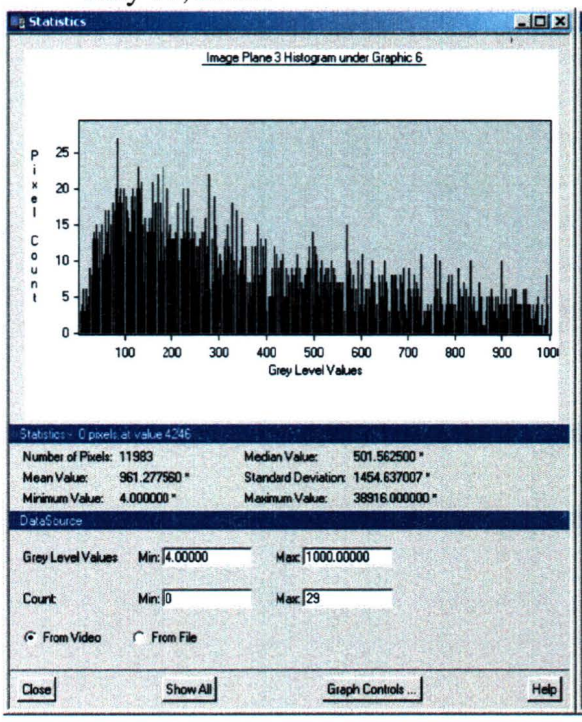

July 18, 2001:

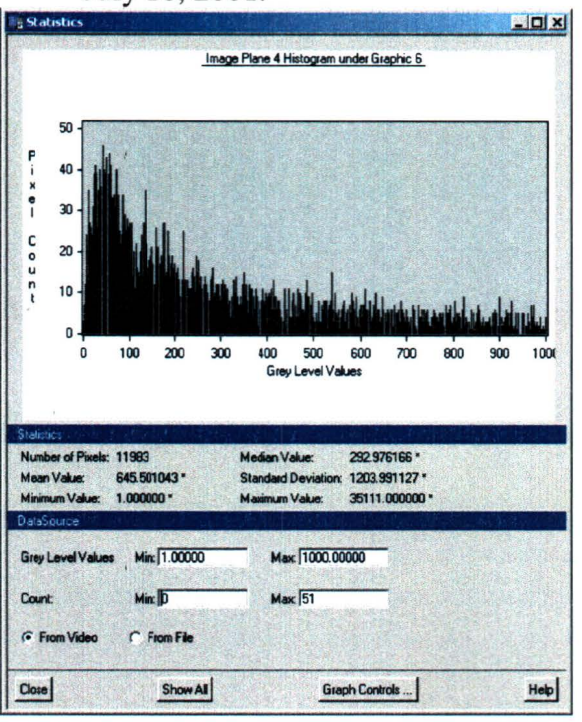

September 19, 2001:

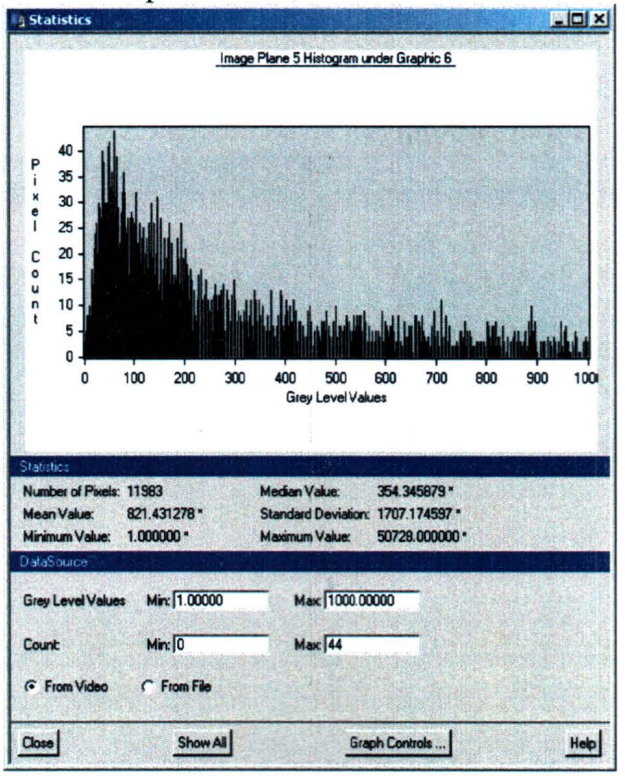

PIXELS DISTRIBUTION FOR TRAINING SITES (2nd SET):

1) Rice: (0-5000)

May7, 2001

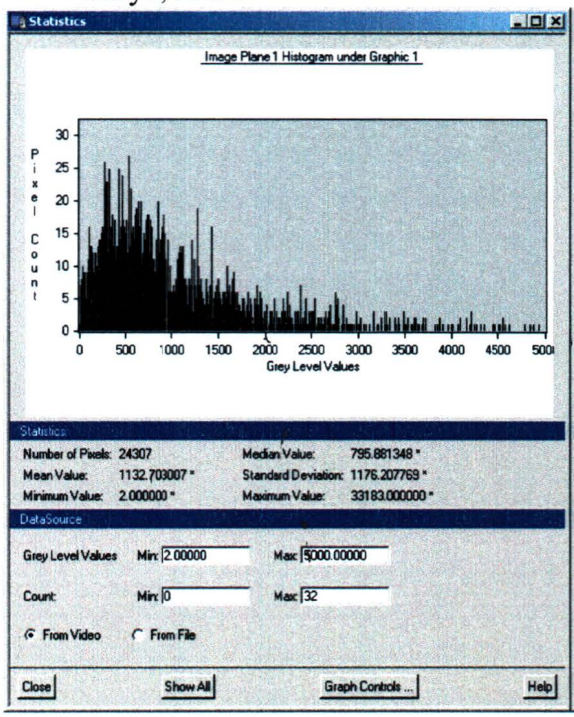

May 24, 2001

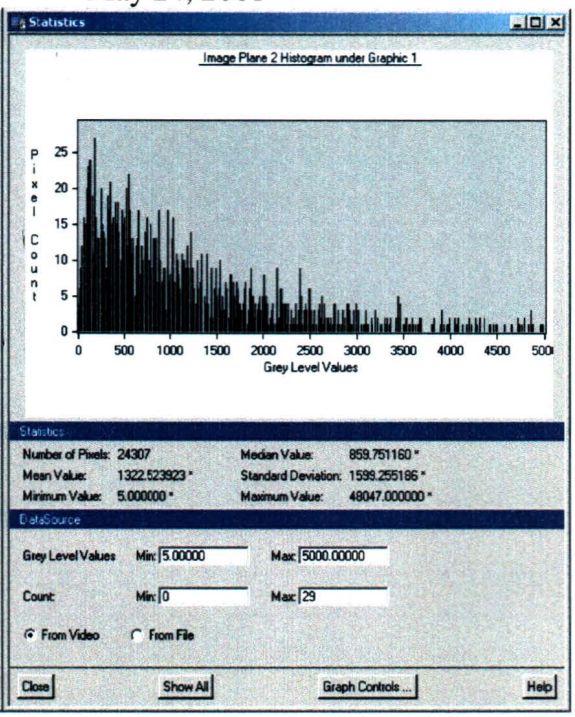

July 11, 2001:

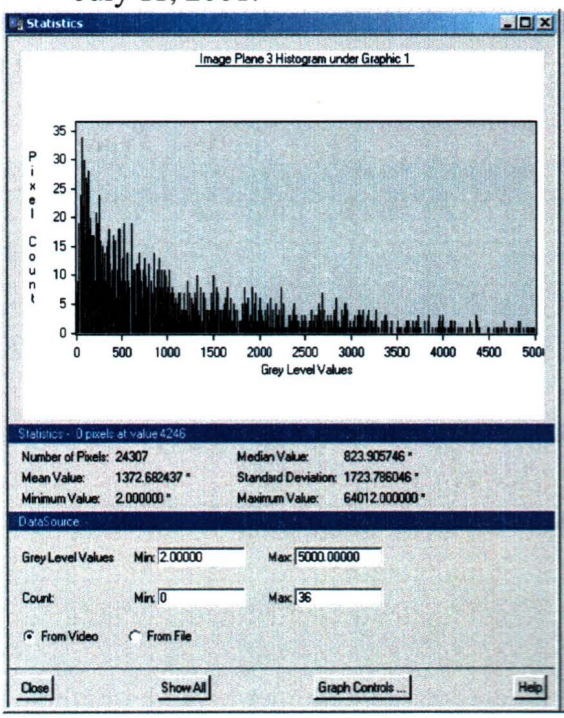

July 18, 2001:

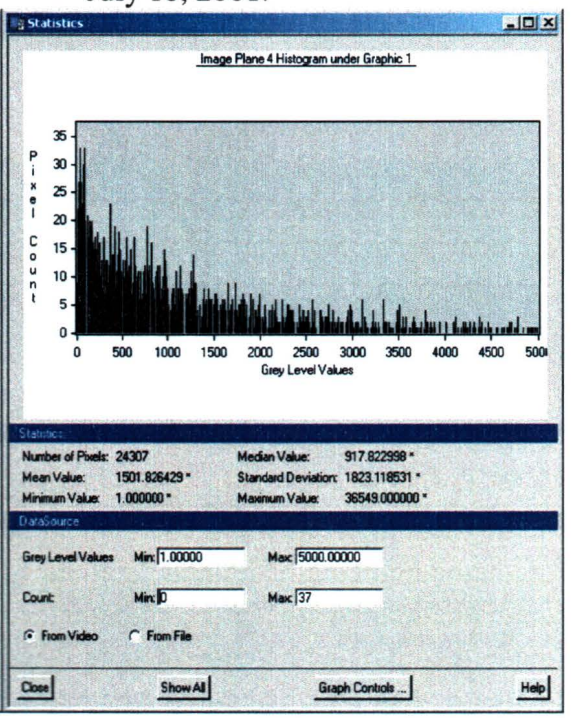

September 19, 2001:

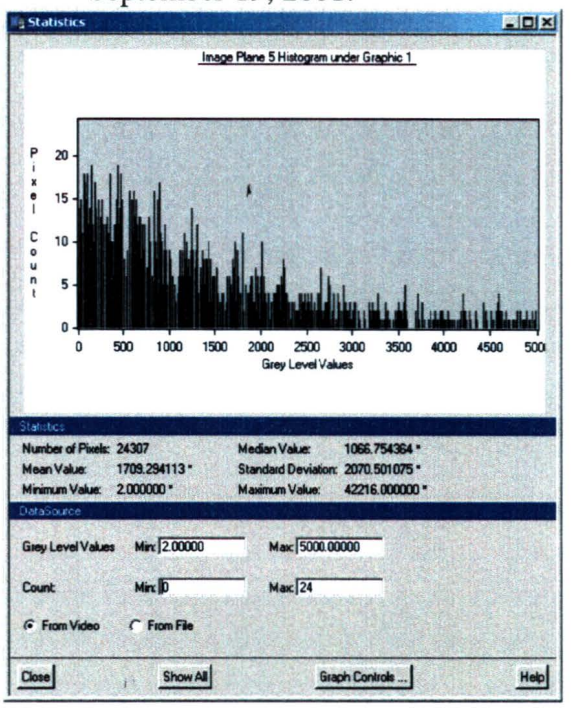

2) Human Settlement: (0-10000)

May7, 2001

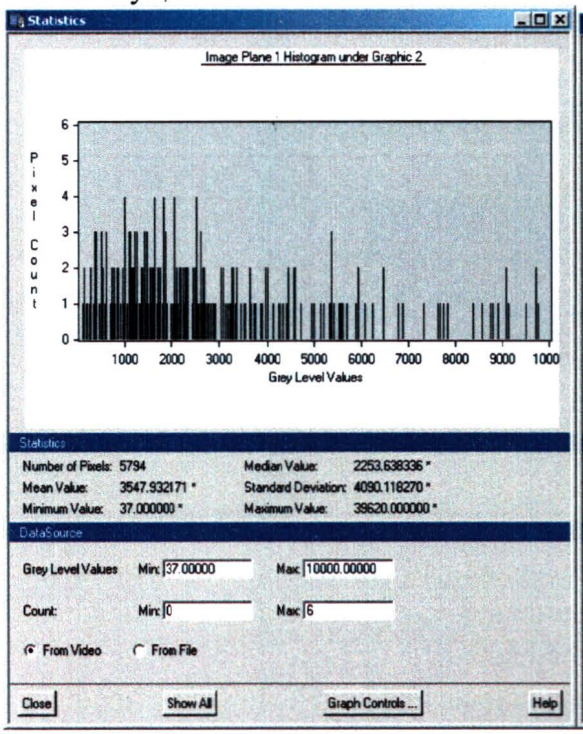

May 24, 2001

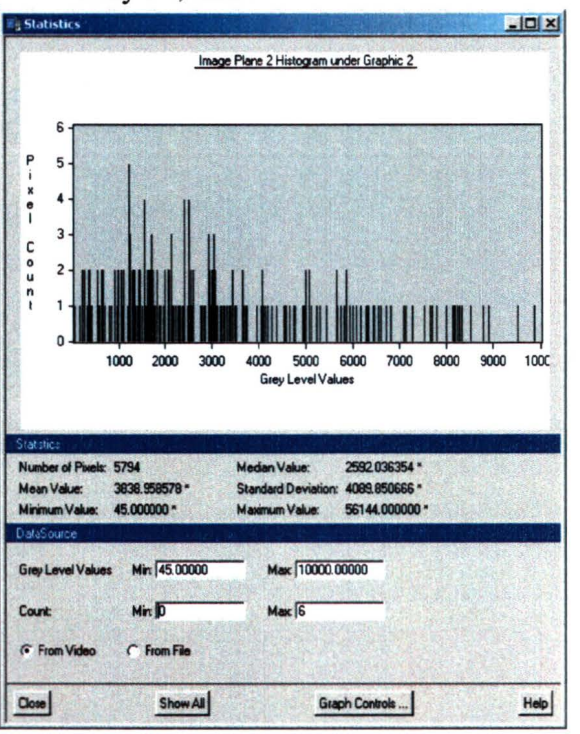

July 11, 2001:

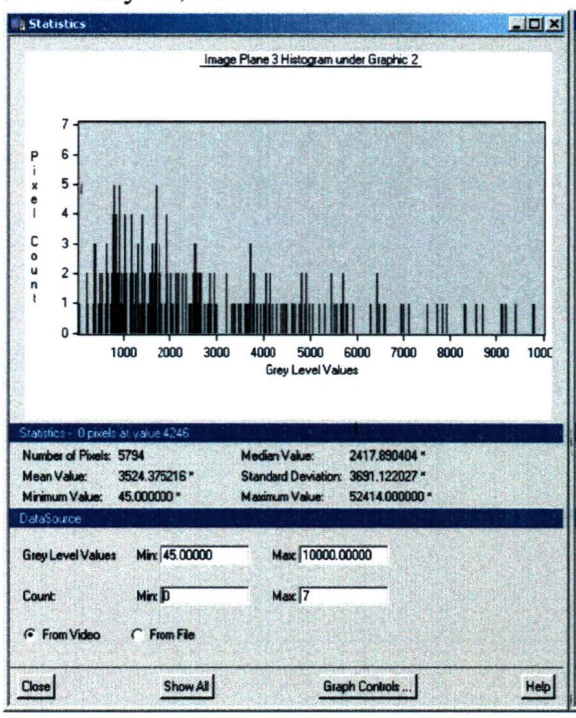

July 18, 2001:

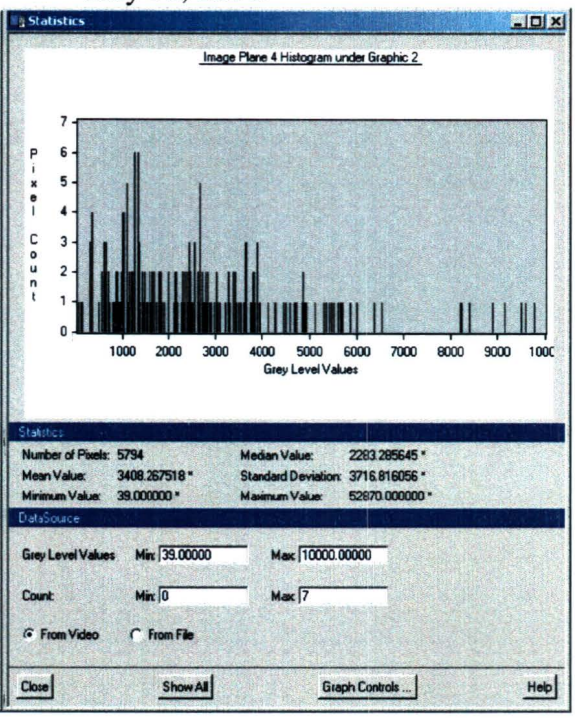

September 19, 2001:

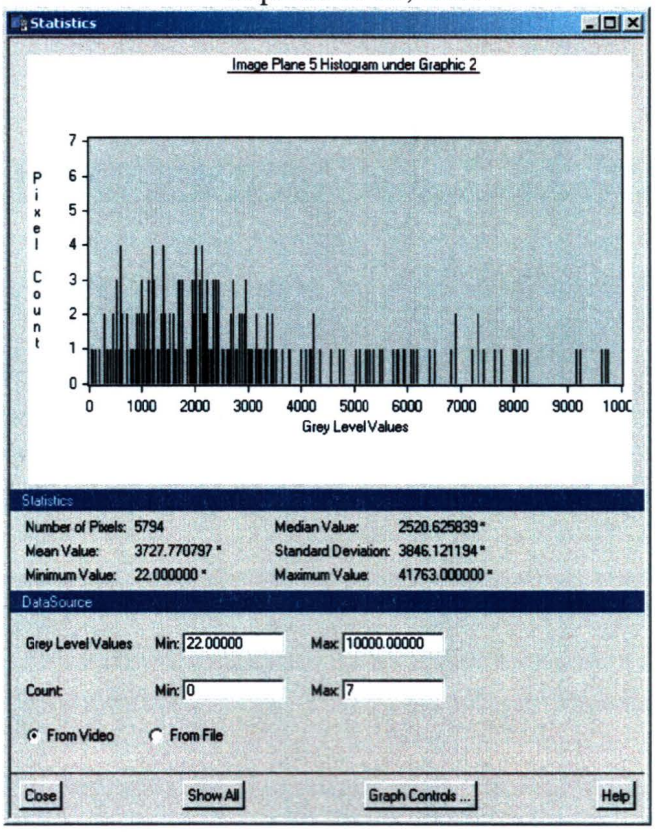

3) Orchards: (0-5000)

May7, 2001

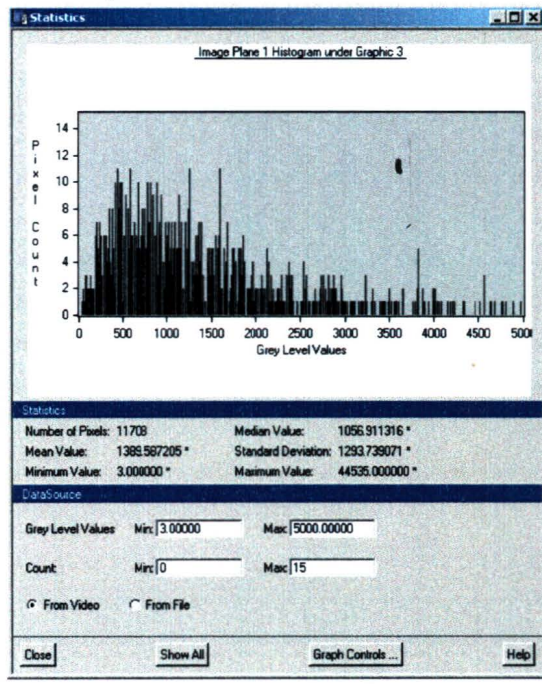

May 24, 2001

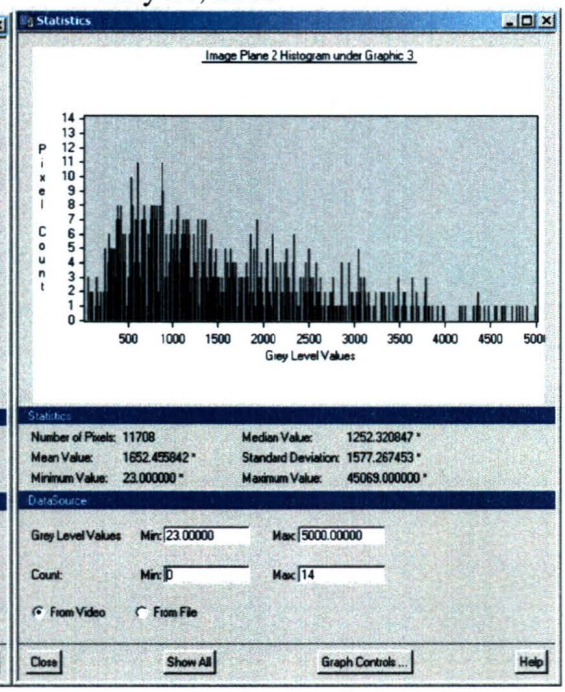

July 11, 2001:

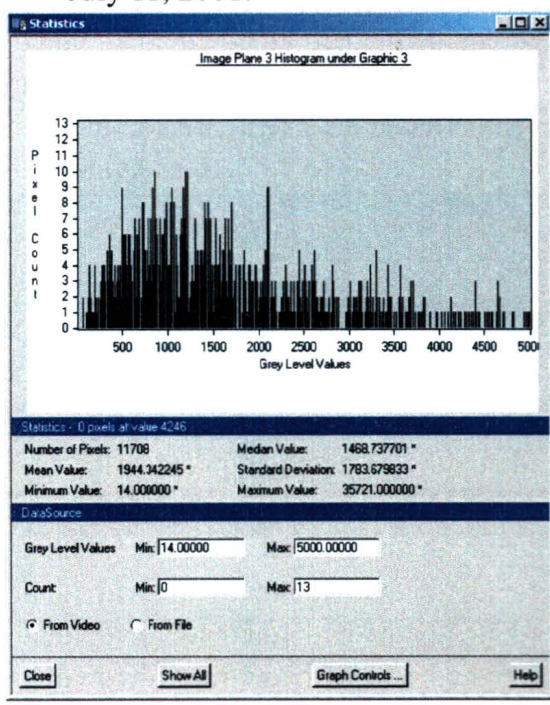

July 18, 2001:

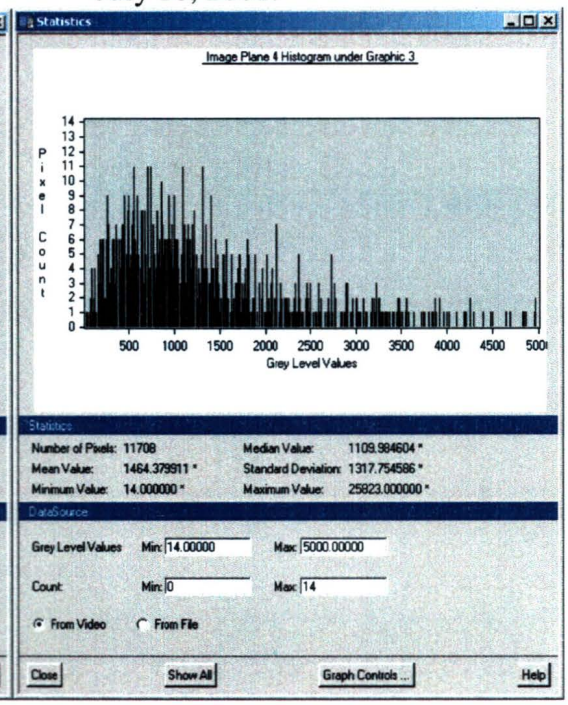

September 19, 2001:

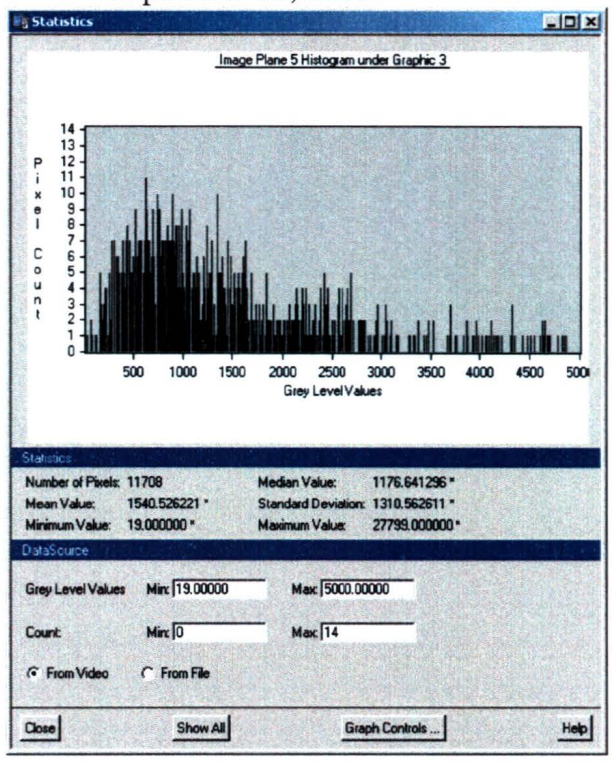

4) Water: (0-200)

May7, 2001

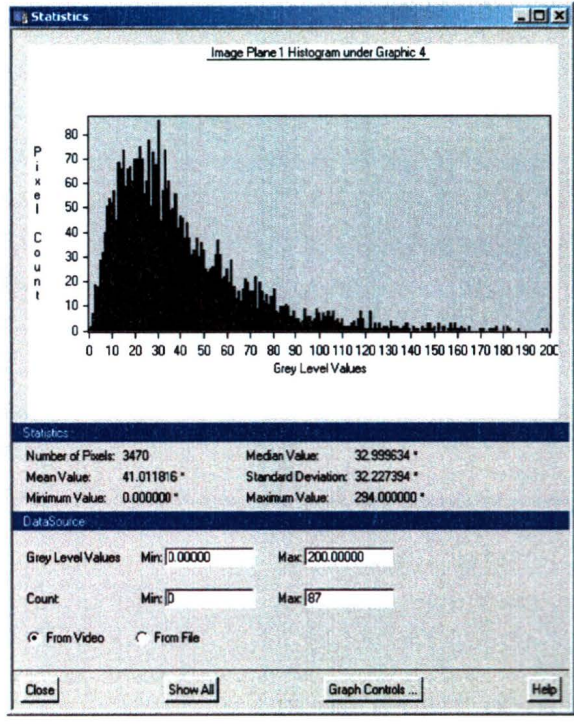

May 24, 2001

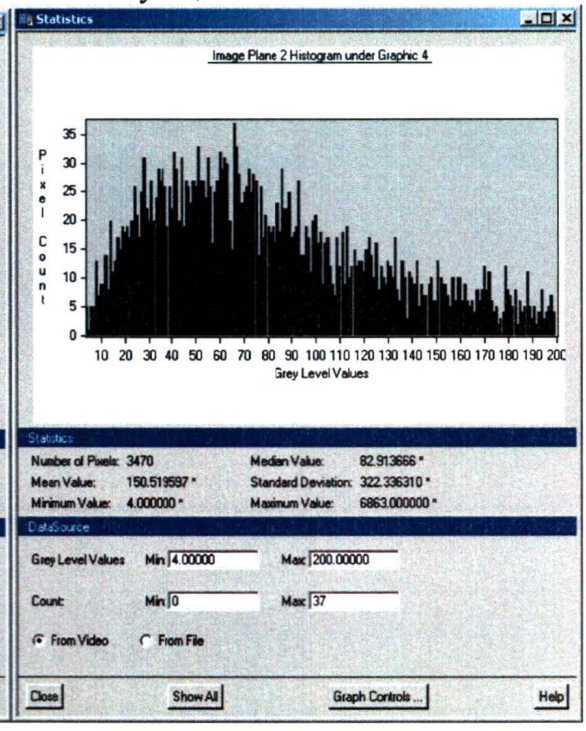

July 11, 2001:

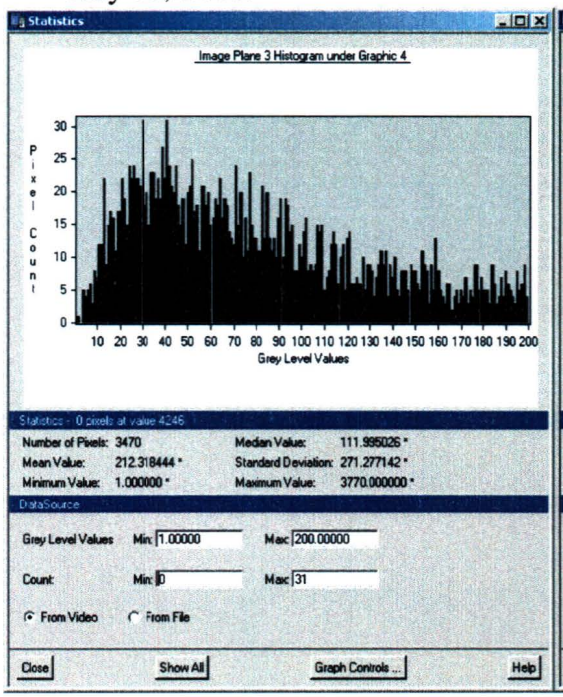

July 18, 2001:

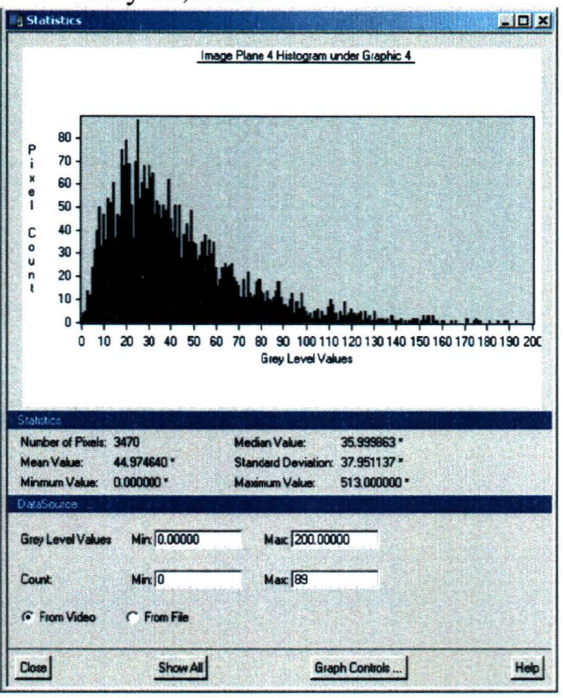

September 19, 2001:

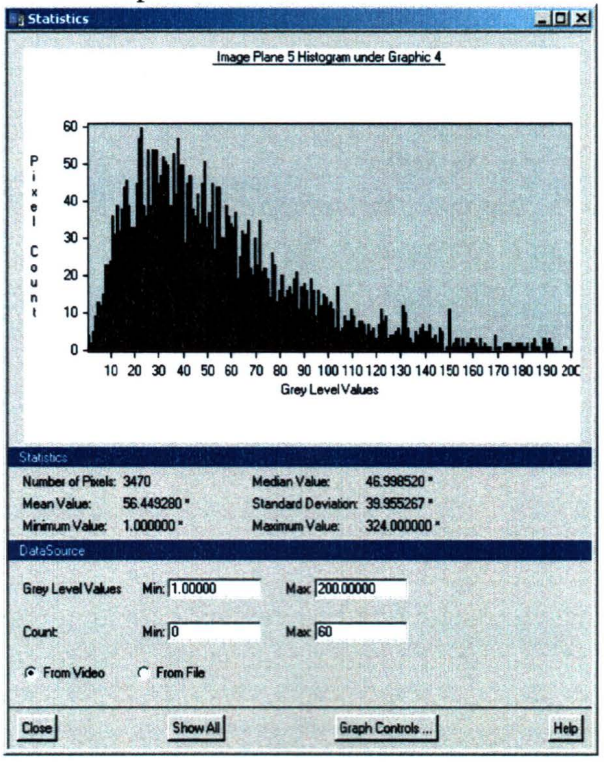

5) Shrimp pond: (0-500)

May7, 2001

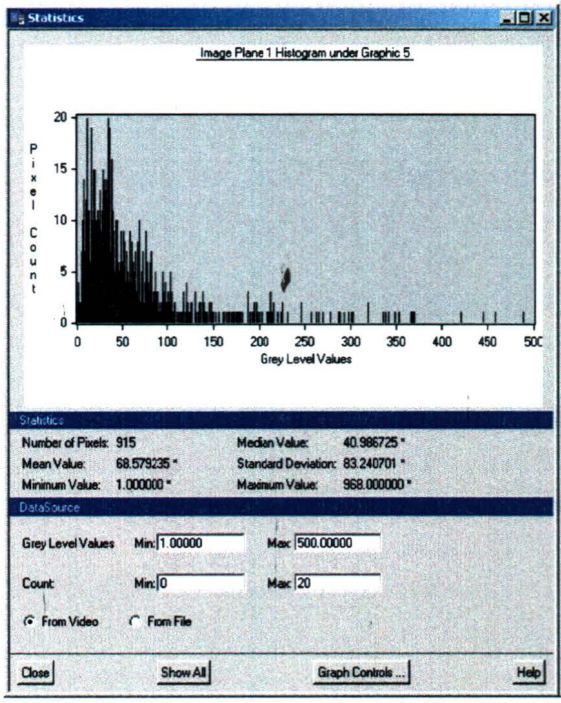

May 24, 2001

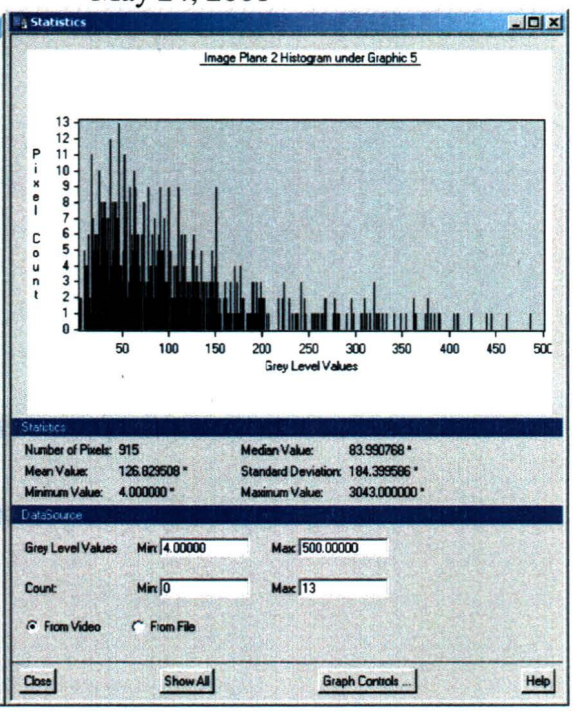

July 11, 2001:

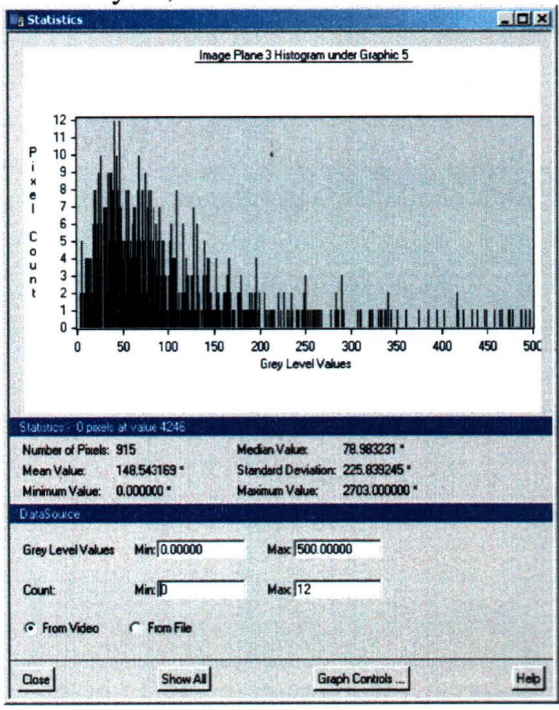

July 18, 2001:

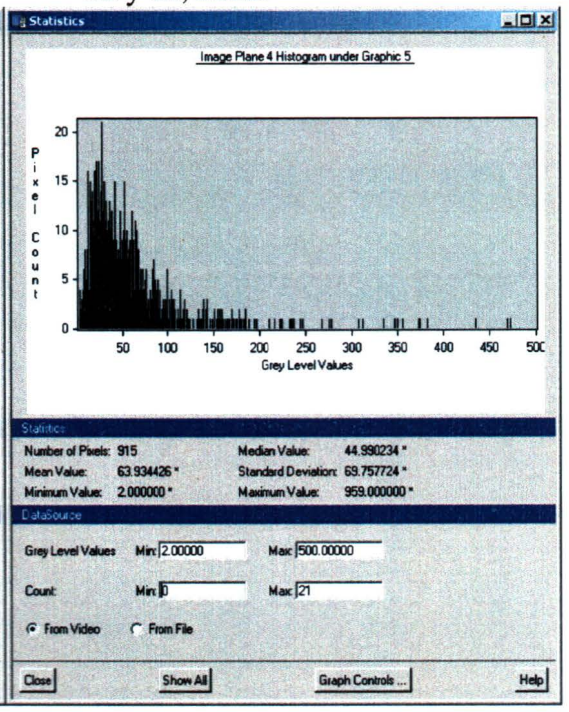

September 19, 2001:

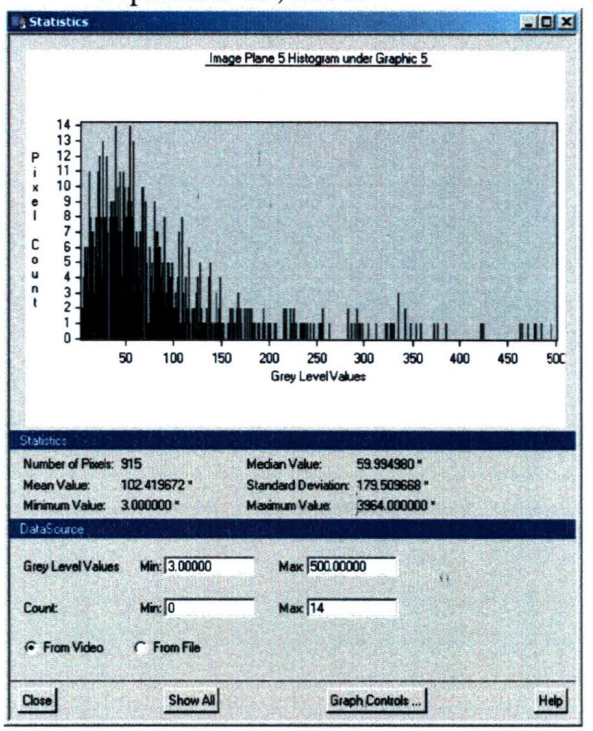

6) Shrimp farm: (0-500)

May7, 2001

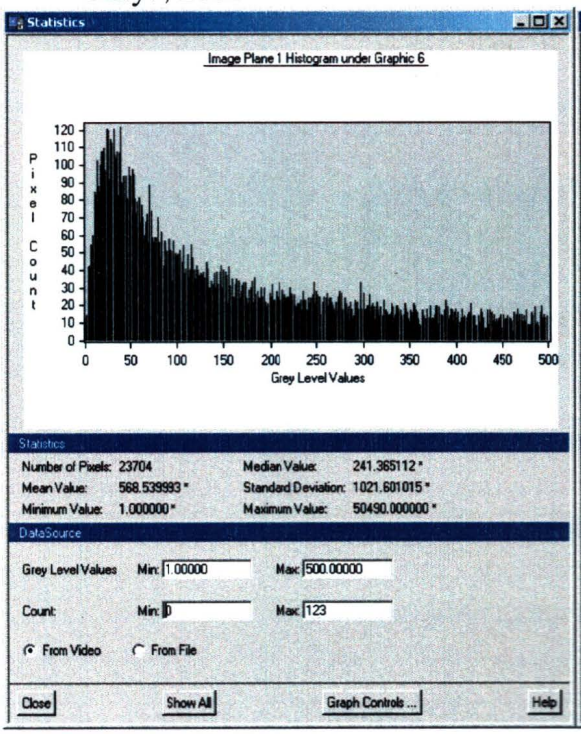

May 24, 2001

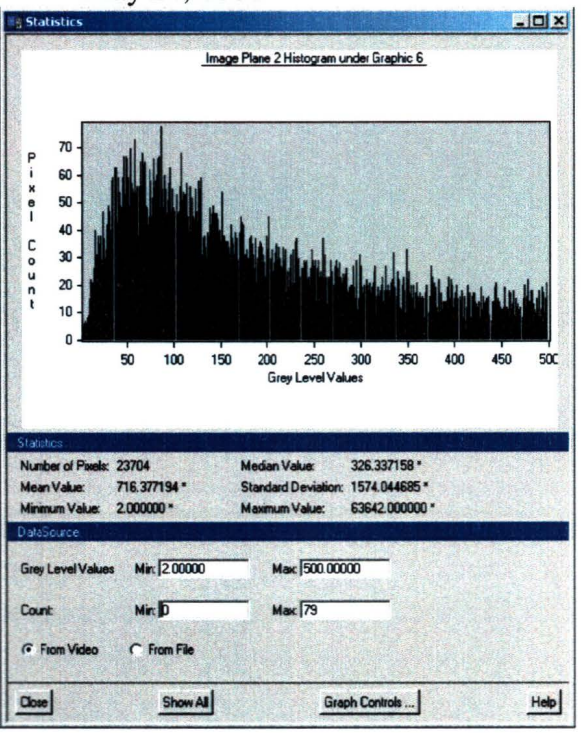

July 11, 2001:

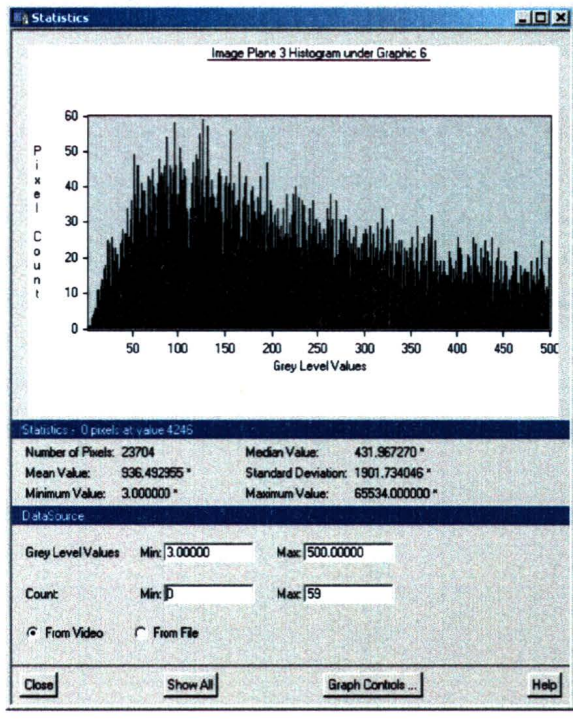

July 18, 2001:

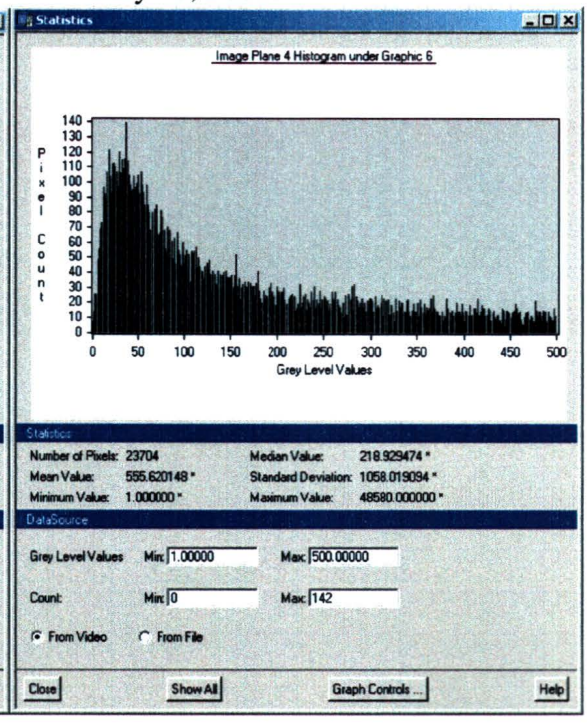

September 19, 2001:

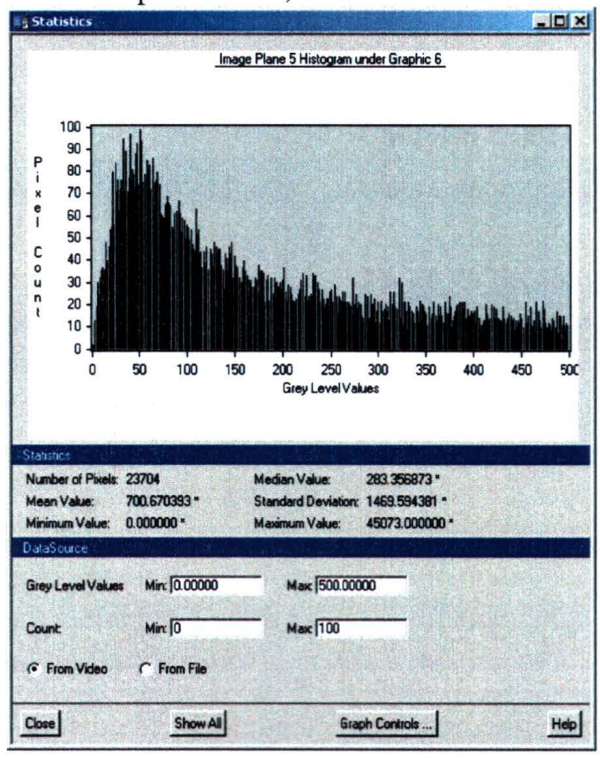

PIXELS DISTRIBUTION FOR ACCURACY SITES:

1) Rice: (0-5000)

May7, 2001

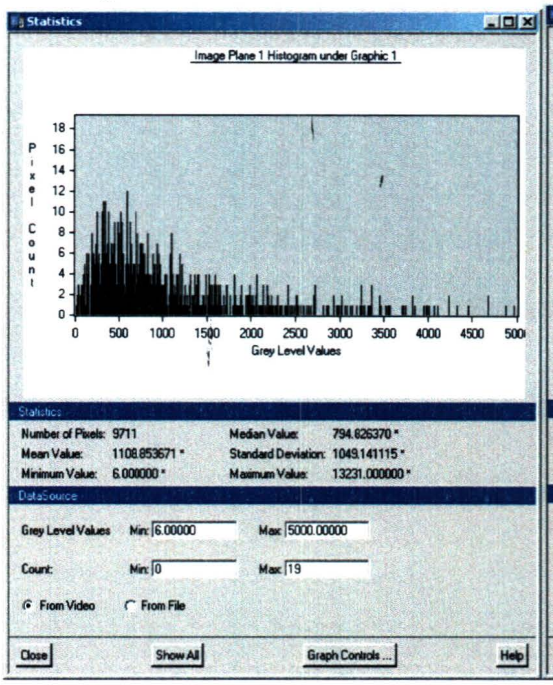

May 24, 2001

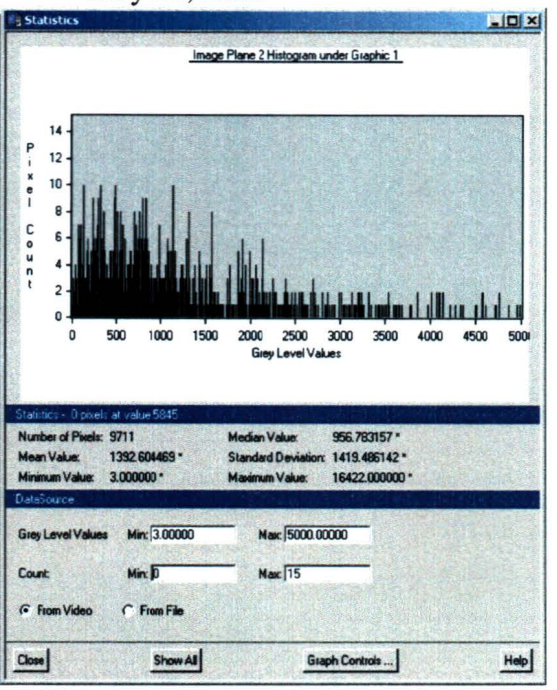

July 11, 2001:

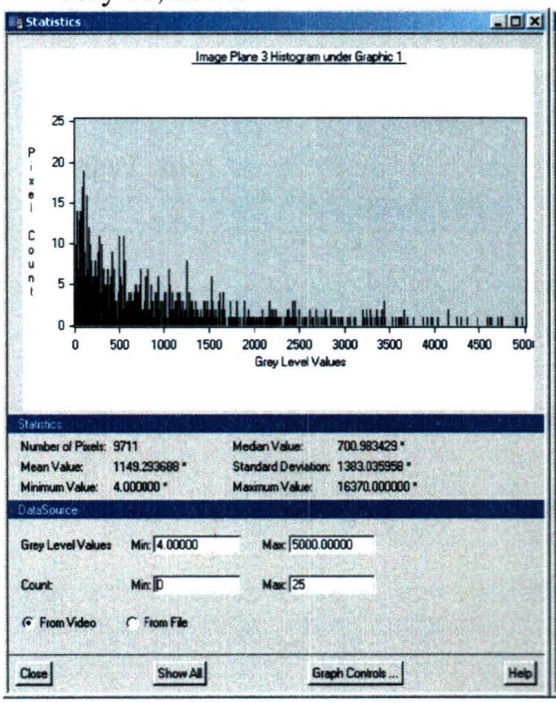

July 18, 2001:

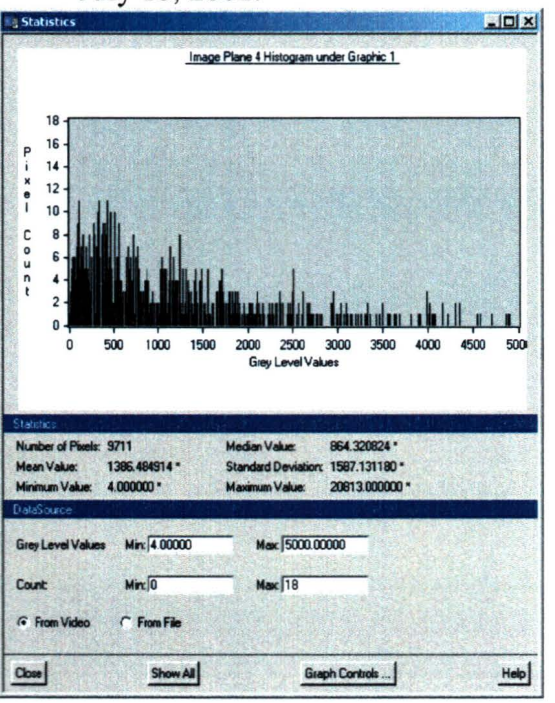

September 19, 2001:

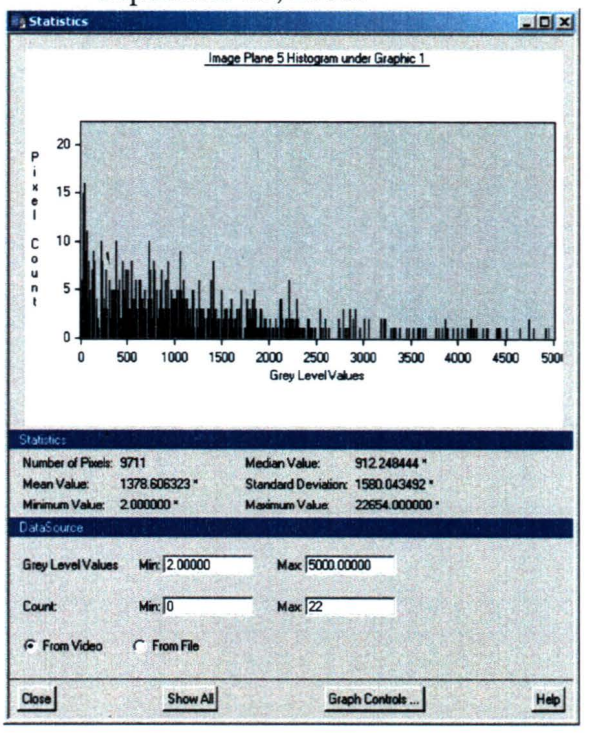

2) Human Settlement: (0-10000)

May7, 2001

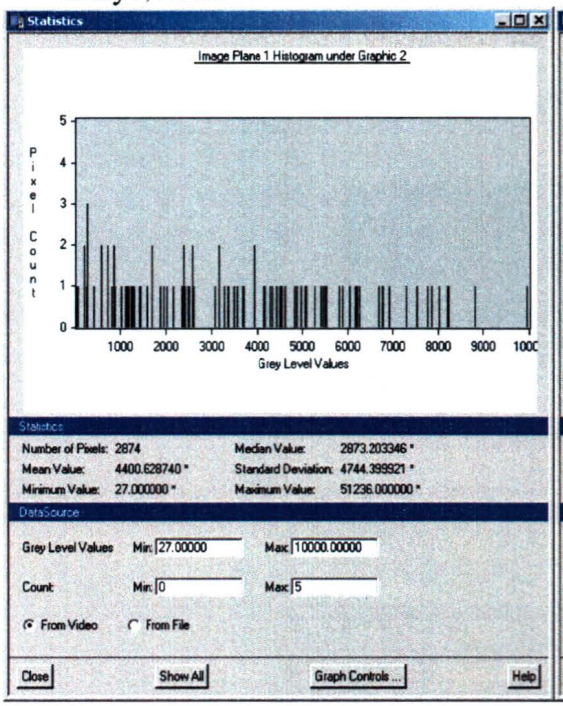

May 24, 2001

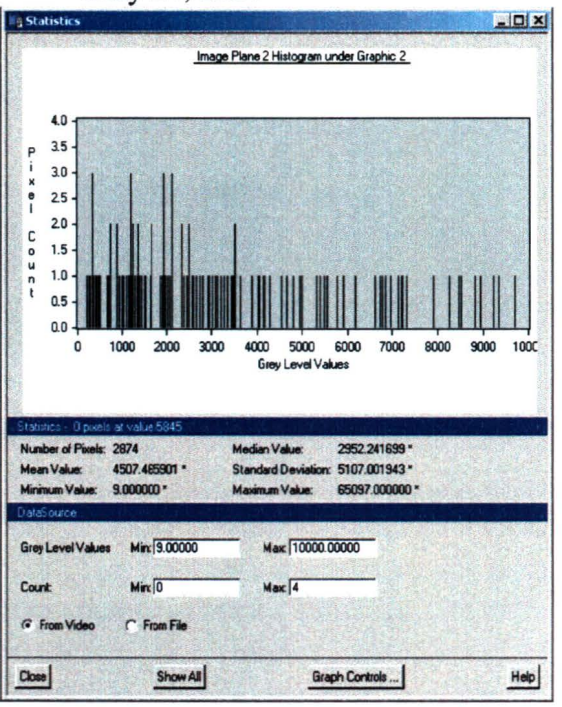

July 11, 2001:

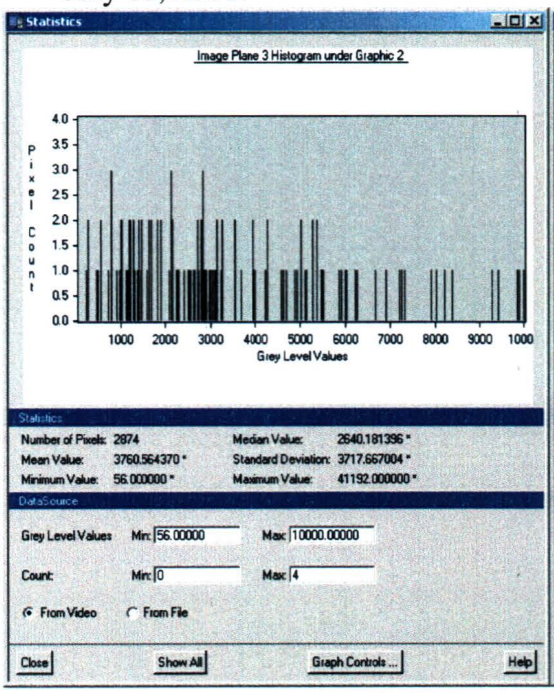

July 18, 2001:

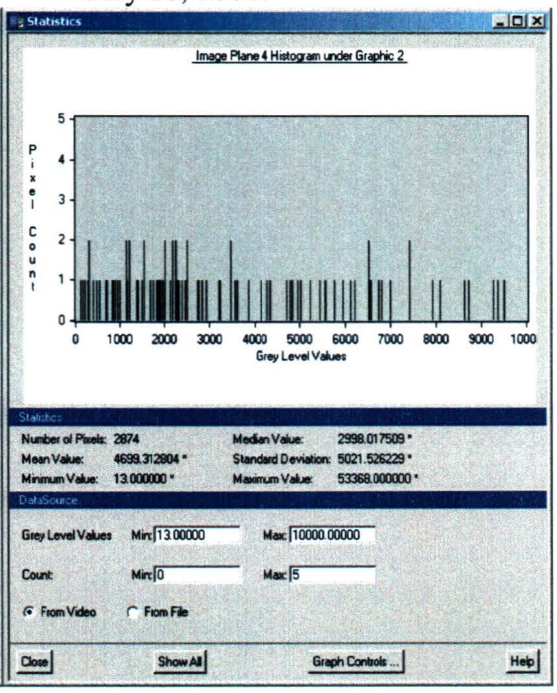

September 19, 2001:

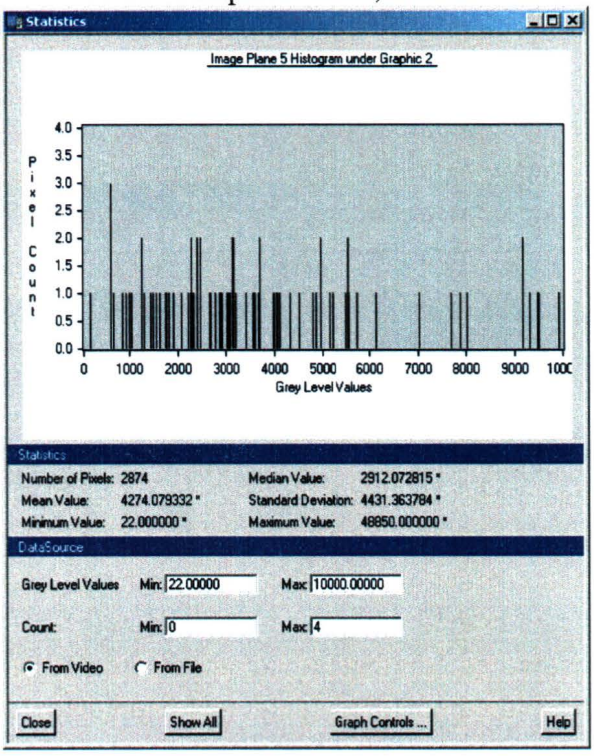

3) Orchards: (0-5000)

May7, 2001

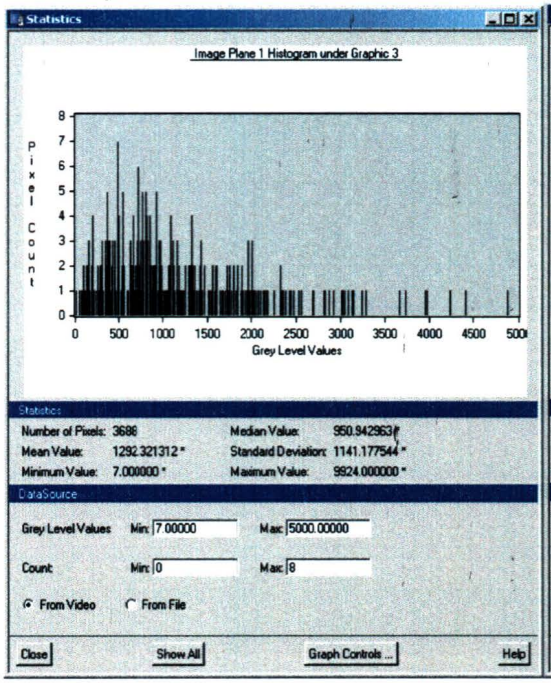

May 24, 2001

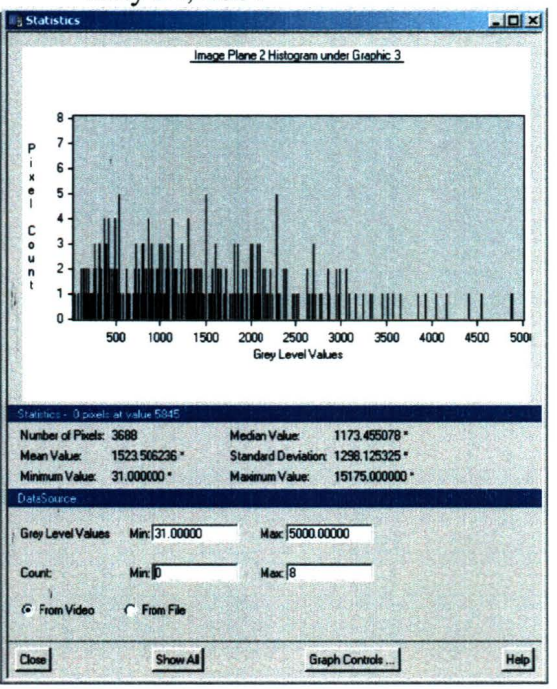

July 11, 2001:

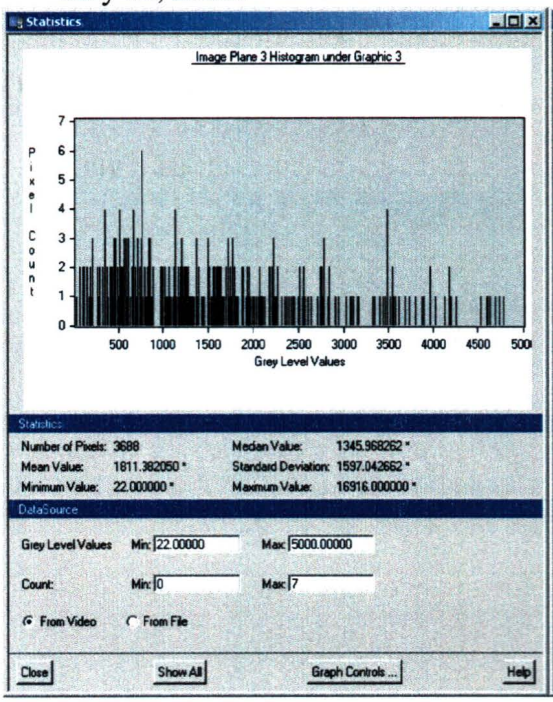

July 18, 2001:

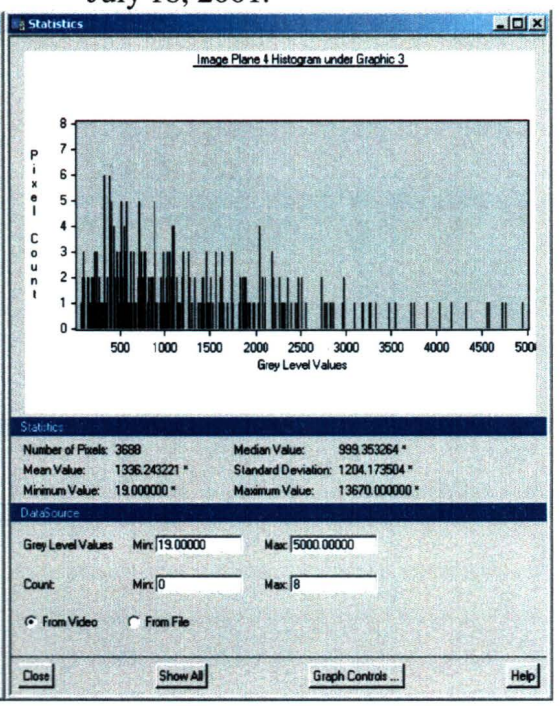

September 19, 2001:

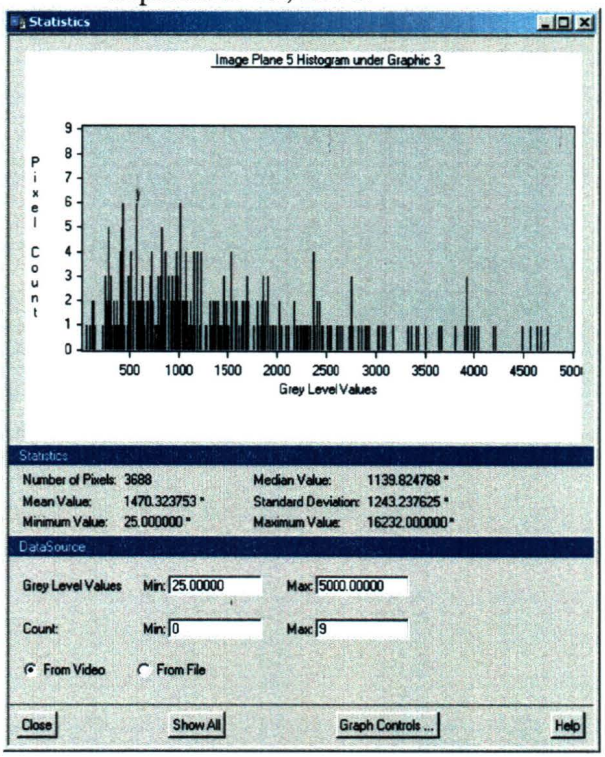

4) Water: (0-200)

May7, 2001

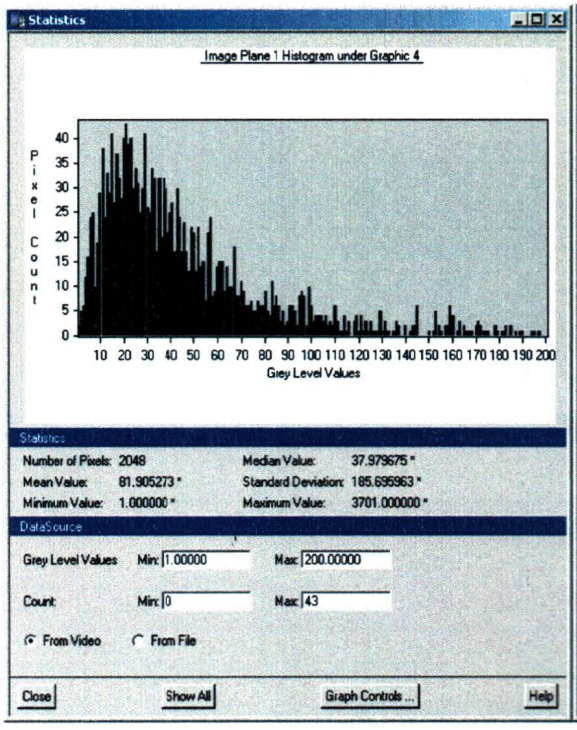

May 24, 2001

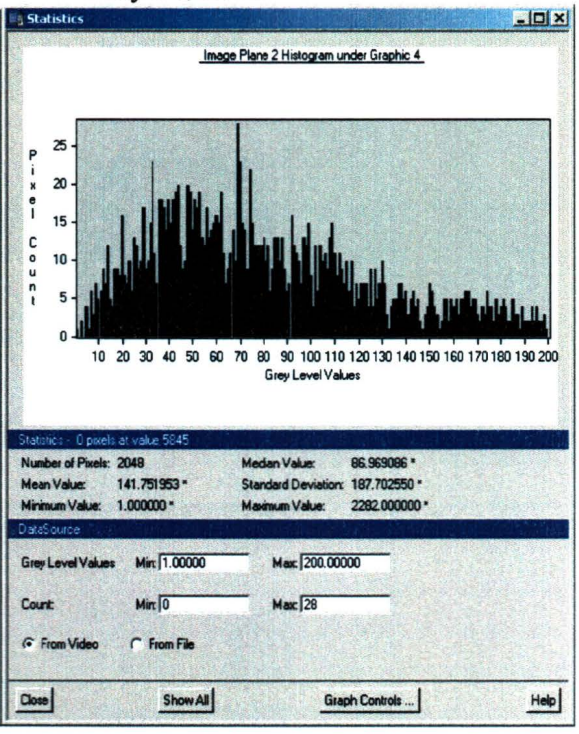

July 11, 2001:

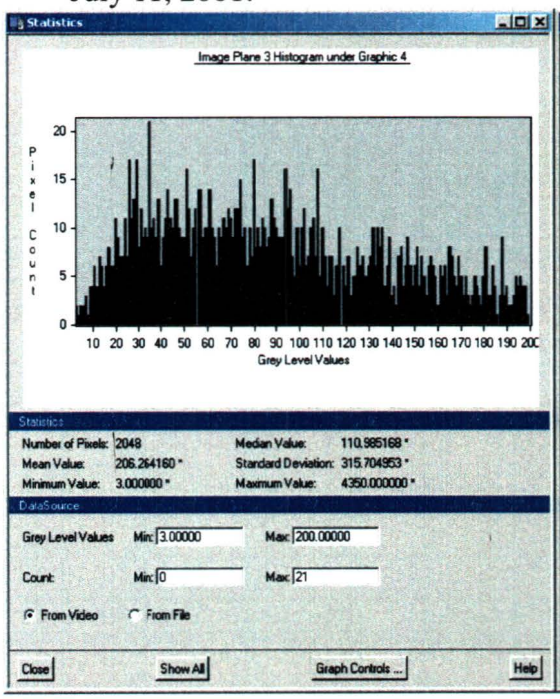

July 18, 2001:

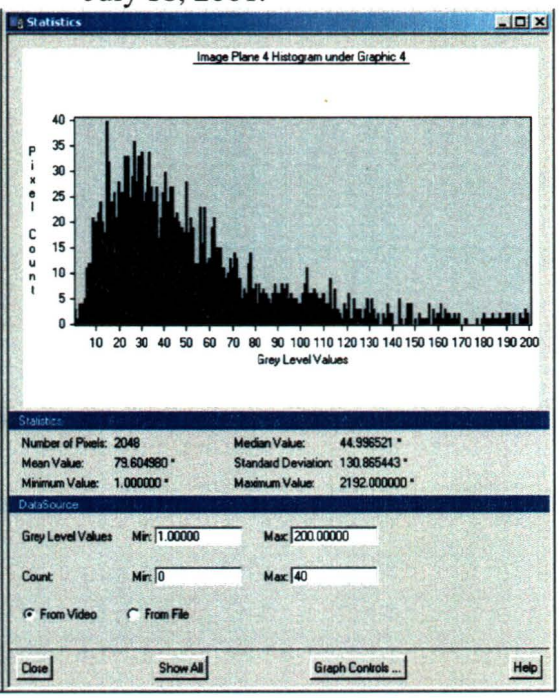

September 19, 2001:

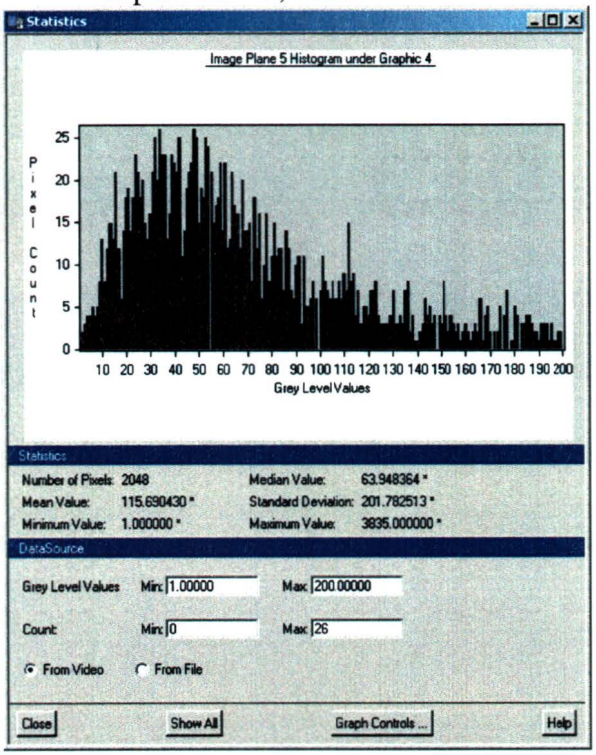

5) Shrimp farm: (0-500)

May7, 2001

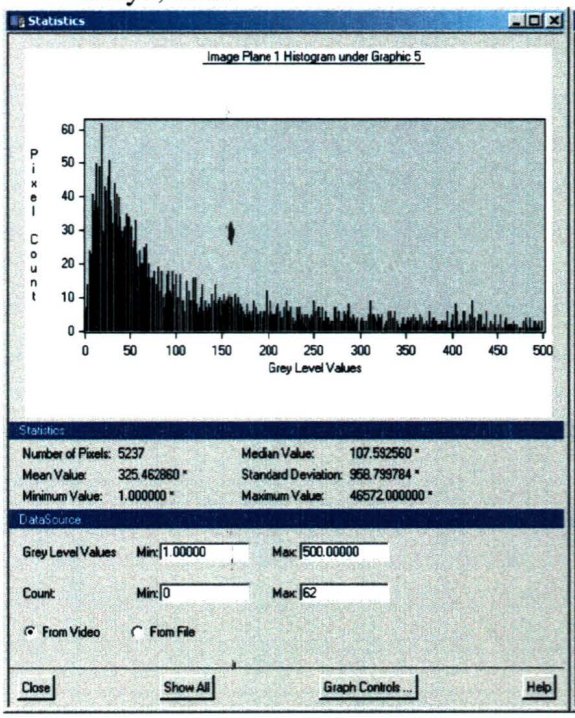

May 24, 2001

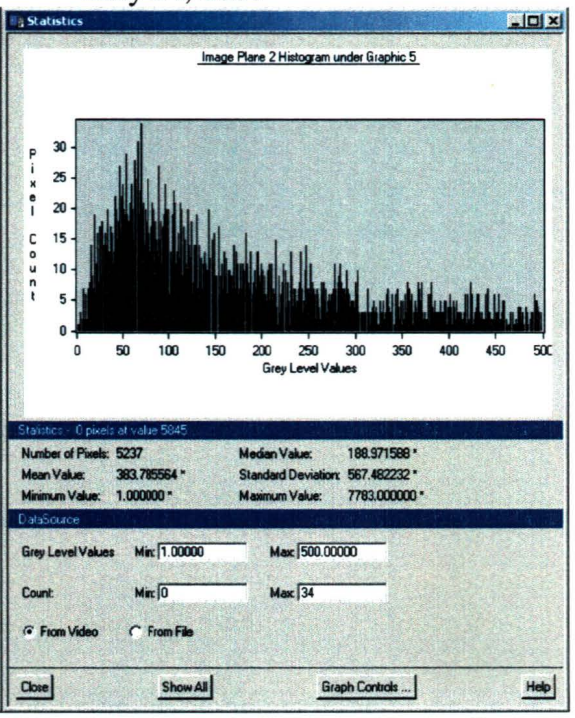

July 11, 2001:

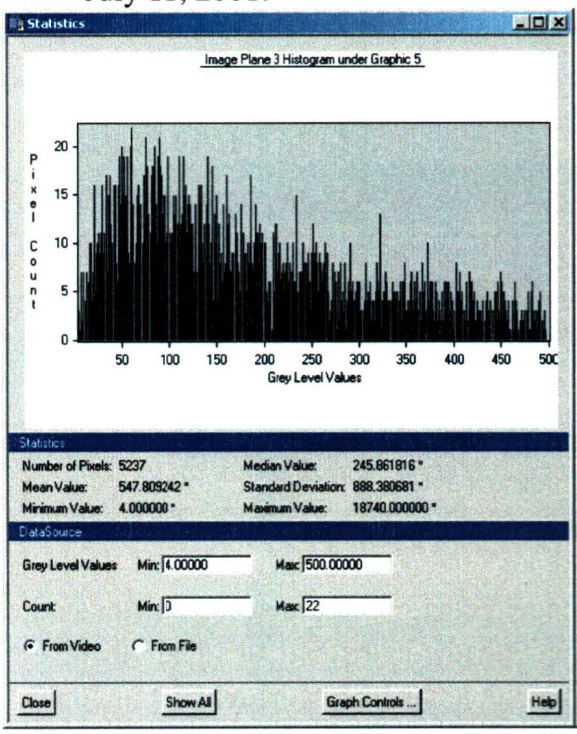

July 18, 2001:

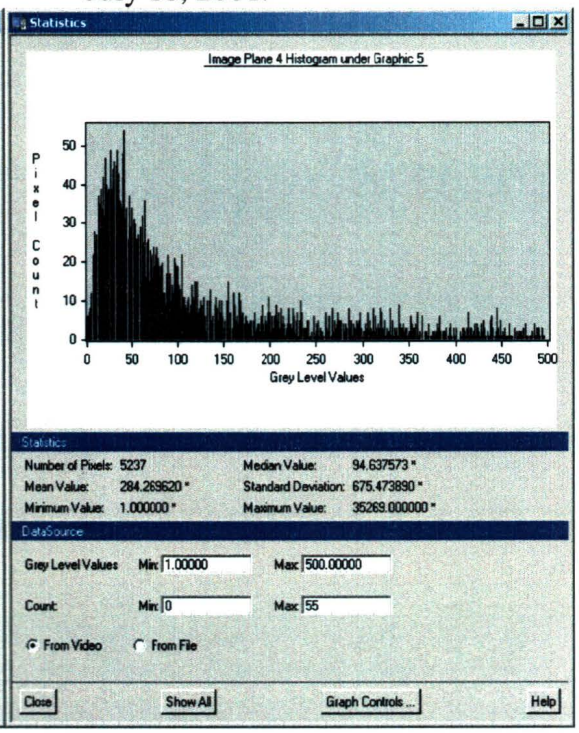

September 19, 2001:

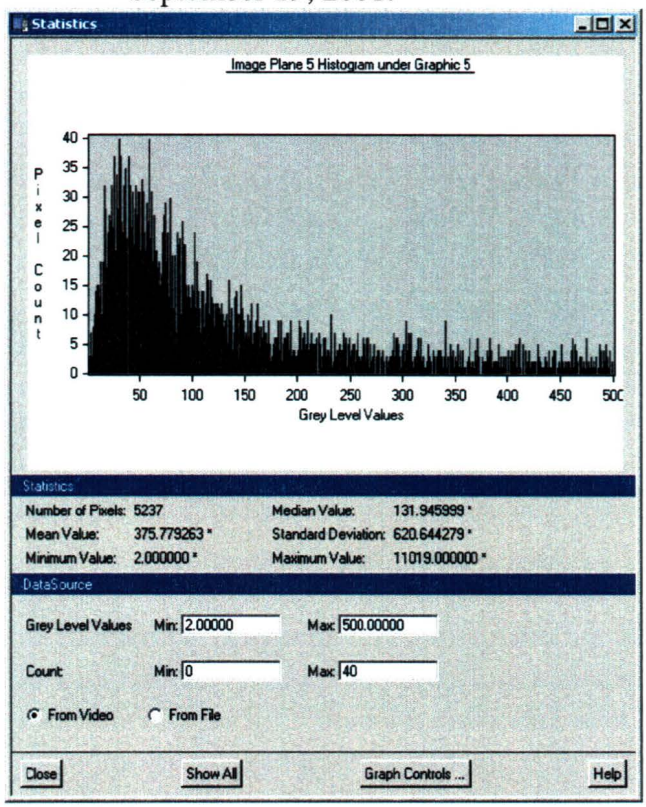

6) *Allwater*: (0-200)

May7, 2001

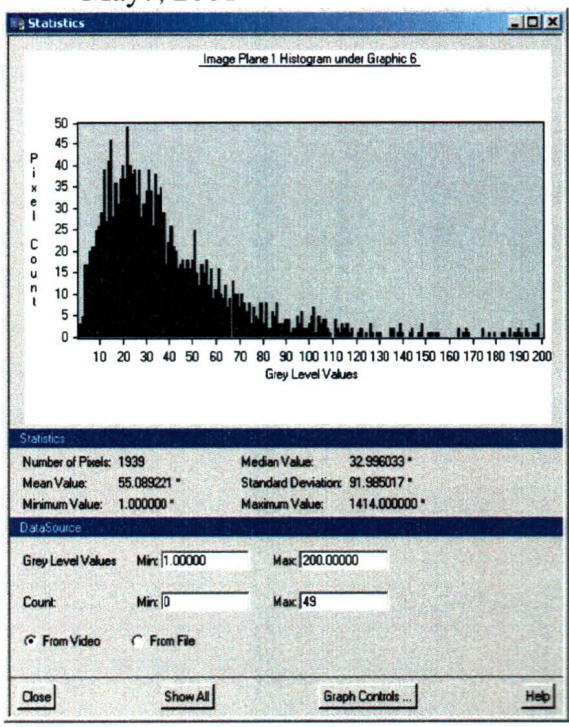

May 24, 2001

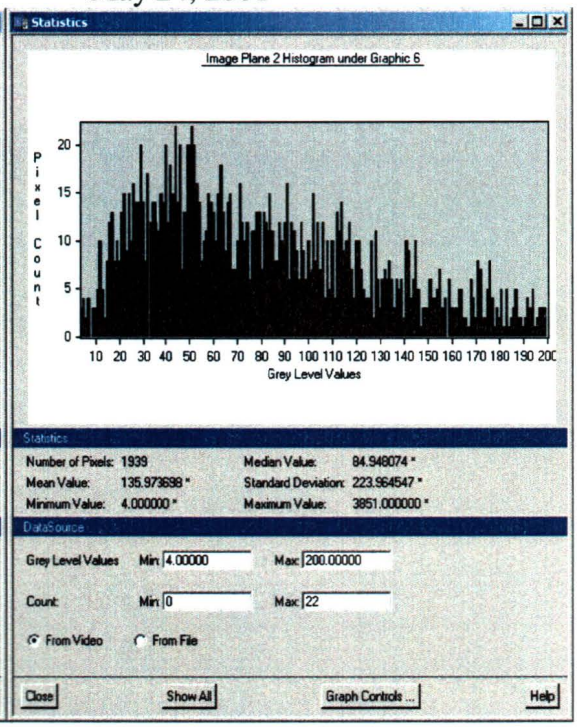

July 11, 2001:

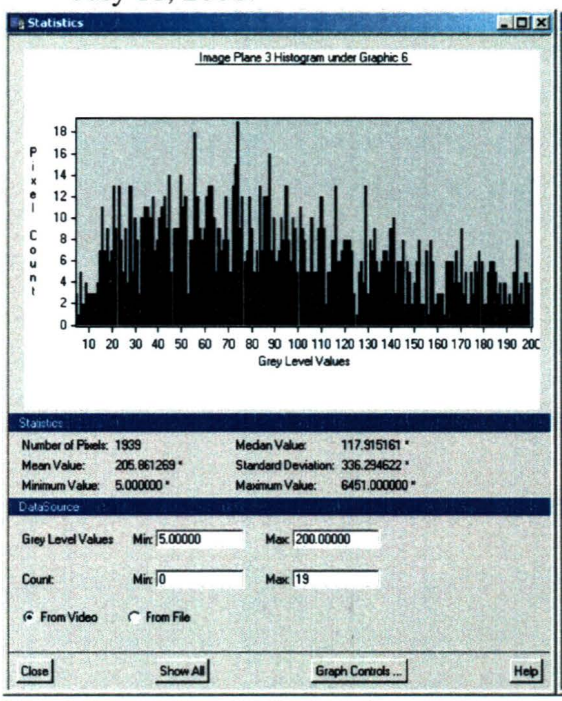

July 18, 2001:

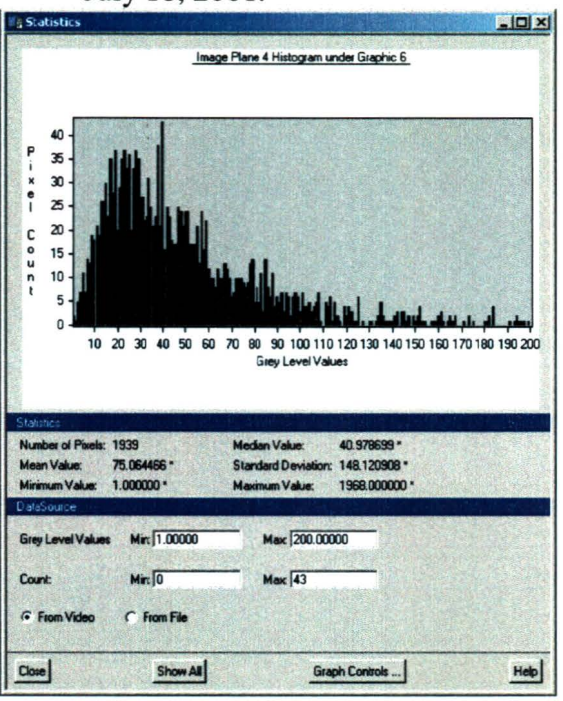

September 19, 2001:

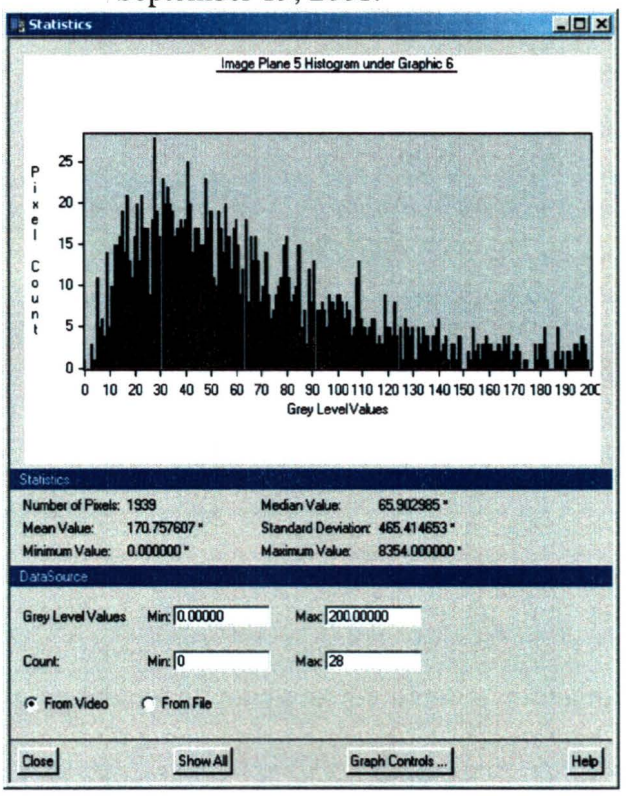

APPENDIX III

TEXTURE ANALYSIS

WINDOW SIZE ANALYSIS
(Tested with the image of May 7, 2001 (F4))

		Mean			Standard Deviation		
Texture (GLCM)	**Signatures**	**3x3**	**5x5**	**7x7**	**3x3**	**5x5**	**7x7**
Homogeneity	Rice	0.371001	0.370341	0.369822	0.110849	0.076249	0.063373
	Human	0.316148	0.31467	0.314375	0.100709	0.060626	0.044036
	Orchard	0.315956	0.316096	0.317173	0.093355	0.05446	0.040388
	Water	0.756154	0.742375	0.721997	0.109039	0.084244	0.080592
	Shrimp Farms	0.436561	0.434355	0.433184	0.163577	0.112211	0.085509
	Shrimp Ponds	0.60162	0.577249	0.54961	0.18896	0.137571	0.108373
Contrast	Rice	7.38409	7.408166	7.433339	4.819309	3.385148	2.858013
	Human	11.271912	11.362003	11.385324	6.9963	4.505496	3.423926
	Orchard	10.162729	10.236324	10.233811	5.544496	3.451797	2.619439
	Water	0.850738	1.171012	1.610818	1.7428	1.804759	1.946132
	Shrimp Farms	7.08419	7.18461	7.231742	6.129049	4.145717	3.173065
	Shrimp Ponds	3.164737	3.757788	4.379729	3.756533	2.88953	2.413946
Dissimilarity	Rice	2.094574	2.098038	2.101673	0.723324	0.514266	0.436732
	Human	2.603755	2.61603	2.618938	0.844678	0.540352	0.407369
	Orchard	2.516172	2.521812	2.518069	0.730253	0.447868	0.338478
	Water	0.537119	0.601131	0.692253	0.379043	0.356863	0.370682
	Shrimp Farms	1.900689	1.915683	1.923165	0.916647	0.631322	0.485597
	Shrimp Ponds	1.127795	1.243685	1.370625	0.758238	0.572533	0.466839
Mean	Rice	6.789992	6.781889	6.773346	1.274261	1.038451	0.92992
	Human	7.539153	7.536987	7.529554	1.540949	1.108009	0.889763
	Orchard	8.002358	7.968786	7.927113	1.48676	1.204898	1.075042
	Water	2.786774	2.878502	3.0146	0.445684	0.500965	0.576304
	Shrimp Farms	5.309711	5.315912	5.323551	1.646552	1.2794	1.051953
	Shrimp Ponds	3.948498	4.119381	4.326267	1.096757	0.939257	0.831032
Standard Deviation	Rice	1.74828	1.926989	1.993484	0.571057	0.449927	0.398934
	Human	2.200528	2.488502	2.591386	0.704638	0.545243	0.457735
	Orchard	2.083712	2.298092	2.379349	0.576946	0.413379	0.341995
	Water	0.532517	0.719041	0.951242	0.375632	0.555945	0.692578
	Shrimp Farms	1.701566	2.042184	2.197022	0.776728	0.636247	0.535784
	Shrimp Ponds	1.066818	1.443406	1.718116	0.671813	0.636905	0.551127
Entropy	Rice	2.769183	3.478232	3.766042	0.407086	0.358017	0.346418
	Human	2.94553	3.771926	4.133762	0.371693	0.290954	0.247318
	Orchard	2.935265	3.736373	4.068151	0.349589	0.254997	0.216337
	Water	1.235337	1.515674	1.760266	0.476629	0.524171	0.613136
	Shrimp Farms	2.537338	3.250564	3.565551	0.628353	0.547201	0.4541
	Shrimp Ponds	1.909647	2.549616	2.955681	0.79011	0.726128	0.611223
Angular 2nd Moment	Rice	0.160955	0.084152	0.064233	0.089519	0.039347	0.028455
	Human	0.13249	0.061391	0.043195	0.073911	0.024894	0.013606
	Orchard	0.131478	0.061843	0.044869	0.063358	0.020623	0.012034
	Water	0.735462	0.590567	0.517832	0.361605	0.206623	0.165851
	Shrimp Farms	0.246768	0.138472	0.104834	0.243947	0.122816	0.073747
	Shrimp Ponds	0.497595	0.321758	0.235794	0.436828	0.270367	0.186036

		Mean			Standard Deviation		
	Signatures	**3x3**	**5x5**	**7x7**	**3x3**	**5x5**	**7x7**
Correlation	Rice	-0.074657	0.097733	0.155527	0.157573	0.148952	0.125267
	Human	-0.09769	0.045503	0.099879	0.155231	0.133891	0.114396
	Orchard	-0.107691	0.047406	0.165099	0.146266	0.178225	0.218013
	Water	-0.033647	0.188846	0.270411	0.161007	0.153862	0.131428
	Shrimp Farms	-0.042605	0.183942	0.288312	0.154195	0.160745	0.142662
	Shrimp Ponds	-0.042605	0.183942	0.288312	0.154195	0.160745	0.142662

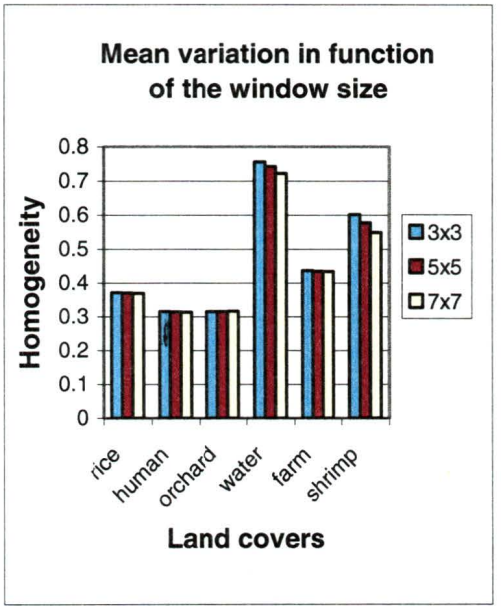

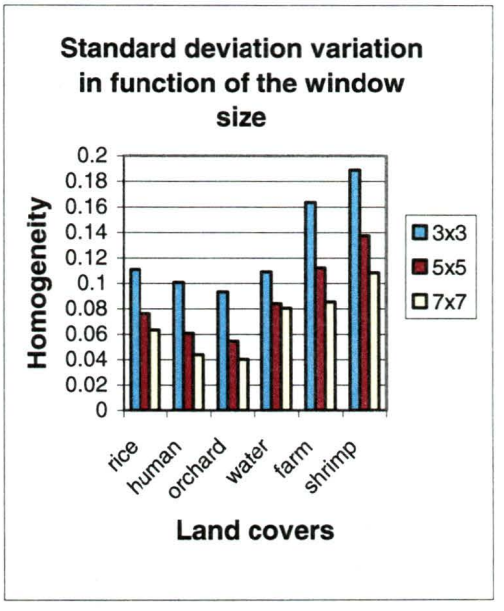

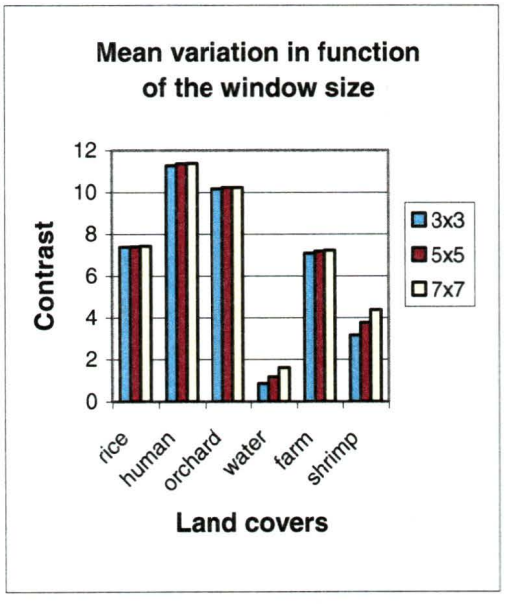

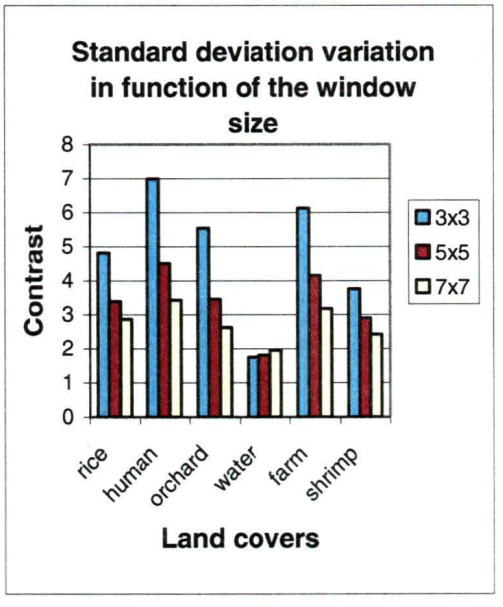

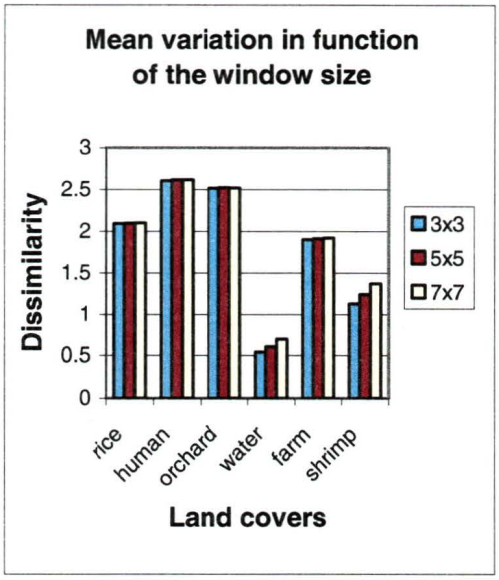
Mean variation in function of the window size
Dissimilarity
3
2.5
2
1.5
1
0.5
0
3x3
5x5
7x7
rice
human
orchard
water
farm
shrimp
Land covers

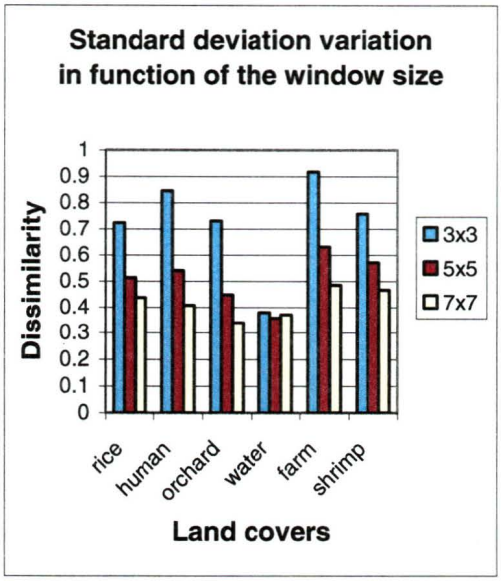
Standard deviation variation in function of the window size
Dissimilarity
1
0.9
0.8
0.7
0.6
0.5
0.4
0.3
0.2
0.1
0
3x3
5x5
7x7
rice
human
orchard
water
farm
shrimp
Land covers

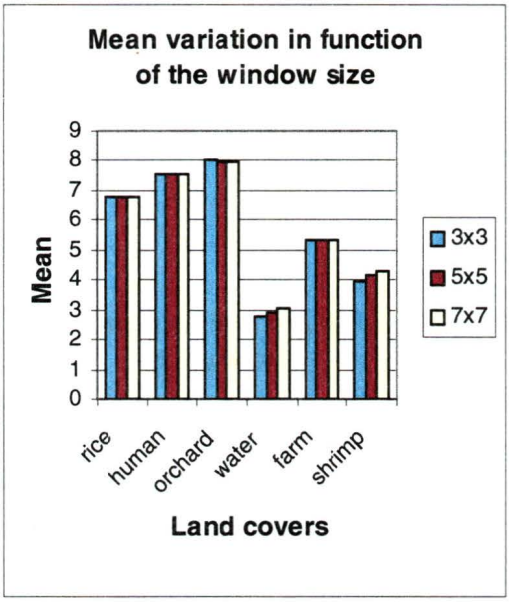
Mean variation in function of the window size
Mean
9
8
7
6
5
4
3
2
1
0
3x3
5x5
7x7
rice
human
orchard
water
farm
shrimp
Land covers

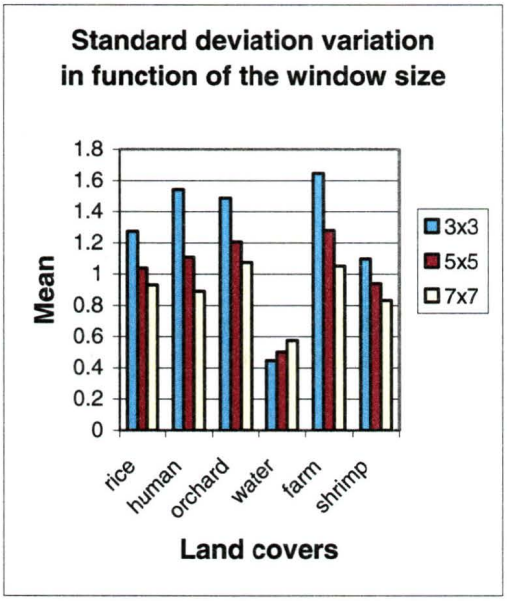
Standard deviation variation in function of the window size
Mean
1.8
1.6
1.4
1.2
1
0.8
0.6
0.4
0.2
0
3x3
5x5
7x7
rice
human
orchard
water
farm
shrimp
Land covers

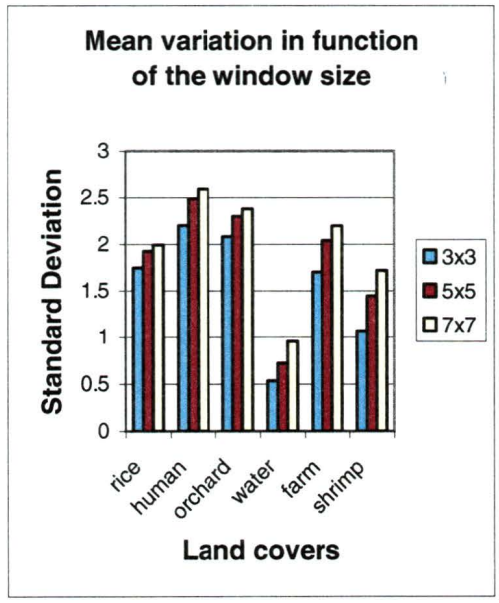
Mean variation in function of the window size
Standard Deviation
3
2.5
2
1.5
1
0.5
0
rice
human
orchard
water
farm
shrimp
Land covers
3x3
5x5
7x7

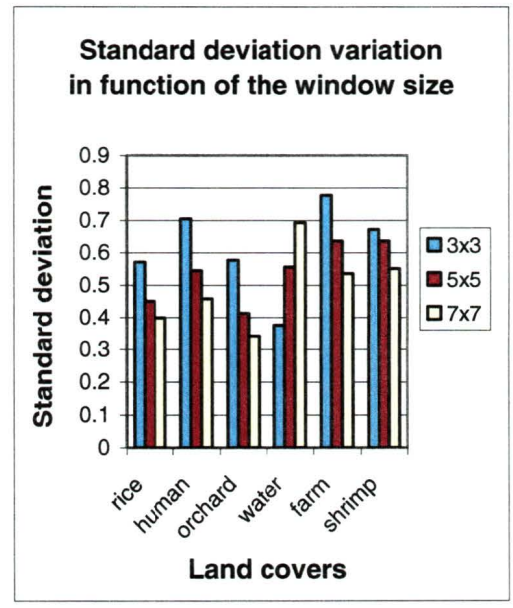
Standard deviation variation in function of the window size
Standard deviation
0.9
0.8
0.7
0.6
0.5
0.4
0.3
0.2
0.1
0
rice
human
orchard
water
farm
shrimp
Land covers
3x3
5x5
7x7

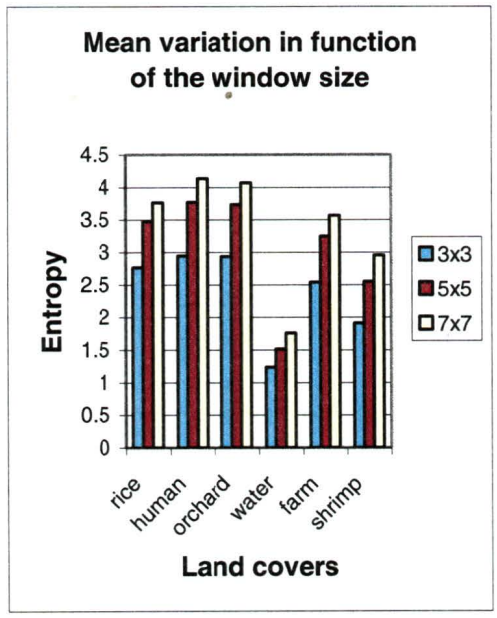
Mean variation in function of the window size
Entropy
4.5
4
3.5
3
2.5
2
1.5
1
0.5
0
rice
human
orchard
water
farm
shrimp
Land covers
3x3
5x5
7x7

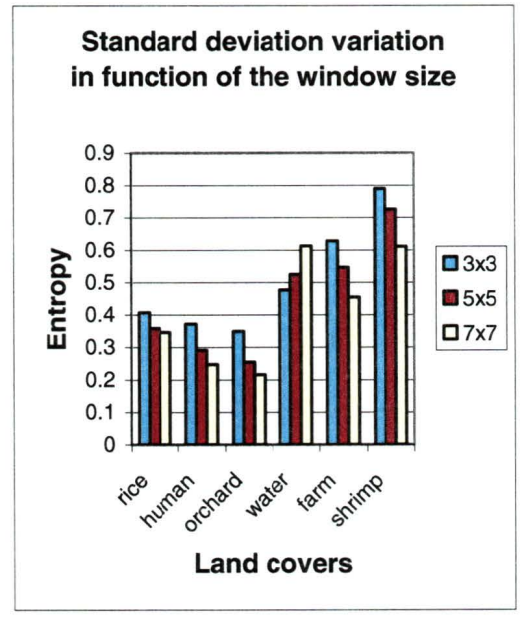
Standard deviation variation in function of the window size
Entropy
0.9
0.8
0.7
0.6
0.5
0.4
0.3
0.2
0.1
0
rice
human
orchard
water
farm
shrimp
Land covers
3x3
5x5
7x7

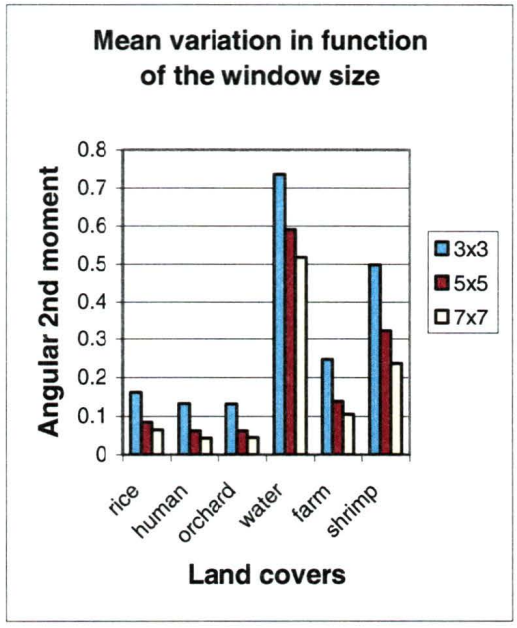
Mean variation in function of the window size
Angular 2nd moment
0.8
0.7
0.6
0.5
0.4
0.3
0.2
0.1
0
3x3
5x5
7x7
rice
human
orchard
water
farm
shrimp
Land covers

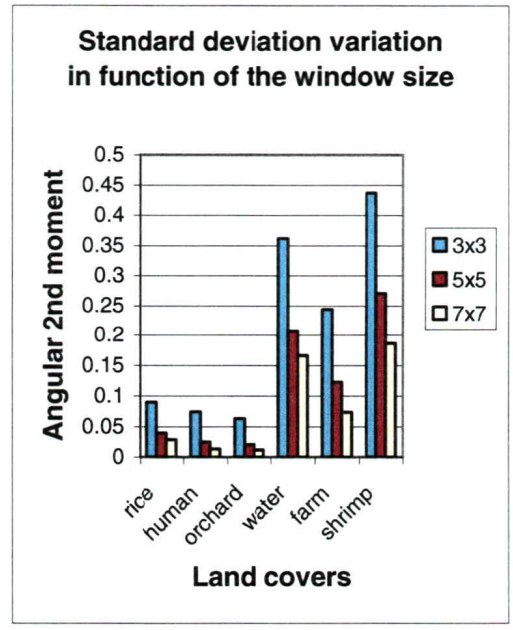
Standard deviation variation in function of the window size
Angular 2nd moment
0.5
0.45
0.4
0.35
0.3
0.25
0.2
0.15
0.1
0.05
0
3x3
5x5
7x7
rice
human
orchard
water
farm
shrimp
Land covers

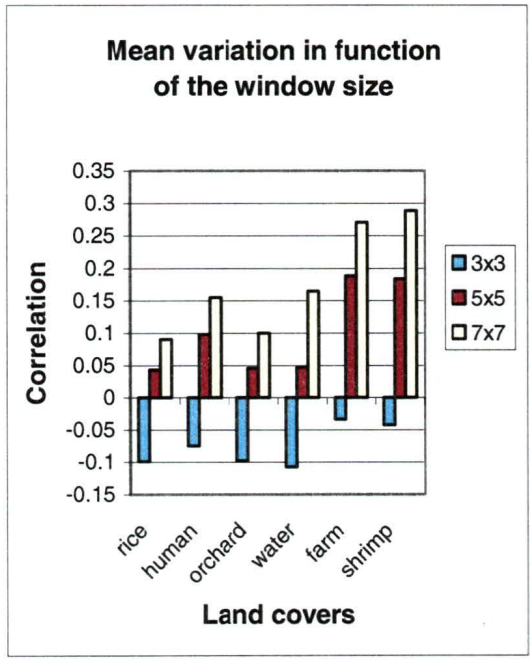
Mean variation in function of the window size
Correlation
0.35
0.3
0.25
0.2
0.15
0.1
0.05
0
-0.05
-0.1
-0.15
3x3
5x5
7x7
rice
human
orchard
water
farm
shrimp
Land covers

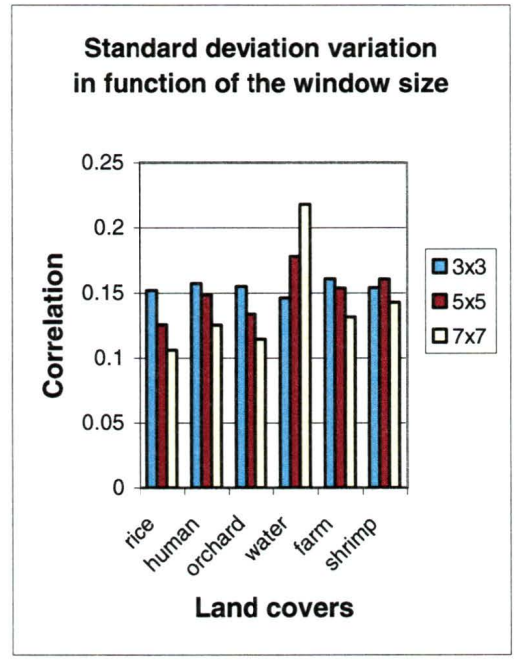
Standard deviation variation in function of the window size
Correlation
0.25
0.2
0.15
0.1
0.05
0
3x3
5x5
7x7
rice
human
orchard
water
farm
shrimp
Land covers

CORRELATION ANALYSIS

(Correlation matrix for each image)

MAY 7, 2001

Rice	Homogeneity	Contrast	Dissimilarity	Mean	Std Dev.	Entropy	Ang. 2nd Moment	Correlation
Homogeneity	1.00							
Contrast	-0.83	1.00						
Dissimilarity	-0.93	0.97	1.00					
Mean	-0.72	0.68	0.73	1.00				
Std Dev.	-0.81	0.94	0.93	0.69	1.00			
Entropy	-0.90	0.80	0.87	0.72	0.85	1.00		
Ang. 2nd Moment	0.86	-0.66	-0.76	-0.66	-0.73	-0.93	1.00	
Correlation	0.14	-0.12	-0.14	-0.02	0.19	0.08	-0.08	1.00

Human	Homogeneity	Contrast	Dissimilarity	Mean	Std Dev.	Entropy	Ang. 2nd Moment	Correlation
Homogeneity	1.00							
Contrast	-0.72	1.00						
Dissimilarity	-0.86	0.97	1.00					
Mean	-0.52	0.53	0.58	1.00				
Std Dev.	-0.62	0.89	0.86	0.56	1.00			
Entropy	-0.83	0.67	0.77	0.52	0.69	1.00		
Ang. 2nd Moment	0.79	-0.52	-0.64	-0.40	-0.53	-0.91	1.00	
Correlation	0.14	-0.02	-0.06	0.09	0.40	0.16	-0.07	1.00

Orchard	Homogeneity	Contrast	Dissimilarity	Mean	Std Dev.	Entropy	Ang. 2nd Moment	Correlation
Homogeneity	1.00							
Contrast	-0.72	1.00						
Dissimilarity	-0.86	0.97	1.00					
Mean	-0.38	0.51	0.51	1.00				
Std Dev.	-0.66	0.89	0.87	0.54	1.00			
Entropy	-0.79	0.64	0.73	0.39	0.71	1.00		
Ang. 2nd Moment	0.77	-0.54	-0.65	-0.30	-0.59	-0.94	1.00	
Correlation	0.12	-0.11	-0.13	0.12	0.32	0.19	-0.13	1.00

Water	Homogeneity	Contrast	Dissimilarity	Mean	Std Dev.	Entropy	Ang. 2nd Moment	Correlation
Homogeneity	1.00							
Contrast	-0.82	1.00						
Dissimilarity	-0.94	0.96	1.00					
Mean	-0.76	0.90	0.89	1.00				
Std Dev.	-0.86	0.97	0.97	0.93	1.00			
Entropy	-0.95	0.85	0.94	0.84	0.91	1.00		
Ang. 2nd Moment	0.87	-0.57	-0.73	-0.45	-0.63	-0.83	1.00	
Correlation	-0.57	0.65	0.66	0.71	0.76	0.74	-0.50	1.00

Shrimp Farms	Homogeneity	Contrast	Dissimilarity	Mean	Std Dev.	Entropy	Ang. 2nd Moment.	Correlation
Homogeneity	1.00							
Contrast	-0.75	1.00						
Dissimilarity	-0.91	0.95	1.00					
Mean	-0.81	0.74	0.83	1.00				
Std Dev.	-0.72	0.92	0.89	0.73	1.00			
Entropy	-0.95	0.72	0.87	0.80	0.75	1.00		
Ang. 2nd Moment	0.86	-0.51	-0.69	-0.63	-0.55	-0.89	1.00	
Correlation	0.16	-0.07	-0.11	-0.02	0.27	0.02	0.03	1.00

Shrimp Ponds	Homogeneity	Contrast	Dissimilarity	Mean	Std Dev.	Entropy	Ang. 2nd Moment	Correlation
Homogeneity	1.00							
Contrast	-0.80	1.00						
Dissimilarity	-0.95	0.95	1.00					
Mean	-0.87	0.81	0.89	1.00				
Std Dev.	-0.81	0.94	0.92	0.81	1.00			
Entropy	-0.97	0.78	0.92	0.86	0.83	1.00		
Ang. 2nd Moment.	0.90	-0.60	-0.78	-0.69	-0.68	-0.93	1.00	
Correlation	-0.17	0.20	0.19	0.23	0.47	0.31	-0.27	1.00

ALL Classes	Homogeneity	Contrast	Dissimilarity	Mean	Std Dev.	Entropy	Ang. 2nd Moment	Correlation
Homogeneity	1.00							
Contrast	-0.78	1.00						
Dissimilarity	-0.91	0.97	1.00					
Mean	-0.65	0.69	0.72	1.00				
Std Dev.	-0.75	0.93	0.91	0.71	1.00			
Entropy	-0.89	0.75	0.85	0.67	0.80	1.00		
Ang. 2nd Moment	0.84	-0.58	-0.71	-0.50	-0.63	-0.91	1.00	
Correlation	-0.07	0.12	0.11	0.23	0.43	0.30	-0.21	1.00

MAY 24, 2001

Rice	Homogeneity	Contrast	Dissimilarity	Mean	Std Dev.	Entropy	Ang. 2nd Moment	Correlation
Homogeneity	1.00							
Contrast	-0.78	1.00						
Dissimilarity	-0.89	0.97	1.00					
Mean	-0.52	0.51	0.55	1.00				
Std Dev.	-0.70	0.90	0.88	0.47	1.00			
Entropy	-0.79	0.69	0.75	0.47	0.74	1.00		
Ang. 2nd Moment	0.78	-0.59	-0.68	-0.42	-0.64	-0.94	1.00	
Correlation	0.18	-0.17	-0.18	-0.09	0.27	0.12	-0.09	1.00

Human	Homogeneity	Contrast	Dissimilarity	Mean	Std Dev.	Entropy	Ang. 2nd Moment	Correlation
Homogeneity	1.00							
Contrast	-0.65	1.00						
Dissimilarity	-0.83	0.96	1.00					
Mean	-0.39	0.53	0.55	1.00				
Std Dev.	-0.54	0.88	0.84	0.60	1.00			
Entropy	-0.84	0.60	0.73	0.39	0.62	1.00		
Ang. 2nd Moment	0.75	-0.37	-0.51	-0.07	-0.34	-0.83	1.00	
Correlation	0.19	-0.03	-0.09	0.17	0.40	0.10	0.04	1.00

Orchard	Homogeneity	Contrast	Dissimilarity	Mean	Std Dev.	Entropy	Ang. 2nd Moment	Correlation
Homogeneity	1.00							
Contrast	-0.74	1.00						
Dissimilarity	-0.87	0.97	1.00					
Mean	-0.40	0.45	0.48	1.00				
Std Dev.	-0.67	0.90	0.88	0.49	1.00			
Entropy	-0.78	0.65	0.72	0.39	0.73	1.00		
Ang. 2nd Moment	0.76	-0.53	-0.63	-0.31	-0.60	-0.93	1.00	
Correlation	0.10	-0.04	-0.07	0.13	0.37	0.26	-0.20	1.00

Water	Homogeneity	Contrast	Dissimilarity	Mean	Std Dev.	Entropy	Ang. 2nd Moment	Correlation
Homogeneity	1.00							
Contrast	-0.78	1.00						
Dissimilarity	-0.94	0.94	1.00					
Mean	-0.76	0.90	0.88	1.00				
Std Dev.	-0.83	0.97	0.96	0.91	1.00			
Entropy	-0.98	0.78	0.94	0.77	0.86	1.00		
Ang. 2nd Moment	0.92	-0.56	-0.78	-0.55	-0.64	-0.91	1.00	
Correlation	-0.50	0.62	0.61	0.67	0.73	0.62	-0.41	1.00

Shrimp Farms	Homogeneity	Contrast	Dissimilarity	Mean	Std Dev.	Entropy	Ang. 2nd Moment	Correlation
Homogeneity	1.00							
Contrast	-0.76	1.00						
Dissimilarity	-0.92	0.95	1.00					
Mean	-0.82	0.72	0.82	1.00				
Std Dev.	-0.72	0.91	0.89	0.70	1.00			
Entropy	-0.94	0.74	0.88	0.82	0.77	1.00		
Ang. 2nd Moment	0.84	-0.52	-0.69	-0.66	-0.57	-0.88	1.00	
Correlation	0.18	-0.08	-0.13	-0.07	0.27	0.03	0.02	1.00

Shrimp Ponds	Homogeneity	Contrast	Dissimilarity	Mean	Std Dev.	Entropy	Ang. 2nd Moment	Correlation
Homogeneity	1.00							
Contrast	-0.79	1.00						
Dissimilarity	-0.94	0.95	1.00					
Mean	-0.86	0.81	0.88	1.00				
Std Dev.	-0.81	0.93	0.93	0.82	1.00			
Entropy	-0.97	0.77	0.91	0.86	0.84	1.00		
Ang. 2nd Moment	0.88	-0.56	-0.74	-0.68	-0.65	-0.90	1.00	
Correlation	-0.16	0.18	0.18	0.24	0.46	0.31	-0.25	1.00

All Classes	Homogeneity	Contrast	Dissimilarity	Mean	Std Dev.	Entropy	Ang. 2nd Moment	Correlation
Homogeneity	1.00							
Contrast	-0.75	1.00						
Dissimilarity	-0.90	0.96	1.00					
Mean	-0.59	0.64	0.67	1.00				
Std Dev.	-0.71	0.92	0.90	0.66	1.00			
Entropy	-0.87	0.70	0.81	0.58	0.76	1.00		
Ang. 2nd Moment	0.82	-0.52	-0.67	-0.41	-0.57	-0.90	1.00	
Correlation	-0.04	0.11	0.09	0.22	0.45	0.28	-0.18	1.00

JULY 11, 2001

Rice	Homogeneity	Contrast	Dissimilarity	Mean	Std Dev.	Entropy	Ang. 2nd Moment	Correlation
Homogeneity	1.00							
Contrast	-0.79	1.00						
Dissimilarity	-0.90	0.98	1.00					
Mean	-0.47	0.46	0.50	1.00				
Std Dev.	-0.70	0.90	0.87	0.45	1.00			
Entropy	-0.81	0.73	0.79	0.48	0.77	1.00		
Ang. 2nd Moment	0.80	-0.64	-0.72	-0.46	-0.67	-0.95	1.00	
Correlation	0.27	-0.23	-0.26	-0.09	0.19	0.03	-0.01	1.00

Human	Homogeneity	Contrast	Dissimilarity	Mean	Std Dev.	Entropy	Ang. 2nd Moment	Correlation
Homogeneity	1.00							
Contrast	-0.63	1.00						
Dissimilarity	-0.81	0.96	1.00					
Mean	-0.24	0.51	0.49	1.00				
Std Dev.	-0.47	0.89	0.83	0.56	1.00			
Entropy	-0.82	0.54	0.67	0.21	0.49	1.00		
Ang. 2nd Moment	0.67	-0.24	-0.38	0.17	-0.16	-0.77	1.00	
Correlation	0.23	0.01	-0.07	0.19	0.43	0.02	0.11	1.00

Orchard	Homogeneity	Contrast	Dissimilarity	Mean	Std Dev.	Entropy	Ang. 2nd Moment	Correlation
Homogeneity	1.00							
Contrast	-0.78	1.00						
Dissimilarity	-0.89	0.98	1.00					
Mean	-0.41	0.46	0.47	1.00				
Std Dev.	-0.68	0.90	0.87	0.47	1.00			
Entropy	-0.76	0.67	0.73	0.39	0.71	1.00		
Ang. 2nd Moment	0.75	-0.58	-0.66	-0.36	-0.62	-0.94	1.00	
Correlation	0.27	-0.21	-0.24	-0.01	0.22	0.07	-0.04	1.00

Water	Homogeneity	Contrast	Dissimilarity	Mean	Std Dev.	Entropy	Ang. 2nd Moment	Correlation
Homogeneity	1.00							
Contrast	-0.83	1.00						
Dissimilarity	-0.95	0.96	1.00					
Mean	-0.82	0.89	0.91	1.00				
Std Dev.	-0.87	0.97	0.97	0.92	1.00			
Entropy	-0.95	0.85	0.95	0.88	0.91	1.00		
Ang. 2nd Moment	0.89	-0.67	-0.81	-0.64	-0.72	-0.89	1.00	
Correlation	-0.50	0.64	0.62	0.69	0.75	0.70	-0.52	1.00

Shrimp Farms	Homogeneity	Contrast	Dissimilarity	Mean	Std Dev.	Entropy	Ang. 2nd Moment	Correlation
Homogeneity	1.00							
Contrast	-0.75	1.00						
Dissimilarity	-0.90	0.96	1.00					
Mean	-0.80	0.70	0.79	1.00				
Std Dev.	-0.71	0.91	0.89	0.68	1.00			
Entropy	-0.92	0.71	0.84	0.79	0.75	1.00		
Ang. 2nd Moment	0.83	-0.50	-0.66	-0.63	-0.55	-0.88	1.00	
Correlation	0.14	-0.08	-0.11	-0.02	0.29	0.07	-0.03	1.00

Shrimp Ponds	Homogeneity	Contrast	Dissimilarity	Mean	Std Dev.	Entropy	Ang. 2nd Moment	Correlation
Homogeneity	1.00							
Contrast	-0.78	1.00						
Dissimilarity	-0.93	0.95	1.00					
Mean	-0.84	0.79	0.87	1.00				
Std Dev.	-0.80	0.92	0.93	0.79	1.00			
Entropy	-0.95	0.75	0.89	0.83	0.83	1.00		
Ang. 2nd Moment	0.90	-0.59	-0.76	-0.71	-0.68	-0.93	1.00	
Correlation	-0.24	0.27	0.28	0.29	0.56	0.43	-0.35	1.00

All Classes	Homogeneity	Contrast	Dissimilarity	Mean	Std Dev.	Entropy	Ang. 2nd Moment	Correlation
Homogeneity	1.00							
Contrast	-0.76	1.00						
Dissimilarity	-0.89	0.96	1.00					
Mean	-0.56	0.62	0.65	1.00				
Std Dev.	-0.70	0.92	0.89	0.64	1.00			
Entropy	-0.86	0.71	0.80	0.56	0.74	1.00		
Ang. 2nd Moment	0.80	-0.54	-0.67	-0.40	-0.57	-0.89	1.00	
Correlation	0.01	0.09	0.06	0.21	0.43	0.25	-0.16	1.00

JULY 18, 2001

Rice	Homogeneity	Contrast	Dissimilarity	Mean	Std Dev.	Entropy	Ang. 2nd Moment	Correlation
Homogeneity	1.00							
Contrast	-0.79	1.00						
Dissimilarity	-0.90	0.98	1.00					
Mean	-0.49	0.44	0.49	1.00				
Std Dev.	-0.70	0.88	0.86	0.44	1.00			
Entropy	-0.80	0.70	0.76	0.49	0.74	1.00		
Ang. 2nd Moment	0.77	-0.59	-0.67	-0.45	-0.63	-0.93	1.00	
Correlation	0.19	-0.18	-0.20	-0.01	0.28	0.10	-0.07	1.00

Human	Homogeneity	Contrast	Dissimilarity	Mean	Std Dev.	Entropy	Ang. 2nd Moment	Correlation
Homogeneity	1.00							
Contrast	-0.66	1.00						
Dissimilarity	-0.84	0.96	1.00					
Mean	-0.57	0.58	0.64	1.00				
Std Dev.	-0.57	0.90	0.86	0.59	1.00			
Entropy	-0.86	0.62	0.76	0.60	0.63	1.00		
Ang. 2nd Moment	0.82	-0.45	-0.62	-0.48	-0.45	-0.91	1.00	
Correlation	0.18	-0.02	-0.09	0.06	0.37	0.07	0.01	1.00

Orchard	Homogeneity	Contrast	Dissimilarity	Mean	Std Dev.	Entropy	Ang. 2nd Moment	Correlation
Homogeneity	1.00							
Contrast	-0.77	1.00						
Dissimilarity	-0.89	0.97	1.00					
Mean	-0.39	0.50	0.50	1.00				
Std Dev.	-0.68	0.90	0.87	0.54	1.00			
Entropy	-0.79	0.69	0.76	0.39	0.73	1.00		
Ang. 2nd Moment	0.76	-0.57	-0.66	-0.31	-0.61	-0.93	1.00	
Correlation	0.19	-0.11	-0.15	0.11	0.31	0.13	-0.08	1.00

Water	Homogeneity	Contrast	Dissimilarity	Mean	Std Dev.	Entropy	Ang. 2nd Moment	Correlation
Homogeneity	1.00							
Contrast	-0.80	1.00						
Dissimilarity	-0.96	0.93	1.00					
Mean	-0.77	0.87	0.88	1.00				
Std Dev.	-0.87	0.95	0.96	0.87	1.00			
Entropy	-0.98	0.80	0.95	0.79	0.89	1.00		
Ang. 2nd Moment	0.92	-0.60	-0.80	-0.50	-0.71	-0.91	1.00	
Correlation	-0.57	0.60	0.63	0.63	0.74	0.68	-0.52	1.00

Shrimp Farms	Homogeneity	Contrast	Dissimilarity	Mean	Std Dev.	Entropy	Ang. 2nd Moment	Correlation
Homogeneity	1.00							
Contrast	-0.76	1.00						
Dissimilarity	-0.92	0.95	1.00					
Mean	-0.84	0.78	0.86	1.00				
Std Dev.	-0.76	0.92	0.91	0.77	1.00			
Entropy	-0.95	0.73	0.88	0.84	0.78	1.00		
Ang. 2nd Moment	0.86	-0.52	-0.70	-0.65	-0.58	-0.89	1.00	
Correlation	0.08	-0.02	-0.05	0.03	0.29	0.10	-0.05	1.00

Shrimp Ponds	Homogeneity	Contrast	Dissimilarity	Mean	Std Dev.	Entropy	Ang. 2nd Moment	Correlation
Homogeneity	1.00							
Contrast	-0.74	1.00						
Dissimilarity	-0.94	0.92	1.00					
Mean	-0.83	0.86	0.91	1.00				
Std Dev.	-0.82	0.93	0.94	0.87	1.00			
Entropy	-0.98	0.72	0.92	0.83	0.84	1.00		
Ang. 2nd Moment	0.92	-0.57	-0.79	-0.67	-0.70	-0.94	1.00	
Correlation	-0.34	0.29	0.34	0.40	0.55	0.46	-0.42	1.00

All Classes	Homogeneity	Contrast	Dissimilarity	Mean	Std Dev.	Entropy	Ang. 2nd Moment	Correlation
Homogeneity	1.00							
Contrast	-0.75	1.00						
Dissimilarity	-0.90	0.95	1.00					
Mean	-0.61	0.65	0.68	1.00				
Std Dev.	-0.73	0.91	0.90	0.66	1.00			
Entropy	-0.88	0.71	0.83	0.62	0.77	1.00		
Ang. 2nd Moment	0.84	-0.56	-0.71	-0.48	-0.62	-0.92	1.00	
Correlation	-0.07	0.12	0.11	0.24	0.45	0.29	-0.22	1.00

SEPTEMBER 19, 2001

Rice	Homogeneity	Contrast	Dissimilarity	Mean	Std Dev.	Entropy	Ang. 2nd Moment	Correlation
Homogeneity	1							
Contrast	-0.80	1.00						
Dissimilarity	-0.91	0.97	1.00					
Mean	-0.60	0.54	0.60	1.00				
Std Dev.	-0.73	0.91	0.89	0.51	1.00			
Entropy	-0.85	0.76	0.83	0.60	0.80	1.00		
Ang. 2nd Moment	0.83	-0.64	-0.74	-0.55	-0.67	-0.94	1.00	
Correlation	0.24	-0.16	-0.19	-0.09	0.23	0.05	-0.01	1.00

Human	Homogeneity	Contrast	Dissimilarity	Mean	Std Dev.	Entropy	Ang. 2nd Moment	Correlation
Homogeneity	1.00							
Contrast	-0.71	1.00						
Dissimilarity	-0.85	0.97	1.00					
Mean	-0.68	0.62	0.69	1.00				
Std Dev.	-0.64	0.93	0.90	0.59	1.00			
Entropy	-0.83	0.67	0.77	0.66	0.69	1.00		
Ang. 2nd Moment	0.80	-0.53	-0.66	-0.61	-0.56	-0.93	1.00	
Correlation	0.15	0.02	-0.05	0.04	0.34	0.14	-0.09	1.00

Orchard	Homogeneity	Contrast	Dissimilarity	Mean	Std Dev.	Entropy	Ang. 2nd Moment	Correlation
Homogeneity	1.00							
Contrast	-0.71	1.00						
Dissimilarity	-0.85	0.97	1.00					
Mean	-0.47	0.59	0.60	1.00				
Std Dev.	-0.60	0.91	0.87	0.60	1.00			
Entropy	-0.79	0.65	0.74	0.50	0.67	1.00		
Ang. 2nd Moment	0.77	-0.50	-0.63	-0.36	-0.51	-0.93	1.00	
Correlation	0.16	0.01	-0.05	0.15	0.39	0.15	-0.08	1.00

Water	Homogeneity	Contrast	Dissimilarity	Mean	Std Dev.	Entropy	Ang. 2nd Moment	Correlation
Homogeneity	1.00							
Contrast	-0.58	1.00						
Dissimilarity	-0.96	0.78	1.00					
Mean	-0.77	0.77	0.85	1.00				
Std Dev.	-0.86	0.84	0.95	0.84	1.00			
Entropy	-0.98	0.54	0.94	0.73	0.86	1.00		
Ang. 2nd Moment mom	0.98	-0.47	-0.91	-0.70	-0.81	-0.98	1.00	
Correlation	-0.13	0.34	0.23	0.39	0.32	0.19	-0.12	1.00

Shrimp Farms	Homogeneity	Contrast	Dissimilarity	Mean	Std Dev.	Entropy	Ang. 2nd Moment	Correlation
Homogeneity	1.00							
Contrast	-0.72	1.00						
Dissimilarity	-0.91	0.94	1.00					
Mean	-0.83	0.74	0.84	1.00				
Std Dev.	-0.71	0.92	0.89	0.75	1.00			
Entropy	-0.96	0.70	0.87	0.85	0.74	1.00		
Ang. 2nd Moment	0.87	-0.50	-0.69	-0.66	-0.55	-0.89	1.00	
Correlation	0.15	-0.06	-0.11	0.03	0.27	0.03	0.02	1.00

Shrimp Ponds	Homogeneity	Contrast	Dissimilarity	Mean	Std Dev.	Entropy	Ang. 2nd Moment	Correlation
Homogeneity	1.00							
Contrast	-0.80	1.00						
Dissimilarity	-0.95	0.94	1.00					
Mean	-0.90	0.84	0.92	1.00				
Std Dev.	-0.83	0.92	0.92	0.85	1.00			
Entropy	-0.98	0.77	0.93	0.90	0.85	1.00		
Ang. 2nd Moment	0.91	-0.60	-0.79	-0.73	-0.71	-0.93	1.00	
Correlation	-0.16	0.13	0.16	0.24	0.44	0.29	-0.27	1.00

All Classes	Homogeneity	Contrast	Dissimilarity	Mean	Std Dev.	Entropy	Ang. 2nd Moment	Correlation
Homogeneity	1.00							
Contrast	-0.70	1.00						
Dissimilarity	-0.90	0.93	1.00					
Mean	-0.67	0.65	0.72	1.00				
Std Dev.	-0.71	0.90	0.90	0.66	1.00			
Entropy	-0.88	0.66	0.83	0.66	0.75	1.00		
Ang. 2nd Moment	0.85	-0.53	-0.73	-0.58	-0.62	-0.93	1.00	
Correlation	0.11	0.03	-0.03	0.10	0.31	0.11	-0.05	1.00

MEAN OF ALL CLASSES FOR ALL DATES	Homogeneity	Contrast	Dissimilarity	Mean	Std Dev.	Entropy	Ang. 2nd Moment	Correlation
Homogeneity	1.00							
Contrast	-0.75	1.00						
Dissimilarity	-0.90	0.95	1.00					
Mean	-0.61	0.65	0.69	1.00				
Std Dev.	-0.72	0.92	0.90	0.66	1.00			
Entropy	-0.88	0.71	0.82	0.62	0.76	1.00		
Ang. 2nd Moment	0.83	-0.55	-0.70	-0.47	-0.60	-0.91	1.00	
Correlation	-0.01	0.09	0.07	0.20	0.41	0.25	-0.17	1.00

SEPARABILITY ANALYSIS

		7 May, 2001		24-May-01		11-Jul-01		18-Jul-01		19-Sep-01	
		Mean	**Std.dev.**	**Mean**	**Std.dev.**	**Mean**	**Std.dev.**	**Mean**	**Std.dev.**	**Mean**	**Std.dev.**
Homogeneity (5x5)	Rice	0.370341	0.076249	0.330034	0.056538	0.321371	0.057561	0.316288	0.055469	0.349009	0.065908
	Human	0.31467	0.060626	0.315165	0.064816	0.30633	0.060081	0.332228	0.064068	0.336084	0.060826
	Orchard	0.316096	0.05446	0.31975	0.052599	0.306881	0.049557	0.327181	0.054728	0.333078	0.055743
	Water	0.742375	0.084244	0.732902	0.105591	0.704413	0.089952	0.809954	0.114229	0.882611	0.131863
	Farm	0.434355	0.112211	0.43039	0.102438	0.398037	0.090196	0.465649	0.115016	0.453578	0.116337
	Shrimp	0.577249	0.137571	0.542297	0.128449	0.512041	0.10661	0.63378	0.14782	0.597527	0.161713
Contrast (5x5)	Rice	7.408166	3.385148	9.005651	3.080384	9.882524	3.372257	10.1044	3.402219	8.506692	3.388827
	Human	11.362	4.505496	11.42974	4.341792	12.17694	4.354359	10.80376	4.359251	9.965006	4.374604
	Orchard	10.23632	3.451797	10.17855	3.553214	10.62817	3.370665	9.585006	3.480365	9.479417	3.645173
	Water	1.171012	1.804759	1.253545	1.677205	1.37953	1.855481	0.940675	1.669761	0.81623	1.594825
	Farm	7.18461	4.145717	6.623235	3.62458	8.10769	4.228231	6.049435	3.741454	6.81134	4.080677
	Shrimp	3.757788	2.88953	3.880794	2.826427	4.677579	3.403455	3.210948	3.04916	3.783166	2.96096
Dissimilarity (5x5)	Rice	2.098038	0.514266	2.366961	0.429022	2.475248	0.457195	2.510678	0.452873	2.263045	0.480155
	Human	2.61603	0.540352	2.626836	0.522581	2.725438	0.512649	2.516699	0.526096	2.428693	0.528959
	Orchard	2.521812	0.447868	2.504299	0.451829	2.5841	0.434075	2.425727	0.455629	2.396522	0.462381
	Water	0.601131	0.356863	0.378148	0.634841	0.696951	0.374847	0.457077	0.395229	0.314947	0.420856
	Farm	1.915683	0.631322	1.869512	0.56844	2.09038	0.591268	1.731586	0.601587	1.835525	0.621265
	Shrimp	1.243685	0.572533	1.327288	0.549168	1.471621	0.555959	1.068352	0.584586	1.216797	0.628888
Mean (5x5)	Rice	6.781889	1.038451	7.502067	0.887107	7.751928	0.988456	8.199002	1.182015	7.191996	0.943332
	Human	7.536987	1.108009	7.630509	1.236779	7.876966	1.200148	7.173077	1.032378	7.146062	0.917088
	Orchard	7.968786	1.204898	7.843297	1.261821	8.002837	0.982352	7.718599	1.140677	7.725419	1.051785
	Water	2.878502	0.500965	3.282077	0.490266	2.852146	0.568414	3.067123	0.539225	3.27129	0.497929
	Farm	5.315912	1.2794	5.411015	1.117296	5.575571	1.157585	5.016617	1.122667	5.260579	1.119816
	Shrimp	4.119381	0.939257	4.335233	0.911166	4.260605	0.941981	3.919204	0.877578	4.327926	0.927165

		7 May, 2001		24-May-01		11-Jul-01		18-Jul-01		19-Sep-01	
		Mean	**Std.dev.**	**Mean**	**Std.dev.**	**Mean**	**Std.dev.**	**Mean**	**Std.dev.**	**Mean**	**Std.dev.**
Standard deviation (5x5)	Rice	1.926989	0.449927	2.169735	0.378765	2.259469	0.390339	2.294771	0.404676	2.092405	0.428199
	Human	2.488502	0.545243	2.490048	0.526373	2.580613	0.526123	2.425469	0.541144	2.292848	0.528215
	Orchard	2.298092	0.413379	2.318206	0.435971	2.34845	0.3791	2.236275	0.427711	2.232682	0.468249
	Water	0.719041	0.555945	0.754278	0.520213	0.80689	0.566423	0.616087	0.533887	0.503346	0.609003
	Farm	2.042184	0.636247	1.940697	0.563547	2.194593	0.601073	1.876431	0.612357	1.992976	0.630167
	Shrimp	1.443406	0.636905	1.465469	0.597806	1.672329	0.674064	1.33025	0.683773	1.453158	0.657799
Entropy (5x5)	Rice	3.478232	0.358017	3.672717	0.264888	3.727987	0.264607	3.749665	0.266316	3.598602	0.30603
	Human	3.771926	0.290954	3.755399	0.305547	3.801521	0.272516	3.69293	0.315693	3.653537	0.289461
	Orchard	3.736373	0.254997	3.736954	0.25811	3.781405	0.232674	3.687382	0.267712	3.672487	0.26623
	Water	1.515674	0.524171	1.676344	0.598916	1.751941	0.550241	1.222867	0.680425	0.796935	0.829339
	Farm	3.250564	0.547201	3.267977	0.496578	3.439574	0.438213	3.106582	0.573308	3.137654	0.591907
	Shrimp	2.549616	0.726128	2.724632	0.670209	2.87906	0.581397	2.258404	0.802745	2.417734	0.878177
Angular 2nd moment (5x5)	Rice	0.084152	0.039347	0.066169	0.022071	0.0626	0.020902	0.061395	0.021938	0.073064	0.028225
	Human	0.061391	0.024894	0.064263	0.037015	0.061305	0.040811	0.068612	0.031944	0.069152	0.026749
	Orchard	0.061843	0.020623	0.062104	0.020527	0.058268	0.016658	0.065649	0.022503	0.066808	0.022607
	Water	0.590567	0.206623	0.627792	0.310279	0.462704	0.16102	0.928678	0.391784	1.373971	0.555846
	Farm	0.138472	0.122816	0.125427	0.10435	0.099768	0.072112	0.164964	0.145799	0.160792	0.149308
	Shrimp	0.321758	0.270367	0.248708	0.220949	0.191015	0.122755	0.461569	0.362496	0.411418	0.395151
Correlation (5x5)	Rice	0.043311	0.12558	0.059336	0.133052	0.05128	0.133403	0.055405	0.138252	0.054693	0.13829
	Human	0.097733	0.148952	0.09202	0.146826	0.09591	0.142183	0.100271	0.143064	0.077892	0.132339
	Orchard	0.045503	0.133891	0.065491	0.139192	0.051508	0.125618	0.058541	0.136882	0.065075	0.138166
	Water	0.047406	0.178225	0.048705	0.173511	0.079042	0.177428	0.053411	0.17227	0.072356	0.17479
	Farm	0.188846	0.153862	0.164685	0.154938	0.194332	0.150712	0.195552	0.152009	0.195598	0.152404
	Shrimp	0.183942	0.160745	0.169506	0.162871	0.211707	0.170405	0.202785	0.166297	0.204627	0.16623

Homogeneity (5x5):

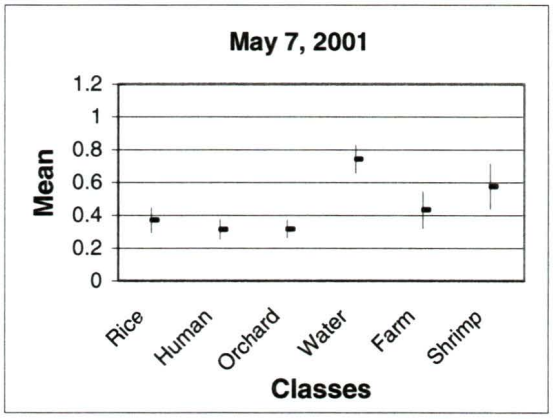

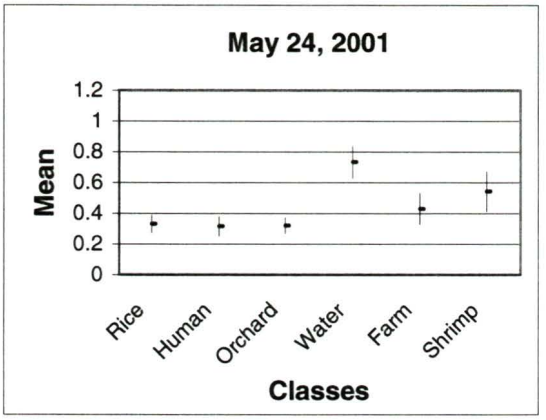

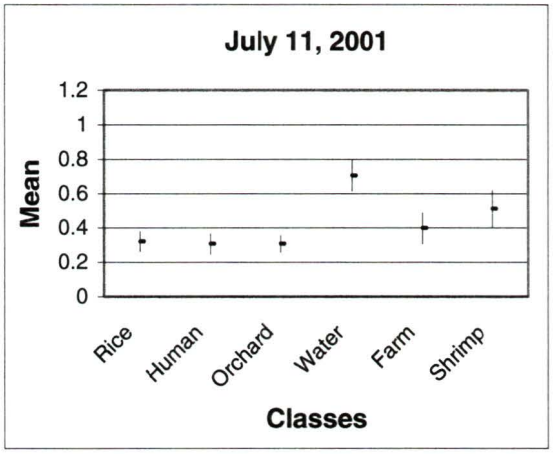

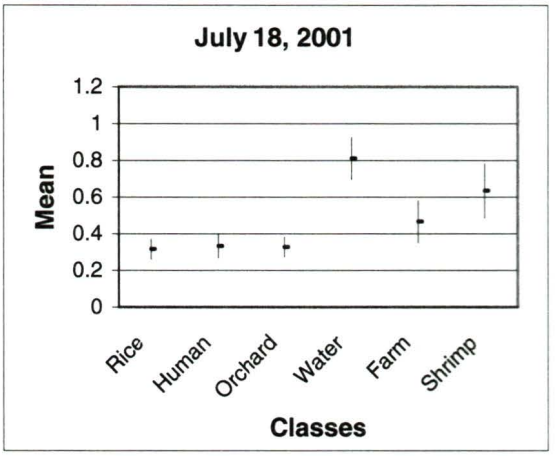

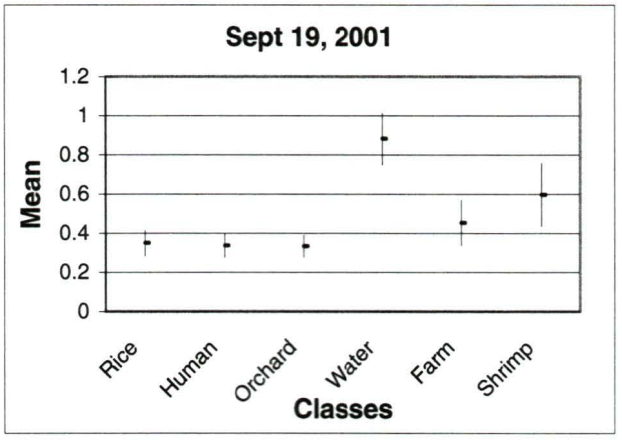

Contrast (5x5):

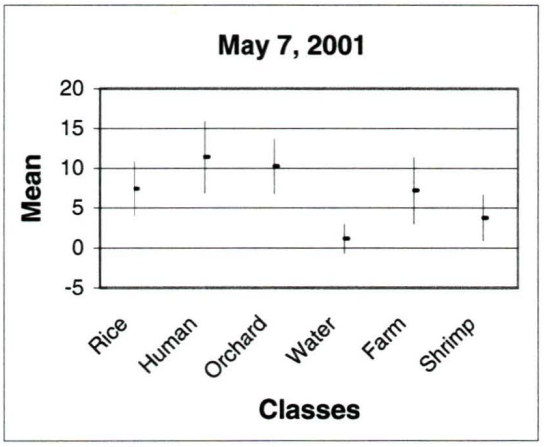

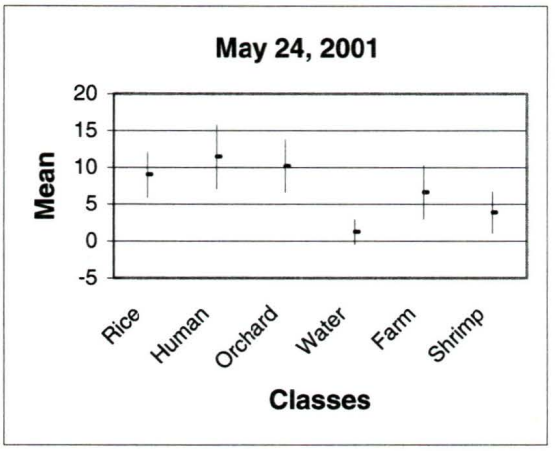

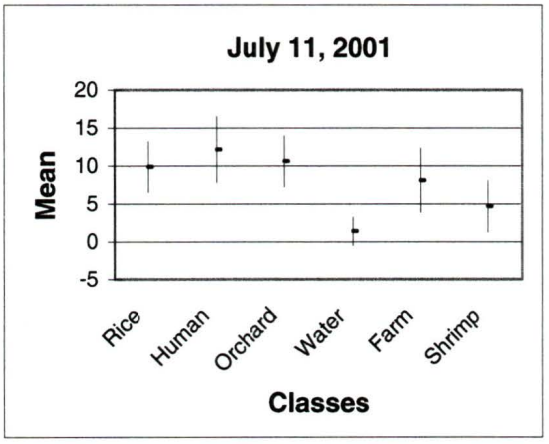

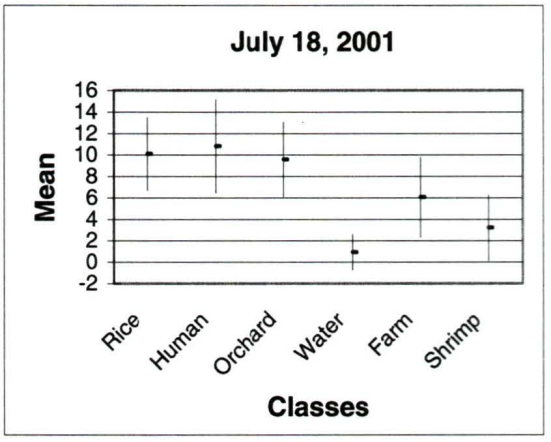

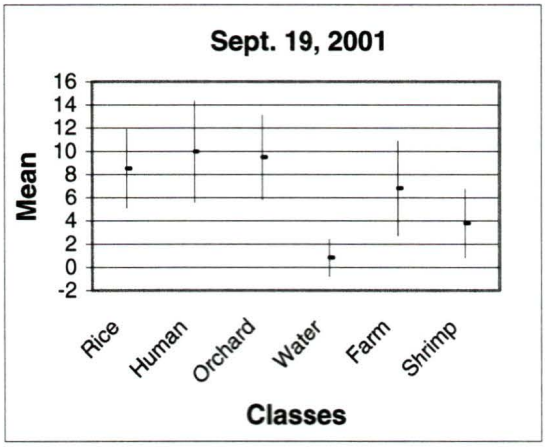

Dissimilarity (5x5):

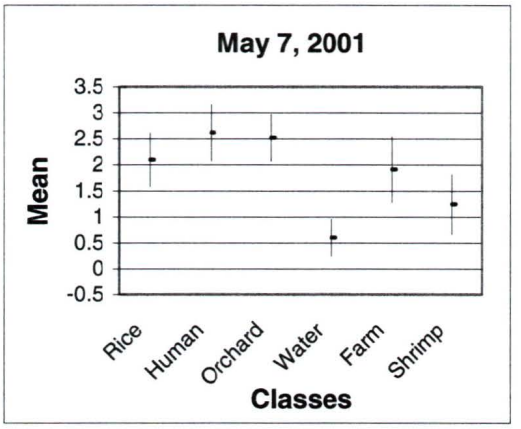

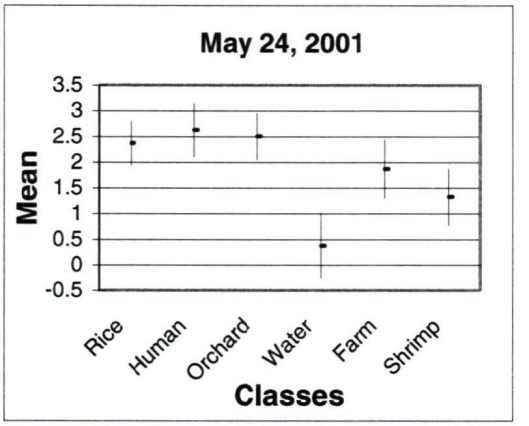

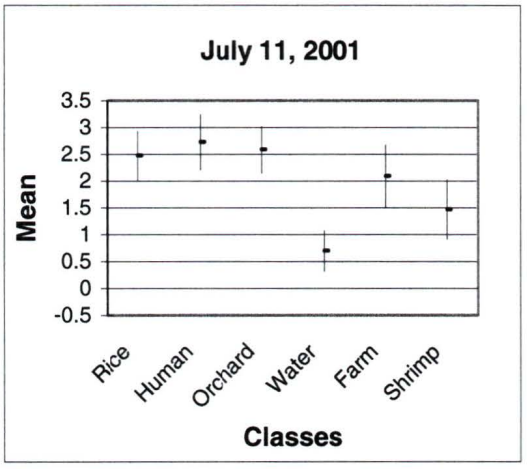

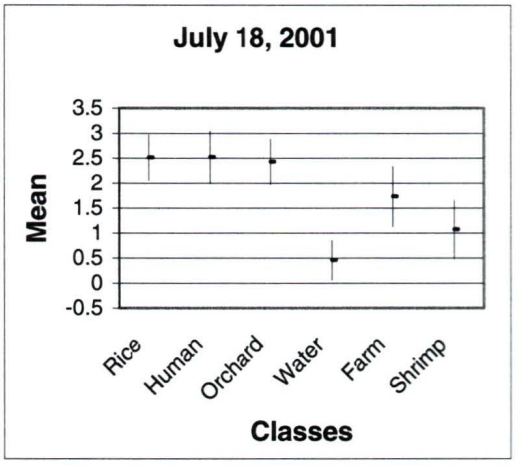

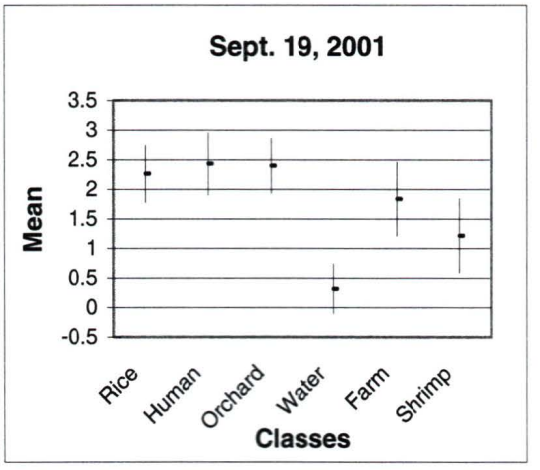

Mean (5x5):

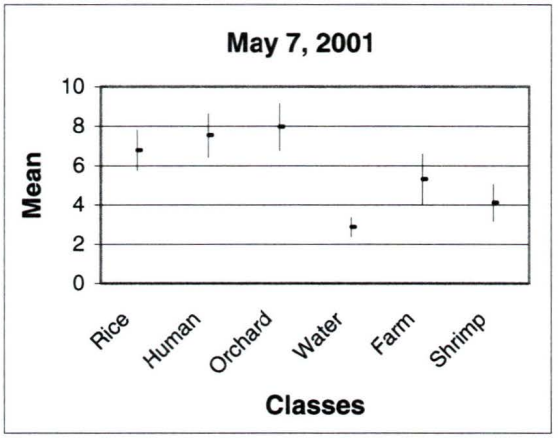
May 7, 2001
Mean
10
8
6
4
2
0
Rice
Human
Orchard
Water
Farm
Shrimp
Classes

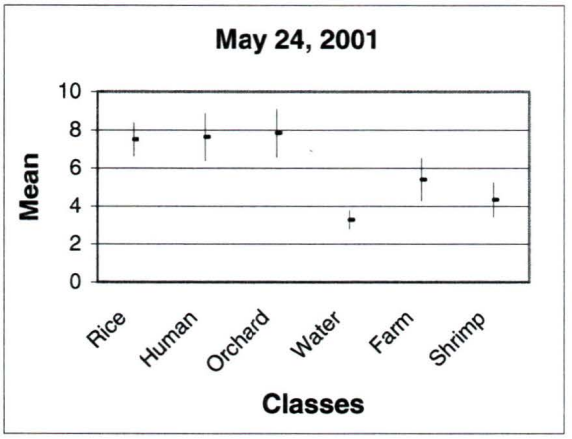
May 24, 2001
Mean
10
8
6
4
2
0
Rice
Human
Orchard
Water
Farm
Shrimp
Classes

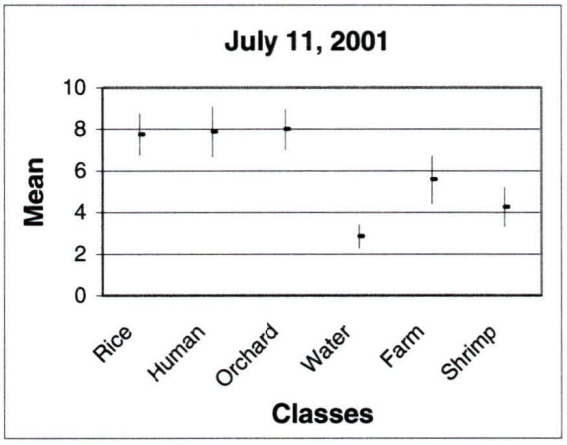
July 11, 2001
Mean
10
8
6
4
2
0
Rice
Human
Orchard
Water
Farm
Shrimp
Classes

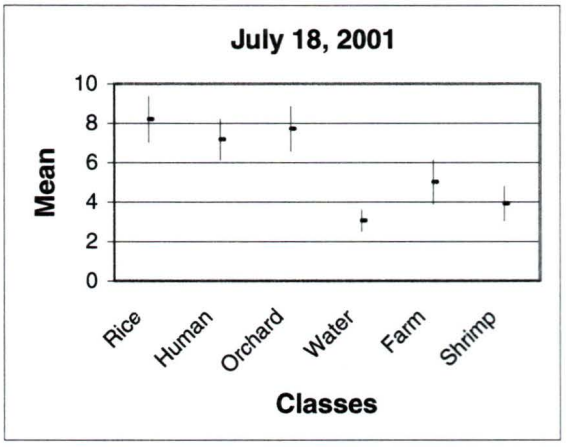
July 18, 2001
Mean
10
8
6
4
2
0
Rice
Human
Orchard
Water
Farm
Shrimp
Classes

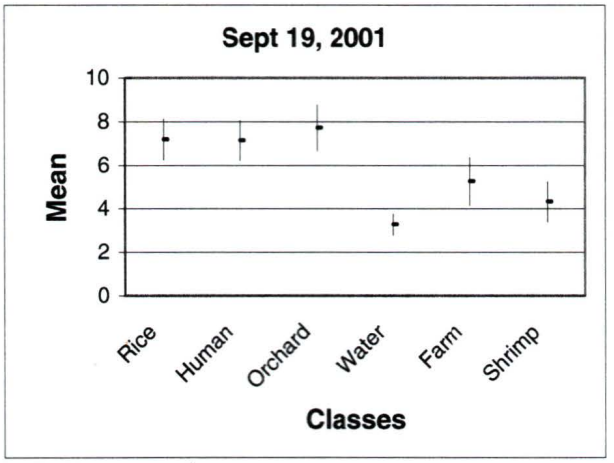
Sept 19, 2001
Mean
10
8
6
4
2
0
Rice
Human
Orchard
Water
Farm
Shrimp
Classes

Standard Deviation (5x5):

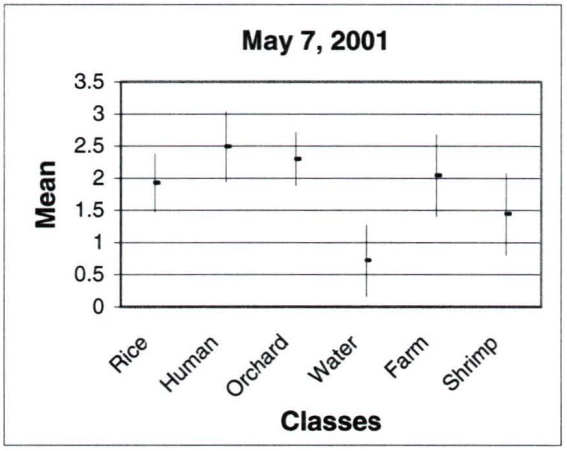

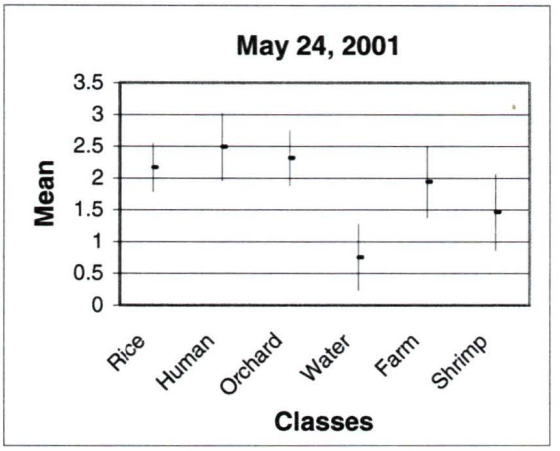

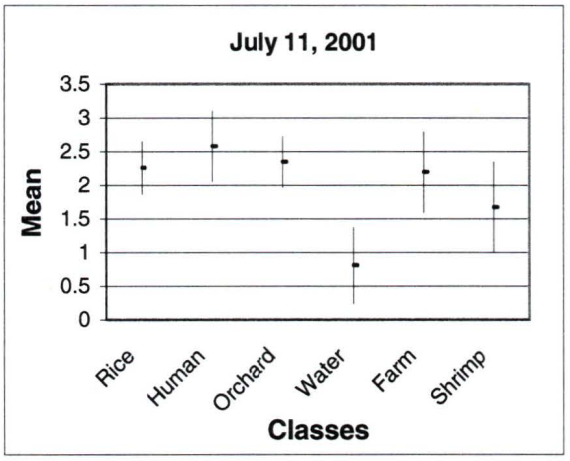

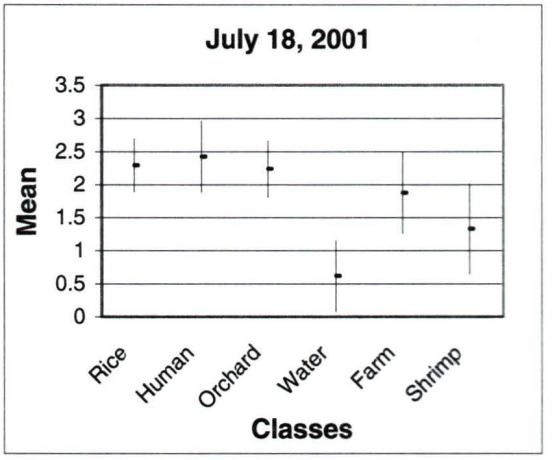

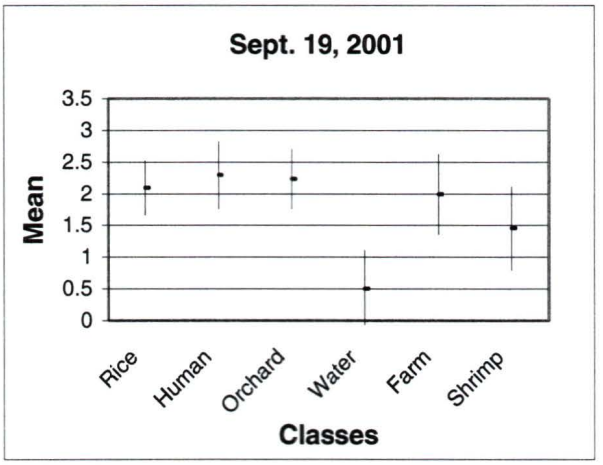

Entropy (5x5):

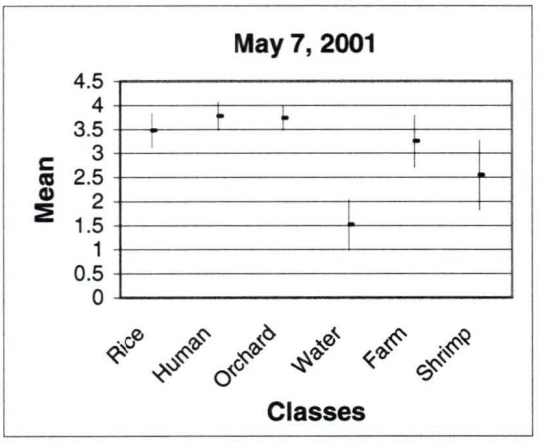
May 7, 2001
Mean
4.5
4
3.5
3
2.5
2
1.5
1
0.5
0
Rice
Human
Orchard
Water
Farm
Shrimp
Classes

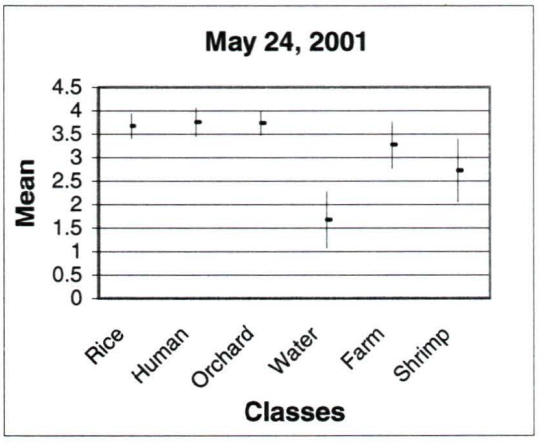
May 24, 2001
Mean
4.5
4
3.5
3
2.5
2
1.5
1
0.5
0
Rice
Human
Orchard
Water
Farm
Shrimp
Classes

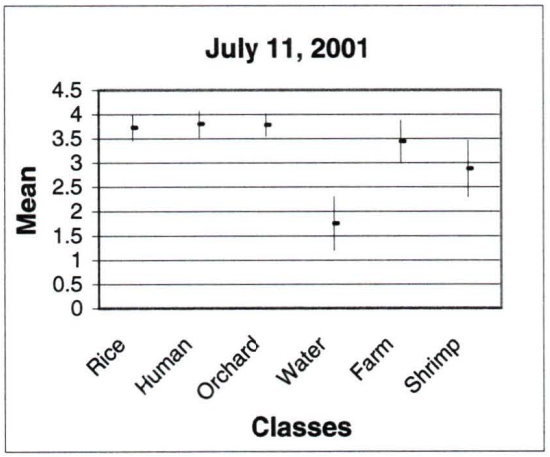
July 11, 2001
Mean
4.5
4
3.5
3
2.5
2
1.5
1
0.5
0
Rice
Human
Orchard
Water
Farm
Shrimp
Classes

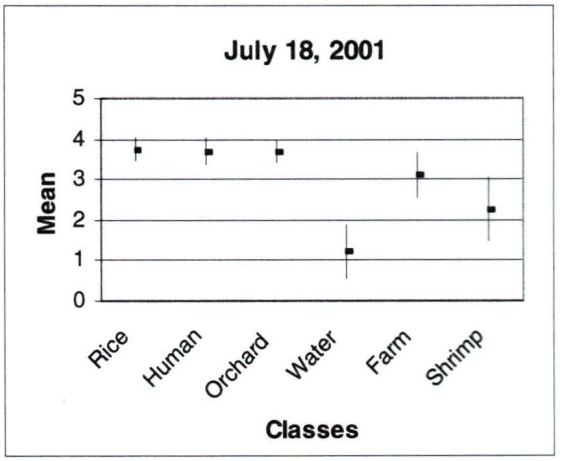
July 18, 2001
Mean
5
4
3
2
1
0
Rice
Human
Orchard
Water
Farm
Shrimp
Classes

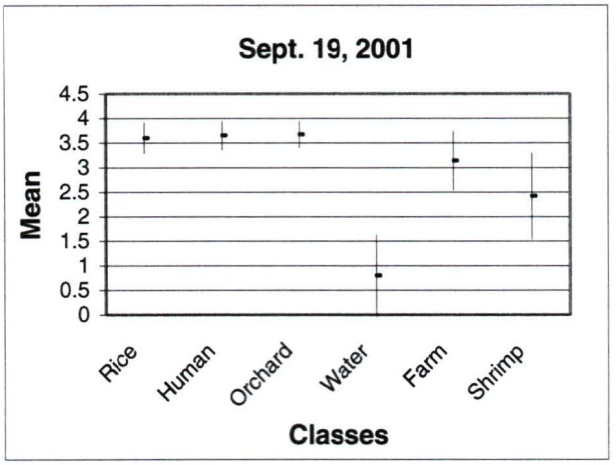
Sept. 19, 2001
Mean
4.5
4
3.5
3
2.5
2
1.5
1
0.5
0
Rice
Human
Orchard
Water
Farm
Shrimp
Classes

Angular 2nd Moment (5x5):

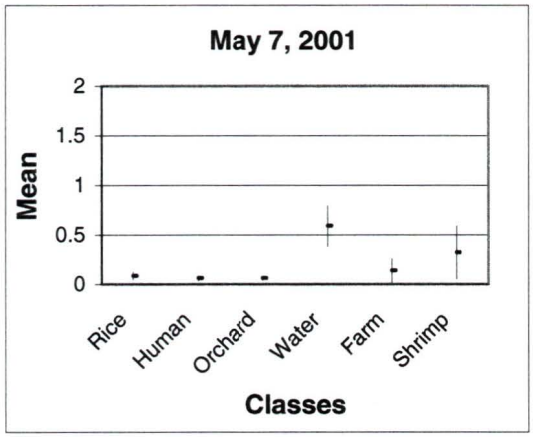

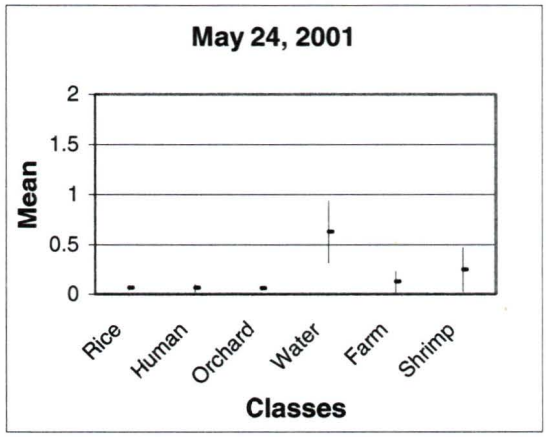

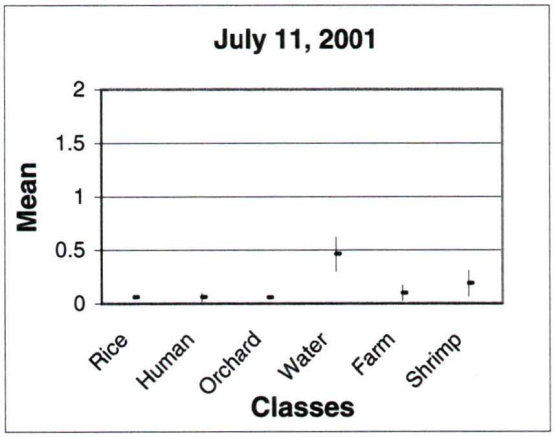

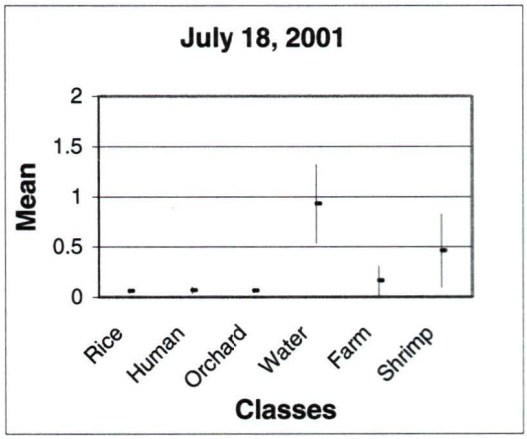

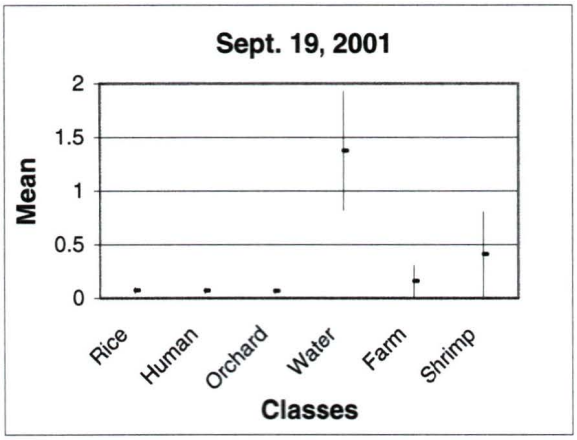

Correlation (5x5):

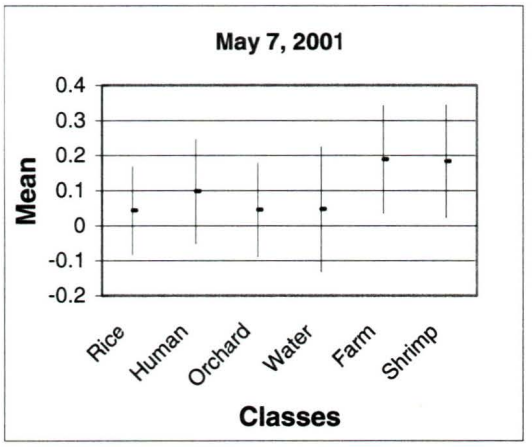

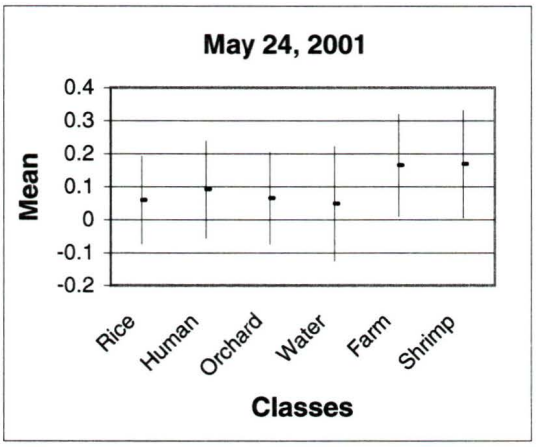

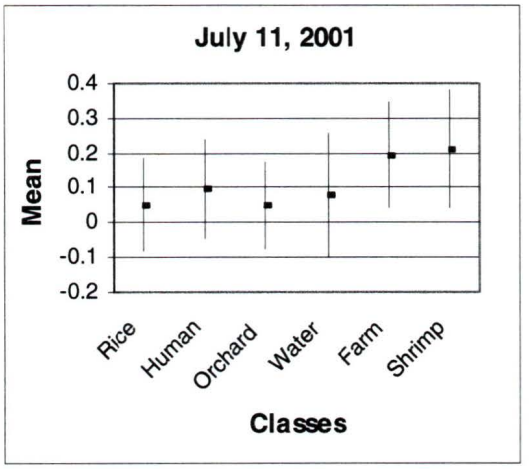

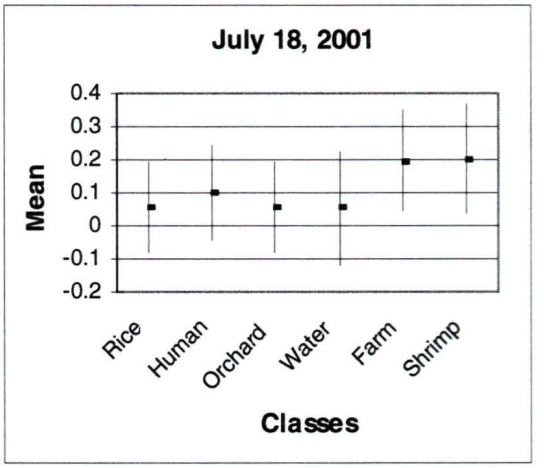

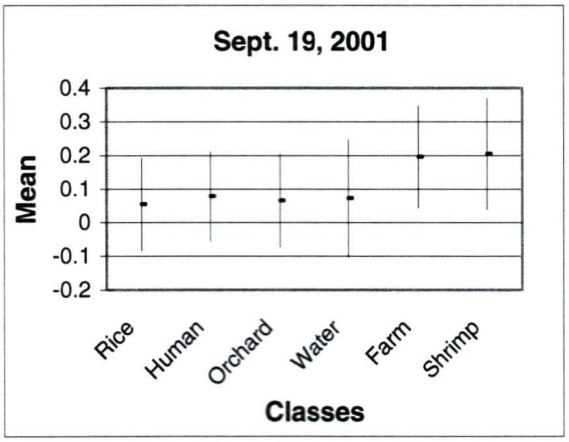

Multi-temporal variation of each signature for each texture components (5x5):

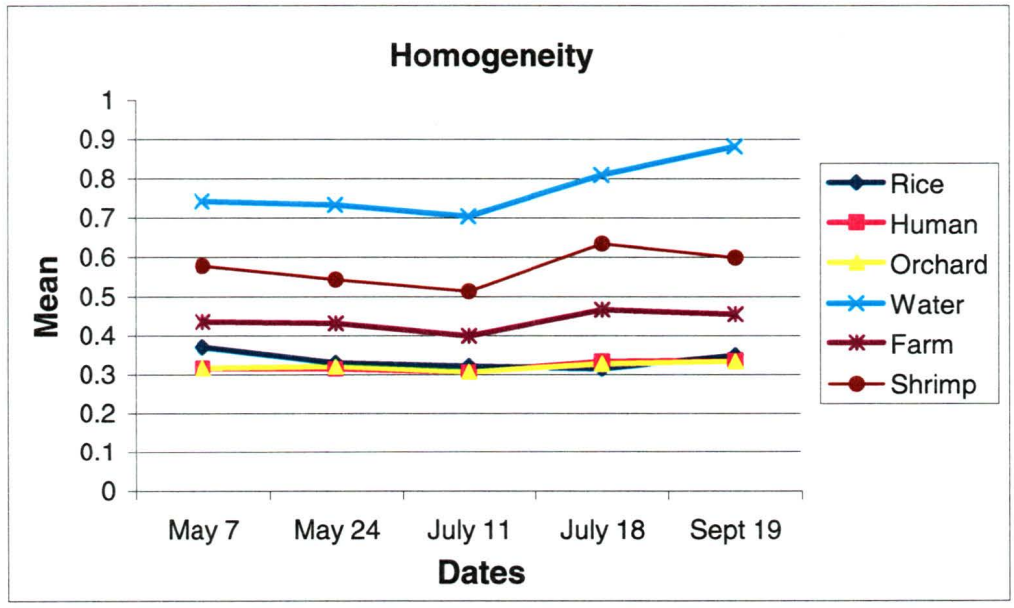

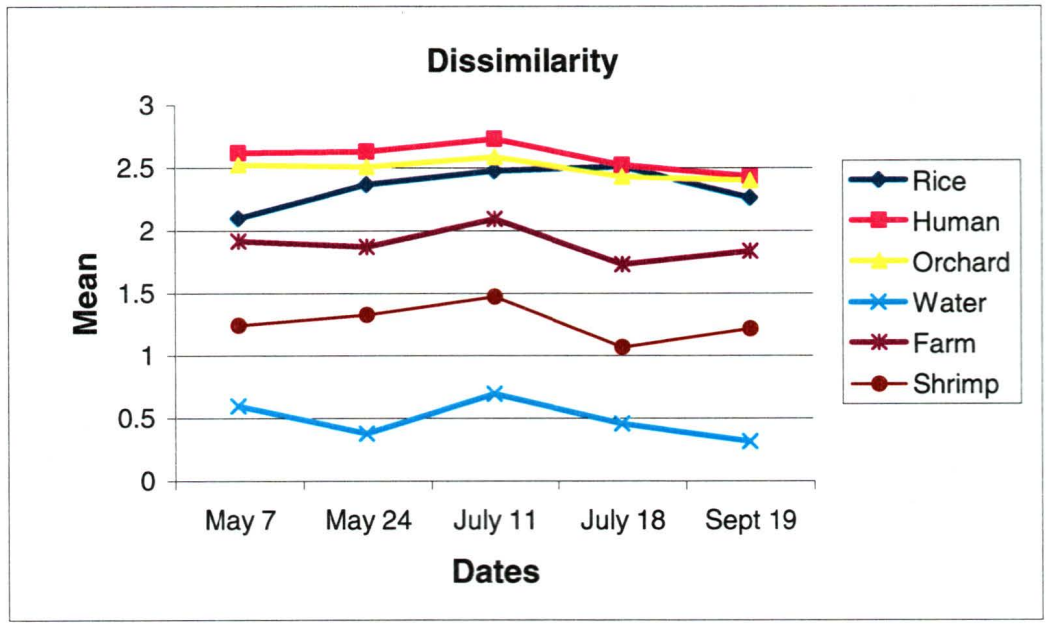

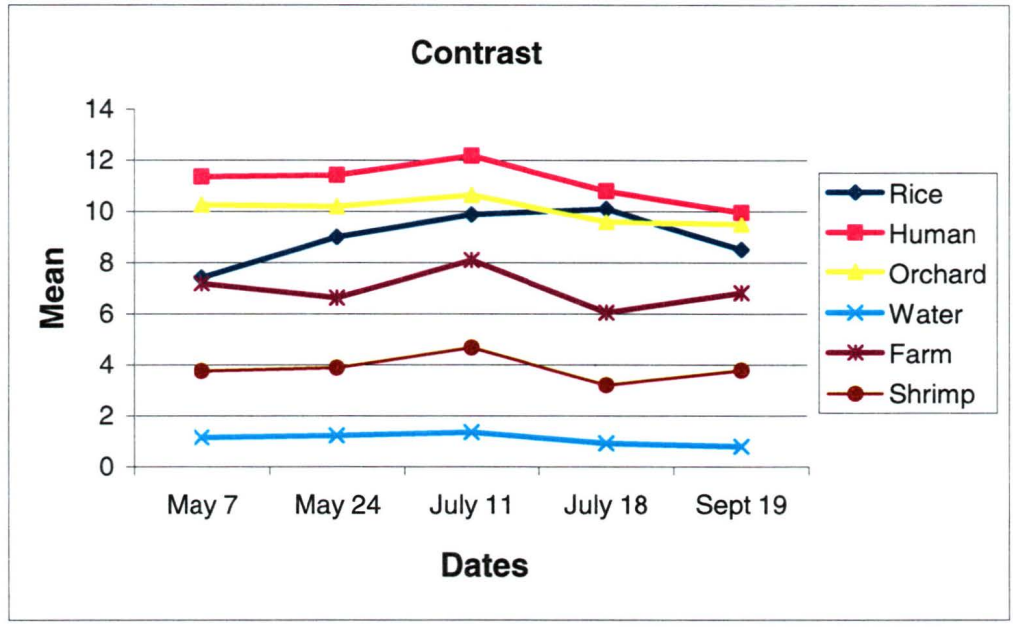
Contrast
14
12
10
8
6
4
2
0
Mean
May 7
May 24
July 11
July 18
Sept 19
Dates
Rice
Human
Orchard
Water
Farm
Shrimp

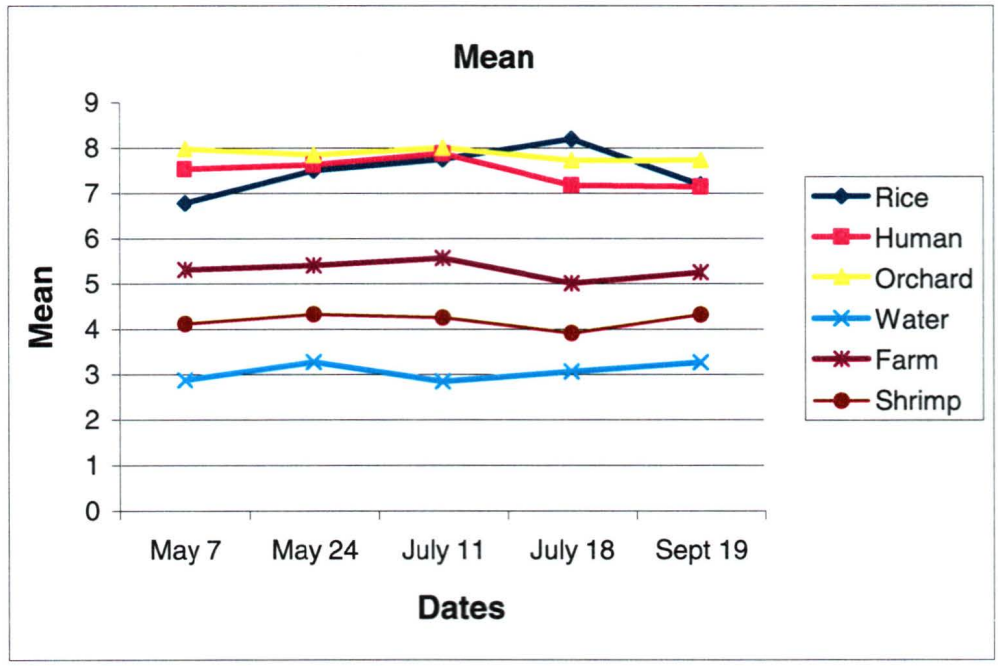
Mean
9
8
7
6
5
4
3
2
1
0
Mean
May 7
May 24
July 11
July 18
Sept 19
Dates
Rice
Human
Orchard
Water
Farm
Shrimp

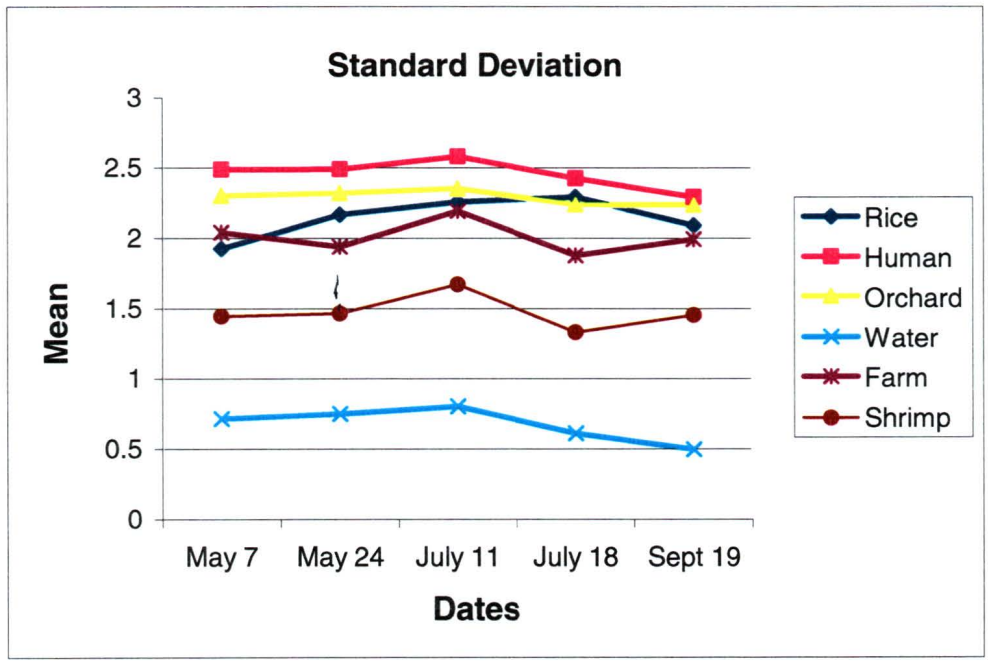
Standard Deviation
Mean
3
2.5
2
1.5
1
0.5
0
May 7
May 24
July 11
July 18
Sept 19
Dates
Rice
Human
Orchard
Water
Farm
Shrimp

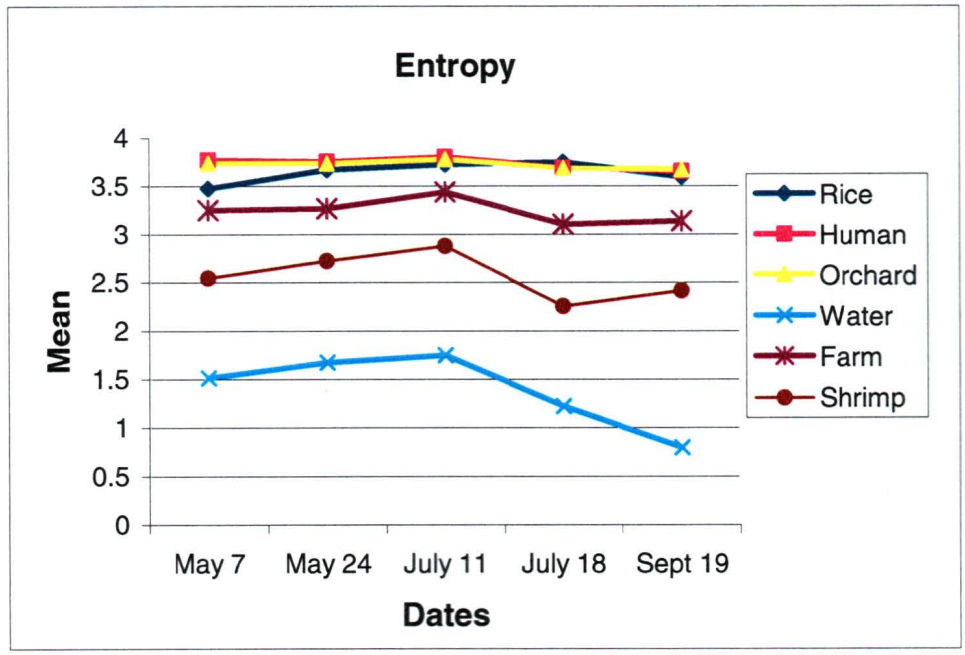
Entropy
Mean
4
3.5
3
2.5
2
1.5
1
0.5
0
May 7
May 24
July 11
July 18
Sept 19
Dates
Rice
Human
Orchard
Water
Farm
Shrimp

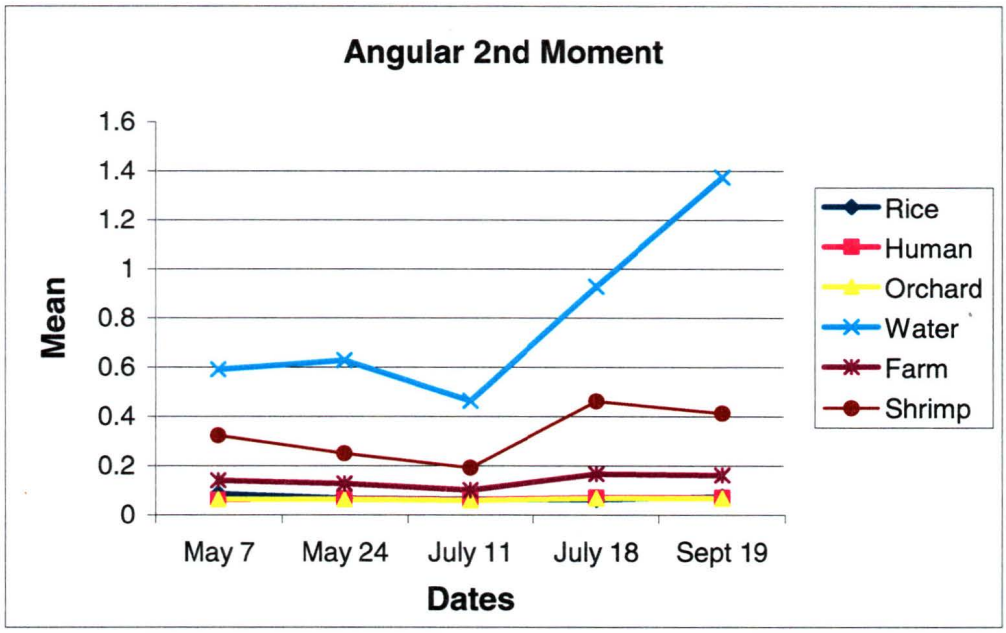
Angular 2nd Moment
Mean
1.6
1.4
1.2
1
0.8
0.6
0.4
0.2
0
May 7
May 24
July 11
July 18
Sept 19
Dates
Rice
Human
Orchard
Water
Farm
Shrimp

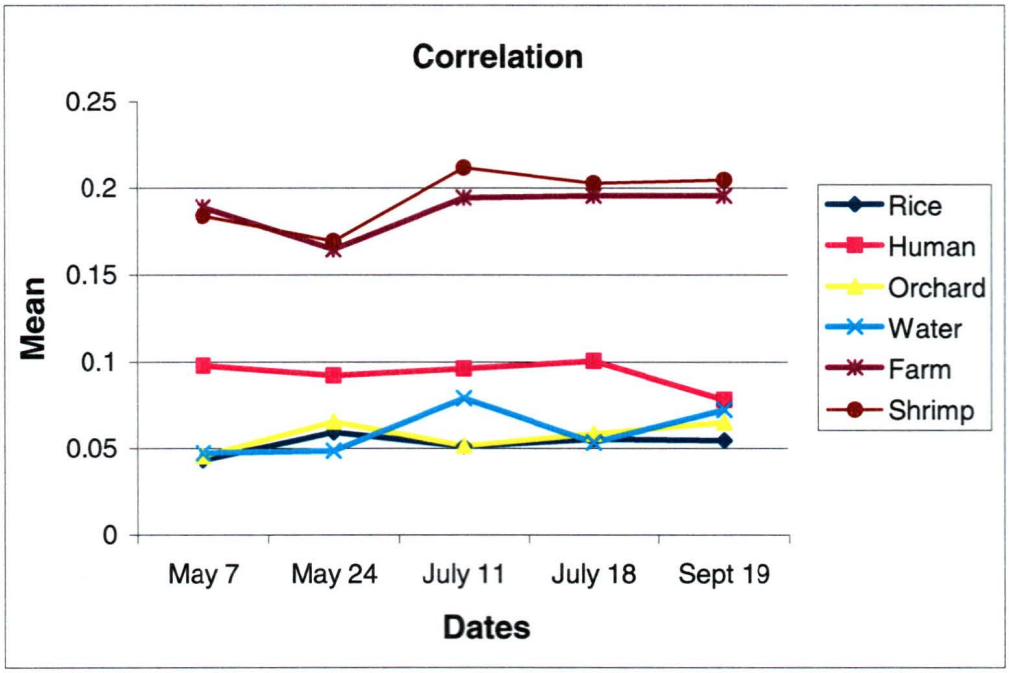
Correlation
Mean
0.25
0.2
0.15
0.1
0.05
0
May 7
May 24
July 11
July 18
Sept 19
Dates
Rice
Human
Orchard
Water
Farm
Shrimp

APPENDIX IV

ACCURACY ANALYSIS

SHRIMP FARM

```
MAT     Matrix Analysis                          V8.0 EASI/PACE  16:49 16Feb2003
G:\MASTER\POWbi16_GOOD\Texture\5x5_tex.p[S  110FIC    1126P    1735L] 21Mar2002
  109 [32R] MAP     Encoded bitmap:432,433,434,435,436                16Feb2003
  100 [32R] imagewo Maximum Likelihood Classification (with NULL class14Feb2003

 Columns = Image Channel **  109 (bitmap)
 Rows    = Image Channel **  100 (classification)
 Output  = Image Channel 93

 COINCIDENCE MATRIX:
      |   1   2   3   4   5 ELSE (bitmap)
 -----+-----------------------
   1  |   1   2   3   4   5   0
   2  |   6   7   8   9  10   0
   3  |  11  12  13  14  15   0
   4  |  16  17  18  19  20   0
   5  |  21  22  23  24  25   0
 ELSE |   0   0   0   0   0   0

 COINCIDENCE STATISTICS:

 output   -------------------- from ---------------------
 class       channel ** 109              channel ** 100          pixel count
                bitmap                   classification
 ------------------------------------------------------------------------------
    1      68% of class   1 overlapping   1% of class   1          6613 (  0%)
    2       8% of class   2 overlapping   0% of class   1           282 (  0%)
    3       2% of class   3 overlapping   0% of class   1            61 (  0%)
    4       0% of class   4 overlapping   0% of class   1             3 (  0%)
    5       1% of class   5 overlapping   0% of class   1            56 (  0%)
    6      19% of class   1 overlapping   0% of class   2          1869 (  0%)
    7      84% of class   2 overlapping   0% of class   2          3106 (  0%)
    8      12% of class   3 overlapping   0% of class   2           332 (  0%)
    9       0% of class   4 overlapping   0% of class   2             0 (  0%)
   10       0% of class   5 overlapping   0% of class   2            10 (  0%)
   11       3% of class   1 overlapping   0% of class   3           260 (  0%)
   12       3% of class   2 overlapping   0% of class   3            96 (  0%)
   13      83% of class   3 overlapping   2% of class   3          2395 (  0%)
   14       0% of class   4 overlapping   0% of class   3             0 (  0%)
   15       0% of class   5 overlapping   0% of class   3             0 (  0%)
   16       0% of class   1 overlapping   0% of class   4             1 (  0%)
   17       0% of class   2 overlapping   0% of class   4             0 (  0%)
   18       0% of class   3 overlapping   0% of class   4             0 (  0%)
   19      85% of class   4 overlapping   1% of class   4          1743 (  0%)
   20      46% of class   5 overlapping   2% of class   4          2391 (  0%)
   21      10% of class   1 overlapping   0% of class   5           955 (  0%)
   22       6% of class   2 overlapping   0% of class   5           204 (  0%)
   23       1% of class   3 overlapping   0% of class   5            16 (  0%)
   24      15% of class   4 overlapping   0% of class   5           302 (  0%)
   25      53% of class   5 overlapping   0% of class   5          2780 (  0%)
------------------------------------------------------------------------------
    0       0% of class   1 overlapping   1% unclassified           13 (  0%)
    0       2% of class   3 overlapping   4% unclassified           70 (  0%)
    0      23% unclassified overlapping  98% of class   1        439078 ( 22%)
    0      36% unclassified overlapping  99% of class   2        687016 ( 35%)
    0       6% unclassified overlapping  98% of class   3        110101 (  6%)
    0       7% unclassified overlapping  97% of class   4        136656 (  7%)
    0      29% unclassified overlapping  99% of class   5        555642 ( 28%)
    0       0% unclassified overlapping  95% unclassified          1559 (  0%)
```

ALLWATER

```
MAT     Matrix Analysis                          V8.0 EASI/PACE  17:43 16Feb2003
G:\MASTER\POWbi16_GOOD\Texture\5x5_tex.p[S  110FIC    1126P    1735L] 21Mar2002
  110 [32R] MAP     Encoded bitmap:437,432,433,434                    16Feb2003
   85 [32R] imagewo Maximum Likelihood Classification (with NULL class11Feb2003

 Columns = Image Channel **  110 (bitmap)
 Rows    = Image Channel 85      (classification)
 Output  = Image Channel 97

 COINCIDENCE MATRIX:
      |   1   2   3   4 ELSE (bitmap)
------+--------------------
  1   |   1   2   3   4   0
  2   |   5   6   7   8   0
  3   |   9  10  11  12   0
  4   |  13  14  15  16   0
ELSE  |   0   0   0   0   0

 COINCIDENCE STATISTICS:

 output   -------------------- from ---------------------
 class        channel **110                channel 85          pixel count
                   bitmap                  classification
-------------------------------------------------------------------------------
   1      96% of class   1 overlapping   1% of class   1          1866 (  0%)
   2       0% of class   2 overlapping   0% of class   1            14 (  0%)
   3       0% of class   3 overlapping   0% of class   1             1 (  0%)
   4       0% of class   4 overlapping   0% of class   1             0 (  0%)
   5       4% of class   1 overlapping   0% of class   2            72 (  0%)
   6      78% of class   2 overlapping   1% of class   2          7546 (  0%)
   7      13% of class   3 overlapping   0% of class   2           484 (  0%)
   8       3% of class   4 overlapping   0% of class   2            76 (  0%)
   9       0% of class   1 overlapping   0% of class   3             1 (  0%)
  10      19% of class   2 overlapping   0% of class   3          1878 (  0%)
  11      84% of class   3 overlapping   0% of class   3          3107 (  0%)
  12      12% of class   4 overlapping   0% of class   3           333 (  0%)
  13       0% of class   1 overlapping   0% of class   4             0 (  0%)
  14       3% of class   2 overlapping   0% of class   4           260 (  0%)
  15       3% of class   3 overlapping   0% of class   4            96 (  0%)
  16      83% of class   4 overlapping   2% of class   4          2395 (  0%)
-------------------------------------------------------------------------------
   0       0% of class   2 overlapping   1% unclassified          13 (  0%)
   0       2% of class   4 overlapping   4% unclassified          70 (  0%)
   0      13% unclassified overlapping  99% of class   1      256875 ( 13%)
   0      45% unclassified overlapping  99% of class   2      876287 ( 45%)
   0      36% unclassified overlapping  99% of class   3      690576 ( 35%)
   0       6% unclassified overlapping  98% of class   4      110101 (  6%)
   0       0% unclassified overlapping  95% unclassified        1559 (  0%)
```

VITA

Surname: Filion **Given Names:** Rébecca

Place of Birth: Québec City, Québec, Canada

Educational Institutions Attended:

Collège Francois-Xavier-Garneau, Québec City	1994 - 1996
Université Laval, Québec City	1997 - 2000
University of Victoria, British Columbia	2000 - 2003

Degrees Awarded:

Diploma in Social Sciences	Collège Francois-Xavier-Garneau	1996
Bachelor in Geography	Université Laval	2000

Honours and Awards:

FCAR, Bourse de maîtrise en recherche (Master's degree Scholarship)	2000 - 2002
President's Research Scholarship, University of Victoria (Master's degree Scholarship)	2000 - 2001
NSERC, Bourse d'emploi d'été (Undergraduate Scholarship)	2000

Publications:

Bernier, M., Ghedira, H., Gauthier, Y., Magadi, R., Filion, R., De Sève, D., Ouarda, T., Villeneuve, J.-P. and Buteau, P. 2003. Détection et Classification de Tourbières Ombrotrophes du Québec à partir d'Images RADARSAT-1. *Canadian Journal of Remote Sensing*. 29(1) :88-98.

Niemann, K.O., Filion, R., Flaherty M. and Steckler, C. 2002. Evaluation of RADARSAT-1 for Monitoring and Mapping Land Use / Land Cover in Thailand. *Proceedings of IGARSS'02*, Toronto, Canada.

Bernier, M., Fortin, J.P., Gauthier, Y., Filion, R., Bouchard, M.C. 2000. Eqeau : Implantation d'Eqeau sur l'Ensemble du Bassin de la Rivière La Grande à l'Hiver 2000. *INRS-Eau, Québec*. 48pages.

UNIVERSITY OF VICTORIA PARTIAL COPYRIGHT LICENSE

I hereby grant the right to lend my thesis to users of the University of Victoria Library, and to make single copies only for such users or in response to a request from the Library of any other university, or similar institution, on its behalf or for one of its users. I further agree that permission for extensive copying of this thesis for scholarly purposes may be granted by me or a member of the University designated by me. It is understood that copying or publication of this thesis for financial gain shall not be allowed without my written permission.

Title of Thesis:

Evaluation of RADARSAT-1 for Monitoring and Mapping Land Use / Land Cover in Thailand.

Author 

Rébecca Filion